

KAISA VUORNOS

**In Vitro Studies of  
Composite Biomaterials  
and Human Adipose Stem  
Cells in Bone and Tendon  
Tissue Engineering  
Applications**



KAISA VUORNOS

*In Vitro* Studies of Composite Biomaterials and  
Human Adipose Stem Cells in  
Bone and Tendon Tissue Engineering Applications

ACADEMIC DISSERTATION

To be presented, with the permission of the  
Faculty of Medicine and Health Technology  
of Tampere University,  
for public discussion in the  
Tietotalo building, Korkeakoulunkatu 1, Tampere,  
on 02 October 2020 12 o'clock.

ACADEMIC DISSERTATION

Tampere University, Faculty of Medicine and Health Technology  
Finland

<i>Responsible supervisor and Custos</i>	Associate Professor Susanna Miettinen Tampere University Finland	
<i>Supervisor</i>	Docent Suvi Haimi Tampere University Finland	
<i>Pre-examiners</i>	PhD Raquel Costa-Almeida University of Porto Portugal	Associate Professor Nicholas David Evans University of Southampton United Kingdom
<i>Opponent</i>	Associate Professor Manuela E. Gomes University of Minho Portugal	

The originality of this thesis has been checked using the Turnitin Originality Check service.

Copyright ©2020 Kaisa Vuornos

Cover design: Roihu Inc.

ISBN 978-952-03-1642-6 (print)  
ISBN 978-952-03-1643-3 (pdf)  
ISSN 2489-9860 (print)  
ISSN 2490-0028 (pdf)  
<http://urn.fi/URN:ISBN:978-952-03-1643-3>

PunaMusta Oy – Yliopistopaino  
Vantaa 2020



To My Family



# ABSTRACT

Critical size bone defects and other musculoskeletal injuries due to illness or trauma continue to contribute to increasing health care costs in connection to the growth of the aging population and obesity related complications in the industrialized countries. Tissue engineering with stem cells, biomaterials, and soluble factors offers feasible solutions to ease the growing need for suitable musculoskeletal implants with the promise of stem cell therapies to remedy failure or lack of tissue function. Adult stem cells, such as multipotent mesenchymal stem cells of adipose tissue, are easily available and abundant stem cells. Human adipose stem cells (hASCs) have the potential to differentiate towards besides adipogenic, also osteogenic, tenogenic, chondrogenic, and myogenic lineages in specific conditions. Critical size bone defects of maxillofacial area have already been treated by combining hASCs with biomaterials and growth factors. A tissue specific functional biomaterial supporting structure, a scaffold, offers physical support and guides stem cell growth, development, and differentiation in combination with the chemical induction provided by specific soluble factors of cell culture media. In particular, the composite biomaterial scaffolds offer an attractive alternative in order to harness the combined feasible properties of the different components. Moreover, the three-dimensional (3D) scaffold offers the differentiating stem cells a microenvironment mimicking the natural.

The aim of this thesis was to investigate novel *in vitro* musculoskeletal applications combining hASCs with suitable biomaterials and soluble factors for bone and tendon tissue engineering and vascularized bone construct applications. Firstly, tenogenic medium (TM) was optimized to support tenogenic differentiation of hASCs and used to induce formation of tendon-like matrix on mechanically suitable braided 3D polymer scaffolds. Secondly, 3D hydrogels supportive of hASC osteogenic differentiation were tested in combination with bioactive glass (BaG) extract based osteogenic medium (BaG OM) with support from evolving hydrogel mechanical properties. Thirdly, concomitant matrix mineralization and microvascularization formation were investigated in composite 3D hydrogels with hASC and human umbilical vein endothelial cell (HUVEC) coculture by comparing BaG extract based endothelial-osteogenic

medium (BaG EM-OM) and endothelial cell growth medium-2 (EGM-2) together with assessing the effect of osteogenic preconditioning of hASCs.

The results showed that the optimized TM with both growth and differentiation factor-5 and L-ascorbic acid together with the support of 3D braided poly(L/D) lactide (PLA) 96L/4D copolymer filament scaffolds significantly enhanced tendon-like matrix production of hASCs compared to other tested media groups or different 3D scaffold structure. The combined optimized chemical support of TM and 3D mechanical support of PLA 96/4 were shown essential for efficient and fast tendon-like matrix formation by hASCs.

In 3D hydrogels, robust hASC osteogenic differentiation and mineralization with BaG OM without any added growth factors was reported. Natural polymers collagen type I (COL) and gellan gum (GG) hydrogels were compared for hASC osteogenic induction for minimally invasive bone tissue engineering applications. In addition, ionic crosslinking of GG with the BaG extract was tested and was found to significantly increase mineralization even in the control condition of regular osteogenic medium. While both the hydrogels elicited strong hASC mineralization, hASCs embedded in COL with the BaG OM induction showed significantly higher gene expression of osteogenic marker genes, and also strong immunocytochemical staining of late osteogenic marker osteocalcin (OCN) was observed, thus confirming efficacious hASC osteogenic differentiation in *in vitro* 3D hydrogel culture mimicking physiological conditions.

In 3D GG-COL composite hydrogels in hASC-HUVEC coculture, both BaG EM-OM and EGM-2 media supported osteogenic as well as endothelial marker gene expression. Whereas hydroxyapatite mineralization and strong OCN staining were detected in the BaG EM-OM condition, in comparison, strong production of mature endothelial marker CD31 and elongated tube-like structures of hASCs and HUVECs with initial prevascular network formation were apparent in the EGM-2 condition. However, osteogenesis and vasculogenesis processes were deemed mutually inhibitory in these conditions in coculture in 3D GG-COL composite hydrogels.

In conclusion, these novel methods for *in vitro* 3D culture have potential for considerable future significance and impact on the field of musculoskeletal regenerative medicine applications.

# TIIVISTELMÄ

Tuki- ja liikuntaelinsairaudet sairauden tai loukkaantumisen johdosta ovat teollistuneissa maissa väestön ikääntymiseen ja ylipainoisuuteen liittyen merkittävä ja kasvava kansantaloudellinen rasite. Kudosteknologia tarjoaa kasvaviin tuki- ja liikuntaelinsovellusten tarpeisiin käyttökelpoisia ratkaisuja yhdistäen kantasoluja, biomateriaaleja sekä solujen kasvua ja erilaistumista edistäviä tekijöitä korjaamaan tai korvaamaan vaurioituneita kudoksia. Aikuisen kantasolut, kuten monikykyiset mesenkymaaliset rasvakudoksen kantasolut, ovat lupaavia kudosteknologiin sovelluksiin perustuen niiden hyvään saatavuuteen, saantoon ja erilaistumiskykyyn useiksi solutyypeiksi, kuten rasva-, luu-, jänne-, rusto- ja lihassoluiksi tietyissä olosuhteissa. Suuria pään ja kallon alueen luupuutoksia on jo hoidettu yhdistäen rasvakudoksen kantasolut biomateriaalin ja kasvutekijöiden kanssa. Kudostyyppikohtainen toiminnallinen biomateriaalitukirakenne eli skaffoldi tukee fyysisesti ja ohjaa kantasolujen kasvua, kehitystä ja erilaistumista yhdessä kasvatusliuoksen tiettyjen liukoisten tekijöiden kemiallisen stimulaation kanssa. Komposiittibiomateriaaleista valmistettujen skaffoldien avulla voidaan yhdistää eri komponenttien hyödylliset ominaisuudet. Kolmiulotteiset (3D) skaffoldit tarjoavat erilaistuville kantasoluille luonnollista jäljittelevän kasvuympäristön.

Tämän väitöstutkimuksen tavoitteena oli kehittää uusia *in vitro* tuki- ja liikuntaelinsovelluksia yhdistämällä rasvakudoksen kantasolut soveltuvien biomateriaalien ja liukoisten tekijöiden kanssa luu- ja jännekudosteknologiin sovelluksiin sekä verisuonittuneen luun kudosteknologisten sovellusten kehittämiseen. Ensimmäisessä osatyössä kehitettiin uusi tehokas solujen jänne-erilaistuskasvatusliuos eli jännemedium rasvakudoksen kantasolujen jänne-erilaistumista tukemaan sekä edistämään jännekudostyyppisen soluväliaineen muodostumista mekaanisilta ominaisuuksiltaan soveltuvien 3D punottujen kuitutukirakenteiden eli kuituskaffoldien avulla. Toisessa osatyössä rasvakudoksen kantasolujen luuerilaistuminen saatiin aikaan 3D hydrogeeleissä bioaktiivisesta lasista valmistetun ekstraktipohjaisen luuerilaistusmediumin sekä luuerilaistumista tukevien mekaanisten ominaisuuksien avulla. Kolmannessa osatyössä tutkittiin luuerilaistumisen lisäksi verisuoniverkoston muodostumista

rasvakudoksen kantasolujen ja ihmisen napalaskimon endoteelisolujen yhteisviljelyn avulla 3D komposiittihydrogeelikasvatuksessa endoteelimedumpohjaisessa bioaktiivisesta lasista valmistetussa ekstraktimediumissa luuerilaistustekijöiden kanssa. Lisäksi työssä tutkittiin rasvakudoksen kantasolujen luuerilaistumisen tehostamista luuviljelymediumilla tapahtuvalla esikasvatuksella.

Kehitetty optimoitu jännemedium, joka sisälsi kasvu- ja erilaistumistekijä 5:tä ja L-askorbiinihappoa, edisti merkittävästi jännekudostyyppisen soluväliaineen muodostumista punotun 3D poly(96L/4D)laktidi (PLA 96/4)-kopolymeeri kuituskaffoldin kanssa verrattuna erilaisiin testattuihin mediumeihin tai erityyppiseen 3D tukirakenteeseen. Tehokkaaseen ja nopeaan rasvakudoksen kantasolujen jännekudostyyppisen soluväliaineen muodostumiseen tarvittiin sekä optimoidun jännemediumin kemiallinen stimulaatio että punottu 3D PLA 96/4-kuiturakenne. Bioaktiivisesta lasista valmistettu ekstraktipohjainen luumedium sai aikaan tehokkaan rasvakudoksen kantasolujen luuerilaistumisen ja mineralisaation ilman lisättyjä kasvutekijöitä 3D gellaanikumi (GG)- ja tyypin I kollageeni (COL)-hydrogeeliskaffoldeissa, joita verrattiin mahdollisimman vähän invasiivisen luukudosteknologisen sovelluksen kehittämiseen. Lisäksi GG:n ristosilloittaminen ionipitoisen bioaktiivisesta lasista valmistetun ekstraktin avulla lisäsi merkittävästi mineralisaatiota jopa kontrolliolosuhteissa luumediumissa. COL hydrogeelissä merkittävästi korkeampi geeniekspressio ja voimakas osteokalsiinituotanto vahvistivat tehokkaan rasvakudoksen kantasolujen luuerilaistumisen *in vitro* 3D hydrogeelikasvatuksessa fysiologisia olosuhteita mallintavissa olosuhteissa. 3D GG-COL -komposiittihydrogeelikasvatuksessa rasvakudoksen kantasolujen ja ihmisen napalaskimon endoteelisolujen yhteisviljelyssä havaittiin sekä luu- että endoteelimarkkereiden geeniekspressiota vertailtavina olleissa endoteelimedumpohjaisessa bioaktiivisesta lasista valmistetussa ekstraktimediumissa luuerilaistustekijöiden kanssa (BaG EM-OM) ja endoteelimediumissa (EGM-2). Voimakas hydroksiapatiittimineralisaatio ja osteokalsiinituotanto olivat havaittavaisissa ainoastaan BaG EM-OM-olosuhteissa, kun taas vahva myöhäisen endoteelimarkkerin CD31 tuotanto, yhteisviljeltyjen levittäytyneiden solujen muodostamia putkirakenteita sekä varhaisia verisuoniverkostorakenteita oli nähtävissä vain EGM-2 -mediumolosuhteissa. Tulosten perusteella luuerilaistuminen ja verisuonituksen muodostuminen olivat toisensa poissulkevia prosesseja näissä kasvatusolosuhteissa yhteisviljelmässä 3D GG-COL -komposiittihydrogeeleissä.

Yhteenvedona voidaan todeta, että nämä uudet *in vitro* 3D kasvatusmenetelmät ovat lupaavia uusien merkittävien regeneratiivisen lääketieteen tuki- ja liikuntaelinsovelluksien kehittämistä varten.





# CONTENTS

1	Introduction.....	25
2	Literature review.....	29
2.1	Stem cells.....	29
2.2	Human adipose stem cells.....	31
2.2.1	Characterization of human adipose stem cells.....	32
2.2.2	Human adipose stem cell heterogeneity.....	33
2.3	Human adipose stem cell differentiation.....	34
2.3.1	Tenogenic differentiation.....	34
2.3.2	Osteogenic differentiation.....	38
2.3.3	Endothelial differentiation and role of subpopulations.....	42
2.4	Three-dimensional cell culture.....	44
2.4.1	Tissue engineering scaffolds.....	44
2.4.2	<i>In vitro</i> tissue models.....	47
2.5	Biomaterials for tendon tissue engineering.....	47
2.5.1	Mechanical properties for tendon constructs.....	48
2.5.2	Filamentous polymer scaffolds.....	49
2.5.3	Foamed polymer scaffolds.....	50
2.6	Biomaterials for bone tissue engineering and vascularized bone.....	50
2.6.1	Mechanical properties for bone constructs.....	51
2.6.2	Hydrogels.....	52
2.6.3	Bioactive glass.....	56
2.7	Vascularized bone tissue engineering.....	58
2.7.1	Coculture for vascularization.....	58

2.7.2	Vascularization in cell-laden hydrogels.....	62
2.8	<i>In vivo</i> studies.....	63
2.9	Clinical case studies.....	64
3	Aims of the study.....	67
4	Materials and methods.....	68
4.1	Human adipose stem cell isolation, characterization and culture .....	68
4.1.1	Human adipose stem cell isolation.....	68
4.1.2	Human adipose stem cell characterization.....	69
4.1.3	Human adipose stem cell culture.....	69
4.2	Human umbilical vein endothelial cell isolation, characterization and culture.....	71
4.2.1	Human umbilical vein endothelial cell isolation.....	71
4.2.2	Human umbilical vein endothelial cell characterization .....	71
4.2.3	Human umbilical vein endothelial cell culture .....	72
4.3	Tenogenic scaffold manufacture and characterization .....	72
4.3.1	Braided filamentous polymer scaffolds .....	72
4.3.2	Foamed polymer scaffolds.....	73
4.3.3	Polymeric tendon scaffold mechanical tensile testing .....	73
4.3.4	Micro-computed tomography imaging of polymeric scaffolds .....	74
4.4	Osteogenic and vascularized bone scaffold manufacture and characterization.....	74
4.4.1	Bioactive glass manufacture.....	74
4.4.2	Gellan gum and collagen type I hydrogel scaffolds... ..	74
4.4.3	Hydrogel scaffold mechanical compression testing .. ..	76
4.4.4	Optical projection tomography and selective plane illumination microscopy imaging of hydrogel scaffolds .....	77
4.5	Cell morphology, viability, and number.....	78

4.6	Differentiation of human adipose stem cells .....	79
4.6.1	Tenogenic differentiation with chemical stimulus and scaffold properties .....	81
4.6.2	Osteogenic differentiation with chemical stimulus and scaffold properties .....	82
4.6.3	Three-dimensional coculture in hydrogels.....	82
4.7	Analysis of human adipose stem cell differentiation .....	83
4.7.1	Quantitative real-time polymerase chain reaction .....	83
4.7.2	Total collagen content.....	84
4.7.3	Mineralization .....	85
4.7.4	Immunocytochemistry .....	85
4.7.5	Raman spectroscopy.....	86
4.7.6	Statistical analyses .....	87
5	Results.....	89
5.1	Biomaterial characterization.....	89
5.1.1	Micro-computer tomography imaging .....	89
5.1.2	Mechanical testing.....	90
5.2	Human adipose stem cell and human umbilical vein endothelial cell characterization .....	92
5.2.1	Human adipose stem cell characterization .....	92
5.2.2	Human umbilical vein endothelial cell characterization .....	93
5.3	Cell morphology, viability, and number.....	93
5.3.1	Cell viability and morphology .....	93
5.3.2	Cell number.....	95
5.4	Tenogenic differentiation of human adipose stem cells in braided polymer scaffolds.....	97
5.4.1	Comparison of tenogenic differentiation media compositions.....	97
5.4.2	Comparison of tenogenic scaffolds .....	98

5.4.3	Human adipose stem cell tenogenic differentiation medium and braided polylactide 96/4 scaffold.....	98
5.5	Osteogenic differentiation of human adipose stem cells in gellan gum and collagen type I hydrogel scaffolds .....	100
5.5.1	Osteogenic gene expression enhanced with bioactive glass extract based osteogenic media .....	100
5.5.2	Robust hydroxyapatite mineralization and late osteogenic differentiation with bioactive glass extract based osteogenic media in three-dimensional hydrogels.....	102
5.6	Osteogenic differentiation of human adipose stem cells and coculture for microvascularization in composite hydrogel scaffolds .....	105
6	Discussion.....	109
6.1	Combined stimulus by soluble factors and scaffold biomaterial needed for human adipose stem cell tenogenic differentiation	109
6.2	Bioactive glass extract based osteogenic medium induced robust osteogenic differentiation of human adipose stem cells in gellan gum and collagen type I hydrogels.....	111
6.3	Bioactive glass soluble factors promoted mineralization and osteogenesis while neovascularization was restricted in coculture in composite hydrogel scaffolds .....	113
6.4	The effect of donor variation and human adipose stem cell endothelial subpopulations.....	115
6.5	Establishing initial three-dimensional <i>in vitro</i> musculoskeletal model.....	117
6.6	Developing three-dimensional hydrogel analysis methods .....	118
6.7	Ethical considerations .....	120
6.8	Future perspectives .....	120
7	Conclusions .....	125
8	Author's contribution .....	127
9	Acknowledgements .....	128

## *List of Figures*

Figure 1. Schematic tendon structure.

Figure 2. Bone tissue structure.

Figure 3. Matrix stiffness influences MSC osteogenesis.

Figure 4. Collagen type I structure.

Figure 5. BaG dissolved ions' effect on angiogenesis.

Figure 6. Microvascularization formation in cell-laden hydrogels.

Figure 7. Micro-CT images of braided PLA 96/4 and foamed PLCL tenogenic scaffolds.

Figure 8. Mechanical compression testing of acellular hydrogels.

Figure 9. Cell viability in study I. The hASC morphology and viability on braided PLA 96/4 scaffolds in MM and TM conditions.

Figure 10. Cell viability in study II. The hASCs embedded within GG-SPD (OM), GG-SPD (BaG OM), COL (OM) and COL (BaG OM) hydrogels.

Figure 11. Cell viability in study III. Cocultured hASCs and HUVECs embedded within composite GG-COL hydrogels in EGM-2 or BaG EM-OM media culture with hASCs cultured in MM or preconditioned in OM prior to cell encapsulation.

Figure 12. Cell number in studies I-III.

Figure 13. Tenogenic differentiation of hASCs in study I.

Figure 14. Osteogenic gene expression and OCN production of hASCs in 3D hydrogels in the GG-SPD (OM), GG-SPD (BaG OM), COL (OM), and COL (BaG OM) conditions in study II.

Figure 15. Mineralization in study II.

Figure 16. Osteogenic and endothelial differentiation of hASCs and HUVECs within composite GG-COL hydrogels in study III.

Figure 17. Mineralization in study III.

## *List of Tables*

Table 1. Tendon markers.

Table 2. Osteogenic markers in MSC osteogenesis process.

Table 3. Angiogenesis process and proangiogenic factors.

Table 4: *In vitro* bone studies with hydrogels.

Table 5. *In vitro* bone vascularization studies in hydrogels and composites.

Table 6. Phase II/III/IV musculoskeletal ATMP clinical trials 2008-2018.

Table 7. The media compositions.

Table 8. Gellan gum and collagen type I hydrogel scaffolds and crosslinkers.

Table 9. Mechanical compression testing of hydrogel scaffolds.

Table 10. Cell viability and cell number analyses' timepoints.

Table 11. Differentiation markers and analyses performed in studies I-III.

Table 12. The primer sequences for qRT-PCR.

Table 13. Immunocytochemical stainings in studies I-III.

Table 14. Raman spectroscopy cell culture media in study II.

Table 15. Surface marker expression of undifferentiated hASCs in studies I-III.

# ABBREVIATIONS AND SYMBOLS

$\alpha$ MEM	Minimum essential medium $\alpha$
$\beta$ -GP	$\beta$ -Glycerophosphate
$\beta$ -TCP	$\beta$ -Tricalcium phosphate
$\epsilon$	Strain
$\sigma$	Stress
2D	Two-dimensional
3D	Three-dimensional
4D	Four-dimensional
ALP	Alkaline phosphatase Homo sapiens alkaline phosphatase gene
ALPL	(liver/bone/kidney)
Ang1	Angiopoietin1
Ang2	Angiopoietin2
ANOVA	Analysis of variance
AsA2P	L-Ascorbic acid 2-phosphate
ASC	Adipose stem cell
ASTM	American Society for Testing and Materials
ATMP	Advanced therapy medicinal product
BaG	Bioactive glass Endothelial basal medium bioactive glass
BaG EM extract	extract
BaG EM-OM	Bioactive glass extract based endothelial- osteogenic medium
BaG OM	Bioactive glass extract based osteogenic medium
bFGF	Basic fibroblast growth factor (see FGF- $\beta$ )
BMSC	Bone marrow stem cell
BMPs	Bone morphogenic proteins
BMP-2	Bone morphogenic protein-2
BMP-7	Bone morphogenic protein-7
BMP-14	Bone morphogenic protein-14 (see GDF-5)
BSA	Bovine serum albumin

BSP	Bone sialoprotein
Calcein AM	Calcein acetoxymethyl ester
CaP	Calcium phosphate
CD	Cluster of differentiation
cDNA	Complementary deoxyribonucleic acid
CD3-PE	Cluster of differentiation 3 with phycoerythrin fluorophore, T cell signal transduction
CD11a-APC	Cluster of differentiation 11a with allophycocyanin fluorophore, lymphocyte function-associated antigen 1
CD14-PE-Cy7	Cluster of differentiation 14 with phycoerythrin cyanine fluorophore, serum lipopolysaccharide binding protein
CD19-PE-Cy7	Cluster of differentiation 19 with phycoerythrin cyanine fluorophore, B lymphocyte-lineage differentiation antigen
CD31	Cluster of differentiation 31, platelet endothelial cell adhesion molecule-1 (see PECAM-1)
CD31-FITC	Cluster of differentiation 31 with fluorescein
CD34+	icothiocyanate fluorophore
CD34-APC	Hematopoietic/progenitor stem cell surface marker positive cell fraction
CD45RO-APC	Cluster of differentiation 34 with allophycocyanin fluorophore, sialomucin-like adhesion molecule, capillary endothelial cells
CD54-FITC	Cluster of differentiation 45 with allophycocyanin fluorophore, leukocyte common antigen
CD73-PE	Cluster of differentiation 54 with fluorescein
	icothiocyanate fluorophore, intercellular adhesion molecule 1
	Cluster of differentiation 73 with phycoerythrin fluorophore, ecto-5'-nucleotidase



CD80-PE	Cluster of differentiation 80 with phycoerythrin fluorophore, B lymphocyte activation and proliferation
CD86-PE	Cluster of differentiation 86 with phycoerythrin fluorophore, B lymphocyte activation and proliferation
CD90-APC	Cluster of differentiation 90 with allophycocyanin fluorophore, T cell surface glycoprotein Thy-1
CD105-PE	Cluster of differentiation 105 with phycoerythrin fluorophore, angiogenesis, TGF- $\beta$ receptor complex
CD144-PE	Cluster of differentiation 144 with phycoerythrin fluorophore, endothelial cell adhesion molecule
CD146-PE	Cluster of differentiation 146 with phycoerythrin fluorophore, endothelial cell adhesion molecule
C-MYC	V-Myc avian myelocytomatosis viral oncogene homolog
COL	Collagen type I hydrogel
COL1	Collagen type I
COL2	Collagen type II
COL3	Collagen type III
CTGF	Connective tissue growth factor
d	Day(s)
Delta-like 4 Notch signaling	Signaling pathway for vascular development
Dex	Dexamethasone
DLX5	Distal-less homeobox 5
DMEM/F-12	Dulbecco's Modified Eagle Medium/Ham's Nutrient Mixture F-12
DNA	Deoxyribonucleic acid
DPBS	Dulbecco's phosphate buffered saline
E'	Elastic modulus or Young's modulus
EBM-2	Endothelial cell growth basal medium-2
EC	Endothelial cell
ECM	Extracellular matrix
EGF	Epidermal growth factor

EGM-2	Endothelial cell growth medium-2
EM	Endothelial medium
EMA	European Medicines Agency
ESC	Embryonic stem cell
EthD-1	Ethidium homodimer-1
EU	European Union
FACS	Fluorescence activated cell sorter
FBS	Fetal bovine serum
FDA	The United States Food and Drug Administration
FEP	Fluorinated ethylene propylene
FGF- $\beta$	Fibroblast growth factor- $\beta$ (see bFGF)
G'	Storage modulus
GDF-5	Growth and differentiation factor-5 (see BMP-14)
GelMA	Methacrylated gelatin
GG	Gellan gum hydrogel
GG-COL	Gellan gum-collagen type I hydrogel
HA	Hyaluronic acid
HAp	Hydroxyapatite
hASC	Human adipose stem cell
hBMSC	Human bone marrow stem cell
HLA-ABC	Human leukocyte antigen (HLA) -A, -B, and -C
HLA-DR-PE	Human leukocyte antigen (HLA) class II, R-phycoerythrin conjugated
hMSC	Human mesenchymal stem cell
hRPLP0	Human large ribosomal protein P0
HS	Human serum
HUVEC	Human umbilical vein endothelial cell
IGF-1	Insulin-like growth factor 1
<i>in vitro</i>	Experiment performed in controlled environment, outside of living organism
<i>in vivo</i>	Experiment performed inside living organism
iPSC	Induced pluripotent stem cell
ISCT	International Society for Cellular Therapy

ISO	International Organization for Standardization
IUPAC	International Union of Pure and Applied Chemistry
KDR	Kinase insert domain receptor
KLF4	Kruppel-like factor 4
LED	Light emitting diode
MA	Methacrylate
Micro-CT	Micro-computed tomography imaging
MM	Maintenance medium
mRNA	Messenger ribonucleic acid
MSC	Mesenchymal stem cell
mTORC1	Mechanistic target of rapamycin complex 1
MTT	NAD(P)H dependent cell metabolic activity analysis
OCN	Osteocalcin
OCT3/4	Octamer binding transcription factor3/4
OM	Osteogenic medium
ON	Osteonectin
OPN	Osteopontin
OPT	Optical projection tomography
OSX	Osterix, homo sapiens Sp7 transcription factor
PBS	Phosphate buffered saline
PCL	Poly( $\epsilon$ -caprolactone)
PDGF	Platelet-derived growth factor
PDMS	Polydimethylsiloxane
PECAM-1	Platelet endothelial cell adhesion molecule-1 (see CD31)
PEGDA	Poly(ethylene glycol) diacrylate
PEGTA	4-arm poly(-ethylene glycol)-tetra-acrylate
PET	Poly(ethylene terephthalate)
PFA	Paraformaldehyde
PGA	Polyglycolide
PLA	Poly lactide
P(L/D)LA	Poly(L/D) lactide
PLCL	Poly(L-lactic-co- $\epsilon$ -caprolactone)
PLGA	Poly(L,D-lactic-co-glycolic acid)

poly(LLA-co-DXO)	Poly(L-lactide-co-1,5-dioxepan-2-one)
P/S	Penicillin/streptomycin
qRT-PCR	Quantitative real-time polymerase chain reaction
RGD	Arginine, glycine, and aspartate amino acid sequence
rpm	Revolutions per minute
RT	Room temperature
RUNX2	Runt related transcription factor 2
SCX	Scleraxis
SD	Standard deviation
SOX2	SRY-box 2
SPD	Spermidine
SPIM	Selective plane illumination microscopy
SSEA-4+	Stage specific early antigen 4 positive cell fraction
TE	Tissue engineering
TERT-hBMSC	Immortalized human TERT-bone marrow stem cell
TGF- $\beta$ 1	Transforming growth factor- $\beta$ 1
TM	Tenogenic medium
TNC	Tenascin-C
TNMD	Tenomodulin
VEGF	Vascular endothelial growth factor
VEGFR2	Vascular endothelial growth factor receptor 2, kinase insert domain receptor (see KDR)
VEGFR3-APC	Vascular endothelial growth factor receptor with allophycocyanin fluorophore
VWF	Von Willebrand factor
Wnt	Wnt cell signal transduction pathway

# ORIGINAL PUBLICATIONS

This thesis is based on the following original publications which are referred to in the text as **I-III**. The publications are reprinted with kind permission from the publishers.

- Publication **I** Vuornos K., Björninen M., Talvitie E., Paakinaho K., Kellomäki M., Huhtala H., Miettinen S., Seppänen-Kajansinkko R., Haimi S. Human adipose stem cells differentiated on braided polylactide scaffolds is a potential approach for tendon tissue engineering. *Tissue Engineering Part A* (2016) 22 (5-6), 513-523.
- Publication **II** Vuornos K., Ojansivu M., Koivisto J.T., Häkkänen H., Belay B., Montonen T., Huhtala H., Kääriäinen M., Hupa L., Kellomäki M., Hyttinen J., Ihalainen J., Miettinen S. Bioactive glass ions induce efficient osteogenic differentiation of human adipose stem cells encapsulated in gellan gum and collagen type I hydrogels. *Mater Sci Eng C Mater Biol Appl*. 2019 Jun; 99: 905-918.
- Publication **III** Vuornos K., Huhtala H., Kääriäinen M., Kuismanen K., Hupa L., Kellomäki M., Miettinen S. Bioactive glass ions for *in vitro* osteogenesis and microvascularization in gellan gum-collagen hydrogels. *J Biomed Mater Res B Appl Biomater*. 2019 Aug 31.



# 1 INTRODUCTION

Presently, the musculoskeletal illnesses continue to contribute to the growing economic burden of the health care systems in the industrialized countries in connection to the increase of the aging population and musculoskeletal complications related to obesity. The musculoskeletal illnesses cause diminished life quality of the patients and considerable economic losses in efficient working life. These complications affect millions worldwide, where 30 million musculoskeletal injuries are treated in the United States yearly (Caliari & Harley 2013). Also, the rate of surgical intervention requiring ruptures of large tendons such as the Achilles tendon has doubled nearly every decade together with a high recurrence rate (Brodie et al., 2011; Chainani et al., 2013). Novel treatment options for musculoskeletal defects are therefore called for urgently. While loss or repair of musculoskeletal tissues have been treated traditionally with tissue autografts from the patient's own tissue or with allografts from a donor as a standard procedure with good results, these are not feasible solutions in the long term. Autologous bone is limited for the treatment of critical size, over 1-cm in graft diameter, bone defects (Chatterjea et al., 2010). Further, in case of repeated injury or any adverse incident, a new bone graft is required thus creating a continued need for bone augmentation solutions (Przekora 2019). However, the shortage of suitable donors persists at present and allografts have been prone to graft rejection due to adverse immunological reactions while xenografts carry risk of zoonosis (Chatterjea et al., 2010; Jakob et al., 2012). Striving to rise up to these challenges, musculoskeletal tissue engineering (TE) has emerged as a promising approach for the development of new treatments for regenerative medicine applications (Przekora 2019).

TE seeks to harness the differentiation potential of stem cells guided with the support and protection provided by a biomaterial scaffold structure and stimulation by growth factors (Langer & Vacanti 1993). TE strategies aim to restore lost tissue function or replace damaged tissue by supporting the natural healing capacity of the body. However, the use of non-physiological concentrations of growth factors has been considered problematic and a shift

towards avoiding the use of excessive amounts of growth factors has taken place. For these reasons, novel functional three-dimensional (3D) biomaterial scaffolds in combination with soluble factors that support cell growth and stimulate stem cell differentiation are researched presently. To this end, functional biomaterials are needed with combined feasible tissue specific material properties such as offered by biomaterial composites. Properties that render the biomaterials feasible include biocompatibility and biodegradability for gradual replacement of the graft by the regenerated tissue. Also, the advantage of a biodegradable TE support structure is that no second operation is needed thus avoiding risks of complications in relation to surgical procedures. Therefore, less invasive methods are demanded, such as injectable hydrogels for bone TE applications. (Kondiah et al., 2016)

Biomedical engineering is a rapidly developing field that potentially offers solutions to the growing need of tissue grafts by combining biomedical knowledge with engineering expertise for novel health technology applications. New interdisciplinary approaches are called for to meet the demands for bone augmentation, vascularized grafts and musculoskeletal constructs to treat large tendon defects. A specifically promising approach to treat musculoskeletal defects is to use patient specific multipotent stem cells such as human adipose stem cells (hASCs) in combination with biomaterial scaffolds for tissue engineered grafts. Described by Zuk and coworkers (Zuk et al., 2001), hASCs are easily available and abundant adult stem cells suitable for the development of bone constructs (Lindroos et al., 2011) and have ability to differentiate also towards tendon, cartilage, muscle, and fat tissue lineages, including potential for endothelial differentiation in specific conditions.

Recently, 3D TE therapies with functional biodegradable biomaterials seeking to mimic the natural cell microenvironment and providing ample opportunities for cell-cell interactions to guide stem cell differentiation with added stability and support have been researched (Pina et al., 2019). Also, novel applications of common biodegradable biomaterials with granted regulatory approval in the European Union (EU) and the United States biomedical product markets such as polylactide (PLA) or common food additive polysaccharide gellan gum (GG) hydrogel have gained interest. The full potential of these biopolymers for TE applications remains to be harnessed. Indeed, their use would help reduce cost barriers in the regenerative healthcare product development and eventually facilitate clinical adoption. Attractive in the case of synthetic biopolymers are their



engineered properties with good processability, reproducibility, and controlled degradation rate that allow mass production and ease of sterilization thus further reducing expenses in biomanufacture. Synthetic biodegradable composite biomaterials with optimized structure have potential to guide stem cell growth and differentiation thus reducing need for added chemical reagents. Indeed, bioceramics, such as bioactive glasses (BaGs) (Hench & Wilson 1986; Hench 1998; Hench & Jones 2015), have been widely applied in the field of regenerative medicine and researched for their osteoinductive properties. What is more, the absence of microvascularization has been a recurrent challenge in the field of TE. Prevascularization is a necessity to ensure graft survival after implantation and for rapid host vasculature ingrowth (Correia, C. et al., 2011; Liu, Y. et al., 2015). What is more, the role of BaG stimulated neovascularization needs to be explored further (Bi et al., 2013; Li, H. et al., 2017). For vascularization, the role of coculture has been reported as relevant (Kang et al., 2013; Mihaila et al., 2017; Pill et al., 2018). In particular, coculture of osteoblastic and endothelial cells has been suggested feasible for prevascularization of bone-like grafts (Laschke & Menger 2016; Mihaila et al., 2017; Muhleder et al., 2018; Pirraco et al., 2014). The limited cell adhesion properties of synthetic polymer biomaterials have restricted their usability for efficient TE applications. In comparison, natural scaffold biomaterials, such as collagen type I (COL) hydrogel, promote good cell adhesion and are attractive biomaterials for engineered prevascular networks, whereas their main limitation has been besides the fast degradation rate *in vivo*, also relatively low mechanical properties. To the point, the mechanical properties of hydrogel scaffolds have not received adequate attention in the past.

Recently, the *in vitro* models have been deemed important for preclinical drug testing and to investigate human tissue function in disease. Further, the optimal 3D biomaterial composite structures or minimal required chemical cues for hASC osteogenic or tenogenic differentiation have not been fully elucidated by previous works in the field. Due to these unmet needs, the aim of this thesis work was to investigate novel *in vitro* musculoskeletal applications by combining hASCs with suitable biomaterial composites and soluble factors for vascularized bone and tendon TE construct development.

The current challenges in the field of musculoskeletal TE of bone and tendon tissue include the need to find suitable cells, optimal biochemical cues, and application specific supporting biomaterial scaffolds with suitable mechanical properties. Also, more cost-effective approaches for engineered tissue implant

production protocols are required due to globally increasing health care system costs.

The rationale for the research consisted of harnessing the multipotent capacity of hASCs for musculoskeletal TE applications by, firstly, optimizing hASC biochemical induction combined with tenogenesis supporting composite biomaterial scaffold; secondly, inducing efficient hASC osteogenesis for establishing an *in vitro* model for mineralized 3D hydrogel and developing a potentially injectable cell-laden mineralized matrix material; thirdly, testing an *in vitro* model for vascularized bone applications with cocultured cells within composite 3D hydrogel.

The expected impacts include, firstly, a potential engineered tendon tissue graft suitable for load-bearing applications for large tendons developed; secondly, *in vitro* model for mineralized 3D hydrogel established and potential cell-laden mineralized hydrogel bone graft material for minimally invasive applications shown; thirdly, initial *in vitro* model with cocultured cells within composite 3D hydrogel for vascularized bone applications tested. In addition, the selected composite biomaterials allow cost-effective engineered tissue construct development.

## 2 LITERATURE REVIEW

### 2.1 Stem cells

Regenerative medicine seeks to answer the unmet need for suitable tissue grafts (Khademhosseini & Langer 2016). The concept of TE was introduced by Langer and coworkers to maintain, restore or replace lost tissue function (Langer & Vacanti 1993). In the paradigm, cells are combined with biomaterials together with biochemical stimuli, for example growth factors. Stem cells are attractive for tissue engineered graft development owing to their capacity to self-renew with unlimited cell division capacity in an undifferentiated state or to differentiate into one or more cell types (Choumerianou et al., 2008; Jensen et al., 2009). Due to their capacity, stem cells have potential for numerous TE applications.

Classification of stem cells is based on their specific differentiation potential. While the zygote is totipotent with capacity to produce all the cell types of an organism, the cells of the inner cell mass of the following blastocyst developmental stage are more restricted in their capacity although still pluripotent with ability to produce all the cell types of a mature organism (Condic 2014). Embryonic stem cells (ESCs) have capacity to produce cell types of all the 3 embryonic layers, namely endodermal, mesodermal, and ectodermal layer cell types. Although ESCs are pluripotent, there are ethical considerations related to their use (Aach et al., 2017), in addition to concerns of immunological reactions towards allogenic cells (de Almeida et al., 2013). Therefore, induced pluripotent stem cells (iPSCs) from somatic cells of an adult individual are researched to an increasing extent.

#### Induced pluripotent stem cells

In their seminal work in 2006, Yamanaka and coworkers were able to produce iPSCs from adult skin tissue fibroblasts (Takahashi & Yamanaka 2006). Consequently, Gurdon and Yamanaka were awarded The Nobel Prize in Physiology or Medicine (Norwegian Nobel Committee., 2012). In the induction method, overexpression of pluripotency factors *octamer-binding transcription factor3/4* (*OCT3/4*), *SRY-box 2* (*SOX2*), *Kruppel-like factor 4* (*KLF4*), and *V-Myc*

*avian myelocytomatosis viral oncogene homolog (C-MYC)* is performed using viral vectors to render the somatic cells, for example, human foreskin fibroblasts (Jungbluth et al., 2019) or blood cells (Loh et al., 2009) to an earlier developmental stage of pluripotency. At present, several clinical trials with iPSCs are anticipated for evaluation including treatment for spinal cord injury (Okubo et al., 2018). Even though immensely appealing for TE applications, there are risks related to the genetic instability of iPSCs. As a consequence of the varied somatic cell induction results, cell line selection is made of several iPS cell lines for more balanced results (Grskovic et al., 2011; Nagoshi et al., 2019). Further, the survival of implanted iPSCs in an immature stage of differentiation in a more mature tissue environment might create other issues. What is more, if the target site also contains diseased tissue, the implanted immature stem cells are less likely to survive or preserve their functionality.

### Adult stem cells

Adult tissues possess stem cells that have more restricted proliferation and differentiation capacity (Lindroos et al., 2011). Adult progenitor stromal stem cells are found in most tissues of a mature body and they are multipotent as to their differentiation capacity (Bourin et al., 2013). To the point, the use of adult stem cells allows to avoid ethical, legal, and political concerns related to the use of ESCs (Lindroos et al., 2011). Compared to the iPSCs, there is also the advantage of greater degree of genetic stability (Turinetto et al., 2017; Yoshihara et al., 2017).

### Mesenchymal stem cells

Mesenchymal stem cells (MSCs) are adult stem cells, originating from the mesodermal embryonic layer, that have potential to differentiate towards multiple tissue lineages. MSCs were originally reported as osteogenic fibroblast-like cells of the bone marrow in 1968 (Friedenstein et al., 1968), however, their naming and more specific characterization took place some 2 decades later (Caplan 1991). MSCs have been defined by the International Society for Cellular Therapy (ISCT) as plastic-adherent cells that express cluster of differentiation markers (CDs) CD105, CD73, and CD90, whereas they lack the expression of CD11b, CD14, CD34, CD45, CD19, CD79a, and HLA-DR. In addition, according to the ISCT definition, they have capacity to differentiate *in vitro* into cells of bone, adipose, and cartilage tissues, according to the minimal criteria (Dominici et al., 2006). MSCs are an inherently heterogenous stem cell population with more restricted

self-renewal and limited nonmesodermal differentiation capacity (Russell et al., 2010). For these reasons, the potential differences in MSC subpopulations should be given appropriate consideration already at the design phase of *in vitro* testing (Kramer et al., 2012). For example, hASCs, human bone marrow stem cells (hBMSCs), dental pulp stem cells, are different types of multipotent MSCs (Khanna-Jain et al., 2012; Lindroos et al., 2011). Nevertheless, MSCs are actively researched with 665 studies recruiting, active or completed found from the United States National Library of Medicine database [clinicaltrials.gov](http://clinicaltrials.gov) with search for “mesenchymal stem cells” for a range of TE applications encompassing cardiovascular diseases, immunological graft-versus-host disease, diabetes, neurological Alzheimer’s disease and ischemic stroke (Kobolak et al., 2016).

## 2.2 Human adipose stem cells

The hASCs have been researched for a variety of regenerative medicine applications within the field of TE following the reported discovery by Zuk and coworkers in 2001 of stromal progenitor cells within adipose tissue of an adult (Zuk et al., 2001). Adipose tissue originates from embryonic mesodermal layer (Martin et al., 1998) and hence also hASCs are of mesodermal origin although some adipogenic progenitors originate from ectodermal neural crest (Sowa et al., 2013).

In literature, challenges with nomenclature have been discussed (Mazini et al., 2019). The nomenclature has included different combinations of terms “adipose-derived stromal/stem cells” (Bora & Majumdar 2017; Casteilla et al., 2011) and the International Federation for Adipose Therapeutics and Science (IFATS) has recommended the term adipose-derived stem cells (Bourin et al., 2013). In studies **I-III**, the term hASC is used throughout. Although the discussion continues on the specific properties of hASCs (Baer 2014; Bora & Majumdar 2017), they have been established as abundant, easily accessible and multipotent adult stem cells (Lindroos et al., 2011; Patrikoski et al., 2019).

The multipotent hASCs are more easily harvested with lower risk of adverse complications or pain to the patient than in the harvesting of bone marrow (Lindroos et al., 2011). In addition, hASCs are obtained in higher amounts per tissue sample compared to hBMSCs (Aust et al., 2004). Although the exact localization of undifferentiated hASCs within adipose tissue remains undetermined partly due to lack of specific markers (Baer 2011), it has been

suggested that hASCs colocalize in perivascular location with endothelial cells (ECs) and pericytes (Traktuev et al., 2008; Zimmerlin et al., 2013). What is more, hASCs possess excellent proliferation ability and are efficiently expanded in cell culture flasks (Zuk et al., 2001; Zuk et al., 2002). This is important since a large number of cells are needed for initial *in vitro* experiments and eventual tissue engineered construct development (Baer 2011; Patrikoski et al., 2019). With patient specific hASCs, graft rejection and adverse immunological reactions can be avoided (Argentati et al., 2018). Although hASC osteogenic differentiation capacity has been reported more moderate compared to that of hBMSCs (Mohamed-Ahmed et al., 2018), they have higher proliferation capacity and are morphologically and genetically more stable in long-term culture (Izadpanah et al., 2006; Strioga et al., 2012). Importantly, hASCs have ability to differentiate towards besides adipose tissue, also bone, cartilage, tendon, and muscle tissue lineages (Dai et al., 2016; Lindroos et al., 2011). In addition, the use of patient specific autologous cells helps to avoid any adverse immunoreactions. What is more, their reported anti-inflammatory, immunoregulatory properties and advantageous paracrine effects, (Lee, Jung Min et al., 2012; Lindroos et al., 2011; McIntosh et al., 2006) render hASCs the attractive for a variety of indications (Dai et al., 2016). Also, use of allogenic hASCs is proposed due to variance in clinical results using autologous hASCs (Patrikoski et al., 2019). In addition, use of allogenic hASCs would permit careful characterization of cells prior to treatment with more assured differentiation capacity, larger amounts of cells immediately available, and also lower production costs (Gimble & Guilak 2003; Patrikoski et al., 2019). Nevertheless, there are persistent risks related to tumorigenicity since the paracrine effects potentially also stimulate tumor microenvironment. The risk of metastasis promotion has been linked to hMSCs and hASCs (Albarenque et al., 2011; Kamat et al., 2015; Meng et al., 2015). Therefore, knowledge of target tissue microenvironment is of major importance for the safety of stem cell therapies.

## 2.2.1 Characterization of human adipose stem cells

The hASCs are characteristically spindle-like vessel-shaped stromal stem cells (Lindroos et al., 2011). According to ISCT issued minimal criteria, hASCs are plastic adherent cells with multipotent capacity to differentiate towards adipogenic, osteogenic, and chondrogenic lineages *in vitro*, in addition to

possessing a specific surface marker expression pattern (Bourin et al., 2013; Dominici et al., 2006).

#### Surface marker expression

The immunophenotype of undifferentiated hASCs determined by flow cytometric analysis includes expression of adhesion molecules CD26, CD49d, CD54, and CD105; surface enzymes CD10, CD13, and CD73; glycoproteins CD90 and CD146. Also, hASCs produce proteins CD55, CD59, collagen type I (COL1), collagen type III (COL3), osteopontin (OPN), osteonectin (ON), intracellular  $\alpha$ -smooth muscle actin, vimentin, and histocompatibility protein HLA-ABC (Bourin et al., 2013; Dominici et al., 2006; Gimble & Guilak 2003). On the other hand, surface markers not present on hASC surface include CD3, CD11b, CD45 or CD62, hematopoietic marker CD14 or histocompatibility protein HLA-DR (Bourin et al., 2013; Dominici et al., 2006; Gimble & Guilak 2003).

### 2.2.2 Human adipose stem cell heterogeneity

Contradicting the ISCT criteria, some variation has been observed, for example, in the expression of cell adhesion and hematopoietic markers CD11, CD14, CD34, and CD45 with lower passages of hASCs (McIntosh et al., 2006; Tapp et al., 2009). What is more, the harvesting location of adipose tissue as well as donor age and sex have been identified as factors that contribute to hASC heterogeneity (Aksu et al., 2008; Baglioni et al., 2012; Oedayrajsingh-Varma et al., 2006). Further, culture conditions during cell expansion and experiment phase affect cell population heterogeneity and might contribute to selection of subpopulations that are enriched during *in vitro* culture (Patrikoski et al., 2013). To resolve this, cell heterogeneity requires careful characterization to ensure eventual clinical reproducibility and safety (Meng et al., 2015). In the past, fetal bovine serum (FBS) has been widely applied in *in vitro* cell culture, however, the currently preferred use of autologous or allogenic human serum (HS) (Josh et al., 2012; Koellensperger et al., 2014) allows to avoid xenozyoonosis complications and better satisfies regulatory safety concerns. Still, different subpopulations together with donor dependent variation continue to contribute to inconsistencies in *in vitro*, *in vivo* and clinical testing results (Baer 2014; Lv et al., 2014; Meng et al., 2015; Selich et al., 2016; Yi et al., 2015). Although hASCs are intrinsically a heterogeneous population of cells, careful *in vitro* characterization

would allow their safe application for therapeutic applications. For these reasons, new effective methods for cell culture characterization and functional *in vitro* models are urgently called for.

## 2.3 Human adipose stem cell differentiation

In the following chapters, hASC differentiation potential is presented for tendon, bone, and vascularization applications. Bioactive substances, such as growth factors, cytokines, and inductive soluble factors, can be applied to stimulate stem cell differentiation towards a specific lineage. Growth factors are cell stimulating natural molecules such as proteins promoting cell growth, proliferation, differentiation, and survival. They also regulate cell and tissue metabolism homeostasis and healing. In comparison, cytokines are small protein molecules that influence cell-cell interactions or communications. (Zhang & An 2007)

### 2.3.1 Tenogenic differentiation

#### Tendon tissue

Tendon attaches muscle to bone and transmits the force of muscle contraction to bone movement. Tendon also functions as a mechanical spring enhancing the movements. (Kannus 2000) For these reasons, great tensile strength and elasticity are key properties of tendon. The principal large tendons of human body that typically require surgical intervention upon serious injury are the Achilles tendon of leg, patellar tendon of the knee, and shoulder rotator cuff tendon (Butler et al., 2004).

In the tissue structure, collagen fibers form bundles and tenocytes are located in between them. Tendon matrix is avascular and consists of COL1 up to 80 % of tendon dry mass. In addition, tendon matrix consists of several different types of collagen, elastin fibers, proteoglycans, glycosaminoglycans, and glycoproteins (Gross & Hoffmann 2013). COL1 polypeptide alpha chains form a soluble tropocollagen molecule with triple-helix structure (Kannus 2000). After crosslinking in the extracellular matrix (ECM), insoluble collagen molecules aggregate into collagen fibrils, and consequently these fine fibrils form collagenous fibers (Kannus 2000) (Figure 1). Indeed, high elastic properties of tendons are based on parallel, continuous, and uniaxially oriented collagen fibers



gliding against each other (James et al., 2008). Collagenous fibers are packed into primary, secondary, and tertiary fiber bundles surrounded by sheaths of connective tissue; endotenon, epitenon, and paratenon. The connective tissue sheaths contain COL3 which has a role in organizing the collagenous fiber bundle (Franchi et al., 2007; James et al., 2008). The endotenon sheath is innervated whereas the loose sheath of paratenon connective tissue is vascularized and allows flexible movement of tendon (Franchi et al., 2007).

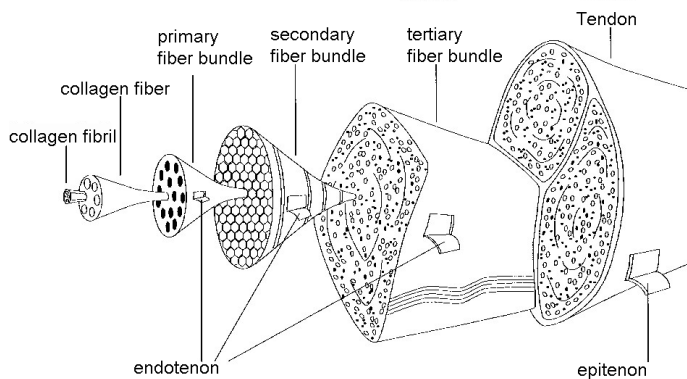


Figure 1. Schematic tendon structure consisting of collagen fibrils, collagen fibers, the primary, secondary and tertiary collagen fiber bundles wrapped in endotenon sheaths forming the tendon unit enveloped by the epitenon. Modified from (Kannus 2000).

High tensile strength of tendon is due to some collagenous fibers forming intertwined braid-like structures (Kannus 2000). The characteristic crimping and wavy collagenous fiber pattern of tendon tissue is created by proteoglycan crosslinking and the elastin fibers help recover the structure after tendon stretching and elongation in movement (Kannus 2000). Further, tendon mechanical properties are aided by matrix elasticity. Indeed, under shear stress, elasticity of matrix proteoglycans aggrecan, decorin, and biglycan in addition to viscous glycosaminoglycans hyaluronic acid and chondroitin sulphate bestow tendon its biomechanical capabilities (Franchi et al., 2007; Kannus 2000). What is more, essential molecular components in tendon tissue structure and function are also glycoprotein tenascin-C (TNC), early tendon marker transcription factor *scleraxis* (*SCX*), and late tendon marker transmembrane protein tenomodulin (TNMD), as listed in Table 1 (Giblin & Midwood 2015; James et al., 2008; Kuo, C. K. et al., 2010; Midwood et al., 2016; Pauly et al., 2010).

Table 1. Tendon markers (Giblin & Midwood 2015; James et al., 2008; Kuo, C. K. et al., 2010; Midwood et al., 2016; Pauly et al., 2010).

Early	Late
SCX	COL1
COL3	TNMD
	TNC
	Aggrecan
	Biglycan
	Decorin
	Chondroitin sulphate
	Elastin

Abbreviations: COL1, collagen type I; COL3, collagen type III; SCX, *scleraxis*; TNC, tenascin-C; TNMD, tenomodulin.

It is important to point out that although the aforementioned molecular markers are not tendon tissue specific, nevertheless, a panel of relevant tenogenic markers is deemed sufficient to verify tenogenic phenotype. Primary tenocytes are not feasible for TE purposes due to their low yield upon isolation, loss of phenotype and risk of dedifferentiation in *in vitro* culture outside native tissue microenvironment, and significant loss of viability that decreases with increase of cell passage number. Importantly, there is no tenocyte supportive optimal culture media or growth matrix currently available commercially (Costa-Almeida et al., 2019).

### Tenogenic medium

For biochemical stimulation of MSC and ASC tenogenic differentiation process, the proposed media have sought to mimic the healing process of tendon. In the healing process for tendon ECM synthesis, production of COL1 is increased, the collagenous fibers are organized and packed densely by crosslinking where COL3 is involved (Molloy et al., 2003). A high COL1/COL3 ratio has been deemed to indicate active matrix deposition (Costa-Almeida et al., 2018), whereas a high COL3/COL1 ratio has been reported to mark tendon matrix disruption and a repair response (Shearn et al., 2011).

Different growth factors orchestrate tendon healing process by triggering cell signaling, influencing cell metabolism and inducing ECM production (Park, A. et al., 2010). Growth factors active early on during tendon healing include connective tissue growth factor (CTGF), vascular endothelial growth factor (VEGF) and insulin-like growth factor 1 (IGF-1) (Chen, C. H. et al., 2008). The

gene expression and production of transforming growth factor- $\beta$ 1 (TGF- $\beta$ 1), IGF-1, and platelet derived growth factor (PDGF) peak both early on and again in later phases of matrix remodeling (Chen, C. H. et al., 2008; Dahlgren et al., 2005). PDGF stimulates IGF-1 early on and is active in late remodeling when IGF-1 and PDGF contribute to collagen synthesis and ECM production together with basic fibroblast growth factor (bFGF) (Molloy et al., 2003; Raghavan et al., 2012). VEGF and bFGF increase MSC proliferation and support cell-matrix interactions (Molloy et al., 2003; Raghavan et al., 2012), and also epidermal growth factor (EGF) stimulates cell proliferation and migration during the healing process (Baer et al., 2009).

### Tenogenesis

For MSC tenogenesis, the applied biochemical cues have included growth and differentiation factor-5 (GDF-5) (James et al., 2011; Jenner et al., 2007; Park, A. et al., 2010; Raabe et al., 2013; Tan et al., 2012) and the transforming growth factor- $\beta$ 1 (TGF- $\beta$ 1) (Jenner et al., 2007). GDFs are bone morphogenic proteins (BMPs), and GDF-5 is also known as BMP-14. GDF-5 helps maintain tenocyte phenotype (Caliari & Harley 2013) by upregulating *SCX* and *TNC* gene expression as well as *COL1* and *COL3* production (Bolt et al., 2007)

In a 3D filamentous scaffold study by Jenner and coworkers, the combination of ascorbic acid and TGF- $\beta$ 1 stimulated significantly hBMSC proliferation and total collagen production (Jenner et al., 2007). In comparison, James and coworker study using GDF-5 stimulation in 3D fibrous scaffolds upregulated rat ASC gene expression of *SCX* and *COL1* (James et al., 2011). With animal-derived tendon matrix components, hASCs have shown increased gene expression of *COL1*, *COL3*, and *TNC* together with total collagen production at 2 weeks in study by Chainani and coworkers (Chainani et al., 2013), whereas uniaxial tension of 3D matrix promoted hASC proliferation and significant *SCX*, *TNC*, and *TNMD* gene expression already within 1 week, as reported by Yang and coworkers (Yang, G. et al., 2013). Further, dynamic stretching of hASCs within a 3D matrix has reportedly induced gene expression of *SCX*, *TNC*, and *COL1* (Vindigni et al., 2013). Also other small molecules, such as ascorbic acid, have promoted tendon ECM and specifically collagenous matrix deposition as well increased cell proliferation. The reported ASC cell seeding densities for tenogenic differentiation have varied between 5 000-21 000 cells/cm<sup>2</sup> (Little et al., 2010; Park, I. S. et al., 2009; Raghavan et al., 2012). These studies exemplify the

importance of 3D culture together with provided biochemical cues and combined with mechanical stimulation for *in vitro* tenogenesis.

### 2.3.2 Osteogenic differentiation

#### Bone tissue

In the musculoskeletal system, bones, muscles, tendons, and ligaments help maintain body position and allow controlled, precise movements. In compact bone tissue structure (Figure 2) on microscopic level, the bone osteons, also known as Haversian systems, form cylindrical units parallel the bone longitudinal axis. The cylindrical units of approximately 100-200  $\mu\text{m}$  of diameter consist of concentric lamellae of bone matrix. The central osteon canal contains blood vessels for cell nutrition and homeostasis. Volkmann's canals connect the osteons and the bone surface. The bone cells, osteocytes, are located within the lamellae in the lacunae pores of approximately 10  $\mu\text{m}$  of length. The lacunae are interconnected by small canals.

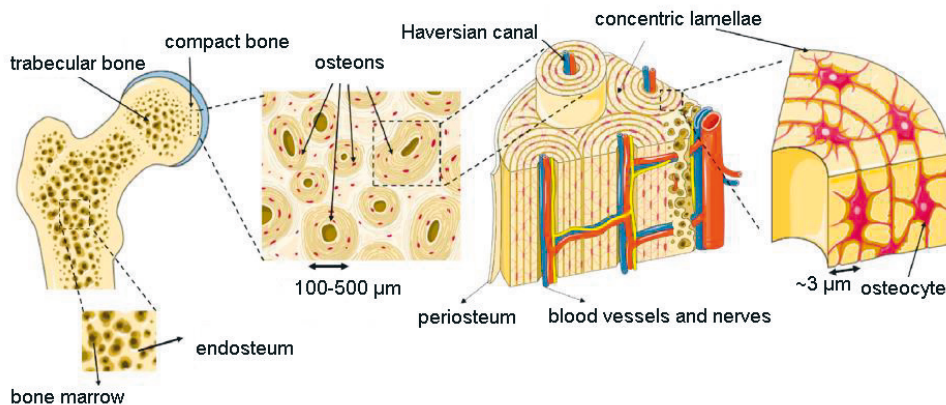


Figure 2. Bone tissue structure. Trabecular bone with bone marrow in endosteum membrane lined cavities and compact bone with osteons and mineralized bone matrix embedded osteocytes. Modified from (Lopes et al., 2018).

Bone tissue matrix consists of an inorganic hydroxyapatite  $\text{Ca}_{10}(\text{PO}_4)_6\text{OH}_2$  mineral component and of an organic collagenous component, mostly COL1. The mineral component forms 75 % of the weight fraction and 40 % of volume of bone tissue. Bone tissue types include compact and trabecular bone which differ in their structure; compact bone forms a continuous solid structure whereas trabecular bone consists of a 3D spongy-like network. Typically, in long bones,

thick compact bone accounts for the long load-bearing shaft of the bone. On the other hand, the ends of the bone consist mainly of brittle trabecular bone while a thin layer of compact bone on the surface gives the bone architecture its mechanical strength. (Doherty, 2009)

### Bone markers

Osteogenic differentiation of MSCs triggered by biochemical cues progresses through a commitment stage, followed by maturation and mineralization of the surrounding matrix (Table 2) (Lian et al., 2012; Wubneh et al., 2018).

Table 2. Osteogenic markers in MSC osteogenesis process (Lian et al., 2012).

<b>Commitment</b>	<b>Maturation</b>	<b>Mineralization</b>
<i>RUNX2</i>	OSX	OCN
<i>DLX5</i>	COL1	<i>DLX5</i>
ALP	ALP	BSP
OPN		

Abbreviations: ALP, alkaline phosphatase; BSP, bone sialoprotein; COL1, collagen type I; *DLX5*, *distal-less homeobox 5*; MSC, mesenchymal stem cell; OCN, osteocalcin; OPN, osteopontin; OSX, *osterix*; *RUNX2*, *runt domain-containing transcription factor*.

Bone marker gene expression activated early in the osteogenic commitment include *RUNX2*, a *runt domain-containing transcription factor*, functioning upstream from *zinc finger protein osterix* (*OSX*). (Desai et al., 2014; Lian et al., 2012; Long 2011; Orimo 2010) Other early osteogenic markers include a transcription factor *distal-less homeobox 5* (*DLX5*) and phosphatase transporting alkaline phosphatase (ALP) protein. In matrix maturation and mineralization, late markers of encompass bone ECM proteins such as COL1, ALP protein, OPN, ON, bone sialoprotein (BSP) and osteocalcin (OCN). (Lian & Stein 1995) Collagenous matrix deposition is typical of hASC osteogenic differentiation, while calcium phosphatase enzyme accumulation is indicated by the activity of the cell membrane protein phosphatase transporting ALP protein which precedes mineralization of matrix. Ca binding matrix protein OPN assists mineralization by forming mineralized hydroxyapatite (Orimo 2010). Bone ECM is mineralized via Ca binding onto fibrillous collagen network. In bone tissue matrix, complexes of CaP form hydroxyapatite.

## Osteogenic medium

Soluble factors for biochemical induction of hASC commitment towards osteogenic lineage have typically included varied concentrations of ascorbate-2-phosphate (AsA2P),  $\beta$ -glycerophosphate ( $\beta$ -GP) and dexamethasone (Dex) (Kyllonen et al., 2013; Zuk et al., 2001; Zuk et al., 2002). In a previous study by Tirkkonen and coworkers, osteogenic medium (OM) was optimized for hASC osteogenic differentiation with 250  $\mu$ M AsA2P, 10 mM  $\beta$ -GP and 5 nM Dex (Tirkkonen et al., 2013). In the process of osteogenesis, AsA2P activates collagen synthesis, increases MSC proliferation and along with  $\beta$ -GP functions as a CaP source for mineral deposits (Coelho, et al. 2000; Choi, et al. 2008). As a synthetic glucocorticoid hormone, Dex upregulates osteogenic *RUNX2* gene expression (Viereck, et al. 2002), although at higher over 100 nM concentrations it suppresses osteogenesis and instead endorses adipogenesis (Zhou, et al. 2006; Liu, et al. 2009). MSC osteogenesis inducing growth factors typically include BMPs which belong to TGF- $\beta$  superfamily. Specifically, bone morphogenic protein-2 (BMP-2) and bone morphogenic protein-7 (BMP-7) have been applied for MSC osteogenic differentiation (Kang, et al. 2004). VEGF is a growth factor with a role in besides vascularization, also in bone healing (Zelzer & Olsen 2004). Upon VEGF stimulus, ECs secrete BMPs that in turn help commit osteoblastic cells towards bone lineage (Deckers, et al. 2002; Brandi, et al. 2006; Dai, et al. 2007). However, the benefit of growth factors is questioned due to lack consensus on physiological, therapeutic, or effective concentrations, especially those required for *in vitro* culture. What is more, the related elevated costs and added risks of chemical factors that are produced exogenously might have unwanted effects on clinical translation (Garrison et al., 2007; Garrison et al., 2010; Zuk et al., 2011).

Besides growth factors, also other soluble factors have potential to efficiently induce osteogenic differentiation of hASCs. A point in fact, BaG is known as a strong osteoinducer (Hench 2006). Recently, research has endeavored to harvest the osteogenic potential of the soluble cues in the form of bioactive glass extract based osteogenic medium (BaG OM) (Ojansivu et al., 2015). Further, in a recent study, Nunez-Toldra and coworkers applied an osteogenic (OM) and endothelial media (EM) mixture based on BaG extract with osteogenic and endothelial media supplements to induce human dental pulp pluripotent-like stem cells to produce mineralized matrix and microvascularization (Nunez-Toldra et al., 2019).

## Osteogenesis

Osteogenesis of MSCs is a sequence of events where differentiation progresses via a pre-osteoblast stage and a compliant osteoid matrix secreted by osteoblasts (Figure 3). In the following, maturing osteoblasts and the evolving mechanical properties direct the developing tissue surroundings towards a more rigid matrix when calcified mineral is deposited.

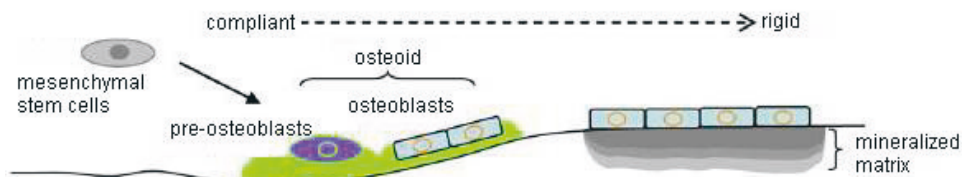


Figure 3. Matrix stiffness influences MSC osteogenesis. Modified from (Engler et al., 2006; Raisz 1999).

Collagenous bone ECM becomes mineralized following accumulation of CaP residues forming mineralized deposits. These cauliflower-like hydroxyapatite crystals are the main structural component of mineralized bone tissue. (Doherty, 2009; Hall, 2005; Long 2011)

The bone maturation can progress either by intramembraneous ossification process with initial MSC condensation followed by differentiation into osteocytes embedded within bone tissue matrix, or by endochondral ossification where MSCs first differentiate into chondrogenic cells prior to osteoblastic maturation and bone ECM production (Lian et al., 2012). Molecular switches and cell signaling pathways including wnt/  $\beta$ -catenin pathway operate in the osteogenic differentiation and maturation process with various cell signaling molecules, cell receptors, transcription factors, growth factors, and cytokines involved (Schaffler & Buchler 2007; Shahabipour et al., 2019). Other suggested strategies to induce osteogenic differentiation even in the absence of added growth factors is, for example, biomechanical stress such as fluid flow caused shear stress (Fritton & Weinbaum 2009; Kim et al., 2014; Wittkowske et al., 2016). For vascularized bone, the mechanistic target of rapamycin complex 1 (mTORC1) protein kinase complex triggers VEGF production of osteoblasts which in turn promotes formation of vascularization. VEGF modulates EC activity by its cell membrane vascular endothelial growth factor receptor 2 (VEGFR2), also called kinase insert domain receptor (KDR). (Shahabipour et al., 2019)

### 2.3.3 Endothelial differentiation and role of subpopulations

#### Vascular structures

Blood vessel structures that ECs take part in encompass capillaries of 5-10  $\mu\text{m}$  of diameter, arterioles of 10-200  $\mu\text{m}$  of diameter, blood vessels or arteries of approximately 400  $\mu\text{m}$  of diameter, veins, and lymphatic vessel structures (Datta et al., 2017). In capillaries, monolayer of ECs is supported by a basement membrane of essentially collagen type IV (Doherty, 2009) with neighbouring pericytes that stabilize the structure (Datta et al., 2017). Autologous and abundant cell sources for ECs are under investigation to develop tissue engineered grafts with vascular structures. Even though widely applied in *in vitro* studies, human umbilical vein endothelial cells (HUVECs) are not clinically available (Datta et al., 2017). What is more, HUVECs originate from a large vein and might not be highly compatible for microvascularization development. Consequently, microvascular endothelial cells as well as endothelial precursor cells circulating in the blood are researched as an alternative source together with multipotent MSCs and also iPSCs with their attractive pluripotency capacity. (Abaci et al., 2016; Amano et al., 2016; Chan et al., 2018; Datta et al., 2017; Tiruvannamalai Annamalai et al., 2016)

#### Endothelial precursor subpopulation

The hASCs have been suggested to possess potential for formation of vascular structures. In a study by Heydarkhan-Hagvall and coworkers, hASCs cultured with EGM-2 formed a branched network of tubular structures (Heydarkhan-Hagvall et al., 2008). Recent studies have discussed the role of the CD34+ subpopulation (Benias et al., 2018a; Benias et al., 2018b). Even though transmembrane phosphoglycoprotein CD34 is considered a hematopoietic stem cell surface marker, it has been suggested also as a marker of active, self-renewing stem cells, or progenitor cells, including vascular endothelial progenitors (Goodell 1999; Sidney et al., 2014; Zimmerlin et al., 2013). What is more, CD34+ subpopulation cells of stromal vascular fraction have been reported to have higher proliferation capacity and greater colony forming ability in addition to reduced osteogenesis or adipogenesis capabilities (Suga et al., 2009) which might be associated with EC phenotypic behavior (Varma et al., 2007; Yoshimura et al., 2006; Zimmerlin et al., 2013). Miranville and coworkers showed hASC CD34+ subpopulation differentiated into endothelial progenitor cells with VEGF and IGF-1 containing media which increased CD31 and Von Willebrand factor



(VWF) production (Miranville et al., 2004). In comparison, Mihaila and coworkers presented stage specific early antigen 4 (SSEA-4+) hASC subpopulation with endothelial and osteogenic differentiation potential (Mihaila et al., 2013; Mihaila et al., 2017). Indeed, hASCs would be a readily available, characterized cell source for vascularized structures although the proportion of hASC CD34+ subpopulation cells is presumed limited.

### Vasculogenesis and angiogenesis

Vasculogenesis and angiogenesis promoting soluble factors commonly encompass VEGF, bFGF, heparin, and ascorbic acid (Chae et al., 2017; Datta et al., 2017), whereas IGF-1 promotes EC migration and sprouting behavior which refers to early indication of tube formation (Goel et al., 2011; Keifer et al., 2014). VEGF triggers multiple vascular processes including EC signalling, proliferation, migration, and functionality (Ferrara 2001; Ruhrberg 2003) as well as EC sprouting behavior and vascular lumen formation (Gerhardt 2008; Iruela-Arispe & Davis 2009). The VEGF cellular actions are regulated by delta-like 4-Notch signaling active in effective vascular branching (Gerhardt 2008; Hellstrom et al., 2007). Likewise, bFGF induces angiogenesis and stimulates capillary growth (Cross & Claesson-Welsh 2001), whereas PDGF is active in recruitment of supporting pericytes and stabilization of vascular structures (Abramsson et al., 2003; Xue et al., 2011). Angiopoietins have a dual role in vascular structures in supporting stability of cell-cell interactions while they are activated again in vascular remodeling (Folkman 2007; Sakurai & Kudo 2011). Factors that promote angiogenesis and vasculogenesis processes are presented in Table 3.

Table 3. Angiogenesis process and proangiogenic factors (Kant & Coulombe 2018; Rouwkema & Khademhosseini 2016; Sakurai & Kudo 2011).

<b>EC sprouting</b>	<b>Tube formation</b>	<b>Cell recruitment</b>	<b>Stabilization</b>
VEGF	VEGF	VEGF	PDGF
bFGF	bFGF	bFGF	Ang1
Ang2	Ang2	PDGF	
TGF-β	TGF-β	TGF-β	
IGF-1			

Abbreviations: Ang1, Angiopoietin1; Ang2, Angiopoietin2; bFGF, basic fibroblast growth factor; EC, endothelial cell; IGF-1, insulin-like growth factor 1; PDGF, platelet derived growth factor; TGF-β, transforming growth factor-β; VEGF, vascular endothelial growth factor.

In addition, hydrocortisone has a supportive effect on the angiogenic process (Goding 2009). Mature collagen type IV is deposited onto the basement membrane in the blood vessel maturation process and ascorbic acid is essential for correct folding of the collagenous protein (Myllyla et al. 1978) and thus vasculature formation.

### Endothelial medium

Commercial endothelial media like Lonza's EGM-2 contains different growth factors and supplements including EGF, FGF- $\beta$ , IGF-1, VEGF, low concentration of AsA2P, hydrocortisone, and heparin that help maintain EC morphology and function. However, the exact concentrations are not disclosed.

## 2.4 Three-dimensional cell culture

### 2.4.1 Tissue engineering scaffolds

#### Biomaterials

Materials are grouped typically into polymers, ceramics, metals, and natural materials (Narayan, 2009). In addition, composite materials consist of 2 or more components. A biomaterial is in general terms any material used in a biomedical application to provide structure and/or function to an implantable construct (Burdick & Mauck, 2011; Vert et al., 2012).

#### Biomaterial scaffolds

The advantage of 3D scaffolds over the conventional two-dimensional (2D) cell cultures on hard polystyrene plastic surface include a microenvironment more similar to native tissue and topographical cues offered by the 3D structure. Cell-cell interactions are pivotal for stem cell differentiation and cell growth and development into tissue.

For regenerative medicine implants, biocompatible, biodegradable, and possibly bioactive materials are processed into supporting scaffold structures that will eventually be replaced by the growth of neotissue at the implantation site. Ideally, a biomaterial scaffold provides the seeded cells a supporting structure onto which the cells can adhere. (Webber et al., 2015) The main TE biomaterial

categories generally include synthetic, organic, inorganic and composite biomaterials (Narayan, 2009).

In general terms, there are 3 different approaches to tissue engineered implantable constructs; firstly, the use of a biomaterial structure, a scaffold, alone and subsequent cell ingrowth from surrounding tissue; secondly, combining the biomaterial scaffold with *in vitro* seeded differentiated stem cells, for example; or thirdly, implanting cell-seeded construct to a different tissue location before transplantation of a matured construct to the target site (Thesleff et al., 2011).

### Biocompatibility

For TE applications, the biomaterial needs to be biocompatible, support cell adhesion, cell growth, proliferation, and differentiation (Khademhosseini & Langer 2016; Kohane & Langer 2010). The biomaterial structure is meant to mimic natural ECM that supports and promotes cell growth towards functional tissue. To this end, biocompatibility is an essential factor. Biocompatibility can be defined as “the ability of a material to perform with appropriate host response in a specific application” (EN ISO 10993-5. 2009).

Also, biocompatibility implies avoidance of adverse effects (Vert et al., 2012). Therefore, biocompatibility is a process where multiple interactions and factors between the biomaterial and host tissue come into play in a specific application. Importantly, it is not an intrinsic biomaterial property (Williams 2014) but refers to the intended function in a specified situation (Williams, 1990). Therefore, *in vitro* tests of application specific cells and biomaterials are generally performed to evaluate cytotoxicity according to Biological Evaluation of Medical Devices standard (EN ISO 10993-5. 2009).

Organic polymers, such as polysaccharide GG or COL hydrogels, are naturally derived biomaterials which are biocompatible and highly malleable but possess weak mechanical properties and are marked by fast degradation rate *in vivo* (Coutinho et al., 2010). According to American Society for Testing and Materials (ASTM) standard, hydrogels can be characterized based on their biological properties such as biocompatibility, kinetics including matrix degradation, physical and chemical stability comprising mechanical properties, and cell encapsulation. In addition, cell migration, transport of nutrients and waste as well as release of bioactive agents are considered (ASTM International. 2011).

In comparison, inorganic biomaterials such as solid BaGs are mechanically stronger and have been applied to bone TE constructs because BaG stimulates bone mineral phase-like apatite layer formation in contact with physiological fluids (Drnovsek et al., 2012; Xynos et al., 2000). Protein-surface interactions are preceded by water molecules bonding with the biomaterial surface. Here, biomaterial's hydrophobic or hydrophilic properties are important. In the next phase, a layer of proteins from physiological fluids is adsorbed onto the surface. In the following, cells that recognize suitable protein binding sites adhere to the implant surface and determine implant integration into tissue. (McKenzie & Webster, 2009) Failing to do so, this might result in formation of a fibrous capsule and eventual implant failure.

A large surface to volume ratio and a large effective surface area promote cell adhesion onto a biomaterial scaffold. Moreover, the 3D scaffold structure as well as its surface topography, porosity, interior architecture with interconnected porous structure, surface roughness, surface charge, and degradation rate all play a role in the eventual clinical performance and effectiveness of the tissue engineered construct. The biomaterial scaffold needs to allow maintenance of tissue homeostasis that encompasses diffusion of soluble factors, nutrients such as glucose and waste products as well as gas exchange including oxygen. Ideally, the scaffold architecture and biomaterial properties stimulate cell growth and differentiation offering structure and mechanical support long enough time for the implanted cells to grow and differentiate to be gradually replaced by the growing tissue.

As TE scaffolds, natural hydrogels, also as composites thereof, offer malleable support for cell growth and differentiation although their degradation rate is challenging to control (Kondiah et al., 2016; Osmalek et al., 2014; Xu et al., 2018). Due to their high malleability, specific hydrogels also allow minimally invasive TE applications of injectable hydrogel bone fillers (Kuo, K. C. et al., 2015).

### Scaffold mechanical properties

In general terms, mechanical properties refer to the elastic and inelastic properties of the material upon the application of forces and relaxation. The applied forces create stress and strain which describe the material mechanical characteristics. The mechanical properties of a 3D scaffold such as stiffness and elasticity determine scaffold properties for stem cell growth and differentiation for their part. (Evans & Gentleman 2014; Gentleman et al., 2003; Gentleman et al., 2006)

### 3D microenvironment

3D TE scaffolds offer besides mechanical protection and support to the implanted cells, also bioactive stimuli for stem cell differentiation process. Thus, an important aspect is creating scaffolds that provide cells with appropriate topographical and biochemical cues. The ensemble of these stimuli might be referred to as constituting a 3D microenvironment. Indeed, 3D cell culture mimics better the native tissue microenvironment than conventional 2D *in vitro* culture on cell culture plastic. (Evans et al., 2009; Evans et al., 2010; Evans & Gentleman 2014; Gomes et al., 2017; Loaiza et al., 2018; Shah & Singh 2017)

#### 2.4.2 *In vitro* tissue models

In addition to tissue engineered graft development, 3D cell culture is researched to establish *in vitro* tissue models of tissue development, function in health and disease. Engineered tissue models would also facilitate toxicology testing and help avoid animal testing. To achieve this, 3D cell microenvironment which provides cells with biological, biochemical and biophysical signals mimicking the native needs to be defined and recreated (Calejo et al., 2020).

Further, 3D cell culture allows more natural cell-cell interactions. In fact, 3D aggregate culture of ASCs has promoted stronger secretion of ECM proteins fibronectin and laminin, for example, compared to 2D monolayer culture. Also, ASC endothelial differentiation and growth of functional tissue structures such as capillary-like tubes, for example, have been better supported in 3D over 2D culture. (Qiu et al., 2015; Zhao et al., 2016)

Importantly, coculture of different cell types is promoted in 3D culture with more degrees of freedom for cellular interactions. With *in vitro* models, the aim is in general terms to create a simplified tissue construct with specific functionality that is studied in more detail. Naturally, *in vivo* tissues are more complex and contain multiple different cell types and are in constant interaction with systemic signals influencing tissue homeostasis in the whole body.

## 2.5 Biomaterials for tendon tissue engineering

### Tenogenic scaffold structure and function

The structure and function within the engineered tissue graft need to support one another for optimal performance. Since large tendons transmit significant forces between muscle and bone in the body, tendon graft biomaterials have to possess high elasticity and sufficient properties for mechanical load-bearing (Butler et al., 2004; Gaspar et al., 2015; James et al., 2011; Kannus 2000). Material properties and processing techniques should benefit biomaterial scaffold production. For example, foamed PLA 96/4 would be too hard and brittle a material for tendon applications (Font Tellado et al., 2015), and in similar terms, poly(L-lactic-co-ε-caprolactone) (PLCL) 70/30 filaments are excessively adhesive for the fabrication of a braided structure although highly elastic (Nair & Laurencin 2006). On the other hand, by combining the right polymer properties vastly increases the feasibility of application.

### Tendon scaffold requirements

In the case of tendon tissue, one important point to consider is the slow healing profile of damaged tendons (de Mos et al., 2008). The biodegradable biomaterial scaffold should offer besides immediate support and possess sufficient load-bearing properties upon implantation, also continued mechanical support long enough to allow for cellular ingrowth and tissue regeneration (Kuo, C. K. et al., 2010). PLA biomaterial degradation rate ranging from months to a year (Rasal et al., 2010) would therefore be suitable for tendon application. In particular, braided structures mimicking the native tendon tissue have been researched due to high tensile strength (Vaquette et al., 2010). Considering tendon tissue, pore sizes in the range of 150–240 μm have been found apt in large animal model. Too small pore size of 55 μm was found to cause growth of cell aggregates and clustering on the edge regions of the scaffold. (Caliari et al., 2011)

## 2.5.1 Mechanical properties for tendon constructs

Native tendon tissue is best characterized by its high tensile strength and elasticity; the Young's modulus related to the tensile strength of human Achilles tendon and ligaments has been measured ranging between 200-870 MPa (Kuo, C. K. et al., 2010; Yang, S. et al., 2001). For tendon applications, PLCL as a highly elastic synthetic copolymer has been applied. For instance, Vaquette and coworkers (Vaquette et al., 2010) reported the elastic modulus of electrospun

PLCL microfiber scaffold as approximately 150 MPa which is in the same order of magnitude as that of native tendon tissue (Kuo, C. K. et al., 2010; Yang, S. et al., 2001). For surface stiffness, a range of ~30-50 kPa has been found to promote MSC tendon-like phenotype (Sharma & Snedeker 2010; Sharma & Snedeker 2012).

## 2.5.2 Filamentous polymer scaffolds

Further specifications to consider in the case of tendon tissue scaffold are the properties of filamentous structures. Filamentous scaffolds are thought to structurally imitate native tendon tissue while filamentous structures permit a variety of scaffold geometries (Lu et al., 2005). Physical properties of filamentous scaffolds that affect cell adhesion and growth encompass fiber diameter, orientation and surface topography (Vaquette et al., 2010), in addition to other material properties. For example, anisotropic alignment has been reported to support tenogenesis (Zouani et al., 2012). What is more, Erisken and coworkers found that microfibers of poly(L,D-lactic-co-glycolic acid) (PLGA) aligned human tenocytes more efficiently than nanofibers (Erisken et al., 2013). To the point, the diameter of human tendon collagen fibrils has been reported in the 1-300  $\mu\text{m}$  scale (Erisken et al., 2013). In a study by Vaquette and coworkers, the aligned 2  $\mu\text{m}$ -microfiber electrospun PLCL scaffolds promoted rat BMSCs to produce ECM rich in COL1 and COL3, both which are typical tendon and ligament matrix proteins (Vaquette et al., 2010). In comparison, Deng and coworkers tested 20-30  $\mu\text{m}$  diameter fiber polyglycolide (PGA) nonaligned fiber mesh with human dermal fibroblast culture under static strain for 14 weeks and reported increased COL1 production and higher tensile strength (Deng et al., 2009). The potential limitations of the filamentous scaffolds include the varied porosity which might lead to seeded cells either flushing through the structure or lack of cell penetration interior the braided structure (Vaquette et al., 2010).

### Poly lactide

Biodegradable and biocompatible PLA is widely applied in biomedical applications (Lasprilla et al., 2012). PLA is a polyester, synthesized from monomers of lactic acid by ring-opening polymerization (Rasal et al., 2010). In the chemical process, lactic acid is polycondensated into a polymer followed by depolymerization resulting into cyclic lactide ring. In a metal catalyzed ring-opening polymerization, the lactide ring is opened and the aliphatic polyester PLA

polymer is formed either according to ionic, co-ordination or free radical polymerization process depending on the choice of metal catalyst (Rasal et al., 2010). P(L/D)LA is bioadsorbable (Lasprilla et al., 2012), hydrophobic, and consists of the natural L-lactic acid as well as isoform D-lactic acid (Rasal et al., 2010) which are fully metabolized by the body in a normal tissue homeostasis condition (Middleton & Tipton 2000). *In vivo*, PLA degradation occurs typically by bulk hydrolysis when the ester bond of the polymer chain is hydrolyzed by water. This reaction leaves hydrophilic hydroxyl groups exposed in the polymer thus causing further hydrolysis reactions to occur. Depending on the tissue environment, hydrolysis of PLA fibers takes from several months up to a couple of years *in vivo* (Rasal et al., 2010). PLA is mechanically tailorable (Nair & Laurencin 2006).

### 2.5.3 Foamed polymer scaffolds

#### Poly(L-lactide-co-ε-caprolactone)

PLCL is a highly elastic hydrophobic copolymer of PLA and poly(ε-caprolactone) (PCL). PCL is a polyester, synthesized by ring-opening polymerization of ε-caprolactone. PCL polymer chain undergoes bulk or surface hydrolysis in aqueous environment, and its degradation product is caproic acid. (Yoon & Fisher, 2009) PCL degrades at a slow rate, approximately up to 2 years *in vivo* (Yang, S. et al., 2001), however, in PLCL copolymer the degradation rate is increased (Yoon & Fisher, 2009).

## 2.6 Biomaterials for bone tissue engineering and vascularized bone

#### Vascularized bone scaffold structure and function

Specific biomaterial properties required for a tissue engineered bone construct include sufficient mechanical stability, mineralization capacity, and possibly anti-bacterial properties (Douglas et al., 2014). Desirable bone biomaterial properties include osteoconductivity, which means that the biomaterial allows endogenous osteoblastic cells to adhere, grow, and divide, whereas an osteoinductive biomaterial actively recruits and induces precursor cells to grow new bone (Turner, 2009).



The scaffold pore size is an important factor influencing, for example, hASC osteogenic differentiation (Kyllonen et al., 2013) and a pore size of 200-600  $\mu\text{m}$  has been reported suitable for osteogenesis (Van Blitterswijk, 2008; Wubneh et al., 2018). The structural properties of a suitable bone scaffold include porosity in the minimal range of 50 % (James et al., 2011) for exchange of nutrients and oxygen diffusion as well as waste removal *in vitro* and also after implantation (Caliari et al., 2011). The pore structure and pore interconnectedness affect cell adhesion and migration as well as the rate and depth of cell ingrowth during tissue regeneration (Vaquette et al., 2010). The porosity and pore interconnectedness of the structure naturally also affect ingrowth of host vasculature following implantation. Pore sizes surpassing 300  $\mu\text{m}$  have been deemed necessary for vascularization. (Wubneh et al., 2018)

Different technologies have potential for engineering of microvascularization, such as 3D bioprinting of cells encapsulated within biocompatible hydrogels, for example. The 3D bioprinting of tissue and organs is a rapidly developing field with wide applicability. However, the feasibility between different applications varies and, particularly the state of maturation of the bioprinted construct with the aid of bioreactors, for example, would necessitate further research.

### 2.6.1 Mechanical properties for bone constructs

The biomaterial mechanical loading capacity requirements for load-bearing bone applications are considerable. In comparison, the developing osteoblast osteoid is a soft material and mechanically comparable to hydrogels at Young's modulus ranging between 11-30 kPa (Engler et al., 2006; Gantar et al., 2014; Huebsch et al., 2010; Wen et al., 2014). Hydrogels could be applied as mineralized bone defect filler materials as minimally invasive injectable grafts, for example (Engler et al., 2006).

#### Stiffness for osteogenesis

The biomaterial substrate stiffness influences the differentiation of anchorage-dependent stem cells. The mechanotransduction process involves transduction of a mechanical signal such as material stiffness into altered protein expression on cellular level. Adhered cells pull on the integrin adhesion sites and therein linked cellular actin filaments. This in turn induces changes in the cell behavior, morphology and function (Evans & Gentleman 2014). Interestingly, cells can also

sense the surrounding harder surfaces of cell culture plastic even though encapsulated within 3D hydrogel matrix, for example. This is due to the activity of the cells pulling on the hydrogel matrix (Evans & Gentleman 2014). In the osteogenesis process, a higher stiffness substrate enhances hMSC osteogenic differentiation, even in similar cell culture media conditions (Engler et al., 2006; Huebsch et al., 2010; Walters & Gentleman 2015). Therefore, substrate mechanical properties and stiffness importantly influence cell fate (de Peppo et al., 2014; Vogel 2018).

## 2.6.2 Hydrogels

According to a simplified International Union of Pure and Applied Chemistry (IUPAC) definition, a gel is nonfluid colloidal or polymer network expanded by a fluid. In the case of a hydrogel, the polymer network is water-swollen and therefore a hydrogel can be defined as a hydrophilic nonfluid polymer network with capacity to retain water. (ASTM International. 2011)

Cellular interactions are better supported when the cells are encapsulated within a 3D matrix, such as hydrogel, that has structure and functions resembling the natural ECM. What is more, similar mechanical properties support the native niche mimicking effect (Vogel 2018).

Depending on the polymer source, hydrogels can be divided into natural, synthetic, or hybrid hydrogels (Zhu & Marchant 2011). Natural biomaterials, such as natural biopolymer COL, have specific advantages over synthetic biomaterials since they offer natural adhesion and recognition sites for cells because of their similarity with native ECM proteins (Yoon & Fisher, 2009). Although attractive, natural biomaterials like COL lack sufficient mechanical properties. Therefore, different strategies have been tested to improve the weak mechanical performance (Marques et al., 2019). Natural polymer polysaccharide and protein hydrogels are typically hydrophilic and biocompatible. However, their restrictions include besides low mechanical strength, also fast *in vivo* degradation. Polysaccharides GG, mammalian ECM glucosaminoglycan hyaluronan, and alginate extracted from brown algae are water soluble and well biocompatible with most cells but lack of adhesion sites (Diekjürgen & Grainger 2017).

Natural polymer based hydrogels, such as COL (Figure 4) and GG (Oliveira, J. T. et al., 2010; Smith et al., 2007), are biodegradable, biocompatible and can

accommodate various shapes and sizes as potentially injectable biomaterial hydrogels.

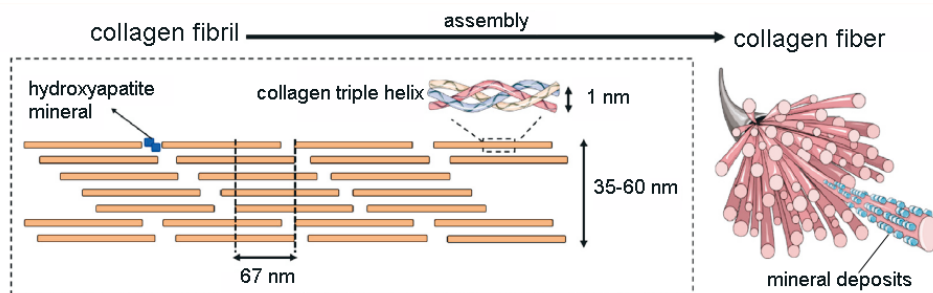


Figure 4. Collagen type I structure. Collagen triple-helix secondary and tertiary structure forms staggered (67 nm periodic spacing) quaternary structure of collagen fibrils. Mineralized collagen fiber hydroxyapatite deposits located in fibril gaps. Modified from (Lopes et al., 2018).

### Collagen type I hydrogel

Collagen is a natural ECM protein and therefore promotes excellent cell adhesion and spreading due to abundant arginine, glycine, and aspartate (RGD) amino acid sequences. Different collagen proteins compose the most part of musculoskeletal tissues and are thus vital for tissue integrity and functioning of cells therein (Friess 1998; Yoon & Fisher, 2009). Collagen has been utilized also as a coating biomaterial to enhance cytocompatibility and adhesion. As a hydrogel biomaterial, COL has been widely applied in TE constructs. However, there is an issue of lot-to-lot variation of COL and other natural polymers, too. Furthermore, COL is a weak gel which means that gelled COL fails to retain its shape without external support when taken out of the mold (ASTM International, 2011). COL contracts *in vitro* due to cell induced contraction forces, hence it is mechanically weak, and therefore methods to improve COL mechanical properties are investigated (Gentleman et al., 2003; Gentleman et al., 2006).

### Gellan gum

Gellan gum is an extracellular bacterial polysaccharide produced by *Sphingomonas elodea* bacteria. The linear polysaccharide structure consists of 4 repeating units of  $\beta$ -D-glucose,  $\beta$ -D-glucuronic acid,  $\beta$ -D-glucose, and  $\alpha$ -L-rhamnose (Ferris et al., 2013). In aqueous solution, anionic GG polysaccharide chains can be gelled with a monovalent or divalent cationic crosslinker into tight double-helix coils in an ionotropic physical crosslinking reaction (Ferris et al., 2013). The heating of non-gelated aqueous GG solution

prior to crosslinker addition to approximately 38 °C enhances the gelation reaction and thus forms more stable hydrogels (Osmalek et al., 2014). GG forms true gels according to ASTM standard meaning that the gelled hydrogel retains its shape when taken out of the cast (ASTM International. 2011). GG is optically transparent thus allowing optical microscopic imaging analysis of hydrogel scaffolds (Belay, et al. 2017). In physiological environment, enzymatic degradation of GG takes place by lysozyme, trypsin, and amylase (Ferris et al., 2013; Xu et al., 2018). The crosslinking reaction can be further enhanced with higher ionic strength. GG hydrogel elasticity and stiffness can be modified by altering ion concentration of the crosslinker (Fialho et al., 2008). To that end, trivalent bioamine spermidine (SPD) cation has been tested for effective GG hydrogel gelation where the amine groups form ammonium groups in aqueous solution (Lopez-Cebal et al., 2013; Soto et al., 2016). Furthermore, GG is approved by the European Medicines Agency (EMA) and the United States Food and Drug Administration (FDA) as a gelling and stabilization agent E418 for use in food, cosmetic, and chemical industries. As such, GG is an economical gelling additive and therefore enables cost-effective industrial scale solutions.

GG was initially reported feasible for cell encapsulation and TE applications by Smith and coworkers (Smith et al., 2007). Since, interest within the field of regenerative medicine applications has continued to grow (Coutinho et al., 2010; Oliveira, J. T. et al., 2010; Stevens et al., 2016). What is more, GG has been evaluated to possess reduced risk of zoonosis compared to animal derived natural hydrogels thus improving the safety of the engineered construct (Gantar et al., 2014). However, GG is rather inert as a biomaterial requiring functionalization to promote cell adhesion and spreading (Bacelar et al., 2016). Interestingly, the inert character of GG might not impede osteogenic differentiation of hASCs according to an Oliveira and coworker study (Oliveira, M. B. et al., 2016).

### Composite hydrogels

The benefits of different components are sought when combining different hydrogels into a composite hydrogel. For example, hiPSC-derived cardiomyocyte adhesion and functionality in GG hydrogel has been demonstrated by combining GG with gelatin, a collagen derivative (Koivisto et al., 2019). GG has also been modified with the aid of a double network to functionalize it for MSC culture (Choi et al., 2019). Also, COL has been applied for improved biofunctionalization of inert alginate hydrogel (Guillaume et al., 2015).

## Hydrogels for bone

COL is a highly suitable choice for bone grafts since collagenous fibers constitute the main part of bone organic matrix. Moreover, collagenous matrix functions as a natural platform for CaP mineral residue deposition and for apatite crystal nucleation and growth (Ferreira et al., 2012; Gelse et al., 2003). For minimally invasive bone defect reparation, an injectable hydrogel would be an attractive alternative, although hydrogels have restricted applicability for load-bearing or large volume bone constructs (Douglas et al., 2014). In a previous study, GG hydrogel has been combined with solid BaG particles (Douglas et al., 2014) for bone applications. Table 4 presents *in vitro* hydrogel studies for bone TE applications.

Table 4. *In vitro* bone studies with hydrogels.

Biomaterial	Cells	Media	Results	Reference
GG-MA beads, Ca-enriched	hASCs	Ca bead-MM	Metabolic activity ↑, proliferation +, mineralization +	(Vieira et al., 2019)
GG-MA, GG-MA/COL, alginate	hASCs	MM, OM	GG-MA (E') 30 kPa, GG-MA/COL (E') 3 kPa, MM: OCN ↑	(Oliveira, M. B. et al., 2016)
GG with BaG nanoparticles	hASCs	SBF	Mechanical properties +, good viability, HAp layer formed	(Gantar et al., 2014)
GG/HA	human osteoblasts	SBF	GG/HA (E') 4 kPa, ECM deposition +, mineralization +	(Bellini et al., 2015)
GG with BaG particles	rat BMSCs	MM	Highest ALP with 45S5	(Douglas et al., 2014)
GG/HAp	rabbit osteoblasts	MM	Good viability, proliferation +	(Vieira et al., 2015)
GG/HAp	rabbit osteoblasts	MM	Bone-like layer (E') 80-180 kPa, osteoblasts: good viability, proliferation +, mineralization +	(Pereira et al., 2018)
Dense COL with BaG nanoparticles	murine osteoblasts	MM	ALP ↑, mineralization +	(Marelli et al., 2011)
GG/PEGDA/PLA	murine BMSCs	MM	Good viability, proliferation +	(Hu et al., 2018)

Abbreviations: ↑ =upregulated; + =increased; 45S5, the original Bioglass®, ALP, alkaline phosphatase activity; BaG, bioactive glass; BMSCs, bone marrow stem cells; COL, collagen type I hydrogel; E', Young's modulus; ECM, extracellular matrix; GG, gellan gum; HA, hyaluronic acid; HAp, hydroxyapatite; hASCs, human adipose stem cells; MA, methacrylate; MM, maintenance medium; OCN, osteocalcin; OM, osteogenic medium; PEGDA, Poly(ethylene glycol) diacrylate; PLA, polylactide; SBF, simulated body fluid.

## Hydrogel characterization

Hydrogels are for the most part mechanically elastic and soft biomaterials. The hydrogel biomaterial mechanical properties are linked to the hydrogel microstructure of water-filled voids, including polymer network mesh size, and hydrogel porosity (Li, J. & Mooney 2016). In fact, the hydrogel microstructure facilitates the diffusion of nutrients and waste products to cells encapsulated within the hydrogel. The mesh size is determined by the distance between crosslinking points whereas porosity is defined as larger voids in the hydrogel microstructure than the mesh size (Li, J. & Mooney 2016). In a study by Soto and coworkers, microstructure of unmodified GG with mesh size allowing mass transport diffusion of small molecules of approximately 20 kDa in size and with larger pores, was deemed sufficient for diffusion of cellular nutrients and growth factors (Soto et al., 2016). Nonetheless, no consensus on optimal hydrogel pore size has been posited although it should be considered separately for each cell type and the desired property, for example, cell motility (Guan et al., 2017).

### 2.6.3 Bioactive glass

BaGs which are a type of bioceramic were discovered by Larry Hench in the late 1960's and were immediately appreciated for their ability to bond directly to bone (Hench & Wilson 1986). By tuning the BaG composition, the rate of bonding can be directly controlled (Turner, 2009). Typical BaG composition consists of SiO<sub>2</sub>, CaO, K<sub>2</sub>O, Na<sub>2</sub>O, P<sub>2</sub>O<sub>5</sub>, B<sub>2</sub>O<sub>3</sub> and MgO (Jones 2015). BaG dissolved ions (Figure 5) stimulate precursor cells to differentiate into osteoblastic cells, bone growth, and importantly, also angiogenesis (Day 2005; Kargozar et al., 2018).

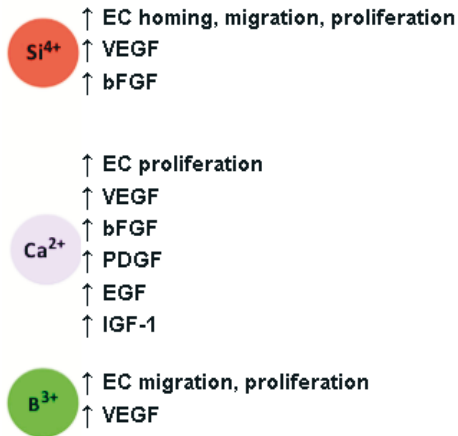


Figure 5. BaG dissolved ions' effect on angiogenesis including Si<sup>4+</sup>, Ca<sup>2+</sup>, and B<sup>3+</sup> multivalent cations. Modified from (Kargozar et al., 2018). Abbreviations: ↑=upregulated; bFGF, basic fibroblast growth factor; EC, endothelial cell; EGF, epidermal growth factor; IGF-1, insulin-like growth factor-1; PDGF, platelet derived growth factor; VEGF, vascular endothelial growth factor.

Although their brittleness limits the applications to non-load-bearing sites, BaG abrasion resistance is excellent (Turner, 2009). When exposed to physiological fluids, BaGs elicit formation of a biologically reactive hydroxycarbonate apatite layer that has composition similar to inorganic bone matrix (Hench 2006). This in turn promotes tissue bonding at the reactive interface, and what is important for graft survival and success, fibrous capsule will not be formed (Turner, 2009). The bioactive property is due to free exchange of ions between the BaG and fluids of the body. For these favorable properties, the BaG should contain <60 mol% SiO<sub>2</sub>, high CaO and Na<sub>2</sub>O content and high CaO:P<sub>2</sub>O<sub>5</sub> ratio. The original 45S5 bioglass formulation contains 45 wt-% SiO<sub>2</sub> with a 5:1 CaO:P<sub>2</sub>O<sub>5</sub> ratio (Turner, 2009). Another well-known bioactive glass composition is that of S53P4 bioactive glass Bonalive® that inhibits bacterial growth. The practical applications of BaGs have been as a coating material or as a filler material for bone constructs (Gantar et al., 2014).

### Bioactive glass extract

As an important discovery (Ojansivu et al., 2015; Ojansivu; Mishra et al., 2018), BaG bioactivity can be harnessed for TE *in vitro* cell culture applications based on the dissolved ions alone. This can be achieved by incubating the solid BaG granules in cell culture media base thus gaining the bioactive component directly

in a soluble form for efficient cell stimulation by BaG ionic dissolution products (da Silva et al., 2017; Nunez-Toldra et al., 2019; Ojansivu et al., 2015).

## 2.7 Vascularized bone tissue engineering

Vascularization of the tissue engineered constructs remains as the principal challenge of the field (Chang & Niklason 2017; Wang et al., 2017). Indeed, engineered microvascularization would not only enhance graft survival but also allow scaling up to clinically relevant volumes of tissue (Datta et al., 2017; Piroso et al., 2018). Cells embedded within constructs thicker than 400  $\mu\text{m}$  suffer from lack of oxygen upon implantation. Therefore, graft prevascularization would support the cell survival. Also, cellular cross-talk between vascular and neuronal cells advances tissue maturation (Ko et al., 2007; Maes et al., 2010). Moreover, prevascularization of the implant promotes faster ingrowth of host tissue vasculature. (Piroso et al., 2018) In view of this, scaffold structure porosity also plays a role since it facilitates diffusion within the tissue engineered construct allowing faster ingrowth of tissue and neovascularization of the construct (Fedorovich et al., 2011). Cell-ingrowth from surrounding tissue promotes bone defect healing and this is likewise rendered faster with prevascular structures already in place (Piroso et al., 2018). Thus, multiple strategies for graft prevascularization have been explored encompassing electrospinning (Hasan et al., 2014), sacrificial conduit materials such as gelatin, particulate leaching (Baker et al., 2011), or bioprinting with extrusion, droplet, and laser techniques (Datta et al., 2017; Rouwkema & Khademhosseini 2016).

### 2.7.1 Coculture for vascularization

The coculture approach offers multiple beneficial aspects for vascularization since MSCs, pericytes, or fibroblasts cultured with ECs have been shown to besides enhance vascular network formation, also increase stability of the network and modulate vascular barrier function (Bajpai & Andreadis 2012; Baldwin et al., 2014). These effects of the supporting cells in close proximity of ECs are mediated via adhesion and paracrine factors (Greco Song et al., 2018). The benefits of cell-cell communication can be harnessed in coculture in the interest of neovascularization formation (Pill et al., 2018; Rouwkema et al., 2006). For example, according to the coculture vascularization scheme, HUVECs



induce stromal cell, such as hASC, endothelial differentiation. The stromal cells support the ECs, in turn. Coculture of hMSCs and HUVECs is mutually beneficial since the factors that stromal cells secrete, promote EC alignment, sprouting and tube formation, in addition to stromal cell stabilizing effect on the capillary basement membrane (Correia, C. et al., 2011).

The hASCs promote angiogenesis, which refers growth of blood vessels from existing vasculature, by secreting stimulating factors (Rehman et al., 2004). Also, hASCs assist vasculogenesis, meaning *de novo* formation of capillaries and blood vessels, and vascular maturation (Cai et al., 2007). Importantly, in a study by Chen and coworkers, the formation of stable capillaries was maintained in hydrogel culture with hMSC provided support for ECs (Chen, Y. C. et al., 2012). Table 5 presents *in vitro* bone vascularization studies in hydrogels and composites.

Table 5. *In vitro* bone vascularization studies in hydrogels and composites.

Biomaterial	Cells (cell ratio)	Media	Main results	Reference
GG-MA/ COL	rat BMSCs	MM, EM	GG-MA (G') 1 kPa, good viability, proliferation +, EM: PECAM-1/VWVF ↑	(Chen, H. et al., 2018)
GG-PCL	TERT-hBMSCs: HUVECs (1:1)	OM	Si <sup>2+</sup> crosslinking: ALP activity ↑, OPN ↑, OCN ↑	(De Giglio et al., 2018)
COL-fibrin ratios (60:40), (50:50), (40:60)	hBMSCs: HUVECs (1:5), (2:3), (1:1), (3:2), (5:1)	N.A.	hBMSCs: HUVECs (1:1) selected for vasculogenesis in COL-fibrin (40:60). Matrix composition ruled over cell ratio.	(Rao et al., 2012)
COL-fibrin/HAP nanoparticles	hBMSCs: HUVECs (1:1)	EGM-2	<2.5 mg/mL HAp good network length, vasculogenesis inhibited with higher HAp content	(Rao et al., 2014)
COL/ gelatin/ fibrin	HUVECs: human lung fibroblasts (1:2)	EGM-2, flow	Bioprinted tubes, capillary network, lumina formed, CD31 production ↑	(Lee, V. K. et al., 2014)
COL/ gelatin	HUVECs	EGM-2, flow	Bioprinted tubes, flow: elongation +, good viability, arterial marker gene expression ↑	(Lee, Vivian K. et al., 2014)
COL	hASCs:HUVECs (1:1), hBMSCs: HUVECs (1:1)	EM	Vascular structures with both set ups <i>in vitro</i> , equal angiogenesis <i>in vivo</i> in murine model	(Ma et al., 2014)
Fibrin	hASCs:HUVECs (1:1), hBMSCs: HUVECs (1:1)	EGM-2	hASCs:HUVECs network density +, VEGF ↑	(Pill et al., 2018)
Fibrin	hBMSCs: HUVECs (1:2)	EGM-2, flow	VEGF+Ang1: perfusable microvascular network	(Jeon et al., 2014)
GelMA, VEGF micropattern	hBMSCs: HUVECs (1:1)	EGM-2	Good viability, metabolic function ↑, proliferation +	(Kazemzadeh-Narbat et al., 2017)

continued

continued

Biomaterial	Cells (cell ratio)	Media (mix)	Main results	Reference
PEG	hBMSCs: HUVECs (1:1)	EGM-2; MM (1:4), OM	BMP-2; osteogenesis +, vasculogenesis +; bFGF: osteogenesis (-), vasculogenesis +	(Blache et al., 2016)
GelMA/alginate/ PEGTA	hBMSCs: HUVECs (1:1)	EGM-2; MM (1:1)	Bioprinted perfusable vascular construct, good viability, vascular marker immunostaining +	(Jia et al., 2016)
RGD-alginate microspheres	hBMSCs: HUVECs (1:2)	EM: OM	Microvascular structures formed, ALP ↑, OCN ↑, mineralization +, VEGF release +	(Grellier; Bareille et al., 2009)
Poly(LLA-co-DXO)	hBMSCs: HUVECs (5:1)	MM, rotation	Coculture: microvascular network formed, gene exp of endothelial and osteomarkers ↑	(Pedersen et al., 2013)

Abbreviations: ↑ =upregulated; + =increased; (-) =inhibited; ALP, alkaline phosphatase; Ang1, angiopoietin1; bFGF, basic fibroblast growth factor; BMP-2, bone morphogenic protein-2; BMSCs, bone marrow stem cells; CD31, Cluster of differentiation 31 (same as PECAM-1); COL, collagen type I hydrogel; EGM-2, endothelial cell growth medium-2; EM, endothelial medium; flow, dynamic fluid flow stimulus applied; G<sup>+</sup>, storage modulus; gene exp, gene expression; GelMA, methacrylated gelatin; GG, gellan gum; HAP, hydroxyapatite; hASCs, human adipose stem cells; hBMSCs, human bone marrow stem cells; HUVECs, human umbilical vein endothelial cells; MA, methacrylate; MM, maintenance medium; N.A., not available; OCN, osteocalcin; OM, osteogenic medium; OPN, osteopontin; PCL, poly(ε-caprolactone); PECAM-1, platelet endothelial cell adhesion molecule-1 (same as CD31); PEGTA, 4-arm poly(ethylene glycol)-tetra-acrylate; poly(LLA-co-DXO), poly(L-lactide-co-1,5-dioxepan-2-one); RGD, arginine, glycine, and aspartate amino acid sequence; rotation, dynamic rotation stimulus applied; TERT-hBMSC, immortalized human TERT-bone marrow stem cell; VEGF, vascular endothelial growth factor; VWF, Von Willebrand factor.

## 2.7.2 Vascularization in cell-laden hydrogels

The formation of vascular network is needed to ensure graft survival and secure graft functionality. For the formation of microvascularization in a tissue engineered graft, a soft hydrogel scaffold material is required at approximately 1 kPa Young's modulus (Sieminski et al., 2007). The hydrogel biomaterial needs to be soft enough to allow the ECs to remodel the 3D hydrogel matrix and eventually form vascular networks (Figure 6).

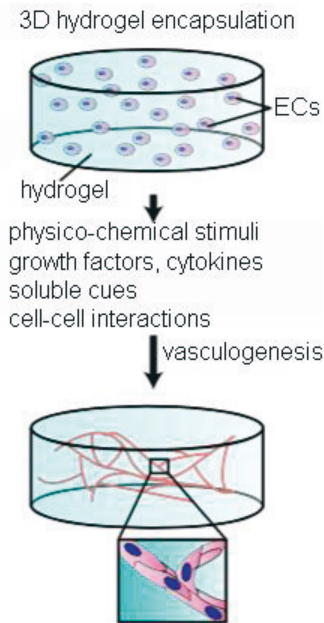


Figure 6. Microvascularization formation in cell-laden hydrogels. Vasculogenesis by self-assembly of endothelial cells into interconnected microvessel network within 3D hydrogel. Modified from (Greco Song et al., 2018).

However, the hydrogel scaffold needs to possess sufficient stability for safe handling of the graft during *in vitro* culture and also implantation process. Functional human vascular network has been reported by Chen and coworkers in gelatin methacrylate hydrogels (Chen, Y. C. et al., 2012) and as an injectable COL construct by Kuo and coworkers (Kuo, K. C. et al., 2015).

## 2.8 *In vivo* studies

*In vivo* testing with an animal model is justified in cases where both tissue and systemic responses are essential for the safety and efficacy assessment of the implant. *In vitro* screening tests of cell-laden biomaterial construct constitute a preliminary step towards *in vivo* testing (Doherty, 2009) and eventual clinical trials. In short, *in vivo* preclinical safety and efficacy testing of medical devices is based on evaluation of irritation and sensitivity, allergic reactions, hemocompatibility, acute and chronic toxicity and inflammation, systemic toxicity, carcinogenicity and mutagenicity (Doherty, 2009; McBlane et al., 2018).

### Tendon constructs *in vivo*

For tendon repair, PLA 96/4 suture has been reported successful in a rabbit model (Viinikainen et al., 2014), whereas direct injections of GDF-5 have improved tendon healing in a rat model (Aspenberg 2007).

### Vascularized bone constructs *in vivo*

*In vivo* neovascularization has been shown to ameliorate with hASCs that have undergone endothelial differentiation (Cao et al., 2005). Liu and coworkers reported enhanced osteogenesis and vascularization with human iPSC-derived MSCs and HUVECs cocultured in a CaP scaffold implanted in a rat model (Liu, X. et al., 2017).

### Limits of *in vivo* testing

An issue remains concerning the use of human cells in an animal model since human cells might be rejected by animal immune system (Seok et al., 2013). The results of *in vivo* testing require an extrapolation step of data interpretation since there are differences between animal and human physiology (Gomes et al., 2017) including differences in species evolution, in cellular composition (Patrikoski et al., 2019), in metabolic and systemic functions (Shah & Singh 2017), and discrepancies between molecular responses (Takao & Miyakawa 2015a; Takao & Miyakawa 2015b). What is more, recovery time between rodent models and humans differs greatly which complicates data interpretation (Patrikoski et al., 2019). For the above reasons, *in vitro* models with human cells could provide more accurate platform for testing of human physiology mimicking functionality and reactions.

## 2.9 Clinical case studies

As their overarching goal, current TE strategies aim to provide novel and innovative solutions in order to help answer the growing need for tissue grafts and personalized medicine applications. Whole organ TE has been reported for skin which is a flat tissue (Centanni et al., 2011) and cartilage (Jiang et al., 2016), hollow organ structures such as urethra (Raya-Rivera, A. et al., 2011), bladder (Atala et al., 2006), and vaginal organs (Raya-Rivera, A. M. et al., 2014), and tubular tissues such trachea (Hamilton et al., 2015) and vascular grafts (Wystrychowski et al., 2014). On the other hand, functional solid organs have proven challenging to generate ascribable to their complexity (Shafiee & Atala 2017). With randomized clinical trials, the efficiency, safety, and clinical end result of different TE techniques can be evaluated (De Francesco et al., 2015).

### Advanced therapy medicinal product European regulatory framework

Since musculoskeletal defects cause a globally growing strain on the health care systems, restrict the working ability with substantial economic losses, and diminish overall the quality of life of the patients, their safe and efficient treatment is of major importance. Tissue-engineered construct treatments are costly at approximately 20,000 USD while the cost of gene therapy is even higher at approximately 400,000-1,200,000 USD (Seoane-Vazquez et al., 2019). These treatments are often considered in cases where conventional treatments are no longer effective and this might be reflected onto the success rate of the aforesaid treatments (Cossu et al., 2018).

Medicines that are based on gene, cell, or tissue therapies are subject to a specific European regulatory framework due to their content of living cells or viral vectors (Eder & Wild 2019). The European regulatory guideline for advanced therapy medicinal products (ATMPs) that encompass gene therapeutics, somatic cell therapy, and tissue engineered products was established with the risk-based approach (Annex I, part IV of Directive/2001/83/EC) and a regulatory framework (1394/2007/EC) for marketing authorisation issued by the EMA was enforced in 2008 (Eder & Wild 2019; Patrikoski et al., 2019).

Up to present, the EMA has given European marketing authorisation to 12 ATMPs most of which have been since withdrawn from the market (Eder & Wild 2019) and the FDA has given authorisation to 16 ATMPs in the United States market (Seoane-Vazquez et al., 2019). Currently the EMA has licensed

5 cell-based ATMPs in the EU; Alofisel® somatic cell therapy medicinal product for Crohn’s disease anal fistula treatment; classified as tissue engineered products, Holoclar® for eye limbal stem cell deficiency and Spherox® for knee cartilage defects; as gene therapy medicinal products Yescarta® for treating two types of nonresponding B-cell lymphoma blood cancer and Zynteglo® for beta thalassaemia treatment.

A case in point, phase II/III/IV ATMP clinical trials concerning musculoskeletal defects have remained limited. Table 6 presents academic cell therapeutic musculoskeletal ATMP clinical trials with European regulatory authorisation. On the other hand, MSCs as ATMPs have been granted European regulatory authorisation and applied for indications ranging from Crohn’s disease anal fistula treatment with autologous ASCs (Phase III trial NCT01803347) to critical limb ischemia with restricted blood and oxygen supply to tissues treated with allogenic BMSCs (Phase II/III trial NCT03042572), and also cardiomyopathy treatment with an autologous BMSC CD34+ subpopulation (Phase II/III trial NCT02248532).

Table 6. Phase II/III/IV musculoskeletal ATMP clinical trials 2008-2018 (Eder & Wild 2019).

Phase	Indication	Intervention	Trial identifier
III	Non-union bone fracture	Autologous BMSCs	EUDRACT2015-000431-32
III	Non-union bone fracture	Autologous BMSCs and biomaterial	NCT03325504
III	Periapical bone healing in infected primary teeth	Autologous leucocyte and platelet rich fibrin	NCT02437708
IV	Osteoarthritis	Autologous bone marrow concentrate	NCT03110679
II/III	Chronic Achilles tendinopathy	Autologous tenocytes	NCT01343836

Abbreviation: BMSCs, bone marrow stem cells.

Summarizing the ATMP clinical trials in Table 6, bone fractures were treated with autologous BMSCs with or without supporting biomaterial, whereas a fibrin matrix with tissue repair promoting leucocytes and platelets were applied for infected primary teeth. For osteoarthritis, a concentrate of autologous bone marrow with a variety of cellular components including hBMSCs was applied while primary tendon cells were used to treat chronic Achilles tendinopathy.

However, regulatory agencies have the power to withdraw the approval of phase II/III clinical trials, as was the case for the treatment of ischemic stroke

with limited brain blood flow by intravenous allogenic hASC therapy (RESSTORE, trial NCT02849613). Indeed, 23 % of ATMP clinical trials are terminated due to lack of efficacy compared to standard treatment options available (Eder & Wild 2019). Subsequently, the RESSTORE preclinical trials have resumed with a new protocol in phase I.

Under certain circumstances, advanced therapy medicines can be authorised nationally by the national competent authorities, when they are custom-made products, prepared on a non-routine basis for an individual patient and administered in hospital under the responsibility of a doctor. In addition, treatments based on human tissue, cell and stem cell products that do not fall under the category of medicinal products are also regulated at national level as tissues or cell transplants (1394/2007/EC). These can be granted national Hospital exemption according to 2001/83/EC. In Finland at the Tampere University Hospital, the national Hospital exemption has up to present allowed bone tissue engineered constructs with hASCs and  $\beta$ -tricalcium phosphate ( $\beta$ -TCP) granules to be applied for over 20 craniomaxillofacial bone regeneration patients since 2008. Thesleff and coworkers reported that the clinical outcomes of 2008-2011 conducted treatments failed to surpass conventional treatment method results (Thesleff et al., 2011). Briefly, autologous cells were expanded in *in vitro* clean room laboratory cell culture and readministered to the defect site with bioceramic granules and osteogenesis promoting BMP-2.



### 3 AIMS OF THE STUDY

The main aim of the study was to develop hASC differentiation methods in combination with tissue specific biomaterials for musculoskeletal tissue engineered graft development. The specific aims of studies **I-III** were:

**I** To evaluate hASC tenogenic differentiation, firstly, by optimizing tenogenic differentiation medium for hASCs and, secondly, by comparing tenogenic differentiation of hASCs in braided PLA 96L/4D and foamed 70L/30CL copolymer scaffolds and, thirdly, by evaluating the combined effect of the optimized tenogenic differentiation medium with the optimized polymeric scaffold.

**II** To determine, firstly, the effect of BaG 2-06 extract based osteogenic medium induction on hASC osteogenic differentiation and mineralization encapsulated in GG and COL hydrogels and, secondly, to compare the effect of BaG 2-06 extract GG crosslinker for hASC mineralization with osteogenic medium culture in 3D GG hydrogel culture.

**III** To evaluate, firstly, osteogenic differentiation of hASCs induced with BaG 2-06 extract based endothelial medium with osteogenic supplements in coculture with HUVECs and, secondly, to evaluate the effect of hASC osteogenic preconditioning for mineralization, and thirdly, to assess microvascularization network formation in 3D composite GG-COL hydrogel coculture.

## 4 MATERIALS AND METHODS

### 4.1 Human adipose stem cell isolation, characterization and culture

#### 4.1.1 Human adipose stem cell isolation

This study was conducted with the favourable opinion of the Regional Ethics Committee of the Expert Responsibility area of Tampere University Hospital, Tampere, Finland, to obtain adipose tissue samples for research purposes (R15161). The hASCs were isolated from subcutaneous adipose tissue in surgeries at the Tampere University Hospital Department of Plastic Surgery that were obtained with the patients' written informed consent. The adipose tissue samples were obtained: in study **I**, from 7 healthy female donors of mean age 52(9) years; in study **II**, from 6 healthy female donors of mean age 52(5) years; in study **III**, from 3 healthy female donors of mean age 56(4) years.

The hASCs isolation was performed as reported previously (Kyllonen et al., 2013). Briefly, subcutaneous adipose tissue was mechanically cut, followed by enzymatic digestion with a solution containing collagenase type I (1.5 mg/mL; Thermo Fisher Scientific, Waltham, MA, USA), Dulbecco's Modified Eagle Medium/Ham's Nutrient Mixture F-12 (DMEM/F-12 1:1; Thermo Fisher Scientific), 1 % L-glutamine (GlutaMAX; Thermo Fisher Scientific), and 1 % antibiotics (100 U/mL penicillin/100 U/mL streptomycin; P/S; Lonza, Basel, Switzerland). The isolated hASCs were expanded in maintenance medium (MM) containing DMEM/F-12, 5-10 % human serum (HS; PAA Laboratories; GE Healthcare, Chicago, IL, USA) in study **I** due to the change of the serum lot, and 5 % HS (Biowest, Nuaille, France) in studies **II** and **III**, 1 % L-glutamine (GlutaMAX, Gibco; Thermo Fisher Scientific), and 1 % P/S. Following isolation, the hASCs were expanded in T75 cm<sup>2</sup> polystyrene flasks (Nunc; Thermo Fisher Scientific) in MM at 37 °C and in 5 % CO<sub>2</sub>. The medium was changed twice a week. Upon passaging, TrypLE Select (Thermo Fisher Scientific) was added to

detach the cells. The isolated hASCs tested negative for mycoplasma contamination.

#### 4.1.2 Human adipose stem cell characterization

Flow cytometry analysis was performed to characterize undifferentiated hASCs of passage 1-2 in studies **I-III**. Briefly, hASCs were analyzed for the multipotency cell surface markers (Lindroos et al., 2011) with flow cytometry (FACS Aria; BD Biosciences, Franklin Lakes, NJ, USA) by measuring fluorophore-conjugated monoclonal antibodies against CD3-PE, CD14-PE-Cy7, CD19-PE-Cy7, CD45RO-APC, CD54-FITC, CD73-PE, CD90-APC (BD Biosciences), CD11a-APC, CD80-PE, CD86-PE, CD105-PE (R&D Systems, Minneapolis, MN, USA), CD34-APC, and HLA-DR-PE (Immunotools, Friesoythe, Germany). Flow cytometric analysis was performed with 10,000 cells per sample, and the positive expression was defined as a level of fluorescence 99 % greater than that of the corresponding unstained cell sample (Jaroszeski & Radcliff 1999; Picot et al., 2012).

#### 4.1.3 Human adipose stem cell culture

In studies **I-III**, hASCs of passages 3-6 were used. In study **I**, the scaffolds were pretreated with DMEM/F-12 and 1 % P/S for 72 h. In study **I**, the cells were allowed to adhere at +37 °C for 3 h before addition of the corresponding medium (Table 7) to the wells.

In studies **II-III**, the cell pellets were resuspended into the non-gelated COL or GG solutions, manually mixed and allowed to gelate in RT. The corresponding medium (Table 7) was added immediately following gelation (studies **II-III**). The 48-well plate format (Nunclon Delta Surface; Merck, Darmstadt, Germany) was used for cell culture experiments in scaffolds in studies **I-III**. Media were changed three times per week in studies **I-III**.

Table 7. The media compositions.

Medium	Study	Composition
MM	I, II	DMEM/F-12, 5-10% (v/v) HS, 1% (v/v) P/S, 1% (v/v) L-glutamine
MM	III	$\alpha$ MEM, 5% (v/v) HS, 1% (v/v) P/S, 1% (v/v) L-glutamine
TM1	I	100 ng/mL GDF-5 in MM
TM2	I	50 ng/mL GDF-5 in MM
TM3 (TM)	I	50 ng/mL GDF-5, 50 $\mu$ g/mL (280 $\mu$ M) L-ascorbic acid EBM-2, hEGF*, hVEGF*, R3-IGF-1*, hFGF- $\beta$ *, heparin*, hydrocortisone*
EGM-2 with HS	III	AsA2P*, GA-1000*, 2% (v/v) HS
OM	II, III	5 nM Dex, 250 $\mu$ M AsA2P, 10 mM $\beta$ -GP in MM
BaG OM	II	OM in BaG extract base
BaG EM-OM	III	OM in BaG EM extract base

Abbreviations and reagents:  $\alpha$ -MEM, Minimum Essential Medium  $\alpha$  (Thermo Fisher Scientific);  $\beta$ -GP,  $\beta$ -glycerophosphate (Merck); AsA2P, L-ascorbic acid 2-phosphate (Merck); ascorbic acid (Lonza); BaG EM extract, bioactive glass extract in EBM-2; BaG EM-OM, bioactive glass extract endothelial-osteogenic medium; BaG extract, bioactive glass extract in MM; BaG OM, bioactive glass extract osteogenic medium; Dex, dexamethasone (Merck); DMEM/F-12, Dulbecco's Modified Eagle Medium/Ham's Nutrient Mixture F-12 (Thermo Fisher Scientific); EBM-2, Endothelial Cell Growth Basal Medium-2 (Lonza); EGM-2, Endothelial Cell Growth Medium-2; GA, 30  $\mu$ g/mL gentamicin/ 15 ng/mL amphotericin-B (Lonza); GDF-5, Growth and Differentiation Factor-5 (Biomol, Hamburg, Germany); hEGF, human Epidermal Growth Factor (Lonza); heparin (Lonza); hFGF- $\beta$ , human Fibroblast Growth Factor-Beta (Lonza); HS, human serum (PAA Laboratories, GE Healthcare (study I); Biowest (studies II-III)); hydrocortisone (Lonza); hVEGF, Vascular Endothelial Growth Factor (Lonza); L-ascorbic acid (Merck); L-glutamine (GlutaMAX; Thermo Fisher Scientific); MM, maintenance medium; OM, osteogenic medium; P/S, 100 U/mL penicillin/streptomycin (Lonza); R3-IGF-1, R3-Insulin-like Growth Factor-1 (Lonza); TM1, tenogenic medium 1; TM2, tenogenic medium 2; TM3, tenogenic medium 3 (selected as the optimized tenogenic medium (TM)). \* indicates EGM-2 SingleQuots supplement (Lonza).

### Bioactive glass extract preparation

In study II, BaG extract and BaG OM solutions were prepared. The granules of BaG 2-06 (Ojansivu et al., 2015) had a nominal composition of 12.1 wt-% Na<sub>2</sub>O, 14.0 wt-% K<sub>2</sub>O, 19.8 wt-% CaO, 2.5 wt-% P<sub>2</sub>O<sub>5</sub>, 1.6 wt-% B<sub>2</sub>O<sub>3</sub>, and 50.0 wt-% SiO<sub>2</sub>. For the preparation of BaG extract and BaG OM, briefly, batches of granules of BaG 2-06 of 500-1 000  $\mu$ m diameter were disinfected with 70 % ethanol washes for 10 min repeated twice (ETAX Aa  $\geq$ 99.5 % ethanol; Altia, Rajamäki, Finland; deionized sterile filtered water). The ethanol was allowed to evaporate in RT for 2 h. The BaG extract contains dissolved ions from 87.5 mg/mL BaG granules incubated for 24 h in DMEM/F-12, 1 % (v/v) P/S (Lonza), and 1 % (v/v) L-glutamine (GlutaMAX; Thermo Fisher Scientific) (study II) or in EBM-2 with 0.1 % (v/v) 30  $\mu$ g/mL gentamicin/ 15 ng/mL

amphotericin-B (Lonza; study **III**), in polystyrene dishes, after which the BaG extract was sterile filtered with 0.2  $\mu\text{m}$  filters. The BaG extracts were stored for a maximum duration of 14 d in studies **II-III**. The BaG OM was prepared by adding 5 % (v/v) HS (Biowest), 10 mM  $\beta$ -GP (Merck), 250  $\mu\text{M}$  AsA2P (Merck), and 5 nM Dex (Merck) to BaG extract (study **II**). Regular OM was made by supplementing 5 % HS (v/v) (Biowest) MM with 10 mM  $\beta$ -GP (Merck), 250  $\mu\text{M}$  AsA2P (Merck), and 5 nM Dex (Merck). In study **III**, BaG EM-OM medium was prepared by incubating 87.5 mg/mL of BaG 2-06 granules (500-1 000  $\mu\text{m}$ ) in EBM-2 with GA (EGM-2 SingleQuots supplements, Lonza) for 24 h to gain the BaG EM extract, after which 5 % HS and osteogenic supplements were added to the BaG EM extract. For hASC pretreatment in study **III**, the hASCs were expanded either in MM or OM.

## 4.2 Human umbilical vein endothelial cell isolation, characterization and culture

### 4.2.1 Human umbilical vein endothelial cell isolation

In study **III**, HUVECs were obtained from 1 donor of 38 years in planned cesarean section at the Tampere University Hospital with the patient's written informed consent and with the favourable opinion of the Regional Ethics Committee of the Expert Responsibility area of Tampere University Hospital (R13019), Tampere, Finland, and isolated according to a previously reported method (Jaffe et al., 1973; Sarkanen et al., 2011). Briefly, the umbilical vein was rinsed with a solution consisting of EBM-2 (Lonza), collagenase type II (1.0 mg/mL; Merck), 2 % P/S (v/v) and 0.1 % (v/v) GA (Lonza).

### 4.2.2 Human umbilical vein endothelial cell characterization

Flow cytometry analysis was performed to characterize HUVECs in study **III**. Briefly, HUVECs were analyzed for the cell surface markers by measuring fluorophore-conjugated monoclonal antibodies against CD31-FITC, CD34-APC (Immunotools), CD73-PE, CD90-APC, CD144-PE, CD146-PE (BD Biosciences), CD105-PE, and VEGFR3-APC (R&D Systems) with flow cytometry (FACSAria; BD Biosciences). The analysis was performed with 10,000

cells per sample. For positive expression the level of fluorescence was 99 % greater than that of the corresponding unstained cell sample (Jaroszeski & Radcliff 1999; Picot et al., 2012).

### 4.2.3 Human umbilical vein endothelial cell culture

In study **III**, HUVECs were expanded prior to plating in EGM-2 medium (see Table 7 in section 4.1.3) consisting of EBM-2 (Lonza), EGM-2 SingleQuots supplements (Lonza), and 2 % HS (Biowest). The HUVECs in study **III** were of passages 6-7. After plating, in the coculture experiments in study **III**, HUVECs were cultured within 3D hydrogels with hASCs in either EGM-2 or BaG EM-OM.

## 4.3 Tenogenic scaffold manufacture and characterization

In study **I**, braided filamentous PLA 96/4 scaffolds and foamed PLCL 70/30 were manufactured, characterized and tested. Consequently, the filamentous and foamed scaffolds were compared for hASC tenogenesis.

### 4.3.1 Braided filamentous polymer scaffolds

In study **I**, the PLA fibers were melt spun from medical grade poly-96L/4D-lactide (PLA 96/4) copolymer with an inherent viscosity of 2.18 dL/g (Purac, Corbion, Amsterdam, the Netherlands) using a Gimac microextruder (Gimac, Gastronno, Italy) with a screw diameter of 12 mm. The multifilament fiber was drawn from a nozzle and oriented by means of caterpillars and infrared ovens. The diameter of a single fiber in the 8-filament braid was 80  $\mu\text{m}$ . The filamentous PLA 96/4 scaffolds were machine braided by Scaffdex Ltd (Tampere, Finland). The finished braid of 4 mm of width and 1.1 mm of height was washed with ethanol and manually cut with a heated blade into scaffolds of 10 mm of length. The scaffolds were gamma irradiated for sterility with a minimum irradiation dose of 25 kGy before cell culture by a commercial service supplier. The filamentous PLA 96/4 scaffolds were pretreated for 72 h with DMEM/F-12 with 1 % P/S (v/v) prior to cell seeding.

### 4.3.2 Foamed polymer scaffolds

In study I, the foamed scaffolds were fabricated from PLCL 70/30 (Purasorb PLC 7015, Purac, Corbion) with an inherent viscosity of 1.5 dL/g. The polymer was melt extruded into rods and processed with a supercritical CO<sub>2</sub> reactor system (Waters Operating Corporation, Milford, MA, USA) to create an irregular porous structure. The samples were manually cut to final dimensions of 10 mm of length, 4 mm of width, and 1.4 mm of height on average. Prior to cell culture experiments, the scaffolds were gamma irradiated for sterility with a minimum irradiation dose of 25 kGy by a commercial service supplier. The foamed PLCL 70/30 were pretreated for 72 h with DMEM/F-12 with 1 % (v/v) P/S prior to seeding of cells.

### 4.3.3 Polymeric tendon scaffold mechanical tensile testing

In study I, the mechanical properties of the braided PLA 96/4 scaffolds and the foamed PLCL 70/30 scaffolds were tested by a tensile test method with a universal material testing machine (Instron 4411, series IX Automated Materials Testing System, Norwood, MA, USA). The direct tensile test was performed according to system manual with a crosshead speed of 30 mm/min, a load cell of 500 N, and gauge length at 10 mm position. Briefly, samples were fastened with tensile grips, the load and strain limits were set and measured sample area entered in the system. The experiment was initiated and stopped when the sample broke or when upper extension limit was reached.

The elastic modulus under tension was calculated by system integrated software based on the slope of the linear region of the stress-strain curve where Hooke's law holds (1) (Callister & Rethwisch, 2014).

Hooke's law

$$\sigma = E * \varepsilon \quad (1)$$

where,  $\sigma$  signifies uniaxial stress (tensile or compressive), E denotes elastic modulus or Young's modulus,  $\varepsilon$  means strain (SFS-EN ISO 604. 2002).

#### 4.3.4 Micro-computed tomography imaging of polymeric scaffolds

The micro-computed tomography (micro-CT) characterization of the braided PLA 96/4 and the foamed PLCL scaffolds was performed with MicroXCT-400 microscope (Carl Zeiss X-ray Microscopy, Pleasanton, CA, USA). Subsequently, image analysis was performed with Fiji open-source platform (Schindelin et al., 2012) with BoneJ plugin (ImageJ; U. S. National Institutes of Health, Bethesda, MD, USA) (Doube et al., 2010).

### 4.4 Osteogenic and vascularized bone scaffold manufacture and characterization

#### 4.4.1 Bioactive glass manufacture

The BaG 2-06 granules were manufactured with analytical grade  $\text{Na}_2\text{CO}_3$ ,  $\text{K}_2\text{CO}_3$ ,  $\text{CaCO}_3$ ,  $\text{MgO}$ ,  $\text{CaHPO}_4(2\cdot\text{H}_2\text{O})$ , and Belgian quartz sand (Merck). Briefly, each batch yielding 300 g of glass granules was melted for 3 h at +1 360 °C in Pt crucible, after which the glass was cast and annealed, followed by a step of crushing and remelting to guarantee homogeneous end product. Following annealing, the glass blocks were crushed corresponding to ISO 719:1985 (2011) glass processing standard omitting milling and sieved to collect granules in 500-1 000  $\mu\text{m}$  diameter size range (EN ISO 719:1985. 2011). The BaG granule batches were washed 5 times in acetone solution with ultrasound to remove grain particles from the surface. Finally, the BaG granules were dried at +120 °C to evaporate residual acetone (Ojansivu et al., 2015).

#### 4.4.2 Gellan gum and collagen type I hydrogel scaffolds

Different hydrogel scaffolds were prepared in studies **II-III** for 3D cell culture experiments (Table 8). Different ionic crosslinkers were compared for GG hydrogel crosslinking in study **II**.



Table 8. Gellan gum and collagen type I hydrogel scaffolds and crosslinkers.

Hydrogel	Study	Polymer	GG crosslinker
GG-SPD	II	GG 0.5 % (w/v)	SPD
GG-BaG	II	GG 0.5 % (w/v)	BaG extract
COL	II	COL 3 mg/mL	-
GG-COL	III	1:1 GG 0.5 % (w/v), COL 3 mg/mL	SPD

Abbreviations: COL, collagen type I hydrogel; GG, gellan gum hydrogel; GG-BaG, bioactive glass extract crosslinked gellan gum hydrogel; GG-COL, 1:1 gellan gum-collagen type I hydrogel mixture; GG-SPD, spermidine crosslinked gellan gum hydrogel; SPD, spermidine.

### Gellan gum hydrogel scaffolds

GG (Mw 1.0 kg/mol; Gelzan CM; Merck) solution of 0.5 % (w/v) concentration was dissolved into sterile filtered (0.2  $\mu$ m) 10 % (w/v) sucrose (BioXtra; Merck) in deionized water. After dissolving, the GG solution was heated to +60 °C on a heat plate and sterile filtered (0.2  $\mu$ m). Different crosslinkers were used to physically crosslink GG hydrogels (0.2 cm<sup>3</sup>). Bioamine SPD trihydrochloride (BioXtra; Merck) of 16 % (v/v) concentration was used to crosslink GG-SPD hydrogels. SPD solution of 0.1 % (w/v) was prepared into 10 % (w/v) sucrose (BioXtra; Merck) in deionized water and sterile filtered (0.2  $\mu$ m). For crosslinking of GG-BaG hydrogels, BaG extract was prepared with bioactive glass 2-06 granules of 16 % (v/v) concentration, containing DMEM/F-12, 1 % L-glutamine (GlutaMAX; Thermo Fisher Scientific), and 1 % P/S (Lonza). For the fabrication of both the cell culture experiment samples (see Table 11 in section 4.6) and compression testing samples (see Table 9 in section 4.4.3), the GG solution and the corresponding crosslinker solution were heated to +37 °C and manually mixed to allow immediate gelation in 48-well plate wells (Nunclon Delta Surface; Merck).

### Collagen type I hydrogel scaffolds

Rat tail collagen type I (Gibco; Thermo Fisher Scientific) hydrogels of 3 mg/mL concentration were gelled by mixing at +4 °C gel solution on ice with 1 N NaOH (Merck) and phosphate buffered saline (PBS; Lonza) after which the hASCs suspended in DMEM/F-12, 1 % (v/v) P/S and 1 % (v/v) L-glutamine were added. In the following, the gels were allowed to gelate briefly in RT before the according media were added on top of the hydrogel scaffold.

### Composite gellan gum-collagen type I hydrogel scaffolds

GG 0.5 % (w/v) hydrogel (Mw 1.0 kg/mol; Gelzan CM; Merck) was crosslinked with 16 % (v/v) SPD (1 mg/mL in 10 % (w/v) sucrose in deionized water; BioXtra; Merck). COL (rat tail, 3.0 mg/mL, Gibco; Thermo Fisher Scientific) was neutralized with 1 N NaOH (Merck) and 10x PBS (Lonza) according to manufacturer protocol. The hASCs and HUVECS were encapsulated into non-gelated GG-COL mixture in RT followed by immediate gelation in 48-well plate wells (Nunclon Delta Surface; Merck), and 0.3 cm<sup>3</sup> of according media (see Table 7 section 4.1.3) were added on top.

#### 4.4.3 Hydrogel scaffold mechanical compression testing

For the mechanical measurements in different time points in studies **II** and **III**, cylindrical shaped acellular hydrogel samples (12 mm diameter, 7 mm height, 870  $\mu$ L volume) were cast into custom-made molds of cut 5 mL-syringes (Table 9).

Table 9. Mechanical compression testing of hydrogel scaffolds.

Hydrogel	Study	Polymer	GG crosslinker	Time points	Medium
GG-SPD	II	GG 0.5 % (w/v)	SPD	0 d, 14 d, 21 d	OM
GG-SPD	II	GG 0.5 % (w/v)	SPD	0 d, 14 d, 21 d	BaG OM
GG-BaG	II	GG 0.5 % (w/v)	BaG extract	0 d, 14 d, 21 d	OM
COL	II	COL 3 mg/mL	-	0 d, 14 d, 21 d	OM
COL	II	COL 3 mg/mL	-	0 d, 14 d, 21 d	BaG OM
GG-COL	III	1:1 COL 3 mg/mL, GG 0.5 % (w/v)	SPD	0 d, 7 d, 14 d	EGM-2
GG-COL	III	1:1 COL 3 mg/mL, GG 0.5 % (w/v)	SPD	0 d, 7 d, 14 d	BaG EM-OM

Abbreviations: BaG EM-OM, bioactive glass extract endothelial-osteogenic medium; BaG OM, bioactive glass extract osteogenic medium; COL, collagen type I hydrogel; EGM-2, endothelial cell growth medium-2; GG, gellan gum hydrogel; GG-BaG, bioactive glass extract crosslinked gellan gum hydrogel; GG-COL, 1:1 gellan gum-collagen type I hydrogel mixture; GG-SPD, spermidine crosslinked gellan gum hydrogel; OM, osteogenic medium; SPD, spermidine.

The mechanical compression testing was performed in air environment with unconfined compression rate and a constant 10 mm/min strain rate in RT to 65 % strain of original height. The compressive modulus of triplicate samples was measured with Bose ElectroForce 5100 BioDynamic system (TA Instruments, New Castle, DE, USA) equipped with a 225 N load sensor to measure the compressive load and with the WinTest 4.1 software (WinTest, Yokohama,

Japan) to record the data. The Young's modulus was calculated based on the slope of the stress-strain curve's linear region where the Hooke's law (1) holds (Callister & Rethwisch, 2014; Koivisto et al., 2017) by MS Excel (Microsoft, Redmond, WA, USA).

#### 4.4.4 Optical projection tomography and selective plane illumination microscopy imaging of hydrogel scaffolds

In study **II**, in-house-built 3D imaging systems, optical projection tomography (OPT) and selective plane illumination microscopy (SPIM), were used to image hASCs encapsulated in the transparent GG-SPD hydrogels (Belay, et al. 2017; Soto et al., 2016). The opacity of the COL hydrogel prevented the OPT or SPIM imaging of hASC-laden COL samples. The brightfield OPT imaging showed the morphology of hASCs and their ECM, whereas the 3D distribution of the OsteoImage (Lonza) stained hydroxyapatite residues was obtained with the SPIM fluorescence imaging.

The hASC-laden GG-SPD hydrogel samples were plated into custom-made 1.0-cm inside diameter fluorinated ethylene propylene (FEP; Adtech Polymer Engineering, Stroud, United Kingdom) tubes on a polydimethylsiloxane (PDMS) platform. For the imaging, the cell-laden hydrogels were punctured with 1.0-mm inside diameter FEP tubes (Adtech Polymer Engineering). The brightfield OPT imaging was conducted with a light emitting diode (LED) emitting white light (LTCL23; Opto Engineering, Mantova, Italy) to illuminate the sample in transmission mode. The sample FEP tube was immersed in a transparent cuvette filled with distilled water. During the sample tube 360° degree-rotation, 400 projection images were captured at 0.9°-degree intervals with a 20x objective. The obtained brightfield images were reconstructed using filtered back projection algorithm (Matlab; MathWorks, Natick, MA, USA) (Figueiras et al., 2014). For the fluorescence imaging of hASC mineralization, the samples were fixed with 4 % paraformaldehyde (PFA; Merck) for 1 h in the 1.0-cm inside diameter FEP tubes, followed by staining of the hydroxyapatite residues for 90 min in RT with the OsteoImage Mineralization Assay (Lonza). In the SPIM fluorescence imaging, samples were excited with a 488-nm wavelength (Custom multi-wavelength laser system, Modulight, Tampere, Finland) illumination light sheet. A notch filter (NF03-405/488/561/635E-25 StopLine Quad-Notch filter; Semrock, Rochester, NY, USA) was used in the detection path to cut out the

excitation light from the fluorescent signal emitted by the fluorescent mineralization. In order to acquire the fluorescence image stack, the sample was translated in the axial direction of the detection path and an image was captured at 3- $\mu$ m intervals with a x20 objective. The image stack was acquired in z direction while x and y directions formed the actual image. Avizo 9.3 analysis software (FEI Visualization Sciences Group; Thermo Fisher Scientific) was used for the 3D visualization of the OPT and SPIM images. Due to differences in technical imaging modalities, the brightfield OPT imaged a cylindrical volume ( $d = 0.67$  mm,  $h = 0.67$  mm), whereas the fluorescence SPIM imaged a rectangular volume ( $x = 0.67$  mm,  $y = 0.67$  mm,  $z = 1$  mm). The 3D reconstructions of the OPT and SPIM images were visually superimposed to combine the information provided by both signals.

## 4.5 Cell morphology, viability, and number

In studies **I-III**, cell morphology was verified by light microscopy prior to cell seeding. Cell adhesion and viability were evaluated qualitatively in studies **I-III** with Live/Dead fluorescence staining (Thermo Fisher Scientific) (Table 10). Briefly, the samples were incubated for 45 min in RT in a solution containing 0.5  $\mu$ M calcein acetoxymethyl ester (calcein AM; green fluorescent dye) indicating intracellular esterase activity of living cells and 0.25  $\mu$ M ethidium homodimer-1 (EthD-1; red fluorescent dye) which indicates loss of plasma membrane integrity of necrotic cells. Images of viable green fluorescent cells and necrotic red fluorescent cells were acquired with an epifluorescence phase contrast Olympus IX51 microscope (Olympus, Tokyo, Japan) fitted with an Olympus DP30BW camera (Olympus).

In studies **I-III**, cell number based on the total amount of DNA of the sample was determined quantitatively with the CyQUANT Cell Proliferation Assay Kit (Thermo Fisher Scientific) according to the manufacturer's protocol (Table 10). Briefly, the cells were lysed with 0.1 % Triton X-100 buffer (Merck), stored in  $-80$  °C until analysis and analyzed after a single freeze-thaw cycle in studies **I-III**. In studies **II** and **III**, the hydrogel samples were mechanically homogenized by the Ultra-Turrax tissue homogenizer (IKA Labortechnik, Staufen, Germany) with the 0.1 % (v/v) Triton X-100 buffer. The thawed samples were treated with kit provided CyQUANT GR dye and Cell lysis buffer. The blue-green

fluorescence of 3 parallel samples was measured at 480/520 nm with Victor 1420 Multilabel Counter microplate reader (PerkinElmer, Waltham, MA, USA).

Table 10. Cell viability and cell number analyses' timepoints.

<b>Analysis</b>	<b>Study</b>	<b>Time points</b>
Cell viability	I	7 d, 14 d
	II	7 d, 14 d
	III	7 d, 14 d
Cell number	I	1 d, 7 d, 14 d
	II	14 d, 21 d
	III	7 d, 14 d

## 4.6 Differentiation of human adipose stem cells

Different factors guide hASC growth and differentiation, including the biomaterial scaffold design and soluble cues. The cell seeding densities, the applied biomaterials, and the selected scaffolds varied depending on the study. In studies **I-III**, hASC was analyzed with several different analysis methods (Table 11).

Table 11. Differentiation markers and analyses performed in studies I-III.

Differentiation markers	Analyses	Time point	Study
<i>Tenogenic markers</i>			
Cell morphology	Live/Dead analysis	7 d, 14 d	I
Proliferation	Cell number	7 d, 14 d	
SCX, COL3A1, COL1A1, TNMD expression	Real-time polymerase chain reaction	7 d, 14 d	
COL I, II, III, IV, V production	Total collagen content	14 d	
Calcium deposit staining	Mineralization (Alizarin Red S)	14 d	
COL1, TNMD production	Immunocytochemistry	14 d	
<i>Osteogenic markers</i>			
Cell morphology	Live/Dead analysis	3 d, 14 d	II
Cell morphology, ECM growth	OPT 3D imaging	21 d	
Proliferation	Cell number	14 d, 21 d	
ALPL, RUNX2, DLX5, OSX expression	Real-time polymerase chain reaction	14 d, 21 d	
Hydroxyapatite staining	Mineralization (OsteoImage): Quantitative measurement and imaging	21 d	
	SPIM 3D imaging	21 d	
Hydroxyapatite residues	Raman spectroscopy	21 d	
OCN production	Immunocytochemistry	21 d	
Cell morphology	Live/Dead analysis	7 d, 14 d	III
Proliferation	Cell number	7 d, 14 d	
RUNX2, DLX5, OSX expression	Real-time polymerase chain reaction	7 d, 14 d	
Hydroxyapatite staining	Mineralization (OsteoImage) imaging	14 d	
OCN production	Immunocytochemistry	14 d	
<i>Endothelial markers</i>			
Cell morphology	Live/Dead analysis	7 d, 14 d	III
Proliferation	Cell number	7 d, 14 d	
PECAM-1, VWF expression	Real-time polymerase chain reaction	7 d, 14 d	
CD31 production	Immunocytochemistry	14 d	

Abbreviations: ALPL, alkaline phosphatase (liver/bone/kidney) transcript variant 1; CD31, cluster of differentiation 31; COL1A1, collagen type I alpha 1 chain; COL3A1, collagen type III alpha 1 chain; DLX5, distal-less homeobox 5; ECM, extracellular matrix; OCN, osteocalcin; OSX, osterix transcript variant 2; PECAM-1, platelet endothelial cell adhesion molecule-1; RUNX2, runt related transcription factor 2 transcript variant 1; SCX, scleraxis; TNMD, tenomodulin; VWF, von Willebrand factor.

#### 4.6.1 Tenogenic differentiation with chemical stimulus and scaffold properties

In the preliminary 2D medium optimization in study **I**, the hASCs were plated at a density of  $1.5 \times 10^4$  cells in 24-well plate wells (Nunclon Delta Surface; Merck) ( $79,000$  cells/cm<sup>2</sup>). Tenogenic induction was initiated 5 d after plating in the preliminary 2D experiments by adding tenogenic medium (TM) of different formulations (see Table 7 in section 4.1.3). In the following 3D experiments, the selected optimized TM3 was added 24 h after plating to induce tenogenic differentiation. The control cell cultures were maintained in MM.

In study **I** preliminary 2D medium optimization experiments, 3 different differentiation medium compositions TM1, TM2, and TM3 (see Table 7 in section 4.1.3) were tested for hASC tenogenic differentiation and hASCs from 3 donors were cultured in MM were used as a control. The tested chemical stimuli included 50 ng/mL or 100 ng/mL of GDF-5 and 50 ng/mL of GDF-5 in combination with 280  $\mu$ M L-ascorbic acid.

##### Cell seeding density in study **I**

In study **I** scaffold experiments, the hASCs were seeded on top of the pretreated filamentous PLA 96/4 and foamed PLCL 70/30 scaffolds at a density of  $1.5 \times 10^5$  hASCs in a volume of 30  $\mu$ L of MM.

##### Scaffold structure in study **I**

In study **I**, 2 different 3D scaffold architectures were compared for tenogenic differentiation of hASCs; the filamentous braided PLA 96/4 scaffolds and foamed PLCL 70/30 scaffolds. The mechanical properties of the supporting scaffold protect and provide mechanical support to the seeded cells during tissue engineered construct growth and maturation. The mechanical tensile testing of the braided PLA 96/4 and foamed PLCL 70/30 scaffolds was performed (see section 4.3.3).

The structure of the filamentous PLA 96/4 scaffold consisted of an 8-filament braid where the diameter of a single fiber was 80  $\mu$ m. The porosity of the structure affects stem cell growth and differentiation, and the porosity of the foamed PLCL 70/30 scaffolds was analyzed with micro-CT.

## 4.6.2 Osteogenic differentiation with chemical stimulus and scaffold properties

### Cell seeding densities in studies II-III

In study **II**, the hASCs were suspended at a density of  $1.9 \times 10^5$  cells in a hydrogel volume of 200  $\mu$ L ( $9.5 \times 10^5$  cells/mL) prior to gelation. In study **III**, the hASCs and HUVECs were mixed in a 1:1 ratio for a total cell density of  $2.0 \times 10^5$  cells in a total hydrogel volume of 200  $\mu$ L prior to gelation (final cell density  $1.0 \times 10^6$  cells/mL).

### Osteogenic preconditioning of human adipose stem cells

In study **III**, hASCs were expanded in MM followed by a 7-day preconditioning with OM (OM-primed) in cell culture flasks prior to cell seeding into 3D hydrogel and cultured with either EGM-2 with 2 % HS or BaG EM-OM (see Table 7 in section 4.1.3) in the experiment.

### Chemical stimuli and scaffold properties in study II

In study **II**, BaG OM was compared with regular OM in 3D hydrogel culture to determine the effect on hASC osteogenic differentiation in a 21-day experiment. The GG and COL hydrogels in study **II** offered hASCs a 3D environment.

Osteogenic induction began immediately after plating with the addition of 0.3 cm<sup>3</sup> of either OM (see Table 7 in section 4.1.3) or BaG OM to the hASC-laden hydrogels. For the sake of avoiding phenol red caused interference to Raman spectra, hASCs were cultured in phenol red free media for the Raman analysis (Ojansivu et al., 2015) (see Table 14 in section 4.7.5). The control samples for Raman spectroscopic analysis were cultured in OM. What is more, mechanical properties of different hydrogels were measured following incubation in OM or BaG OM media.

## 4.6.3 Three-dimensional coculture in hydrogels

3D coculture of hASCs and HUVECs in 1:1 ratio was performed in study **III** in composite GG-COL hydrogels for microvascularization of bone-like tissue. Following cell suspension into GG and COL hydrogels, manual mixing of cell-laden hydrogels equally in 1:1 ratio and consequent gelation, either EGM-2 or BaG EM-OM media were added to initiate osteogenic differentiation and



promote initial growth of microvascularization. Final volume of composite GG-COL hydrogel samples was 0.2 cm<sup>3</sup>. The composite GG-COL hydrogels were cast into 48-well plate wells (Nunclon Delta Surface; Merck). After gelation, 0.3 cm<sup>3</sup> of either EGM-2 or BaG EM-OM media were added on top.

## 4.7 Analysis of human adipose stem cell differentiation

### 4.7.1 Quantitative real-time polymerase chain reaction

Quantitative real-time polymerase chain reaction (qRT-PCR) analysis was used to compare the relative expression of tenogenic, osteogenic and endothelial genes. In study **I**, total sample RNA was isolated at 14 d for the medium optimization experiments, and at 7 d and 14 d for the scaffold experiments with the NucleoSpin RNA II kit (Macherey-Nagel, Düren, Germany) according to manufacturer's instructions. In study **II**, total sample RNA was isolated 14 d and 21 d time points, whereas in study **III**, 7 d and 14 d samples were analyzed. First strand cDNA of total RNA was synthesized using High-Capacity cDNA Reverse Transcriptase Kit (Applied Biosystems, Foster City, CA, USA). The obtained data was normalized using human acidic ribosomal phosphoprotein P0 (*bRPLP0*) (Oligomer) as a housekeeping gene. In study **I**, the gene expression of *collagen type I* (*COL1A1*, abbreviated as *COL1*; TAG Copenhagen, Frederiksberg, Denmark), *collagen type II* (*COL2A1*, abbreviated as *COL2*; Oligomer, Helsinki, Finland), *collagen type III* (*COL3A1*, abbreviated as *COL3*; Oligomer), *SCX* (Oligomer) and *tenomodulin* (*TNMD*; Oligomer) was measured. In study **II**, gene expression of osteogenic genes *ALPL*, *DLX5*, *RUNX2* and *OSX* was measured at 14 d and 21 d. In study **III**, osteogenic gene expression of *DLX5*, *RUNX2*, and *OSX* was measured in addition to endothelial gene expression of *VWF* and *PECAM-1* (QuantiTect Primer Assays; 10x). Relative gene expression of each sample in relation to *bRPLP0* was calculated according to a mathematical data analysis model (Pfaffl 2001). The qRT-PCR mixture contained 50 ng cDNA, 300 nM forward and reverse primers, and SYBR Green PCR Master Mix (Applied Biosystems; Thermo Fisher Scientific). The used primer sequences and accession numbers are presented in Table 12. The qRT-PCR reactions were performed with ABI PRISM 7300 Sequence Detection System (Applied Biosystems; Thermo Fisher Scientific) initially at +95 °C for 10 min enzyme

activation, and by 45 cycles at +95 °C for 15 s denaturation followed by 60 s at +60 °C for annealing and extension.

Table 12. The primer sequences for qRT-PCR.

Name	Primer	5'-Sequence-3'	Accession number
<i>hRPLP0</i>	Fwd	AATCTCCAGGGGCACCATT	NM_001002
	Rev	CGCTGGCTCCCACTTTGT	
<i>SCX</i>	Fwd	CAGCGGCACACGGCGAAC	BK000280
	Rev	CGTTGCCAGGTGCGAGATG	
<i>COL3A1</i>	Fwd	CAGCGGTTCTCCAGGCAAGG	NM_000090
	Rev	CTCCAGTGATCCAGCAATCCC	
<i>COL1A1</i>	Fwd	CCAGAAGAACTGGTACATCAGCAA	NM_000088.3
	Rev	CGCCATACTCGAACTGGAATC	
<i>COL2A1</i>	Fwd	GAGACAGCATGACGCCGAG	NM_001844
	Rev	GCGGATGCTCTCAATCTGGT	
<i>TNMD</i>	Fwd	CCATGCTGGATGAGAGAGGTT	NM_022144
	Rev	TTGGTAGCAGTATGGATATGGGT	
<i>ALPL</i>	Fwd	CCC CCG TGG CAA CTC TAT CT	NM_000478.4
	Rev	GAT GGC AGT GAA GGG CTT CTT	
<i>RUNX2</i>	Fwd	CTTCATTGCGCTCACAAACAAC	NM_001024630.3
	Rev	TCCTCCTGGAGAAAAGTTTGCA	
<i>OSX</i>	Fwd	TGAGCTGGAGCGTCATGTG	NM_152860.1
	Rev	TCGGGTAAGCGCTTGGA	
<i>DLX5</i>	Fwd	ACCATCCGTCTCAGGAATCG	NM_005221.5
	Rev	CCCCCGTAGGGCTGTAGTAGT	
<i>VWF</i>	Fwd	AGAAACGCTCCTTCTCGATTATTG	NM_000552
	Rev	TGTCAAAAAATTCCCCAAGATACAC	
<i>PECAM-1</i>	Fwd	AAGTGGAGTCCAGCCGCATATC	NM_000442.4
	Rev	ATGGAGCAGGACAGGTTTCAGTC	

#### 4.7.2 Total collagen content

In study **I**, the total collagen content was analyzed at 14 d using a quantitative Sircol Soluble Collagen Assay (Biocolor, Carrickfergus, Northern Ireland, United Kingdom) for analysis of acid or pepsin soluble mammalian collagen types I-V. In brief, acid soluble collagen was extracted from the samples with 0.5 M acetic acid (Merck) containing 0.1 mg/mL pepsin (Merck). Sircol Dye reagent (Biocolor), comprised of Sirius Red and picric acid, was added to liquid samples and incubated for 30 min in order for the mammalian collagen types I-V with a [Gly-X-Y] peptide sequence to form a complex with the dye. The collagen-dye

pellet was washed to remove any unbound dye and alkali reagent of 0.5 M sodium hydroxide solution (Biocolor) was added in order to resolubilize the collagen. Finally, the intensity of red dye in 2 parallel samples was measured with Victor 1420 microplate reader at 540 nm (PerkinElmer).

### 4.7.3 Mineralization

#### Alizarin Red S calcium deposit mineralization assay

Late osteogenic differentiation of hASCs was studied by Alizarin Red S method at 14 d in study **I**. Briefly, the PFA-fixed cell-scaffold constructs were stained with filtered 2 % Alizarin Red S (pH 4.2; Merck). Dye was extracted with cetylpyridinium chloride (100 mM, Merck) and the intensity of the dye was determined by measuring absorbance at 540 nm with microplate reader Victor 1420 (PerkinElmer). In study **I**, mineralization was measured at 14 d in order to exclude unwanted mineralization indicating bone-like matrix formation.

#### OsteoImage hydroxyapatite mineralization assay

In study **II**, hydroxyapatite deposits were analyzed by OsteoImage Mineralization Assay (Lonza) at 21 d time point, whereas in study **III**, the cell-laden hydrogel samples were stained at 14 d. Briefly, cell-laden samples as well as acellular controls were fixed by 4 % PFA and stained according to kit instructions. The sample hydroxyapatite portion was quantitatively measured with Victor 1420 microplate reader at 492/520 nm (PerkinElmer) in study **II**. In study **III**, the unhomogeneous and fractured properties of the GG-COL composite hydrogels prevented the quantitative measurement. After subsequent 4',6-diamidino-2-phenylindole (DAPI, Merck) staining detected at 361 nm, mineralized hydroxyapatite residues were imaged at 492/520 nm using a phase contrast Olympus IX51 microscope with fluorescence optics and Olympus DP30BW camera (Olympus).

### 4.7.4 Immunocytochemistry

Immunocytochemical stainings were performed for qualitative observation of different tenogenic, osteogenic, or endothelial markers. In study **I**, tenogenic marker production was detected at 14 d. In study **II**, osteogenic marker production was observed at 21-day time point, whereas in study **III**, endothelial

and osteogenic marker proteins were stained at 14 d. Prior to immunocytochemical stainings in studies **I-III**, the samples were fixed with 4 % PFA (Merck) in Dulbecco's phosphate buffered saline (DPBS; Merck). In study **I**, a blocking solution of 0.05 % Triton X-100 buffer (Merck) and 10 % goat serum (Thermo Fisher Scientific) in DPBS was used to block nonspecific binding sites. In study **II**, the blocking solution contained 10 % normal donkey serum (Merck) and 1 % bovine serum albumin (BSA; Merck) in 0.1 % Triton X-100 (Merck) in PBS, whereas in study **III**, the blocking solution contained 10 % goat serum (Thermo Fisher Scientific). The primary antibodies, secondary antibodies and the dilutions thereof are presented in Table 13. Cell nuclei were stained with DAPI (Merck, dilution 1:2000) in PBS in studies **I-III**. Imaging was performed using a confocal LSM 780 microscope (ZEISS, Oberkochen, Germany) in study **I** and for Z-stacks of hydrogel samples in study **III**. In study **II**, immunocytochemical imaging was conducted with an Olympus IX51 phase contrast microscope with fluorescence optics and Olympus DP30BW camera (Olympus).

Table 13. Immunocytochemical stainings in studies I-III.

Primary antibody	Study	Dilution	Secondary antibody	Dilution
Mouse anti-human COL1	<b>I</b>	1:2000	A488 Goat anti-mouse IgG (H+L)	1:200
Rabbit anti-human TNMD	<b>I</b>	1:50	A594 Goat anti-rabbit IgG (H+L)	1:100
Mouse anti-human CD31	<b>III</b>	1:20	A488 Goat anti-mouse IgG (H+L)	1:200
Mouse anti-human OCN	<b>II</b>	1:100	A488 Donkey anti-mouse IgG (H+L)	1:400
Rabbit anti-human OCN	<b>III</b>	1:25	A594 Goat anti-rabbit IgG (H+L)	1:100

Abbreviations: CD31, platelet endothelial cell adhesion molecule (mouse anti-human CD31, Dako, Glostrup, Denmark); COL1, collagen type I (mouse anti-human COL1, Abcam, Cambridge, United Kingdom); OCN, Osteocalcin (mouse anti-human OCN, Abcam (study **II**), rabbit anti-human OCN, Bio-Rad, Hercules, CA, USA (study **III**)); TNMD, tenomodulin (rabbit anti-human TNMD, Santa Cruz, Biotechnology, Dallas, TX, USA). Highly cross-adsorbed Alexa Fluor (A488, A594) secondary antibodies manufactured by Thermo Fisher Scientific.

#### 4.7.5 Raman spectroscopy

In study **II**, hASC osteogenic differentiation and mineralized ECM hydroxyapatite residues containing inorganic phosphate  $\text{PO}_4^{3-}$  were analyzed with Raman spectroscopy. Raman shift at  $960 \text{ cm}^{-1}$  indicated hydroxyapatite inorganic phosphate. For the semi-quantitative method, hASCs from 1 donor embedded

within GG-SPD, GG-BaG, and COL 3D hydrogels were cultured with phenol red free medium along with acellular control hydrogel samples to avoid interference of phenol red fluorescence to Raman spectra (Table 14, for other media compositions see Table 7 in section 4.1.3).

Table 14. Raman spectroscopy cell culture media in study II.

Medium	Composition
Raman spectroscopy cell culture medium	Phenol red free DMEM/F-12 1:1 including L-glutamine, 5 % (v/v) HS, 1 % (v/v) P/S
Raman spectroscopy phenol red free BaG OM	OM in phenol red free BaG ext base

Abbreviations: BaG OM, bioactive glass extract osteogenic medium; phenol red free DMEM/F-12, Phenol Red Free Dulbecco's Modified Eagle Medium/Ham's Nutrient Mixture F-12 (Thermo Fisher Scientific); HS, human serum (Biowest); L-glutamine (GlutaMAX; Thermo Fisher Scientific); OM, osteogenic medium; P/S, 100 U/mL penicillin/streptomycin (Lonza).

Preceding analysis at 21 d, samples were washed with 1x PBS and the Raman spectra was obtained as described previously (Ruokola et al., 2014). The reference spectra of acellular samples were subtracted from the measured spectra of cell-laden hydrogel samples.

#### 4.7.6 Statistical analyses

Non-parametric tests were applied due to non-Gaussian distribution and relatively small  $n$  values. For statistical significance,  $p$ -values  $< 0.05$  were considered. The data were analyzed with IBM SPSS Statistics versions 19, 22 and 23 software (IBM, Armonk, NY, USA). The data are presented as mean and SD.

In study I, the significance of differences between means was determined using one-way analysis of variance (ANOVA) with Bonferroni's *post hoc* test to determine which groups were significantly different. The 3D scaffold experiments were conducted with hASCs from 3 different donors and with 3 parallel samples in the analyses of cell number, total collagen content, and Alizarin Red S mineralization resulting in  $n = 9$  for each assay, whereas the gene expression analysis was performed with 2 parallel samples resulting in  $n = 6$ .

In study II, the significance of differences between the means was determined using Mann-Whitney U Test. 3-6 parallel samples were tested for hydrogel mechanical compression testing ( $n = 3-6$ ). The experiments with cells were repeated with hASCs from 3 different donors. The analysis for cell number was repeated with 3 parallel samples ( $n = 9$ ), whereas the gene expression analysis was

performed with 2 parallel samples ( $n = 6$ ). The OsteoImage mineralization assay was conducted with 1-2 parallel samples for the GG-SPD in OM and BaG OM groups ( $n = 5$ ), whereas for COL in BaG OM only 2 hASC donors were tested with 2 parallel samples ( $n = 4$ ) due to contracted hydrogels.

In study **III**, the significance of differences between mean ranks for equal distributions was analyzed using Mann-Whitney U Test. 3 parallel samples were tested for hydrogel mechanical compression testing ( $n = 3$ ). The cell number analyses were repeated with 3 different hASC donors with 3 samples for each condition ( $n = 9$ ). The gene expression analyses were repeated with 3 different hASC donors with 1-2 samples due to values below analysis threshold ( $n = 3-6$ ).

## 5 RESULTS

### 5.1 Biomaterial characterization

The braided PLA 96/4 and foamed PLCL scaffolds that were used in study **I** were imaged with micro-CT in order to visualize the biomaterial structures that hASCs directly adhered to. The influence of biomaterial scaffold surface topography on cell behavior, including cell adhesion and stem cell differentiation capacity, has been widely reported (Ahn et al., 2014; de Peppo et al., 2014; Kolind et al., 2012). In addition, interior architecture of biomaterial scaffold is of great importance in allowing diffusion of nutrients, removal of waste products and cell growth, also in the interior parts of the cell-seeded construct (Boschetti et al., 2006).

Overall, the micro-CT characterization of the braided PLA 96/4 and foamed PLCL polymer scaffolds showed the different scaffold surfaces, structures, and topographies available for hASCs. Further, in study **I**, the braided PLA 96/4 and the foamed PLCL scaffolds were characterized by mechanical tensile testing. In studies **II-III**, the hydrogel scaffolds were characterized by mechanical compression testing, however, the hydrogel scaffolds were not imaged with optical methods such as OPT due to opacity of the COL hydrogel which also restricted comparison of hydrogel textures.

#### 5.1.1 Micro-computer tomography imaging

##### Poly lactide scaffolds

In study **I**, micro-CT imaging with 5  $\mu\text{m}$ -resolution (MicroXCT-400, Zeiss) of the PLA 96/4 scaffolds showed the braided filamentous architecture of the biomaterial scaffold structure for tendon applications (Figure 7A). In the PLA 96/4 scaffold structure, each braid consisted of 8 parallel 80  $\mu\text{m}$ -diameter filaments. The scaffold structure was practically 2D which impeded detailed analysis of the porosity of the braided PLA 96/4 scaffold structure in study **I**.

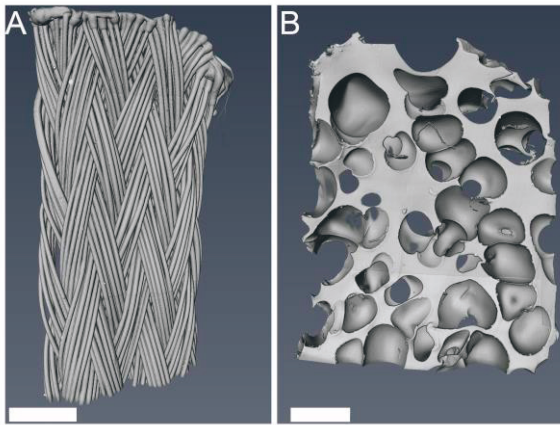


Figure 7. Micro-CT image of A) Braided PLA 96/4 tenogenic scaffold;  
 B) CO<sub>2</sub>-processed foamed PLCL tenogenic scaffold. Scale bar 1 000  $\mu$ m.

### Poly(L-lactic-co- $\epsilon$ -caprolactone) scaffolds

Micro-CT imaging (MicroXCT-400, Zeiss) in study **I** showed the complex irregular porous structure of the foamed polymer PLCL scaffolds for tendon TE applications (Figure 7B). The porosity of the CO<sub>2</sub>-processed foamed PLCL scaffold was analyzed based on micro-CT imaging and reported as 66(2) % with a range of pore sizes between 300-500  $\mu$ m. Porosity and pore size were calculated from micro-CT images with Fiji (Schindelin et al., 2012) using BoneJ plugin (Doube et al., 2010).

## 5.1.2 Mechanical testing

### Tensile testing

For tendon TE applications, the biomaterial mechanical properties were analyzed with tensile testing in study **I**. The elastic modulus, or Young's modulus, of the braided PLA 96/4 scaffolds was reported to be 280(20) MPa. In contrast, for the foamed PLCL scaffolds, the elastic modulus was 1.6(0.6) MPa.

### Compression testing

The compression testing of acellular GG-SPD, GG-BaG and COL hydrogels in study **II** for bone TE applications and composite GG-COL hydrogels in study **III** for vascularized bone TE was conducted. To assess the effect of cell culture media on hydrogel mechanical properties, the compression testing of the



cell-free hydrogel samples was performed with or without serum containing media incubation in studies **II** and **III**. In study **II**, the incubation media for GG-SPD and COL hydrogels were OM or BaG OM, whereas OM alone was used for GG-BaG hydrogels in GG crosslinker comparison testing (Figure 8A). In study **III** for vascularized bone applications, the incubation media for composite GG-COL hydrogels were EGM-2 and BaG EM-OM (Figure 8B). The 0 d testing samples were incubated overnight at 37 °C without media in custom-made molds of cut 5 mL-syringes covered with parafilm.

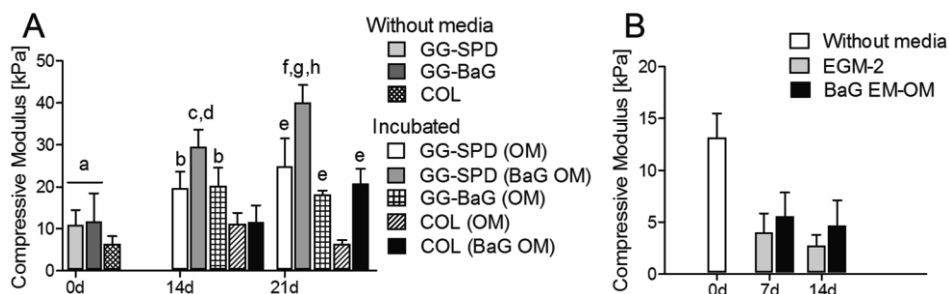


Figure 8. Mechanical compression testing of acellular hydrogels. A) GG-SPD, GG-BaG, and COL hydrogel samples incubated in OM or BaG OM media were tested at 0, 14, and 21 d in study **II** ( $n = 3-6$ ). Data are presented as mean + SD. Significant difference with  $p < 0.05$ : **a**: from COL hydrogel samples at 0 d; **b**: from COL (OM) at 14 d; **c**: from GG-SPD (OM) at 14 d; **d**: from GG-BaG (OM) at 14 d; **e**: from COL (OM) at 21 d; **f**: from GG-SPD (OM) at 21 d; **g**: from GG-BaG (OM) at 21 d; **h**: from COL (BaG OM) at 21 d; B) GG-COL hydrogel samples incubated in EGM-2 or BaG EM-OM media tested at 0, 7, and 14 d in study **III** ( $n = 3-6$ ).

In the results of study **II**, the compressive moduli of GG-SPD hydrogels with OM and BaG OM media incubation and that of GG-BaG with OM incubation increased. Even without media incubation, the tested GG hydrogel samples had significantly higher Young's modulus than COL hydrogel samples. In media incubation, the OM condition increased the compressive moduli of all hydrogels until 14 d, however, the modulus of GG-SPD alone increased towards 21 d in OM. The measured Young's modulus of GG-SPD hydrogels persisted higher compared to GG-BaG hydrogels with OM incubation at 14 d and 21 d. However, COL hydrogels incubated in OM had the lowest compressive modulus in all the measured time points. In contrast, BaG OM incubation increased the moduli of both COL and GG-SPD hydrogels with a growing trend towards 21 d. Indeed, the compressive moduli of BaG OM-incubated GG-SPD hydrogels were significantly higher compared to those of OM-incubated samples at both 14 d and 21 d. At 3 weeks, the BaG OM-incubated GG-SPD hydrogels had the

highest Young's modulus at 40.2(4.1) kPa which was significantly higher compared to GG-BaG samples with OM incubation at 18.1(1.0) kPa or that of COL with BaG OM incubation at 20.9(3.4) kPa or with OM incubation at 6.3(1.1) kPa. Overall, the GG-SPD samples had higher stiffness and were more brittle with a clear fracture point in the stress-strain curve, whereas COL and GG-BaG samples demonstrated ductile behavior and plastic deformation properties without a fracture point in the stress-strain curve.

In study **III**, the GG-COL compression testing results showed the degradation of composite hydrogel mechanical properties. The highest Young's modulus value was measured for the 0 d GG-COL hydrogel samples at 12.9(1.9) kPa. The Young's moduli of acellular GG-COL hydrogel samples continued to decrease in time from 7 d to 14 d of incubation in EGM-2 or BaG EM-OM media. However, the measured mechanical properties persisted higher in the BaG EM-OM condition compared to the EGM-2 incubation at both 7 d to 14 d.

## 5.2 Human adipose stem cell and human umbilical vein endothelial cell characterization

### 5.2.1 Human adipose stem cell characterization

The flow cytometric analysis showed that hASCs expressed the surface markers CD73, CD90, and CD105, and lacked the expression of the CD3, CD11a, CD14, CD19, CD45, CD80, and CD86, whereas the expression of CD34, CD54, and HLA-DR was moderate (Table 15). The ISCT guideline defines strong negative expression as that below 2 % and positive expression as that above 95 %. In studies **I-III**, the expression average of CD73 was below 95 %, and that of CD105 was equally below 95 % in study **I**, which might have been due to hASC low passage although expected to increase with higher passages (Mitchell et al., 2006). There was a slight albeit non-significant increase of CD45 expression average of hASCs in study **II**. The elevation of CD34 and CD54 expressions in studies **I-III** was attributed to low hASC passage and to a known effect of HS as a medium component (Patrikoski et al., 2013). Overall, the cell surface marker flow cytometry analysis indicated the mesenchymal origin of the cells in accordance with the ISCT minimal criteria for multipotent MSCs (Dominici et

al., 2006; Lindroos et al., 2011; McIntosh et al., 2006). The isolated hASCs tested negative for mycoplasma contamination.

Table 15. Surface marker expression of undifferentiated hASCs in studies I-III. The data are presented as mean and SD.

Antigen	Surface protein	Study I	Study II	Study III
CD 3	T cell signal transduction	0.2(0.1)	0.5(0.4)	0.5(0.4)
CD 11a	Lymphocyte function-associated antigen 1	0.4(0.3)	1.3(0.6)	1.3(0.8)
CD 14	Serum lipopolysaccharide binding protein	0.9(0.8)	0.9(0.8)	1.0(0.8)
CD 19	B lymphocyte-lineage differentiation antigen	0.6(0.5)	0.6(0.4)	0.5(0.4)
CD 34	Sialomucin-like adhesion molecule	8.9(6.1)	31.9(19.4)	24.8(19.0)
CD 45	Leukocyte common antigen	1.3(0.9)	2.2(0.7)	2.0(1.2)
CD 54	Intercellular adhesion molecule 1	4.9(2.8)	13.8(6.0)	11.9(9.5)
CD 73	Ecto-5'-nucleotidase	78.5(11.2)	93.4(7.7)	89.1(8.8)
CD 80	B lymphocyte activation antigen B7	0.4(0.3)	0.9(0.8)	0.9(0.9)
CD 86	B lymphocyte activation antigen B7-2	0.6(0.6)	0.9(0.8)	1.1(0.8)
CD 90	Thy-1 (T cell surface glycoprotein)	97.8(4.1)	98.9(1.3)	98.7(1.5)
CD 105	SH-2 endoglin	93.2(4.5)	98.2(1.1)	96.4(3.4)
HLA-DR	Human leukocyte antigen HLA class II	1.3(1.1)	1.0(0.7)	1.0(0.9)

## 5.2.2 Human umbilical vein endothelial cell characterization

In study **III**, the flow cytometric analysis showed that HUVECs expressed the surface markers CD31 (99.5 %), CD34 (42.9 %), CD73 (99.9 %), CD105 (70.7 %), and CD146 (99.9 %), whereas the expression of VEGFR3 (27.8 %) and CD144 (12.9 %) was moderate. The isolated HUVECs lacked the expression of CD90 (5.7 %).

## 5.3 Cell morphology, viability, and number

### 5.3.1 Cell viability and morphology

In the results of Live/Dead analysis in studies **I-III**, the viable cells were imaged with green fluorescent calcein AM stain, excitation/emission at 494/517 nm, whereas the necrotic cells were imaged with red fluorescent EthD-1 stain, excitation/emission at 517/617 nm.

In study **I**, the hASCs were viable in both the MM and TM conditions. In the TM condition, the well elongated hASCs formed a uniform cell layer on the braided PLA 96/4 scaffolds, whereas in the MM condition, the cells remained in small clusters (Figure 9).

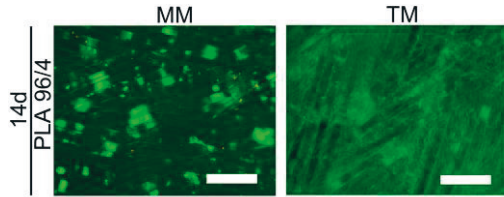


Figure 9. Cell viability in study I. The effect of the optimized TM shown on hASC morphology and viability on braided PLA 96/4 scaffolds in MM and TM conditions at 14 d. Viable cells stained green and necrotic cells stained red. Representative images with hASCs from 1 donor. Scale bar 500  $\mu$ m.

In study **II**, good viability of hASCs encapsulated in GG-SPD (OM), GG-SPD (BaG OM), COL (OM) and COL (BaG OM) 3D hydrogels was observed at 3 d and 14 d (Figure 10). As an exception, the COL (OM) samples contracted after 3 d and were therefore unavailable at 14 d.

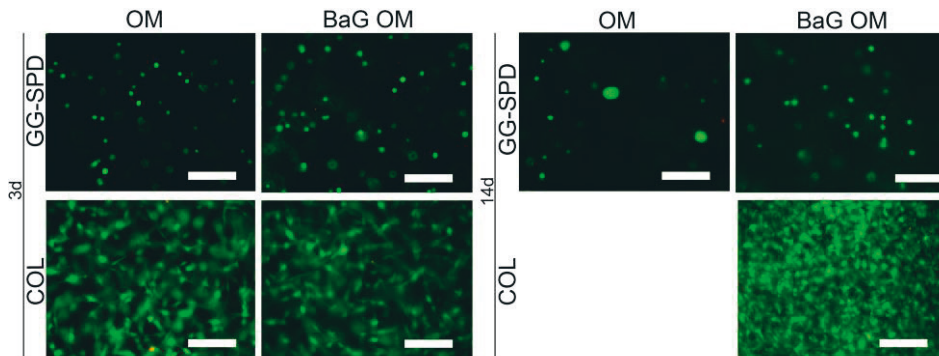


Figure 10. Cell viability in study II. The hASCs embedded within GG-SPD (OM), GG-SPD (BaG OM), COL (OM) and COL (BaG OM) hydrogels at 3 d and 14 d. The hASCs were isolated from 1 donor. The COL (OM) samples contracted after 3 d. Scale bar 200  $\mu$ m.

In study **III**, Live/Dead staining portrayed good hASC viability encapsulated within GG-COL composite hydrogels with elongated cell morphologies

(Figure 11). Formation of reticular structures was observed in the EGM-2 conditions with both the non-primed MM-cultured and OM-primed cells at 7 d and 14 d. In contrast, the hASCs cultured in the BaG EM-OM condition showed restricted elongation and reticulated structures were less visible.

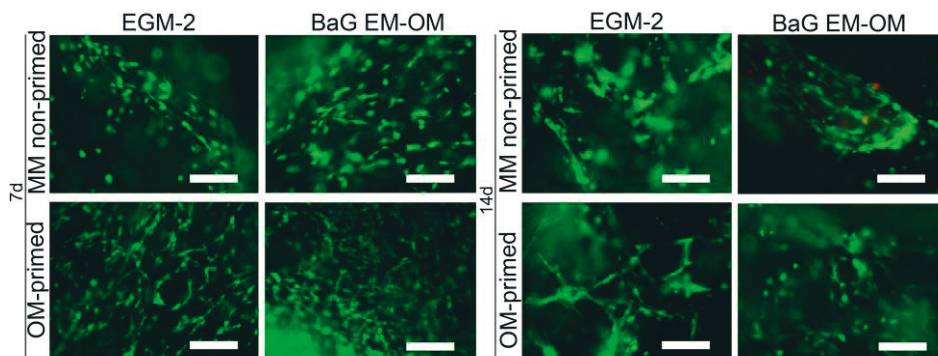


Figure 11. Cell viability in study III. Cocultured hASCs and HUVECs embedded within composite GG-COL hydrogels in EGM-2 or BaG EM-OM media culture with hASCs cultured in MM or preconditioned in OM prior to cell encapsulation. Analyzed at 7 d and 14 d. The hASCs were isolated from 2 donors and HUVECs from 1 donor. Scale bar 200  $\mu\text{m}$ .

Overall, good cell viability was observed in studies **I-III**. The different biomaterial scaffolds and media conditions showed a visible impact on cell adhesion, morphology, and elongation.

### 5.3.2 Cell number

In study **I**, the relative cell number based on the total DNA content of hASCs cultured with the optimized TM was higher in the braided PLA 96/4 scaffolds compared to the foamed PLCL scaffolds at 7 d and 14 d (Figure 12A). Further, significantly higher hASC proliferation was measured in the TM condition in the braided PLA 96/4 scaffolds compared to the MM condition at 7 d and 14 d (Figure 12B).

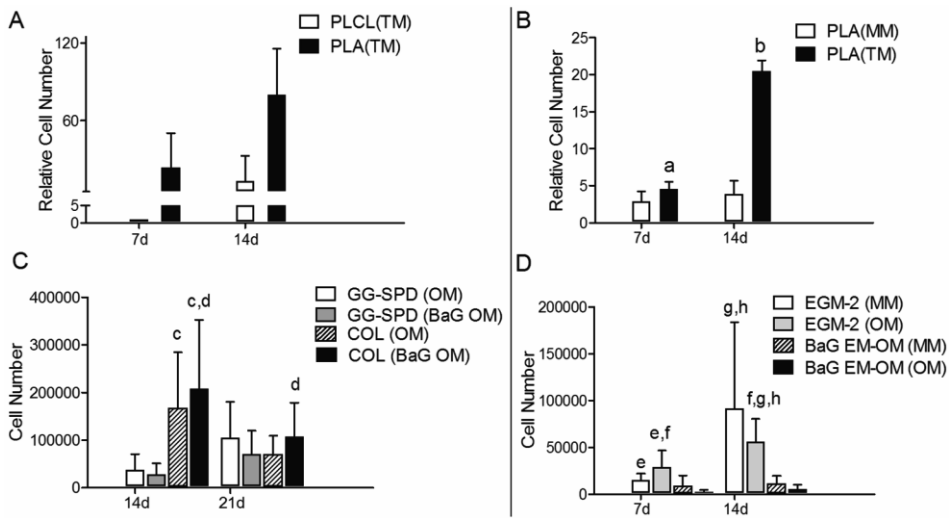


Figure 12. Cell number in studies I-III. Data are presented as mean + SD. Results based on hASCs from 3 donors ( $n = 9$ ). **A)** Relative cell number of hASCs cultured with TM in the braided PLA 96/4 scaffolds compared to the foamed PLCL scaffolds at 7 d and 14 d in study I; **B)** Relative cell number of hASCs in the braided PLA 96/4 scaffolds cultured with TM compared to MM at 7 d and 14 d in study I. Significant difference with  $p < 0.05$ : **a:** from MM at 7 d; **b:** from MM at 14 d; **C)** The hASC cell number in 3D GG and COL hydrogels measured at 14 d and 21 d in study II. Significant difference with  $p < 0.05$ . **c:** Combined COL (OM) and COL (BaG OM) group cell numbers significantly higher compared to combined GG-SPD (OM) and GG-SPD (BaG OM) group cell numbers at 14 d; **d:** Combined 14 d COL (BaG OM) and 21 d COL (BaG OM) group cell numbers significantly higher compared to combined 14 d GG-SPD (BaG OM) and 21 d GG-SPD (BaG OM) group cell numbers; **D)** The hASC and HUVEC coculture cell number in 3D composite GG-COL hydrogels cultured with EGM-2 or BaG EM-OM media analyzed at 7 d and 14 d in study III. The hASCs were OM-primed (OM) or non-primed (MM). Results based on hASCs from 3 donors and HUVECs from 1 donor ( $n = 9$ ). Significant difference with  $p < 0.05$ . **e:** Significantly higher combined cell numbers of the EGM-2 (MM) and EGM-2 (OM) conditions compared to the combined cell numbers of the BaG EM-OM (MM) and BaG EM-OM (OM) conditions at 7 d ( $p = 0.026$ ); **f:** Significantly higher combined cell numbers of the EGM-2 (OM) condition at 7 d and 14 d compared to the BaG EM-OM (OM) condition at 7 d and 14 d ( $p = 0.002$ ); **g:** Significantly higher combined cell numbers of the EGM-2 (MM) and EGM-2 (OM) conditions at 14 d compared to the combined cell numbers of the BaG EM-OM (MM) and BaG EM-OM (OM) conditions at 14 d ( $p = 0.002$ ); **h:** Significantly higher combined cell numbers of the EGM-2 (MM) and EGM-2 (OM) conditions at 14 d compared to the combined cell numbers of the EGM-2 (MM) and EGM-2 (OM) conditions at 7 d ( $p = 0.015$ ).

In study II, the highest hASC cell numbers were measured in the COL (BaG OM) hydrogel samples at both 14 d and 21 d (Figure 12C). The combined COL (OM) and COL (BaG OM) cell numbers at 14 d were significantly higher compared to the combined GG-SPD (OM) and

GG-SPD (BaG OM) cell numbers at 14 d. Further, the combined 14 d COL (BaG OM) and 21 d COL (BaG OM) cell numbers were significantly higher compared to the combined 14 d GG-SPD (BaG OM) and 21 d GG-SPD (BaG OM) cell numbers. However, hASCs embedded within GG-SPD hydrogel and cultured with OM showed an increasing trend from 14 d to 21 d, whereas the cell number result in the COL hydrogels receded over 3 weeks.

In study **III**, the highest cell number of cocultured hASCs and HUVECs at 14 d was measured in the EGM-2 (MM) condition whereas the lowest was in the BaG EM-OM (OM) condition (Figure 12D). The combined cell amount of the EGM-2 (MM) and EGM-2 (OM) conditions was significantly higher compared to the combined cell amount of the BaG EM-OM (MM) and BaG EM-OM (OM) conditions separately at both 7 d and 14 d time points. Also, the combined EGM-2 (MM) and EGM-2 (OM) condition cell numbers at 14 d were significantly higher compared to the combined EGM-2 (MM) and EGM-2 (OM) condition cell numbers at 7 d. Further, there was an increasing trend in the cell numbers of all the tested conditions over 2 weeks. Specifically, the combined cell number result of EGM-2 (MM) and EGM-2 (OM) conditions at 14 d was significantly higher compared to the combined cell number result of EGM-2 (MM) and EGM-2 (OM) conditions at 7 d.

## 5.4 Tenogenic differentiation of human adipose stem cells in braided polymer scaffolds

### 5.4.1 Comparison of tenogenic differentiation media compositions

#### Tenogenic medium optimization

Based on the higher cell number at 7 d and 14 d together with higher relative total collagen content at 14 d results of the 2D preliminary experiments (data not shown), TM3 was selected as TM for the following 3D experiments in study **I**. In addition, higher gene expression of tendon matrix components COL1 and COL3 was observed in the TM3 condition compared to the other tested media at 14 d (data not shown).

## 5.4.2 Comparison of tenogenic scaffolds

In study **I**, the braided PLA 96/4 scaffold and the foamed PLCL scaffold were compared for tenogenic differentiation of hASCs with the optimized TM. The braided PLA 96/4 scaffold was selected based on the low cell number result in the foamed PLCL scaffolds (data not shown) and the lower gene expression of tendon markers *COL1* and *TNMD* compared to the braided PLA 96/4 scaffolds (unpublished data). The combined optimized TM and the braided PLA 96/4 scaffold were selected for the following experiments.

## 5.4.3 Human adipose stem cell tenogenic differentiation medium and braided polylactide 96/4 scaffold

In study **I**, hASC gene expression of tenogenic marker genes *SCX*, *COL3*, *COL1*, and *TNMD* was analyzed with qRT-PCR at 7 d and 14 d in the braided PLA 96/4 scaffolds with the optimized TM and compared to the control condition of MM (Figure 13A-E). For the analysis of late tendon markers, hASC-produced matrix total collagen content indicating tenogenic matrix formation was analyzed at 14 d. In addition, hASC production of *COL1* and *TNMD* was analyzed with immunocytochemical staining (Figure 13F).



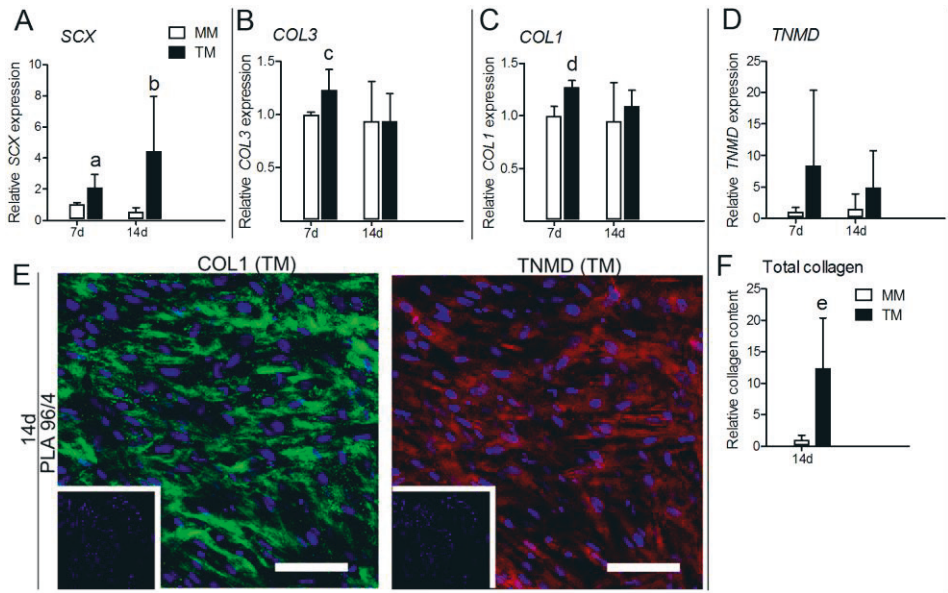


Figure 13. Tenogenic differentiation of hASCs in study I. Gene expression of hASCs in braided PLA 96/4 scaffolds in TM compared to MM. Relative gene expression of **A) SCX**; **B) COL3**; **C) COL1**; and **D) TNMD**. **E**) Immunocytochemical staining of hASC production of late tendon markers COL1 (green) and TNMD (red) in the braided PLA 96/4 scaffolds in the TM condition at 14 d. Cell nuclei stained with DAPI (blue). Cell-free blanks in lower left. **F**) Relative total collagen content of hASCs in the braided PLA 96/4 scaffolds in the TM condition compared to MM. Data presented as mean + SD. Significant difference with  $p < 0.05$ : **a**: from MM at 7 d; **b**: from MM at 14 d; **c**: from MM at 7 d; **d**: from MM at 7 d; **e**: from MM at 14 d. For the gene expression results, the results were relative to the control condition of MM at 7 d and the results were based on hASCs isolated from 3 donors with 2 parallel samples ( $n = 6$ ). For the relative total collagen content results, the results were based on hASCs isolated from 3 donors with 3 parallel samples ( $n = 9$ ).

In study **I**, hASC gene expression of early tenogenic marker *SCX* in braided PLA 96/4 scaffolds was significantly higher in the TM condition compared to the MM condition at 7 d and 14 d. Also, hASC gene expression of another early tenogenic marker *COL3* in the braided PLA 96/4 scaffolds was significantly higher in the TM condition compared to that of MM at 7 d. Further, hASC gene expression of late tenogenic marker *COL1* in the braided PLA 96/4 scaffolds was significantly higher in the TM condition compared to the MM condition at 7 d. Furthermore, the hASC gene expression of late tenogenic marker *TNMD* was higher in the TM condition compared to the MM condition at both 7 d and 14 d. The hASC-produced total collagen content in the braided PLA 96/4 scaffolds was significantly higher with the TM culture compared to MM at 14 d indicating tenogenic matrix production. In addition, hASC matrix mineralization analyzed

with the Alizarin Red S mineralization assay was lower in TM culture compared to MM in the braided PLA 96/4 scaffolds at 14 d (unpublished data). The hASC immunocytochemical staining results in the braided PLA 96/4 scaffolds indicated strong COL1 and TNMD production only in the TM condition at 14 d.

## 5.5 Osteogenic differentiation of human adipose stem cells in gellan gum and collagen type I hydrogel scaffolds

### 5.5.1 Osteogenic gene expression enhanced with bioactive glass extract based osteogenic media

In study **III**, the hASC gene expression of osteogenic marker genes *DLX5*, *OSX*, *RUNX2*, and *ALPL* was analyzed with qRT-PCR at 14 d and 21 d in 3D hydrogels in the GG-SPD (OM), GG-SPD (BaG OM), COL (OM), and COL (BaG OM) conditions (Figure 14A-D).

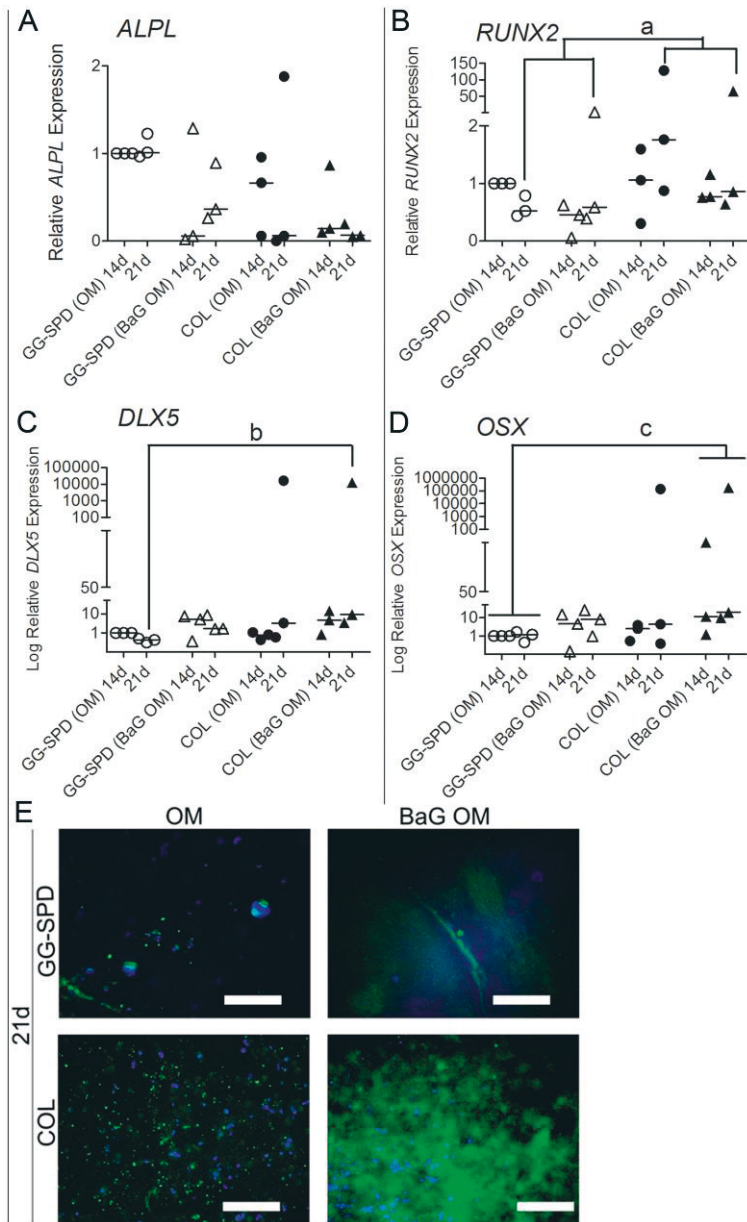


Figure 14. Osteogenic gene expression and OCN production of hASCs in 3D hydrogels in the GG-SPD (OM), GG-SPD (BaG OM), COL (OM), and COL (BaG OM) conditions in study II. Relative gene expression of **A)** *ALPL*; **B)** *RUNX2*; **C)** *DLX5*; and **D)** *OSX* at 14 d and 21 d. Data are presented as mean + SD. Significant difference with  $p < 0.05$ : **a:** For combined COL (OM) and COL (BaG OM) conditions compared to combined GG-SPD (OM) and GG-SPD (BaG OM) conditions at 21 d; **b:** In COL (BaG OM) compared to GG-SPD (OM) at 21 d; **c:** For combined COL (OM) and COL (BaG OM) conditions compared to combined GG-SPD (OM) and GG-SPD (BaG OM)

conditions at 14 d and 21 d. Results based on hASCs isolated from 3 donors with 2 parallel samples ( $n = 6$ ). Results relative to the control condition of GG-SPD (OM) at 14 d. *DLX5* and *OSX* gene expression showed high variance and were therefore presented partly in Log(10) scale. Group medians are indicated with horizontal line; **E**) Representative images of hASC OCN production at 21 d. The hASCs isolated from 3 donors ( $n = 3$ ). Scale bar 200  $\mu\text{m}$ .

Overall, significantly higher hASC osteogenic marker gene expression was observed with the COL (OM) or COL (BaG OM) conditions compared to the GG-SPD (OM) or GG-SPD (BaG OM) conditions with the exception of *ALPL* expression. In detail, hASC gene expression of *DLX5* was significantly higher in the COL (BaG OM) condition compared to the GG-SPD (OM) condition at 21 d. Also, *OSX* gene expression was significantly higher for the combined 14 d and 21 d COL (BaG OM) results compared to the combined 14 d and 21 d results of the GG-SPD (OM) condition. Further, hASC gene expression of *RUNX2* of the combined COL (OM) and COL (BaG OM) conditions at 21 d was significantly higher compared to the combined GG-SPD (OM) and GG-SPD (BaG OM) results at 21 d.

### 5.5.2 Robust hydroxyapatite mineralization and late osteogenic differentiation with bioactive glass extract based osteogenic media in three-dimensional hydrogels

#### Hydroxyapatite mineralization in gellan gum and collagen type I hydrogels

The hASC-secreted matrix hydroxyapatite residues were stained with the OsteoImage assay at 21 d after which the fluorescence was measured, followed by staining of hASC nuclei with DAPI and imaging of the mineralized residues with epifluorescence microscope (Figure 15).

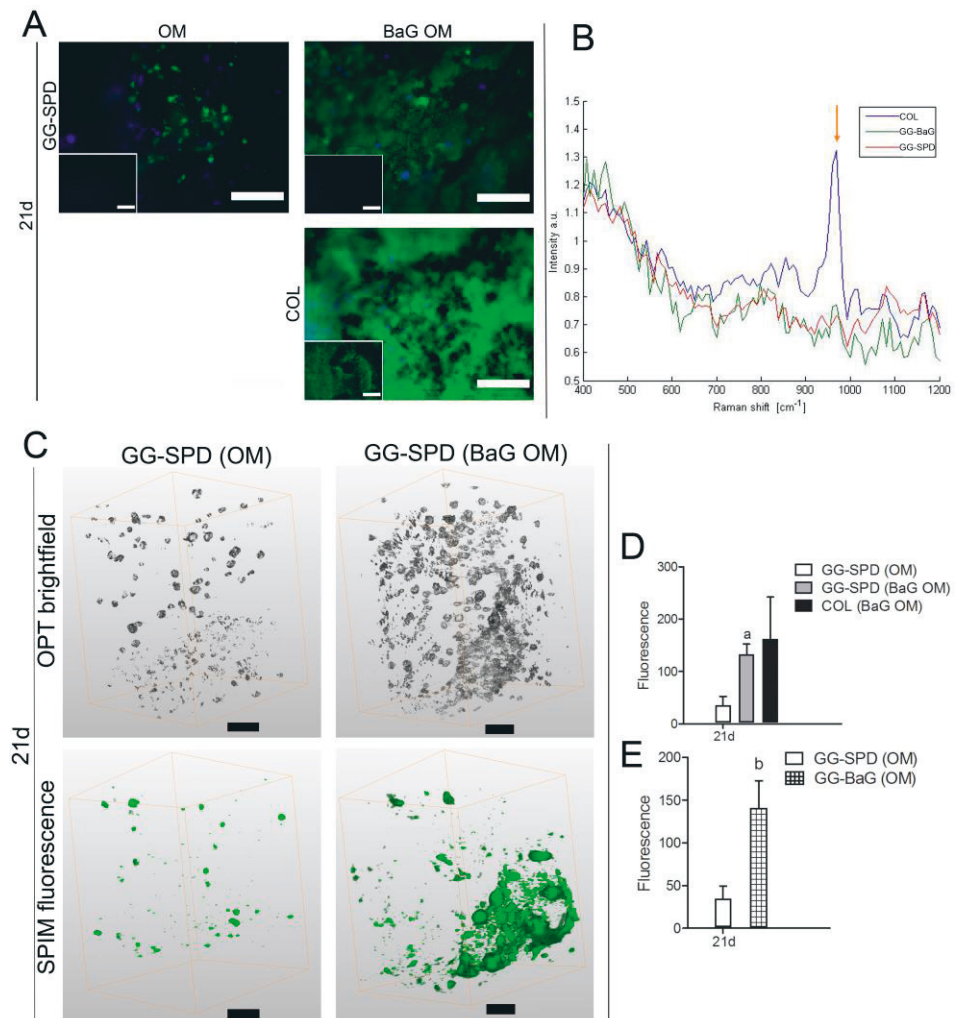


Figure 15. Mineralization in study II. **A**) Representative images of hASC matrix hydroxyapatite residues stained with Osteolmage assay and cell nuclei stained with DAPI in GG-SPD (OM), GG-SPD (BaG OM), and COL (BaG OM). COL (OM) samples contracted after 3 d. Images of acellular blank controls on lower left. The hASCs were isolated from 1 donor ( $n = 1$ ). Scale bar 200  $\mu\text{m}$ ; **B**) Raman spectroscopic analysis of hASC-secreted matrix mineralized residue Raman shifts in 3D hydrogel at 21 d in GG-SPD (BaG OM) (red), GG-BaG (BaG OM) (green) and COL (BaG OM) (blue) conditions. Arrow pointing the phosphate peak at Raman shift 960  $\text{cm}^{-1}$ . The hASCs were isolated from 1 donor ( $n = 1$ ). Spectra normalized to average intensity between 475-560  $\text{cm}^{-1}$ ; **C**) Representative brightfield OPT 3D reconstructed images of hASCs embedded within GG-SPD (OM), and GG-SPD (BaG OM) hydrogels, and representative Osteolmage hydroxyapatite (green) fluorescence stained 3D reconstructed SPIM images of hASCs encapsulated in GG-SPD (OM) and GG-SPD (BaG OM) hydrogels at 21 d. The analyzed hASCs were from 1 donor ( $n = 1$ ). Scale bar 100  $\mu\text{m}$ ; **D**) The measured fluorescence of stained hydroxyapatite residues

in GG-SPD (OM), GG-SPD (BaG OM), and COL (BaG OM) hydrogels at 21 d. The hASCs were isolated from 3 donors with 1-2 parallel samples for GG-SPD (OM) and GG-SPD (BaG OM) ( $n = 5$ ), whereas hASCs from 2 donors with 2 parallel samples ( $n = 4$ ) were available for analysis for COL (BaG OM) due to contracted hydrogels. **a:** Significant difference with  $p < 0.05$  compared to GG-SPD (OM) at 21 d; **E** Mineralization with different gellan gum crosslinkers. The measured fluorescence of stained hASC hydroxyapatite mineralization in GG-SPD (OM) and GG-BaG (OM) at 21 d. **b:** Significant difference with  $p = 0.002$  compared to GG-SPD (OM) at 21 d. Data are presented as mean + SD.

Both the imaging of hydroxyapatite residues and the measured mineralization results showed the highest hydroxyapatite content for the COL (BaG OM) condition and strong hydroxyapatite staining was observed in the GG-SPD (BaG OM) condition, whereas only moderate staining was seen in the GG-SPD (OM) at 21 d.

### Hydroxyapatite mineralization 3D distribution

OsteoImage-stained hASC hydroxyapatite mineralization 3D distribution was imaged OPT and SPIM (Figure 15C). The reconstructed brightfield OPT analysis showed label-free images of hASCs and matrix within 3D GG-SPD hydrogel based on variation in light attenuation between the cells and the surrounding hydrogel. The cells and matrix were visible as shaded objects in projection images acquired in transmission mode. SPIM imaging was acquired as a 3D stack of multi-focal images in fluorescence emission mode. The SPIM imaging showed the 3D distribution of OsteoImage-labeled hydroxyapatite residues. The hydroxyapatite staining result was strong in the GG-SPD (BaG OM) condition while the labeled hydroxyapatite was scarce in the GG-SPD (OM) condition. The COL hydrogel optical opacity impeded the OPT and SPIM imaging.

### Raman spectroscopic analysis of calcium phosphate species

In study **II**, we verified the hASC ECM mineralization CaP species as hydroxyapatite with Raman spectroscopic analysis (Figure 15B). The hASCs embedded in GG-SPD (BaG OM), GG-BaG (BaG OM) and COL (BaG OM) 3D hydrogels were cultured 21 d with phenol red free media (see Table 14 in section 4.7.5) to avoid interference to Raman spectra. The Raman spectra showed the hydroxyapatite phosphate peak at Raman shift  $960 \text{ cm}^{-1}$  which semi-quantitatively measured hydroxyapatite content. The highest result was obtained for the COL (BaG OM) condition, followed by those of GG-BaG (BaG OM) and GG-SPD (BaG OM), respectively. The slightly higher hydroxyapatite

content measured for the GG-BaG (BaG OM) condition showed that GG mineralization was enhanced with BaG ext crosslinking.

#### Immunocytochemical staining of osteocalcin production

In study **II**, OCN production of hASCs in 3D hydrogels was analyzed (Figure 14E). The OCN- and DAPI-stained hASCs in GG-SPD (OM), GG-SPD (BaG OM), COL (OM), and COL (BaG OM) conditions were analyzed at 21 d. Strong hASC OC production was observed in the COL (OM) and COL (BaG OM) conditions while moderate OCN production was also visible in the GG-SPD (OM) and GG-SPD (BaG OM) conditions.

## 5.6 Osteogenic differentiation of human adipose stem cells and coculture for microvascularization in composite hydrogel scaffolds

#### Bioactive glass extract based endothelial-osteogenic media and coculture for osteogenic and endothelial gene expression

In study **III**, hASC and HUVEC gene expression of osteogenic marker genes *DLX5*, *RUNX2*, and *OSX*, together with endothelial marker genes *VWF* and *PECAM-1* was analyzed with qRT-PCR in the EGM-2 (MM), EGM-2 (OM), BaG EM-OM (MM), and BaG EM-OM (OM) conditions at 7 d and 14 d (Figure 16A-E).



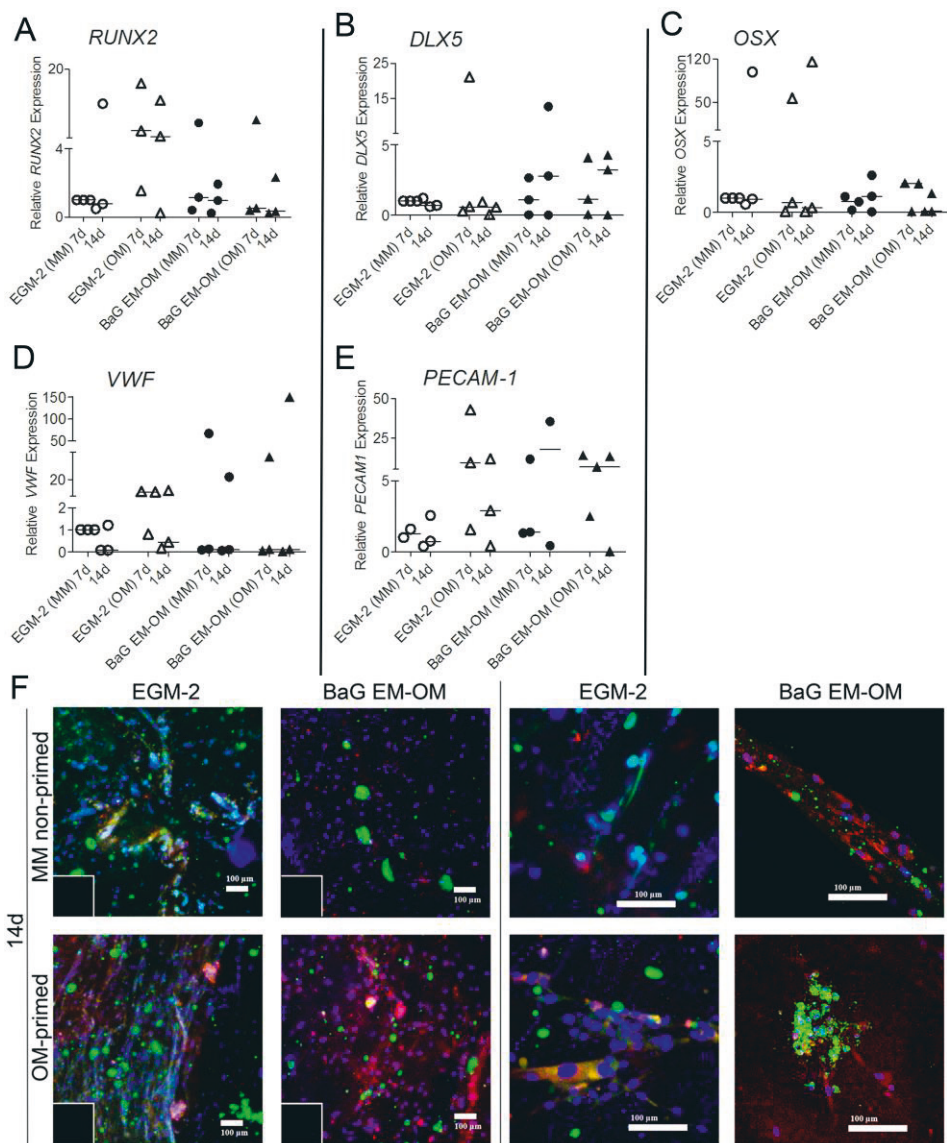


Figure 16. Osteogenic and endothelial differentiation of hASCs and HUVECs within composite GG-COL hydrogels in study III. Relative gene expression of **A**) *RUNX2*; **B**) *DLX5*; **C**) *OSX*; **D**) *VWF*; and **E**) *PECAM-1* with EGM-2 or BaG EM-OM media culture for 7 d and 14 d. The hASCs were OM-primed or non-primed (MM). Results relativized to the control condition of EGM-2 (MM) at 7 d. The hASCs isolated from 3 donors and HUVECs from 1 donor ( $n = 3$ ). Group median indicated by horizontal line; **F**) Immunocytochemical staining of OCN and CD31 production in study III. Representative Z-stack confocal microscope images of hASCs and HUVECs in GG-COL 3D hydrogel with EGM-2 and BaG EM-OM media culture at 14 d. OCN (red); CD31 (green); DAPI (blue). On left side: 10x objective images. Acellular blank controls lower left; On right side: 25x objective images. Scale bar 100  $\mu\text{m}$ . The hASCs were OM-primed or



non-primed (MM). The hASCs were isolated from 2 donors and HUVECs from 1 donor ( $n = 2$ ).

Osteogenic gene expression of *DLX5* peaked at 14 d in the BaG EM-OM (MM) and BaG EM-OM (OM) conditions. The highest medians of gene expression of bone marker *RUNX2* were measured in the EGM-2 (OM) condition at 7 d and 14 d. Osteogenic marker *OSX* gene expression showed highest values for single donors in EGM-2 culture at 7 d and 14 d although the highest gene expression median was observed for the BaG EM-OM (OM) condition at 7 d. The highest gene expression of endothelial marker VWF was detected for single donors in BaG EM-OM culture at 7 d and 14 d albeit the highest median was observed for the EGM-2 (OM) condition at 7 d. The highest gene expression median of endothelial marker *PECAM-1* was observed for the BaG EM-OM (MM) condition at 14 d while also EGM-2 (OM) at 7 d, BaG EM-OM (MM), and BaG EM-OM (OM) conditions at 7 d and 14 d showed elevated medians.

#### Hydroxyapatite mineralization

In study III, hASC and HUVEC coculture mineralization hydroxyapatite residues were stained with OsteoImage assay and the cell nuclei with DAPI in composite GG-COL hydrogels at 14 d (Figure 17).

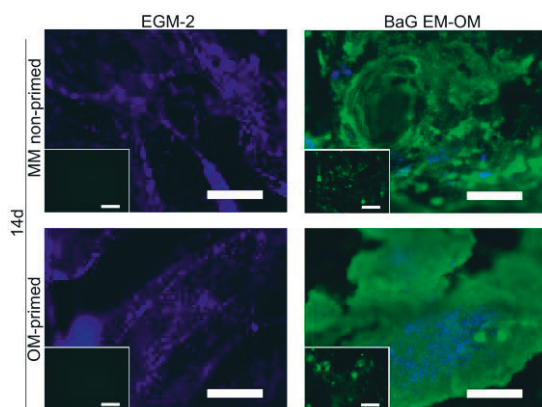


Figure 17. Mineralization in study III. Representative images of OsteoImage hydroxyapatite (green) stain, hASC and HUVEC nuclei (DAPI; blue) encapsulated in 3D GG-COL hydrogels in EGM-2 and BaG EM-OM conditions at 14 d. The hASCs were OM-primed or non-primed (MM). Scale bar 500  $\mu\text{m}$ . Acellular blank controls shown on lower left. The hASCs were isolated from 1 donor and HUVECs from 1 donor ( $n = 1$ ).

The strongest mineralization content of hASC and HUVEC coculture in GG-COL hydrogels was visually analyzed in the BaG EM-OM (OM) condition at 14 d. Also, strong hydroxyapatite residue content was observed in the BaG EM-OM (MM) condition. Some background was visible for both the BaG EM-OM conditions. However, no mineralization was detected in either of the EGM-2 media conditions.

#### Immunocytochemical staining of endothelial and osteogenic markers

In study **III**, mature endothelial marker CD31 and late bone marker OCN production in hASC and HUVEC coculture in GG-COL hydrogels was analyzed with immunocytochemical staining at 14 d and the cell nuclei were stained with DAPI (Figure 16F). The strongest OCN staining was observed in the BaG EM-OM (OM) condition at 14 d. Also, strong OCN staining was seen in the BaG EM-OM (MM) condition. Some OCN staining of hASCs and HUVECs was observed in the EGM-2 conditions and accentuated with OM preconditioning of hASCs. Reticular structures were visible with both EGM-2 and BaG EM-OM media culture, however, tubular structures and initial microvessel-like networks were visible in the EGM-2 conditions alone. The most developed tubular-like structures were seen with hASC and HUVEC coculture in the EGM-2 (MM) condition.

## 6 DISCUSSION

### 6.1 Combined stimulus by soluble factors and scaffold biomaterial needed for human adipose stem cell tenogenic differentiation

The increasing trend of musculoskeletal diseases and related restricted physical abilities call for new therapeutical options (Calejo et al., 2020). The study **I** examined *in vitro* tissue engineered tendon-like construct development with hASC tenogenic differentiation. To the best of our knowledge, this was the first study to combine GDF-5 and L-ascorbic acid to stimulate tenogenic differentiation of hASCs *in vitro*. Importantly, micro-CT imaging of scaffold microstructures provided pivotal knowledge of the topographic environment directing cell behavior in study **I** (Cengiz et al., 2018).

The hASCs are an interesting cell source for tendon TE since they are available, abundant, and have been shown to improve *in vivo* tendon injuries although the exact mechanism remains undetermined (Costa-Almeida et al., 2019). Our approach was to combine a mechanically suitable and relatively slowly biodegradable supporting biocompatible scaffold structure and hASCs with efficient tenogenic chemical induction.

Once ruptured, large load-transmitting tendons such as the Achilles tendon are difficult to suture into bone and importantly, heal slowly with high risk of reinjury. Therefore, a mechanically stable engineered tendon-like tissue construct would offer a feasible solution. The mechanical stability of the construct is a necessity since tendon transmits the mechanical muscle contraction to bone in the musculoskeletal system. Our mechanical testing results showed Young's modulus at 280(20) MPa for the braided PLA 96/4 with similarities to that of human Achilles tendon measured at 800-900 MPa (Kuo, C. K. et al., 2010; LaCroix et al., 2013). What is more, the biomaterial PLA 96/4 has been found suitable for *in vivo* tendon repair (Viinikainen et al., 2014). Also, cell-seeded grafts

show typically faster tissue ingrowth, tissue integration, and healing response than cell-free implanted constructs.

Our results were consistent with a previous study demonstrating the beneficial effect of fibrous scaffolds for tenogenic differentiation of hMSCs (Czaplewski et al., 2014). In 2D cell culture, Park and coworkers induced tenogenic differentiation of rat ASCs with GDF-5 which significantly enhanced cell proliferation, increased gene expression of *SCX*, *TNMD*, *TNC*, *COL1*, *COL3*, *aggrecan*, and *decorin*. In addition, an increase in protein production of TNMD and TNC was reported. (Park et al. 2010) We were similarly able to confirm the beneficial effect of GDF-5 on ASC tenogenic gene expression and protein production. Jenner and coworkers studied hBMSCs for ligament application in woven PLGA scaffold stimulated with a combination of ascorbic acid with either TGF- $\beta$ 1 or GDF-5, when TGF- $\beta$ 1 stimulation was found to increase significantly cell proliferation and total collagen production (Jenner et al. 2007). Although this result was reported for hBMSCs, hASCs could also be tested with TGF- $\beta$ 1 in filamentous scaffolds for tenogenesis stimulation. James and coworkers studied *in vitro* the effect of GDF-5 stimulation on rat ASCs cultured on PLGA fiber scaffold, where the gene expression of tenogenic markers *SCX* and *COL1* was upregulated with 3D scaffolds (James et al. 2011). Our results confirmed these observations. Although mechanical stimulation has been shown to induce tendon-like matrix production in previous works (Gaspar et al., 2015; Kuo, C. K. & Tuan 2008; Raabe et al., 2013; Vindigni et al., 2013; Yang, G. et al., 2013), our result with PLA 96/4 scaffolds was interesting due to the fact that we obtained abundant COL1 production in a static condition in a 3D structure without mechanical stimulation. The selected braided PLA 96/4 scaffold possessed anisotropic surface structures which have been suggested to promote tenogenesis due to resemblance to native fibrous organization (Calejo et al., 2020; Domingues et al., 2016; Laranjeira et al., 2017). However, we did not observe uniaxially oriented COL1 fiber structures that in native tissue glide against each other and endow tendon with characteristic elastic properties (James et al., 2008).

Our results showed that inducing soluble factors were required to support hASC tenogenic differentiation because the PLA 96/4 scaffold alone in the MM condition was not sufficient to promote hASC tenogenesis. In the future, different spun textile fiber scaffolds and anisotropic fibrous scaffolds could be compared for further tendon graft development (Domingues et al., 2016; Miranda et al., 2020; Silva et al., 2020; Wu et al., 2017). Overall, the results with

hASCs seeded on PLA 96/4 scaffolds and cultured in TM condition showed potential for further *in vivo* studies to test the functionality of the engineered tendon construct.

## 6.2 Bioactive glass extract based osteogenic medium induced robust osteogenic differentiation of human adipose stem cells in gellan gum and collagen type I hydrogels

In study **II**, we investigated the effect of BaG OM induction on hASC osteogenesis within 3D GG and COL hydrogels for minimally invasive bone graft development. The mechanical properties of the non-incubated GG and COL hydrogels were in line with previous studies (Raub et al., 2010; Silva-Correia et al., 2013). The moderate mechanical properties of GG and COL as well as the weak stability of COL have limited their application for hard tissue applications (El-Fiqi et al., 2013; Oliveira, M. B. et al., 2016). In contrast, we were able to show significantly enhanced mechanical properties for both GG-SPD and COL hydrogels in the BaG OM incubation albeit still insufficient for load-bearing applications. The GG-SPD (BaG OM) sample compressive modulus resembled that reported for osteoblastic matrix at 30 kPa (Engler et al., 2006; Gantar et al., 2014; Huebsch et al., 2010; Wen et al., 2014). Interestingly, the mechanical properties increased gradually and this might have enhanced even more the osteogenesis process (Engler et al., 2006; Lopes et al., 2018).

The rapid *in vivo* degradation of COL is a valid source of criticism. To the point, the COL mechanical stability was significantly increased in the BaG OM incubation. Indeed, the BaG OM-incubated COL scaffold might also have capacity to resist more the rapid degradation although this would require additional verification with degradation analysis or, eventually, *in vivo* testing. The traction forces that adhered cells exert on the substrate and the pericellular milieu could be studied by traction force microscopy, for example, to better understand mechanisms of mechanotransduction (Ribeiro et al., 2016).

The observed rounded hASC morphology in 3D GG hydrogels was assumed to be linked to lack of adhesion sites (Karvinen et al., 2017; Koivisto et al., 2017). Nevertheless, it has been postulated that the round cell morphology might not hinder hASC osteogenesis (Huebsch et al., 2010; Oliveira, M. B. et al., 2016). This has been based on the assumption that once the encapsulated cells have formed their own niche microenvironment, the inert surrounding hydrogel bulk

interferes little with cell growth and differentiation. Contrastingly, hASCs were elongated in 3D COL albeit their exaggerated pulling action caused COL matrix to contract (El-Fiqi et al., 2013; Gentleman et al., 2007) in the OM condition without the extra mechanical stability offered by BaG OM incubation. The issue of uncontrollable change of shape of COL constructs has been addressed by various attempts, for example, by the addition of short COL1 fiber composites. In a study by Gentleman and coworkers, the higher mass of COL1 fibers supported the construct to maintain its shape longer (Gentleman et al., 2007). It is important to note that the hydrogel bulk mechanical properties might not correlate with the unhomogenous fibrous ECM pericellular stiffness at close range of the cells. In fact, cells remodel elastically and plastically the heterogenous surrounding fibrous matrix thus creating a wide range of local stiffnesses. The heterogeneity of cell microenvironment stiffness influences cell-ECM interactions that would warrant more specific investigations (Binner et al., 2017; Keating et al., 2017).

The hASCs cell number within GG-SPD hydrogel in OM showed an increasing trend from 14 d to 21 d, whereas the cell number in the COL hydrogels decreased over 3 weeks, possibly due to COL hydrogel contraction and lack of space for cell growth. This indicates the feasibility of GG-SPD hydrogel for long term hASC culture permitting cell proliferation and providing space for cell growth avoiding premature hydrogel contraction. This might also indicate that hASCs required a longer time of adjustment into inert GG-SPD hydrogel to produce their own ECM and initiate growth, proliferation, and differentiation. Therefore, later time points of analysis past 3 weeks might have yielded improved differentiation results also for the GG-SPD hydrogel culture conditions.

The robust mineralization results verified efficacious hASC osteogenic differentiation with rich hydroxyapatite residue deposition in hASC matrix with BaG OM incubation in both the GG and COL conditions. The accumulation of mineralized matrix was confirmed by qualitative OsteoImage hydroxyapatite staining and quantification in addition to semi-quantitative Raman spectroscopic analysis with a prominent peak of inorganic phosphate for the COL (BaG OM) condition. Providing attractive 3D imaging results, 3D reconstructed OPT and stacked fluorescence SPIM images showed homogenous distribution of hydroxyapatite residues in the pericellular space or surrounding hASCs. The intensive and strongly accumulated hydroxyapatite mineralization was visible in the nonspecific OPT images and the stained fluorescent SPIM images in the

BaG OM condition. The wet-state 3D imaging of cell-laden hydrogels is an emerging and promising analysis method the likes of which are keenly needed for TE graft development *in vitro* studies. Moreover, the image analysis of the entire 3D volume is important to gain advanced understanding of the whole volume and not limiting the observations on the mere mineralized surface (Killion et al., 2013). Other studies have reported more moderate results for MSC osteogenesis encapsulated in 3D hydrogels compared to our strong hydroxyapatite accumulation (Castillo Diaz et al., 2016). Most significantly, we were able to show homogenous mineralization with the BaG ionic dissolution products also in the interior region of the GG-SPD hydrogel constructs. This showed that the GG hydrogel allowed diffusion of soluble species also to the central parts of the construct. Therefore, our results aligned with those presented by Gantar and coworkers although their system incorporated solid BaG nanoparticles in the hydrogel (Gantar et al., 2014).

Also acellular COL samples mineralized, attributed to COL functioning naturally as a platform for mineral residue nucleation (Marelli et al., 2011; Miri et al., 2016) albeit the mineralization was clearly accentuated with the cell-laden samples. Overall, the superior mineralization and mature osteogenic differentiation with OCN staining results verified BaG OM as efficient hASC osteoinducer in *in vitro* 3D hydrogel culture.

### 6.3 Bioactive glass soluble factors promoted mineralization and osteogenesis while neovascularization was restricted in coculture in composite hydrogel scaffolds

In study **III**, we investigated the blend of GG and COL hydrogels for vascularized bone graft development. In the study, soluble BaG ions' effect on hASC osteogenic differentiation was researched. Further, we tested the impact of HUVEC coculture for growth of microvasculature in 3D hydrogel culture in BaG EM-OM media. Similarly to the study **II** results, BaG ion-media enhanced hydrogel mechanical stability. The mechanical properties of the acellular composite hydrogel samples remained soft at 1-3 kPa which has been deemed suitable for vascularization (Rouwkema & Khademhosseini 2016; Sieminski et al., 2007). To the point, matrix mechanical properties and stiffness gradients have been reported as factors that modulate vascular processes (Rao et al., 2012; Rouwkema & Khademhosseini 2016).

Importantly, the Live/Dead analysis imaging displayed reticular structures in all the experiment groups thus indicating cellular crosstalk and initial EC tube formation capacity (Correia, C. R. et al., 2017; Kirkpatrick et al., 2011). Further, the Live/Dead imaging results confirmed the cell number results where lower cell amount was detected in the BaG EM-OM condition, and in particular with osteogenic preconditioning of hASCs.

In study **III** cell number results, hASC cell number in the EGM-2 condition was significantly higher than in the BaG EM-OM condition. This showed the BaG ions' restricting effect on cell proliferation. However, the lower cell number might have been due to progressed hASC differentiation as evidenced by the strong mineralization result. The BaG EM-OM condition restricted cell elongation and caused distinctly different truncated cell morphology. To the point, the effect of  $B^{3+}$  cations on cell morphology has been reported also by others (Brown et al., 2009; Rodriguez et al., 2004), in addition to the changes to cytoskeleton organization, cell signaling pathways, and adhesion (Ojansivu et al., 2015; Ojansivu; Hyvari et al., 2018). Furthermore,  $B^{3+}$  cations also induce EC proliferation and migration along with VEGF production (Kargozar et al., 2018) which might have been beneficial for the combined osteogenesis and vasculogenesis scheme. The EGM-2 condition supported good cell viability and cell elongation, high cell number regardless of hASC preconditioning status, abundant capillary-like structures, and moderate vascular-like network growth indicating microvascularization. This was deemed as the main result of the compared 3D GG-COL coculture conditions including a novelty for the study. However, no perfusable functionality was tested.

Interestingly, the EGM-2 (OM) condition induced osteogenic gene expression. This opposed the Mihaila and coworker report on absence of osteogenic differentiation in coculture of hASCs and ECs with EGM-2 media despite osteogenic priming (Mihaila et al., 2017). In our results, the BaG EM-OM condition enhanced endothelial marker gene expression with the highest median with OM-preconditioned hASCs. The high endothelial gene expression medians and single peaks in coculture might have indicated hASC endothelial subpopulation, as also noted by other researchers (Huttala et al., 2015; Mihaila et al., 2017). Indeed, the effect of an endothelial precursor population of hASCs merits further research. Interestingly, some OCN staining was observed in the EGM-2 condition which indicated that it supported restricted osteogenesis. The effect was accentuated by hASC osteogenic preconditioning as seen in the bone



marker gene expression results. This would warrant more detailed research in the future. The immunofluorescence imaging results showed that the BaG EM-OM condition was required for strong OCN production, whereas the EGM-2 condition supported strong CD31 production and vessel-like structure formation, similarly to a report by Ma and coworkers demonstrating *in vitro* capillary growth with hASC and HUVEC coculture in endothelial medium within COL hydrogel (Ma et al., 2014).

Overall, the lack of CD31 staining or vascular-like networks indicated that the BaG EM-OM condition late osteogenic differentiation prevented vessel growth and tubular network formation. This observation showed that simultaneous osteogenesis and vasculogenesis were inhibited similarly to previous studies (Blache et al., 2016), although synergistic cellular crosstalk has been reported for MSCs undergoing osteogenic differentiation and ECs forming microvascular networks (Bidarra et al., 2011; Grellier; Granja et al., 2009; Pedersen et al., 2013; Saleh et al., 2011). Indeed, direct cell-cell contacts between MSCs, osteoblastic cells, and HUVECs have been observed to increase VEGF secretion and consequentially VEGFR2 expression and ALP activity in the following (Grellier et al., 2009; Shahabipour et al., 2019).

#### 6.4 The effect of donor variation and human adipose stem cell endothelial subpopulations

There were some discrepancies in the osteogenic and endothelial gene expression results specifically in study **III** and these were addressed as instances of donor dependent variation in the analysis. The endothelial culture condition seemed to promote osteogenesis in cocultured hASCs of individual donors and vice versa for osteogenic culture conditions enhancing endothelial gene expression. In part, this can be addressed to VEGF stimulation of vascular ECs that in turn promote MSC osteogenesis in the intramembranous ossification process (Shum et al., 2004; Zelzer & Olsen 2004). For the BaG EM-OM condition, the BaG extract component might have induced angiogenesis and vasculogenesis markers in the cocultured HUVECs (Kargozar et al., 2018). What is more, biomineralization glycoprotein BSP has been reported to stimulate HUVEC angiogenesis (Bellahcene et al., 2000), although BSP was not targeted in any of the study **III** analyses and, therefore, its presence in the mineralized matrix cannot be neither confirmed nor dismissed.

The isolated hASCs used for experiments in study **III** showed upregulated endothelial marker CD54, CD31, and hematopoietic/progenitor marker CD34 expression in the flow cytometric analysis results. Some studies have suggested that ASCs would in fact be of CD34+, CD90-, CD31-, CD45- and CD145- phenotype and localized within perivascular niche (Varma et al., 2007; Yoshimura et al., 2006; Zimmerlin et al., 2013). The CD34+ fraction of blood cells indicating similarity with endothelial and hematopoietic stem cells has been researched for clinical limb ischemia trials, however, albeit seemingly efficient for vascular injury treatment, convincing evidence based on clinical trials still needs to be shown (Trounson & McDonald 2015).

On the other hand, other reports have remarked on the presence of a subpopulation of CD34+ fibroblast-like vascular endothelial precursors in what seems to be hydrogel-like native tissue located in reticular collagenous structures of fluid-filled interstitial space of submucosa (Benias et al., 2018a; Benias et al., 2018b). The identity of the cell population and tissue environment would require more elucidation although this shows the heterogeneity of the MSCs and ECs in the body (Sidney et al., 2014). The characteristics of CD34+ subpopulation are still being unfolded but CD34+ cells have been shown to include vascular endothelial progenitors and to possess enhanced progenitor activity (Bora & Majumdar 2017; Mazini et al., 2019), in fact, a portion of heterogeneous MSCs express CD34 contrary to what has been postulated in most literature (Sidney et al., 2014; Zimmerlin et al., 2013). Our results were in line with this emerging view and role of different hASC subpopulations. Furthermore, Mihaila and coworkers have presented SSEA-4+hASCs as another potential hASC subpopulation for both endothelial and osteogenic differentiation (Mihaila et al., 2013). To control the heterogeneity of MSC subpopulations, standardization methods have been proposed to increase reproducibility and safety in view of clinical applications. The cell number increasing expansion step in cell-based therapies is challenging also in view of phenotypic drift. The fact remains, that within a hASC population, cells are most likely at different stages of differentiation (Baer 2014). The cell population heterogeneity could be better controlled with careful method standardization such as defined *in vitro* culture conditions (Patrikoski et al., 2019). Another method to drive MSC differentiation and thus limit subpopulation enrichment is the priming of cultured cells with biochemical stimuli. This would potentially also enhance the efficacy of stem cell-based treatments (Neri 2019) even though the use of exogenously added growth factors should be minimized in cell cultures. However, in practice, the use of specific and limited hASC

subpopulations might not be feasible for clinical treatments which require large amounts of cells (Baer 2011).

## 6.5 Establishing initial three-dimensional *in vitro* musculoskeletal model

While *in vivo* tests are still used for the safety evaluation of implantable medical devices in the preclinical phase, *in vitro* tissue models are increasingly developed to replace, refine, and reduce use of animals. An *in vitro* tissue model permits the study of simplified cell and tissue function in a controlled and defined laboratory cell culture setting. (Papadimitropoulos et al., 2011) Ideally, an *in vitro* tissue model would facilitate 3D analysis of cell-cell interactions with controlled 3D growth of tissue in the matrix material of choice. They are sought to establish a research platform to recapitulate tissue development and functions by combining engineering and biology. With human cells, they could be utilized as research models to explore disease mechanisms and screen for drug effects in a more representative manner than animal models. A research platform is to mimic functional tissue and facilitate exploring disease mechanisms and to screen for drug effects (Loaiza et al., 2018). The impact and value of a novel and simple to apply *in vitro* disease model or a drug screening platform with specific and simplified functionality for bone cancer testing, for example, would be considerable.

Establishing an *in vitro* assay, for biomedical graft safety evaluation that satisfies regulatory control includes separate phases of development, validation, and acceptance. The final phase would entail acceptance by the regulatory bodies, manufacturers and assay users. The urgent need for a variety of validated *in vitro* assays therefore persists. Validated *in vitro* cytotoxicity tests currently exist as International Organization for Standardization (ISO) standard procedures. According to ISO 10993-5 standard, evaluation of biomaterial cytotoxicity can be by qualitative or quantitative methods. Even though qualitative or subjective, semi-quantitative assessment of the results satisfy the international standard, these might not produce relevant data for more efficient comparisons between different institutions or teams of researchers. What is more, testing of human cell lines is preferred and further, cells from more than 1 donor should be tested in addition to relevant negative and positive controls. (EN ISO 10993-5. 2009) Another important aspect that affects meaningful assessment and comparison of

*in vitro* test results are the donor dependent differences, and these factors should be carefully discussed in each case. Therefore, reproducibility of *in vitro* testing is a relevant cause of concern. Indeed, a quantifiable *in vitro* model for precision analysis would allow more accurate comparisons (Loaiza et al., 2018).

In view of these issues, our results in study **I** offered reproducible and relevant data on *in vitro* screening of suitable tenogenic media, scaffold materials, and structures potential for further *in vivo* safety evaluation. In study **III**, the results offered important insights into the intricate interplay of factors affecting vascularized bone formation *in vitro*. Although the *in vitro* results were conducted with hASCs from 3 donors satisfying the commonly held criteria for *in vitro* testing, they fell short of providing statistically significant results in all areas of analysis, for example on gene expression of various bone and endothelial markers. The discrepancies in gene expression of differentiation markers might have been partly attributable to hASC subpopulations which, therefore, merit further research. Importantly, in study **II**, the BaG extract-based protocol for creation of mineralized 3D hydrogel matrix with hASCs was the most successful in establishing an *in vitro* bone tissue mineralized matrix model potential for wider application in the field. Although some aspects of bone-like, vascularized bone-like and tendon-like tissue were achieved with expression of specific markers with gene expression or protein production, these models remained limited in their scope. Indeed, *in vivo*-resembling tissue model would require more complex functionality provided by microfluidics, for example. A vascularization model could be utilized for study of cancer tumor vascularization (Haase & Kamm 2017; Song et al., 2014), for example.

In terms of impact on the research field, these studies provided relevant human cell data and feasible composite biomaterial combinations for musculoskeletal tissue engineered *in vitro* model development although some components such as differentiation media might call for more optimization. The *in vitro* models developed in this thesis work offer themselves up for further development in future research.

## 6.6 Developing three-dimensional hydrogel analysis methods

Quantitative *in vitro* analyses are increasingly developed to facilitate transfer and direct comparison of data between different research groups. Novel and reliable analysis methods are therefore urgently needed for 3D hydrogel cell culture

characterization. As one of the principal achievements of this thesis work overall, study **II** established reproducible quantitative analysis methods for 3D cell-hydrogel constructs together with qualitative 3D imaging modalities. Importantly, repeatable mechanical testing of hydrogel scaffolds was reported in studies **II-III** which are valued for hydrogel biomaterial testing research. So far, 3D mineralized hydrogels have been challenging to produce and analyze *in vitro* and there has been a lack of methods to analyze 3D distribution of hydrogel encapsulated cells and of cell matrix mineral residues (Marro et al., 2016). What is more, OPT and SPIM techniques allowed hydrogel, cell, and ECM characterization in the wet-state which mimics the natural tissue environment instead of freeze-drying of samples as required for micro-CT (Cengiz et al., 2018). Instead, the wet-state analysis allowed to observe the water-swollen hydrogel polymer network intact together with embedded cells. Therefore, 3D OPT and SPIM imaging have important new applicability and potential for relevant impact on the *in vitro* research of 3D hydrogel cell cultures. In addition, semi-quantitative Raman spectroscopic analysis holds great promise and applicability for mineralized cell-laden hydrogel analysis also in the future.

In order to study cell proliferation, analysis of cell number from 3D hydrogel culture has been challenging due to lack of hydrogel biomaterial specific extraction methods. We opted to mechanically mince the cell-laden hydrogels because the digestion methods of COL and GG hydrogel scaffolds differed and with no feasible enzymatic digestion protocol available for GG. In addition, cell-laden COL contracted strongly and therefore robust mechanical mincing was the preferred method for reproducible quantitative DNA amount analysis. For a similar reason, RNA isolation from contracted or mineralized COL matrix was made possible with the mechanical mincing method. These established analysis methods were essential for the execution of the following study **III** with the added complexity of composite GG-COL hydrogel scaffolds. Indeed, reproducible analysis methods have been deemed essential for the quality and ensuing development of 3D *in vitro* cell culture protocols.

Overall, these established 3D hydrogel cell culture biochemical analysis protocols and 3D imaging applications possess important novelty and carry a potential impact on the basic research field on cell-laden and mineralized hydrogels enabling new *in vitro* hydrogel characterization research for tissue engineered bone graft development. The established *in vitro* hydrogel

characterization and analysis methods have therefore applicability to the wider TE field not restricted solely on musculoskeletal applications.

## 6.7 Ethical considerations

The use of autologous MSCs such as hASCs for tissue engineered constructs helps to avoid ethical dilemmas and political issues (Dai et al., 2016). Therefore, hASCs are an easily acceptable and feasible option for regenerative medicine and graft development. However, there are ethical concerns related to possible MSC induced tumor growth and metastasis (Volarevic et al., 2018), for example, due hASC paracrine factor induced stimuli (Patrikoski et al., 2019). However, these risks can be minimized with careful evaluation of implantation site microenvironment (Patrikoski et al., 2019). With allogenic cells, such as HUVECs, there are potential ethical aspects to consider due to the fact that the cells originate from another donor. Nevertheless, HUVECs are generally viewed as a useful component of preclinical assessment before they can be replaced by a more suitable EC source (Muehleider et al., 2014).

## 6.8 Future perspectives

Cell-based therapies are emerging as advanced medicinal products with a growing impact on the treatment of various indications and especially those with limited conventional treatment options. As a matter of fact, musculoskeletal TE is a growing line of regenerative medicine applications.

On a critical note, MSC clinical trials have been the most frequent although they have also failed. The safety of MSCs has been assessed even if their fate after implantation is still not clear and might indicate rapid turnover in tissues. Both autologous and allogenic MSCs have been deemed almost equally promising thus allowing development of off-the-shelf cell-based therapies with well characterized and well suitable cells. The downside is that the exact mechanism of action that MSCs trigger upon implantation still remains to be elucidated. (Trounson & McDonald 2015)

## I

Tissue engineered tendon grafts are greatly anticipated for the treatment of large tendon defects. In study I, the results showed potential for future development with tenogenic differentiation of hASCs in a mechanically suitable filamentous PLA 96/4 scaffold. The developed TM could be optimized even further with different growth factor stimuli, for example, GDF-7 has been reported feasible (Gomes et al., 2017). What is more, sequential stimuli of different growth factors could be beneficial for enhanced hASC tenogenesis. Further, the tenogenic differentiation could be stimulated and supported by surface topography (Kishore et al., 2012), which would help diminish the need to use growth factors in the differentiation process, thus promoting the production process stability and the patient safety. Modifications of the PLA material surface could enhance hASC adhesion, proliferation and differentiation (Rasal et al., 2010). The bioactivity of the PLA scaffold could be improved by a coating treatment consisting of an electroactive polymer such as polypyrrole (Ateh et al., 2006; Bendrea et al., 2011). Further studies with bioactive coatings that mimic the native ECM could be applied (Chainani et al., 2013; Yang, G. et al., 2013), for example, fibronectin (Liu, Y. et al., 2008; Lu et al., 2005). Moreover, mechanical stimulation under cyclic tension, for example, could improve the orientation of collagenous matrix and mature the tissue organization and structure. What is more, since tendon cell niche is naturally hypoxic (Calejo et al., 2020), the effect of oxygen tension on tenogenesis could be tested with hASCs. In comparison, hBMSCs have been shown to undergo tendon-like tissue development under hypoxic conditions (Tsiapalis & Zeugolis 2019).

In critical terms, quantified cell viability analysis might be relevant in the future (Gering et al., 2019). Quantified data would be needed for easily comparable data between different researchers and research institutes. What is more, metabolism-based cell number analysis such as the MTT analysis based on mitogenic activity that essentially discerns living and necrotic cells would be beneficial since the current DNA-based cell number assay fails to make this relevant distinction and requires Live/Dead results to support the interpretation.

## II

Mineralized natural hydrogels such as COL have proven challenging to produce *in vitro*. In study II, hydrogel mineralization was induced with BaG 2-06 ionic dissolution products. Due to the rounded morphology of hASCs embedded in

GG hydrogel suggesting lack of adhesion sites, GG hydrogel might benefit from functionalization in future studies. For minimally invasive injectable bone graft development, the GG and COL hydrogels could be modified to allow an injectable application. The OPT and SPIM systems could be combined and allow simultaneous imaging. The 3D OPT-SPIM imaging of Live/Dead-stained hASCs and the distribution of osteogenic markers would be an advantage. A Raman line scan of a mineralized hydrogel scaffold instead of a measured spectrum from a single location could elucidate distribution of mineral deposits and potentially identify different mineral species (Evans et al., 2012; Volponi et al., 2015). Further, calculating the mineral-to-matrix ratio based on the area of the measured Raman inorganic phosphate peak could be utilized to characterize the pattern of mineralization (Evans et al., 2012) in different hydrogel scaffolds. An established *in vitro* bone model would facilitate research on musculoskeletal diseases and allow *in vitro* testing of drugs (Foyt et al., 2018). Interestingly, also hypoxic conditions could be tested to activate hMSC mechanosensitive pathways for musculoskeletal differentiation (Foyt et al., 2019).

### III

In study **III**, the mutually exclusive mineralization and microvascular network results indicated that the mechanisms that would allow both processes for cocultured hASCs and ECs within 3D hydrogels would require further investigation. The challenge of engineering complex microvascular networks still remains. (Shen et al., 2016) Our approach was to trigger vasculogenesis with bottom-up approach although the method has been suggested to result into unorganized, dense, and possibly resemble tumor-like vessel growth. In the approach, no control is exerted on vessel diameter or branching of the network or its density, all impacting *in vivo* anastomosis (Greco Song et al., 2018). Further, the choice of coculture media influences besides the cosurvival of both hASCs and HUVECs, also the osteogenesis and vasculogenesis processes although no superior media formulation has been postulated to date (Kolbe et al., 2011; Nunez-Toldra et al., 2019). The synergistic endothelial-osteogenic cellular crosstalk could be harnessed for more effective results in the future. This could be explored by observing morphology of intercellular barrier junctions with vascular endothelial cadherin analysis and testing barrier permeability. EC polarity and EC membrane receptor locations have also been suggested as a factor in tubular structure formation. (Greco Song et al., 2018)



The functionality and stability of the microvascular-like network in the EGM-2 (MM) condition could be tested by gentle perfusion to stabilize forming vascular network. To better simulate tissue specific niche microenvironments with multiple cell types integrated into a complex tissue-like structure, bioprinting might be a relevant approach. Specifically, repeatable vascular structure fabrication is expected to take a leap forward with bioprinting technologies and thus globally progress the TE field (Datta et al., 2017). While manual pipetting becomes easily cumbersome after the early stage of fabrication of multilayered hydrogel constructs and more high-throughput technologies are needed for scaling up. They also help avoid worker dependent variabilities thus adding to the repeatability.

Patterned hydrogels with separate endothelial and osteogenic niches was shown to result into organized vascularization with cocultured hBMSCs and HUVECs and mineralized regions with osteoblastic cells (Kazemzadeh-Narbat et al., 2017). Matrix composition has been shown to guide vascular network growth of MSC and EC coculture (Rao et al., 2012). Further, the density of the 3D matrix moderates endothelial sprouting, lumen formation, and capillary morphogenesis (Kniazeva & Putnam 2009), although the mechanical environment most likely cannot be attuned on a fine enough scale to guide capillary networks within a tissue engineered construct (Rouwkema & Khademhosseini 2016).

In the fused deposition bioprinting process, cell-laden bioink which is practically an injectable hydrogel is extruded as a continuous filament layer-by-layer into a structure. This method has the lowest resolution of approximately 200  $\mu\text{m}$ , while droplet-based bioprinting can reach a 100  $\mu\text{m}$  resolution, whereas laser-based techniques can operate at single cell level. (Greco Song et al., 2018) However, past the hype of the bioprinting trend, significant results are yet to materialize to back up the claims and no intact capillary network on cellular level has been achieved to date (Datta et al., 2017). The obstacle of coordinated osteogenesis and vasculogenesis processes with controlled osteogenic and endothelial cell-cell interactions remains unsurpassed for 3D bioprinted vascularized bone constructs (Shahabipour et al., 2019). On the topic, four-dimensional bioprinting (4D) that incorporates time into the process meaning that the printed object can shift its shape or functionality with appropriate stimuli in time (Wan et al., 2020), although the nature of the stimuli-responsive materials remains to be determined.

In study **III** results, the differentiation media compositions could be optimized since the BaG extract-based media promoted truncated cell morphologies and

aggregation of HUVECs. For example, the BaG extract could be diluted to diminish the harshness of the chemical stimulus for the cells. The ratio of cocultured cells as well as their application sequence should be tested further. Similarly, the effect of the differentiation media application sequence in time could be further analyzed. Supplementary analysis would be needed on hASC subpopulation characteristics and potential for multiple lineage differentiation. The 3D OPT-SPIM imaging of the distribution of osteogenic and endothelial immunocytochemical markers would be an advantage for mineralized matrix and vascular network analysis.

## 7 CONCLUSIONS

The main findings of the thesis and the conclusions reached in studies **I-III** were:

### **I**

Optimized TM with GDF-5 and L-ascorbic acid induced efficient hASC toward tendon lineage. PLA 96/4 structure supported cell adhesion and elongation compared to PLCL scaffolds in TM. Late tenogenesis markers COL1 and TNMD were strongly expressed on PLA 96/4 scaffolds in TM. The mechanical properties of braided PLA 96/4 scaffolds were suited for tendon TE applications. Nevertheless, PLA 96/4 scaffold alone was not able to induce hASC tenogenic differentiation. To the point, the combined TM with the selected filamentous PLA 96/4 scaffold were both essential. Thus, hASC tenogenic gene expression and collagenous matrix production were induced by TM. Overall, the combination of hASCs in braided filamentous PLA 96/4 scaffolds with TM were found efficacious for future tendon TE strategies and potential for *in vivo* testing.

### **II**

Osteogenic induction of hASC with BaG 2-06 ionic dissolution products in GG-SPD and COL 3D hydrogels was studied in addition to the effect of GG crosslinker for mineralization. The media incubation significantly increased GG and COL hydrogel mechanical properties. Also, gradual stiffening behavior mimicking evolving bone matrix was observed. Good viability was observed in all conditions. GG-SPD promoted rounded cell morphologies while COL supported elongation. Significantly higher bone marker gene expression of hASCs in COL was observed with the BaG OM induction. In the COL (BaG OM) condition, the prominent OCN and hydroxyapatite staining, in addition to the highest Raman spectroscopic measurement result qualified it as the strongest osteoinducer. GG crosslinking with the BaG 2-06 extract induced significantly higher hASC mineralization in GG-BaG hydrogels in OM. OPT and SPIM techniques were found highly utilizable and attractive methods for 3D imaging of transparent cell-laden hydrogels. The significant potential of hASC

osteogenesis with BaG OM induction in 3D hydrogels was demonstrated. New 3D hydrogel culture and analysis methods were presented with importance for *in vitro* bone model development.

### III

We tested the impact of BaG EM-OM with dissolved BaG ions for hASC osteogenesis and vasculogenesis in coculture with HUVECs in composite GG-COL hydrogels. Contrary to our hypothesis, the results indicated mutually exclusive production of late osteogenic and endothelial markers. We showed osteogenic differentiation of hASCs induced with BaG 2-06 extract based endothelial growth medium with osteogenic supplements in coculture with HUVECs. Importantly, we showed the effect of hASC osteogenic preconditioning for mineralization. Priming in OM enhanced hydroxyapatite mineralization of hASC-laden GG-COL hydrogels. The EGM-2 was essential for growth of endothelial tubular structures. However, the results did not confirm microvascularization network formation in 3D composite GG-COL hydrogel coculture. The results presented strong hASC osteogenic differentiation. However, microvessel-like networks were restricted in coculture in 3D GG-COL composite hydrogels. Overall, the results were moderately potential for development of further vascularized bone *in vitro* model.

To conclude, it is important to obtain data on hASC behavior in a controlled *in vitro* environment with specific media, biomaterial scaffold, and cell type, in order to facilitate future tissue engineered construct development. In general terms, this thesis work presents some potential alternatives worthy of considering as attractive starting points with insights into musculoskeletal TE and for further development of regenerative medicine applications.

## 8 AUTHOR'S CONTRIBUTION

**I.** The applicant designed the study in collaboration with all the co-authors. The applicant was responsible for the grand majority of the laboratory analyses, data collection, data analyses, and data interpretation. Statistical analyses were done in collaboration with HHu. The biomaterial scaffolds were produced by MKe, ET, Scaffdex Ltd and KP. JH was responsible for micro-CT imaging. The applicant wrote the article as the first author.

**II.** The applicant planned the study with all the co-authors. The applicant was responsible for the laboratory analyses, collection of the data, data analyses, and data interpretation. Hydrogel mechanical testing and GG hydrogel production were done in collaboration with JK and MKe. Statistical analyses were done independently with SPSS and HHu was consulted. JI and HHä were responsible for the Raman spectroscopic analyses. BB, TM and JH were responsible for the OPT and SPIM imaging and 3D image reconstruction. The applicant wrote the article as the first author.

**III.** The study was designed by the applicant in collaboration with all the co-authors. The applicant performed the laboratory analyses, collection of the data, data analyses, and data interpretation. Tissue samples for cell isolation were procured by MKä and KK. Hydrogel mechanical testing was done independently. GG hydrogel components were provided by MKe. Statistical analyses were done independently with SPSS and HHu was consulted. The applicant wrote the article as the first author.

## 9 ACKNOWLEDGEMENTS

This study was performed in the Adult Stem Cell Group, BioMediTech, Faculty of Medicine and Health Technology, Tampere University, Finland. This thesis work was carried out during the years 2012-2019 in the former Regea Institute of Regenerative Medicine, the BioMediTech Institute of Biosciences and Medical Technology, the University of Tampere, and the Tampere University of Technology as a part of the Pyrotissue project, the Human Spare Parts project, and the Academy of Finland Centre of Excellence Body-on-Chip Research. Firstly, I would like to thank my supervisors, the Adult Stem Group leader, Docent Susanna Miettinen, and Docent Suvi Haimi for their supervision and excellence in research and science. It has been a privilege having had this opportunity to learn about tissue engineering and regenerative medicine which I am grateful for. Secondly, I would like to thank the official reviewers of this thesis, Raquel Costa-Almeida, Ph.D., and Associate Professor Nicholas Evans, Ph.D., for their valuable and constructive criticism and their thorough evaluation of the thesis. They have offered valuable comments for the scientific value of this work. Thirdly, I would like to thank the members of the thesis committee, Docent Kati Juuti-Uusitalo, Docent Mervi Puska, and Niina Ahola, D.Sc., for their valuable contribution to this thesis work with academic expertise and encouraging, wise, and kind comments throughout the thesis process.

Thanks to all my co-authors; Birhanu Belay, Miina Björninen, Suvi Haimi, Heini Huhtala, Leena Hupa, Jari Hyttinen, Heikki Häkkänen, Janne A. Ihalainen, Minna Kellomäki, Janne T. Koivisto, Kirsi Kuismanen, Minna Kääriäinen, Susanna Miettinen, Toni Montonen, Miina Ojansivu, Kaarlo Paakinaho, Riitta Seppänen-Kaijansinkko, and Elina Talvitie for sharing their expertise.

I wish to acknowledge our research collaboration with the Tampere University Hospital, Minna Kääriäinen, M.D., Ph.D., and Kirsi Kuismanen M.D., Ph.D., for the tissue samples. For the cell isolation and flow cytometry analyses I wish to thank Miia Juntunen, M.Sc., Mimmi Patrikoski, Ph.D., and Miina Ojansivu, Ph.D. For the biomaterials, I wish to thank Scaffold Ltd. and Tuija Annala, M.Sc., Professor Minna Kellomäki and the Biomaterials and Tissue Engineering Group,

Tampere University. For expertise in hydrogel mechanical testing I wish to thank Janne T. Koivisto, D.Sc., and for innovative expertise in OPT and SPIM 3D imaging and micro-CT imaging, Professor Jari Hyttinen and the Computational Biophysics and Imaging Group (CBIG), Tampere University. I wish to acknowledge our research collaboration with the Åbo Akademi University and Professor Leena Hupa for the bioactive glass biomaterials and for the Raman spectroscopy measurements, Professor Janne A. Ihalainen, Ph.D., and the Spectroscopy for Detecting Dynamics of Biomolecules Group, Nanoscience Center, the University of Jyväskylä. I wish to acknowledge the Dean of the Tampere University Faculty of Medicine and Health Technology, Professor Tapio Visakorpi, the excellent Tampere University Kauppi Campus and Hervanta Campus research facilities, the services of Biocenter Finland (BF), Tampere Imaging Facility (TIF), Tampere University Cell Tech Laboratories and Core Facility services, and for Adult Stem Cell Group technical support, Anna-Maija Honkala, Bachelor of Laboratory Science, Bachelor of Laboratory Engineering, Miia Juntunen, M.Sc., and Sari Kalliokoski, Medical Laboratory Technician. I wish to acknowledge the former Institute of Medical Technology (IMT), Institute of Biotechnology (IBT), and the BioMediTech Institute (BMT), Tampere, Finland, for their seminal work in scientific education and research. Importantly, I wish to acknowledge the excellent interdisciplinary tissue engineering and stem cell research facilities and the scientific professionalism of the research staff in the former Regea Institute of Regenerative Medicine. I am thankful for all our research collaborators who have been involved in this thesis work. I wish to thank all the members of the Adult Stem Cell Group for expert discussions throughout this work. Especially, thanks to the Adult Stem Cell Group fellow doctoral students Miia Juntunen and Laura Hyväri, M.Sc., for the fun, travels and company on the TERMIS conference trips to San Diego and the typhoon-ravaged Kyoto, among others.

Thanks to my sailing friends for humour and sharing wide horizons in the seven seas. My deepest gratitude goes to my family for their love and support throughout this thesis work and all of my studies. You inspire me.

This work was financially supported by the Academy of Finland Centre of Excellence Body-on-Chip Research, Business Finland (formerly the Finnish Funding Agency for Technology and Innovation, TEKES), the Human Spare Parts project, The Finnish Cultural Foundation's Pirkanmaa Regional Fund (Marjatta Melkas-Rusanen and Anneli Melkas Fund), The Finnish Foundation for

Technology Promotion, the City of Tampere Science Fund, The Finnish Concordia Fund, the Tampere Graduate Program in Biomedicine and Biotechnology, the Tampere University Doctoral School, Tampere University, the former Tampere University of Technology, the former University of Tampere, and the Competitive State Research Financing of the Expert Responsibility area of Tampere University Hospital.

Oulu, 08 June 2020

A handwritten signature in black ink, appearing to read 'Kaisa Vuornos', written in a cursive style.

Kaisa Vuornos



## REFERENCES

- Aach, J., Lunshof, J., Iyer, E., Church, G.M. (2017). Addressing the ethical issues raised by synthetic human entities with embryo-like features. *eLife*, 6, 20674.
- Abaci, H.E., Guo, Z., Coffman, A., Gillette, B., Lee, W.H., Sia, S.K., Christiano, A.M. (2016). Human Skin Constructs with Spatially Controlled Vasculature Using Primary and iPSC-Derived Endothelial Cells. *Advanced Healthcare Materials*, 5(14), 1800-1807.
- Abramsson, A., Lindblom, P., Betsholtz, C. (2003). Endothelial and nonendothelial sources of PDGF-B regulate pericyte recruitment and influence vascular pattern formation in tumors. *The Journal of Clinical Investigation*, 112(8), 1142-1151.
- Ahn, E.H., Kim, Y., Kshitiz, An, S.S., Afzal, J., Lee, S., Kwak, M., Suh, K.Y., Kim, D.H., Levchenko, A. (2014). Spatial control of adult stem cell fate using nanotopographic cues. *Biomaterials*, 35(8), 2401-2410.
- Aksu, A.E., Rubin, J.P., Dudas, J.R., Marra, K.G. (2008). Role of gender and anatomical region on induction of osteogenic differentiation of human adipose-derived stem cells. *Annals of Plastic Surgery*, 60(3), 306-322.
- Albarenque, S.M., Zwacka, R.M., Mohr, A. (2011). Both human and mouse mesenchymal stem cells promote breast cancer metastasis. *Stem Cell Research*, 7(2), 163-171.
- Amano, Y., Nishiguchi, A., Matsusaki, M., Iseoka, H., Miyagawa, S., Sawa, Y., Seo, M., Yamaguchi, T., Akashi, M. (2016). Development of vascularized iPSC derived 3D-cardiomyocyte tissues by filtration Layer-by-Layer technique and their application for pharmaceutical assays. *Acta Biomaterialia*, 33, 110-121.
- Argentati, C., Morena, F., Bazzucchi, M., Armentano, I., Emiliani, C., Martino, S. (2018). Adipose Stem Cell Translational Applications: From Bench-to-Bedside. *International Journal of Molecular Sciences*, 19(11), 3475.
- Aspenberg, P. (2007). Stimulation of tendon repair: mechanical loading, GDFs and platelets. A mini-review. *International Orthopaedics*, 31(6), 783-789.
- ASTM F2900-11 *Standard Guide for Characterization of Hydrogels used in Regenerative Medicine* (2011). ASTM International, West Conshohocken, PA, USA.
- Atala, A., Bauer, S.B., Soker, S., Yoo, J.J., Retik, A.B. (2006). Tissue-engineered autologous bladders for patients needing cystoplasty. *Lancet*, 367(9518), 1241-1246.
- Ateh, D.D., Navsaria, H.A., Vadgama, P. (2006). Polypyrrole-based conducting polymers and interactions with biological tissues. *Journal of the Royal Society, Interface / the Royal Society*, 3(11), 741-752.
- Aust, L., Devlin, B., Foster, S.J., Halvorsen, Y.D., Hicok, K., du Laney, T., Sen, A., Willingmyre, G.D., Gimble, J.M. (2004). Yield of human adipose-derived adult stem cells from liposuction aspirates. *Cytotherapy*, 6(1), 7-14.
- Bacelar, A.H., Silva-Correia, J., Oliveira, J.M., Reis, R.L. (2016). Recent progress in gellan gum hydrogels provided by functionalization strategies. *Journal of Materials Chemistry B*, 4(37), 6164-6174.

- Baer, P.C. (2011). Adipose-derived stem cells and their potential to differentiate into the epithelial lineage. *Stem Cells and Development*, 20(10), 1805-1816.
- Baer, P.C. (2014). Adipose-derived mesenchymal stromal/stem cells: An update on their phenotype in vivo and in vitro. *World Journal of Stem Cells*, 6(3), 256-265.
- Baer, P.C., Schubert, R., Bereiter-Hahn, J., Plosser, M., Geiger, H. (2009). Expression of a functional epidermal growth factor receptor on human adipose-derived mesenchymal stem cells and its signaling mechanism. *European Journal of Cell Biology*, 88(5), 273-283.
- Baglioni, S., Cantini, G., Poli, G., Francalanci, M., Squecco, R., Di Franco, A., Borgogni, E., Frontera, S., Nesi, G., Liotta, F., Lucchese, M., Perigli, G., Francini, F., Forti, G., Serio, M., Luconi, M. (2012). Functional differences in visceral and subcutaneous fat pads originate from differences in the adipose stem cell. *PLoS One*, 7(5), e36569.
- Bajpai, V.K., & Andreadis, S.T. (2012). Stem cell sources for vascular tissue engineering and regeneration. *Tissue Engineering. Part B, Reviews*, 18(5), 405-425.
- Baker, S.C., Rohman, G., Hinley, J., Stahlschmidt, J., Cameron, N.R., Southgate, J. (2011). Cellular integration and vascularisation promoted by a resorbable, particulate-leached, cross-linked poly(epsilon-caprolactone) scaffold. *Macromolecular Bioscience*, 11(5), 618-627.
- Baldwin, J., Antille, M., Bonda, U., De-Juan-Pardo, E.M., Khosrotehrani, K., Ivanovski, S., Petcu, E.B., Huttmacher, D.W. (2014). In vitro pre-vascularisation of tissue-engineered constructs A co-culture perspective. *Vascular Cell*, 6, 13.
- Belay, B., Koivisto, J.T., Vuornos, K., Montonen, T., Koskela, O., Lehti-Polojärvi, M., Miettinen, S., Kellomäki, M., Figueiras, E., Hyttinen, J. (2017). Optical Projection Tomography Imaging of Single Cells in 3D Gellan Gum Hydrogel. Paper presented at the *IFMBE Proceedings EMBEC & NBC 2017*, Tampere, Finland.
- Bellahcene, A., Bonjean, K., Fohr, B., Fedarko, N.S., Robey, F.A., Young, M.F., Fisher, L.W., Castronovo, V. (2000). Bone sialoprotein mediates human endothelial cell attachment and migration and promotes angiogenesis. *Circulation Research*, 86(8), 885-891.
- Bellini, D., Cencetti, C., Meraner, J., Stoppoloni, D., D'Abusco, A.S., Matricardi, P. (2015). An in situ gelling system for bone regeneration of osteochondral defects. *European Polymer Journal*, 72, 642-650.
- Bendrea, A.D., Cianga, L., Cianga, I. (2011). Review paper: progress in the field of conducting polymers for tissue engineering applications. *Journal of Biomaterials Applications*, 26(1), 3-84.
- Benias, P.C., Wells, R.G., Sackey-Aboagye, B., Klavan, H., Reidy, J., Buonocore, D., Miranda, M., Kornacki, S., Wayne, M., Carr-Locke, D., Theise, N.D. (2018a). Author Correction: Structure and Distribution of an Unrecognized Interstitium in Human Tissues. *Scientific Reports*, 8(1), 7610.
- Benias, P.C., Wells, R.G., Sackey-Aboagye, B., Klavan, H., Reidy, J., Buonocore, D., Miranda, M., Kornacki, S., Wayne, M., Carr-Locke, D., Theise, N.D. (2018b). Structure and Distribution of an Unrecognized Interstitium in Human Tissues. *Scientific Reports*, 8(1), 4947.
- Bi, L., Rahaman, M.N., Day, D.E., Brown, Z., Samujh, C., Liu, X., Mohammadkhah, A., Dusevich, V., Eick, J.D., Bonewald, L.F. (2013). Effect of bioactive borate glass microstructure on bone regeneration, angiogenesis, and hydroxyapatite conversion in a rat calvarial defect model. *Acta Biomaterialia*, 9(8), 8015-8026.

- Bidarra, S.J., Barrias, C.C., Barbosa, M.A., Soares, R., Amedee, J., Granja, P.L. (2011). Phenotypic and proliferative modulation of human mesenchymal stem cells via crosstalk with endothelial cells. *Stem Cell Research*, 7(3), 186-197.
- Binner, M., Bray, L.J., Friedrichs, J., Freudenberg, U., Tsurkan, M.V., Werner, C. (2017). Cell-instructive starPEG-heparin-collagen composite matrices. *Acta Biomaterialia*, 53, 70-80.
- Blache, U., Metzger, S., Vallmajo-Martin, Q., Martin, I., Djonov, V., Ehrbar, M. (2016). Dual Role of Mesenchymal Stem Cells Allows for Microvascularized Bone Tissue-Like Environments in PEG Hydrogels. *Advanced Healthcare Materials*, 5(4), 489-498.
- Bolt, P., Clerk, A.N., Luu, H.H., Kang, Q., Kummer, J.L., Deng, Z.L., Olson, K., Primus, F., Montag, A.G., He, T.C., Haydon, R.C., Toolan, B.C. (2007). BMP-14 gene therapy increases tendon tensile strength in a rat model of Achilles tendon injury. *The Journal of Bone and Joint Surgery.American Volume*, 89(6), 1315-1320.
- Bora, P., & Majumdar, A.S. (2017). Adipose tissue-derived stromal vascular fraction in regenerative medicine: a brief review on biology and translation. *Stem Cell Research & Therapy*, 8(1), 145-017-0598-y.
- Boschetti, F., Raimondi, M.T., Migliavacca, F., Dubini, G. (2006). Prediction of the micro-fluid dynamic environment imposed to three-dimensional engineered cell systems in bioreactors. *Journal of Biomechanics*, 39(3), 418-425.
- Bourin, P., Bunnell, B.A., Casteilla, L., Dominici, M., Katz, A.J., March, K.L., Redl, H., Rubin, J.P., Yoshimura, K., Gimple, J.M. (2013). Stromal cells from the adipose tissue-derived stromal vascular fraction and culture expanded adipose tissue-derived stromal/stem cells: a joint statement of the International Federation for Adipose Therapeutics and Science (IFATS) and the International Society for Cellular Therapy (ISCT). *Cytotherapy*, 15(6), 641-648.
- Brodie, M., Vollenweider, L., Murphy, J.L., Xu, F., Lyman, A., Lew, W.D., Lee, B.P. (2011). Biomechanical properties of Achilles tendon repair augmented with a bioadhesive-coated scaffold. *Biomedical Materials*, 6(1), 015014.
- Brown, R.F., Rahaman, M.N., Dwilewicz, A.B., Huang, W., Day, D.E., Li, Y., Bal, B.S. (2009). Effect of borate glass composition on its conversion to hydroxyapatite and on the proliferation of MC3T3-E1 cells. *Journal of Biomedical Materials Research.Part A*, 88(2), 392-400.
- Burdick, J. A., & Mauck, R. L. (Eds.). (2011). *Biomaterials for Tissue Engineering Applications – A Review of the Past and Future Trends*. Vienna: Springer-Verlag.
- Butler, D.L., Juncosa, N., Dressler, M.R. (2004). Functional efficacy of tendon repair processes. *Annual Review of Biomedical Engineering*, 6, 303-329.
- Cai, L., Johnstone, B.H., Cook, T.G., Liang, Z., Traktuev, D., Cornetta, K., Ingram, D.A., Rosen, E.D., March, K.L. (2007). Suppression of hepatocyte growth factor production impairs the ability of adipose-derived stem cells to promote ischemic tissue revascularization. *Stem Cells (Dayton, Ohio)*, 25(12), 3234-3243.
- Calejo, I., Costa-Almeida, R., Reis, R.L., Gomes, M.E. (2020). A Physiology-Inspired Multifactorial Toolbox in Soft-to-Hard Musculoskeletal Interface Tissue Engineering. *Trends in Biotechnology*, 38(1), 83-98.
- Caliari, S.R., & Harley, B.A. (2013). Composite Growth Factor Supplementation Strategies to Enhance Tenocyte Bioactivity in Aligned Collagen-GAG Scaffolds. *Tissue Engineering. Part A*, 19(9-10), 1100-1112.

- Caliari, S.R., Ramirez, M.A., Harley, B.A. (2011). The development of collagen-GAG scaffold-membrane composites for tendon tissue engineering. *Biomaterials*, 32(34), 8990-8998.
- Callister, W. D., Jr, & Rethwisch, D. G. (2014). *Materials science and engineering: an introduction* (9th ed ed.). Hoboken, NJ: John Wiley and Sons.
- Cao, Y., Sun, Z., Liao, L., Meng, Y., Han, Q., Zhao, R.C. (2005). Human adipose tissue-derived stem cells differentiate into endothelial cells in vitro and improve postnatal neovascularization in vivo. *Biochemical and Biophysical Research Communications*, 332(2), 370-379.
- Caplan, A.I. (1991). Mesenchymal stem cells. *Journal of Orthopaedic Research*, 9(5), 641-650.
- Casteilla, L., Planat-Benard, V., Laharrague, P., Cousin, B. (2011). Adipose-derived stromal cells: Their identity and uses in clinical trials, an update. *World Journal of Stem Cells*, 3(4), 25-33.
- Castillo Diaz, L.A., Elsayy, M., Saiani, A., Gough, J.E., Miller, A.F. (2016). Osteogenic differentiation of human mesenchymal stem cells promotes mineralization within a biodegradable peptide hydrogel. *Journal of Tissue Engineering*, 7, 2041731416649789.
- Cengiz, I.F., Oliveira, J.M., Reis, R.L. (2018). Micro-CT - a digital 3D microstructural voyage into scaffolds: a systematic review of the reported methods and results. *Biomaterials Research*, 22, 26.
- Centanni, J.M., Straseski, J.A., Wicks, A., Hank, J.A., Rasmussen, C.A., Lokuta, M.A., Schurr, M.J., Foster, K.N., Faucher, L.D., Caruso, D.M., Comer, A.R., Allen-Hoffmann, B.L. (2011). StrataGraft skin substitute is well-tolerated and is not acutely immunogenic in patients with traumatic wounds: results from a prospective, randomized, controlled dose escalation trial. *Annals of Surgery*, 253(4), 672-683.
- Chae, Y.K., Ranganath, K., Hammerman, P.S., Vaklavas, C., Mohindra, N., Kalyan, A., Matsangou, M., Costa, R., Carneiro, B., Villafior, V.M., Cristofanilli, M., Giles, F.J. (2017). Inhibition of the fibroblast growth factor receptor (FGFR) pathway: the current landscape and barriers to clinical application. *Oncotarget*, 8(9), 16052-16074.
- Chainani, A., Hippensteel, K.J., Kishan, A., Garrigues, N.W., Ruch, D.S., Guilak, F., Little, D. (2013). Multilayered electrospun scaffolds for tendon tissue engineering. *Tissue Engineering. Part A*, 19(23-24), 2594-2604.
- Chan, X.Y., Elliott, M.B., Macklin, B., Gerecht, S. (2018). Human Pluripotent Stem Cells to Engineer Blood Vessels. *Advances in Biochemical Engineering/ Biotechnology*, 163, 147-168.
- Chang, W.G., & Niklason, L.E. (2017). A short discourse on vascular tissue engineering. *NPJ Regenerative Medicine*, 2(7), 10.1038/s41536.
- Chatterjea, A., Meijer, G., van Blitterswijk, C., de Boer, J. (2010). Clinical application of human mesenchymal stromal cells for bone tissue engineering. *Stem Cells International*, 2010, 215625.
- Chen, C.H., Cao, Y., Wu, Y.F., Bais, A.J., Gao, J.S., Tang, J.B. (2008). Tendon healing in vivo: gene expression and production of multiple growth factors in early tendon healing period. *The Journal of Hand Surgery*, 33(10), 1834-1842.
- Chen, H., Zhang, Y., Ding, P., Zhang, T., Zan, Y., Ni, T., Lin, R., Liu, M., Pei, R. (2018). Bone Marrow-Derived Mesenchymal Stem Cells Encapsulated in Functionalized Gellan Gum/Collagen Hydrogel for Effective Vascularization. *ACS Applied Bio Materials*, 1(5), 1408-1415.

- Chen, Y.C., Lin, R.Z., Qi, H., Yang, Y., Bae, H., Melero-Martin, J.M., Khademhosseini, A. (2012). Functional Human Vascular Network Generated in Photocrosslinkable Gelatin Methacrylate Hydrogels. *Advanced Functional Materials*, 22(10), 2027-2039.
- Choi, J.H., Choi, O.K., Lee, J., Noh, J., Lee, S., Park, A., Rim, M.A., Reis, R.L., Khang, G. (2019). Evaluation of double network hydrogel of poloxamer-heparin/gellan gum for bone marrow stem cells delivery carrier. *Colloids and Surfaces B: Biointerfaces*, 181, 879-889.
- Choumerianou, D.M., Dimitriou, H., Kalmanti, M. (2008). Stem cells: promises versus limitations. *Tissue Engineering, Part B, Reviews*, 14(1), 53-60.
- Condic, M.L. (2014). Totipotency: what it is and what it is not. *Stem Cells and Development*, 23(8), 796-812.
- Correia, C., Grayson, W.L., Park, M., Hutton, D., Zhou, B., Guo, X.E., Niklason, L., Sousa, R.A., Reis, R.L., Vunjak-Novakovic, G. (2011). In vitro model of vascularized bone: synergizing vascular development and osteogenesis. *PLoS One*, 6(12), e28352.
- Correia, C.R., Santos, T.C., Pirraco, R.P., Cerqueira, M.T., Marques, A.P., Reis, R.L., Mano, J.F. (2017). In vivo osteogenic differentiation of stem cells inside compartmentalized capsules loaded with co-cultured endothelial cells. *Acta Biomaterialia*, 53, 483-494.
- Cossu, G., Birchall, M., Brown, T., De Coppi, P., Culme-Seymour, E., Gibbon, S., Hitchcock, J., Mason, C., Montgomery, J., Morris, S., Muntoni, F., Napier, D., Owji, N., Prasad, A., Round, J., Saprai, P., Stilgoe, J., Thrasher, A., Wilson, J. (2018). Lancet Commission: Stem cells and regenerative medicine. *Lancet (London, England)*, 391(10123), 883-910.
- Costa-Almeida, R., Calejo, I., Gomes, M.E. (2019). Mesenchymal Stem Cells Empowering Tendon Regenerative Therapies. *International Journal of Molecular Sciences*, 20(12), 10.3390/ijms20123002.
- Costa-Almeida, R., Calejo, I., Reis, R.L., Gomes, M.E. (2018). Crosstalk between adipose stem cells and tendon cells reveals a temporal regulation of tenogenesis by matrix deposition and remodeling. *Journal of Cellular Physiology*, 233(7), 5383-5395.
- Coutinho, D.F., Sant, S.V., Shin, H., Oliveira, J.T., Gomes, M.E., Neves, N.M., Khademhosseini, A., Reis, R.L. (2010). Modified Gellan Gum hydrogels with tunable physical and mechanical properties. *Biomaterials*, 31(29), 7494-7502.
- Cross, M.J., & Claesson-Welsh, L. (2001). FGF and VEGF function in angiogenesis: signalling pathways, biological responses and therapeutic inhibition. *Trends in Pharmacological Sciences*, 22(4), 201-207.
- Czaplewski, S.K., Tsai, T.L., Duenwald-Kuehl, S.E., Vanderby, R., Jr, Li, W.J. (2014). Tenogenic differentiation of human induced pluripotent stem cell-derived mesenchymal stem cells dictated by properties of braided submicron fibrous scaffolds. *Biomaterials*, 35(25), 6907-6917.
- da Silva, J.G., Babb, R., Salzlechner, C., Sharpe, P.T., Brauer, D.S., Gentleman, E. (2017). Optimisation of lithium-substituted bioactive glasses to tailor cell response for hard tissue repair. *Journal of Materials Science*, 52(15), 8832-8844.
- Dahlgren, L.A., Mohammed, H.O., Nixon, A.J. (2005). Temporal expression of growth factors and matrix molecules in healing tendon lesions. *Journal of Orthopaedic Research : Official Publication of the Orthopaedic Research Society*, 23(1), 84-92.

- Dai, R., Wang, Z., Samanipour, R., Koo, K.I., Kim, K. (2016). Adipose-Derived Stem Cells for Tissue Engineering and Regenerative Medicine Applications. *Stem Cells International*, 2016, 6737345.
- Datta, P., Ayan, B., Ozbolat, I.T. (2017). Bioprinting for vascular and vascularized tissue biofabrication. *Acta Biomaterialia*, 51, 1-20.
- Day, R.M. (2005). Bioactive glass stimulates the secretion of angiogenic growth factors and angiogenesis in vitro. *Tissue Engineering*, 11(5-6), 768-777.
- de Almeida, P.E., Ransohoff, J.D., Nahid, A., Wu, J.C. (2013). Immunogenicity of pluripotent stem cells and their derivatives. *Circulation Research*, 112(3), 549-561.
- De Francesco, F., Ricci, G., D'Andrea, F., Nicoletti, G.F., Ferraro, G.A. (2015). Human Adipose Stem Cells: From Bench to Bedside. *Tissue Engineering, Part B, Reviews*, 21(6), 572-584.
- De Giglio, E., Bonifacio, M.A., Ferreira, A.M., Cometa, S., Ti, Z.Y., Stanzione, A., Dalgarno, K., Gentile, P. (2018). Multi-compartment scaffold fabricated via 3D-printing as in vitro co-culture osteogenic model. *Scientific Reports*, 8(1), 15130.
- de Mos, M., van der Windt, A.E., Jahr, H., van Schie, H.T., Weinans, H., Verhaar, J.A., van Osch, G.J. (2008). Can platelet-rich plasma enhance tendon repair? A cell culture study. *The American Journal of Sports Medicine*, 36(6), 1171-1178.
- de Peppo, G.M., Agheli, H., Karlsson, C., Ekstrom, K., Brisby, H., Lenneras, M., Gustafsson, S., Sjoval, P., Johansson, A., Olsson, E., Lausmaa, J., Thomsen, P., Petronis, S. (2014). Osteogenic response of human mesenchymal stem cells to well-defined nanoscale topography in vitro. *International Journal of Nanomedicine*, 9, 2499-2515.
- Deng, D., Liu, W., Xu, F., Yang, Y., Zhou, G., Zhang, W.J., Cui, L., Cao, Y. (2009). Engineering human neo-tendon tissue in vitro with human dermal fibroblasts under static mechanical strain. *Biomaterials*, 30(35), 6724-6730.
- Desai, H.V., Voruganti, I.S., Jayasuriya, C., Chen, Q., Darling, E.M. (2014). Live-cell, temporal gene expression analysis of osteogenic differentiation in adipose-derived stem cells. *Tissue Engineering, Part A*, 20(5-6), 899-907.
- Diekjürgen, D., & Grainger, D.W. (2017). Polysaccharide matrices used in 3D in vitro cell culture systems. *Biomaterials*, 141, 96-115.
- Doherty, P. (2009). Inflammation, Carcinogenicity and Hypersensitivity. In R. Narayan (Ed.), *Biomedical Materials* (pp. 201-214). New York: Springer.
- Domingues, R.M., Chiera, S., Gershovich, P., Motta, A., Reis, R.L., Gomes, M.E. (2016). Enhancing the Biomechanical Performance of Anisotropic Nanofibrous Scaffolds in Tendon Tissue Engineering: Reinforcement with Cellulose Nanocrystals. *Advanced Healthcare Materials*, 5(11), 1364-1375.
- Dominici, M., Le Blanc, K., Mueller, I., Slaper-Cortenbach, I., Marini, F., Krause, D., Deans, R., Keating, A., Prockop, D., Horwitz, E. (2006). Minimal criteria for defining multipotent mesenchymal stromal cells. The International Society for Cellular Therapy position statement. *Cytotherapy*, 8(4), 315-317.
- Doube, M., Klosowski, M.M., Arganda-Carreras, I., Cordelieres, F.P., Dougherty, R.P., Jackson, J.S., Schmid, B., Hutchinson, J.R., Shefelbine, S.J. (2010). BoneJ: Free and extensible bone image analysis in ImageJ. *Bone*, 47(6), 1076-1079.
- Douglas, T.E., Piwowarczyk, W., Pamula, E., Liskova, J., Schaubroeck, D., Leeuwenburgh, S.C., Brackman, G., Balcaen, L., Detsch, R., Declercq, H., Cholewa-Kowalska, K., Dokupil, A., Cuijpers, V.M., Vanhaecke, F., Cornelissen, R., Coenye, T., Boccaccini, A.R., Dubruel, P. (2014). Injectable self-gelling

- composites for bone tissue engineering based on gellan gum hydrogel enriched with different bioglasses. *Biomedical Materials (Bristol, England)*, 9(4), 045014.
- Drnovsek, N., Novak, S., Dragin, U., Ceh, M., Gorenssek, M., Gradisar, M. (2012). Bioactive glass enhances bone ingrowth into the porous titanium coating on orthopaedic implants. *International Orthopaedics*, 36(8), 1739-1745.
- Eder, C., & Wild, C. (2019). Technology forecast: advanced therapies in late clinical research, EMA approval or clinical application via hospital exemption. *Journal of Market Access & Health Policy*, 7(1), 1600939.
- El-Fiqi, A., Lee, J.H., Lee, E.J., Kim, H.W. (2013). Collagen hydrogels incorporated with surface-aminated mesoporous nanobioactive glass: Improvement of physicochemical stability and mechanical properties is effective for hard tissue engineering. *Acta Biomaterialia*, 9(12), 9508-9521.
- EN ISO 10993-5, Biological Evaluation of Medical Devices. Part 5: Tests for in Vitro Cytotoxicity (2009). International Organization for Standardization (ISO), Geneva, Switzerland.
- EN ISO 719:1985. (2011). *Glass. Hydrolytic resistance of glass grains at 98 degrees C.* (No. 719). Geneva, Switzerland:
- Engler, A.J., Sen, S., Sweeney, H.L., Discher, D.E. (2006). Matrix elasticity directs stem cell lineage specification. *Cell*, 126(4), 677-689.
- Erisken, C., Zhang, X., Moffat, K.L., Levine, W.N., Lu, H.H. (2013). Scaffold fiber diameter regulates human tendon fibroblast growth and differentiation. *Tissue Engineering.Part A*, 19(3-4), 519-528.
- Evans, N.D., & Gentleman, E. (2014). The role of material structure and mechanical properties in cell-matrix interactions. *Journal of Materials Chemistry B*, 2(17), 2345-2356.
- Evans, N.D., Gentleman, E., Chen, X., Roberts, C.J., Polak, J.M., Stevens, M.M. (2010). Extracellular matrix-mediated osteogenic differentiation of murine embryonic stem cells. *Biomaterials*, 31(12), 3244-3252.
- Evans, N.D., Minelli, C., Gentleman, E., LaPointe, V., Patankar, S.N., Kallivretaki, M., Chen, X., Roberts, C.J., Stevens, M.M. (2009). Substrate stiffness affects early differentiation events in embryonic stem cells. *European Cells & Materials*, 18, 1-13.
- Evans, N.D., Swain, R.J., Gentleman, E., Gentleman, M.M., Stevens, M.M. (2012). Gene-expression analysis reveals that embryonic stem cells cultured under osteogenic conditions produce mineral non-specifically compared to marrow stromal cells or osteoblasts. *European Cells & Materials*, 24, 211-223.
- Fedorovich, N.E., Kuipers, E., Gawlitta, D., Dhert, W.J., Alblas, J. (2011). Scaffold porosity and oxygenation of printed hydrogel constructs affect functionality of embedded osteogenic progenitors. *Tissue Engineering.Part A*, 17(19-20), 2473-2486.
- Ferrara, N. (2001). Role of vascular endothelial growth factor in regulation of physiological angiogenesis. *American Journal of Physiology.Cell Physiology*, 280(6), C1358-66.
- Ferreira, A.M., Gentile, P., Chiono, V., Ciardelli, G. (2012). Collagen for bone tissue regeneration. *Acta Biomaterialia*, 8(9), 3191-3200.
- Ferris, C.J., Gilmore, K.J., Wallace, G.G., Panhuis, M.i.h. (2013). Modified gellan gum hydrogels for tissue engineering applications. *Soft Matter*, 9(14), 3705-3711.
- Fialho, A.M., Moreira, L.M., Granja, A.T., Popescu, A.O., Hoffmann, K., Sa-Correia, I. (2008). Occurrence, production, and applications of gellan: current state and perspectives. *Applied Microbiology and Biotechnology*, 79(6), 889-900.

- Figueiras, E., Soto, A.M., Jesus, D., Lehti, M., Koivisto, J., Parraga, J.E., Silva-Correia, J., Oliveira, J.M., Reis, R.L., Kellomaki, M., Hyttinen, J. (2014). Optical projection tomography as a tool for 3D imaging of hydrogels. *Biomedical Optics Express*, 5(10), 3443-3449.
- Folkman, J. (2007). Angiogenesis: an organizing principle for drug discovery? *Nature Reviews Drug Discovery*, 6(4), 273-286.
- Font Tellado, S., Balmayor, E.R., Van Griensven, M. (2015). Strategies to engineer tendon/ligament-to-bone interface: Biomaterials, cells and growth factors. *Advanced Drug Delivery Reviews*, 94(Nov 1), 126-140.
- Foyt, D.A., Norman, M.D.A., Yu, T.T.L., Gentleman, E. (2018). Exploiting Advanced Hydrogel Technologies to Address Key Challenges in Regenerative Medicine. *Advanced Healthcare Materials*, 7(8), e1700939.
- Foyt, D.A., Taheem, D.K., Ferreira, S.A., Norman, M.D.A., Petzold, J., Jell, G., Grigoriadis, A.E., Gentleman, E. (2019). Hypoxia impacts human MSC response to substrate stiffness during chondrogenic differentiation. *Acta Biomaterialia*, 89(Apr 15), 73-83.
- Franchi, M., Trire, A., Quaranta, M., Orsini, E., Ottani, V. (2007). Collagen structure of tendon relates to function. *The Scientific World Journal*, 7, 404-420.
- Friedenstein, A.J., Petrakova, K.V., Kurolesova, A.I., Frolova, G.P. (1968). Heterotopic transplants of bone marrow. *Transplantation*, 6(2), 230-247.
- Friess, W. (1998). Collagen--biomaterial for drug delivery. *European Journal of Pharmaceutics and Biopharmaceutics : Official Journal of Arbeitsgemeinschaft Fur Pharmazeutische Verfahrenstechnik E.V.*, 45(2), 113-136.
- Fritton, S.P., & Weinbaum, S. (2009). Fluid and Solute Transport in Bone: Flow-Induced Mechanotransduction. *Annual Review of Fluid Mechanics*, 41, 347-374.
- Gantar, A., da Silva, L.P., Oliveira, J.M., Marques, A.P., Correlo, V.M., Novak, S., Reis, R.L. (2014). Nanoparticulate bioactive-glass-reinforced gellan-gum hydrogels for bone-tissue engineering. *Materials Science & Engineering C, Materials for Biological Applications*, 43, 27-36.
- Garrison, K.R., Donell, S., Ryder, J., Shemilt, I., Mugford, M., Harvey, I., Song, F. (2007). Clinical effectiveness and cost-effectiveness of bone morphogenetic proteins in the non-healing of fractures and spinal fusion: a systematic review. *Health Technology Assessment (Winchester, England)*, 11(30), 1-150, iii-iv.
- Garrison, K.R., Shemilt, I., Donell, S., Ryder, J.J., Mugford, M., Harvey, I., Song, F., Alt, V. (2010). Bone morphogenetic protein (BMP) for fracture healing in adults. *Cochrane Database of Systematic Reviews (Online)*, 2010(6), CD006950.
- Gaspar, D., Spanoudes, K., Holladay, C., Pandit, A., Zeugolis, D. (2015). Progress in cell-based therapies for tendon repair. *Advanced Drug Delivery Reviews*, 84, 240-256.
- Gelse, K., Poschl, E., Aigner, T. (2003). Collagens--structure, function, and biosynthesis. *Advanced Drug Delivery Reviews*, 55(12), 1531-1546.
- Gentleman, E., Dee, K.C., Livesay, G.A., Nauman, E.A. (2007). Operating curves to characterize the contraction of fibroblast-seeded collagen gel/collagen fiber composite biomaterials: effect of fiber mass. *Plastic and Reconstructive Surgery*, 119(2), 508-516.
- Gentleman, E., Lay, A.N., Dickerson, D.A., Nauman, E.A., Livesay, G.A., Dee, K.C. (2003). Mechanical characterization of collagen fibers and scaffolds for tissue engineering. *Biomaterials*, 24(21), 3805-3813.



- Gentleman, E., Livesay, G.A., Dee, K.C., Nauman, E.A. (2006). Development of ligament-like structural organization and properties in cell-seeded collagen scaffolds in vitro. *Annals of Biomedical Engineering*, 34(5), 726-736.
- Gerhardt, H. (2008). VEGF and endothelial guidance in angiogenic sprouting. *Organogenesis*, 4(4), 241-246.
- Gering, C., Koivisto, J.T., Parraga, J., Leppiniemi, J., Vuornos, K., Hytonen, V.P., Miettinen, S., Kellomaki, M. (2019). Design of modular gellan gum hydrogel functionalized with avidin and biotinylated adhesive ligands for cell culture applications. *PLoS One*, 14(8), e0221931.
- Giblin, S.P., & Midwood, K.S. (2015). Tenascin-C: Form versus function. *Cell Adhesion & Migration*, 9(1-2), 48-82.
- Gimble, J., & Guilak, F. (2003). Adipose-derived adult stem cells: isolation, characterization, and differentiation potential. *Cytotherapy*, 5(5), 362-369.
- Goel, S., Duda, D.G., Xu, L., Munn, L.L., Boucher, Y., Fukumura, D., Jain, R.K. (2011). Normalization of the vasculature for treatment of cancer and other diseases. *Physiological Reviews*, 91(3), 1071-1121.
- Gomes, M.E., Rodrigues, M.T., Domingues, R.M.A., Reis, R.L. (2017). Tissue Engineering and Regenerative Medicine: New Trends and Directions-A Year in Review. *Tissue Engineering, Part B, Reviews*, 23(3), 211-224.
- Goodell, M.A. (1999). Introduction: Focus on hematology. CD34(+) or CD34(-): does it really matter? *Blood*, 94(8), 2545-2547.
- Greco Song, H.H., Rumma, R.T., Ozaki, C.K., Edelman, E.R., Chen, C.S. (2018). Vascular Tissue Engineering: Progress, Challenges, and Clinical Promise. *Cell Stem Cell*, 22(4), 608.
- Grellier, M., Bareille, R., Bourget, C., Amedee, J. (2009). Responsiveness of human bone marrow stromal cells to shear stress. *Journal of Tissue Engineering and Regenerative Medicine*, 3(4), 302-309.
- Grellier, M., Granja, P.L., Fricain, J.C., Bidarra, S.J., Renard, M., Bareille, R., Bourget, C., Amedee, J., Barbosa, M.A. (2009). The effect of the co-immobilization of human osteoprogenitors and endothelial cells within alginate microspheres on mineralization in a bone defect. *Biomaterials*, 30(19), 3271-3278.
- Gross, G., & Hoffmann, A. (2013). Therapeutic strategies for tendon healing based on novel biomaterials, factors and cells. *Pathobiology: Journal of Immunopathology, Molecular and Cellular Biology*, 80(4), 203-210.
- Grskovic, M., Javaherian, A., Strulovici, B., Daley, G.Q. (2011). Induced pluripotent stem cells--opportunities for disease modelling and drug discovery. *Nature Reviews. Drug Discovery*, 10(12), 915-929.
- Guan, X., Avci-Adali, M., Alarcin, E., Cheng, H., Kashaf, S.S., Li, Y., Chawla, A., Jang, H.L., Khademhosseini, A. (2017). Development of hydrogels for regenerative engineering. *Biotechnology Journal*, 12(5), 10.1002/biot.201600394.
- Guillaume, O., Naqvi, S.M., Lennon, K., Buckley, C.T. (2015). Enhancing cell migration in shape-memory alginate-collagen composite scaffolds: In vitro and ex vivo assessment for intervertebral disc repair. *Journal of Biomaterials Applications*, 29(9), 1230-1246.
- Haase, K., & Kamm, R.D. (2017). Advances in on-chip vascularization. *Regenerative Medicine*, 12(3), 285-302.
- Hall, B. K. (2005). *Bones and Cartilage: Developmental and Evolutionary Skeletal Biology* (1st ed.). Amsterdam, the Netherlands: Elsevier.

- Hamilton, N.J., Kanani, M., Roebuck, D.J., Hewitt, R.J., Cetto, R., Culme-Seymour, E.J., Toll, E., Bates, A.J., Comerford, A.P., McLaren, C.A., Butler, C.R., Crowley, C., McIntyre, D., Sebire, N.J., Janes, S.M., O'Callaghan, C., Mason, C., De Coppi, P., Lowdell, M.W., Elliott, M.J., Birchall, M.A. (2015). Tissue-Engineered Tracheal Replacement in a Child: A 4-Year Follow-Up Study. *American Journal of Transplantation : Official Journal of the American Society of Transplantation and the American Society of Transplant Surgeons*, 15(10), 2750-2757.
- Hasan, A., Memic, A., Annabi, N., Hossain, M., Paul, A., Dokmeci, M.R., Dehghani, F., Khademhosseini, A. (2014). Electrospun scaffolds for tissue engineering of vascular grafts. *Acta Biomaterialia*, 10(1), 11-25.
- Hellstrom, M., Phng, L.K., Gerhardt, H. (2007). VEGF and Notch signaling: the yin and yang of angiogenic sprouting. *Cell Adhesion & Migration*, 1(3), 133-136.
- Hench, L.L. (1998). Biomaterials: a forecast for the future. *Biomaterials*, 19(16), 1419-1423.
- Hench, L.L. (2006). The story of Bioglass. *Journal of Materials Science. Materials in Medicine*, 17(11), 967-978.
- Hench, L.L., & Jones, J.R. (2015). Bioactive Glasses: Frontiers and Challenges. *Frontiers in Bioengineering and Biotechnology*, 3, 194.
- Hench, L.L., & Wilson, J. (1986). Biocompatibility of silicates for medical use. *Ciba Foundation Symposium*, 121, 231-246.
- Heydarkhan-Hagvall, S., Schenke-Layland, K., Yang, J.Q., Heydarkhan, S., Xu, Y., Zuk, P.A., MacLellan, W.R., Beygui, R.E. (2008). Human adipose stem cells: a potential cell source for cardiovascular tissue engineering. *Cells, Tissues, Organs*, 187(4), 263-274.
- Hu, D., Wu, D., Huang, L., Jiao, Y., Li, L., Lu, L., Zhou, C. (2018). 3D bioprinting of cell-laden scaffolds for intervertebral disc regeneration. *Materials Letters*, 223, 219-222.
- Huebsch, N., Arany, P.R., Mao, A.S., Shvartsman, D., Ali, O.A., Bencherif, S.A., Rivera-Feliciano, J., Mooney, D.J. (2010). Harnessing traction-mediated manipulation of the cell/matrix interface to control stem-cell fate. *Nature Materials*, 9(6), 518-526.
- Huttala, O., Vuorenpaa, H., Toimela, T., Uotila, J., Kuokkanen, H., Ylikomi, T., Sarkanen, J.R., Heinonen, T. (2015). Human vascular model with defined stimulation medium - a characterization study. *Altex*, 32(2), 125-136.
- Iruela-Arispe, M.L., & Davis, G.E. (2009). Cellular and molecular mechanisms of vascular lumen formation. *Developmental Cell*, 16(2), 222-231.
- Izadpanah, R., Trygg, C., Patel, B., Kriedt, C., Dufour, J., Gimble, J.M., Bunnell, B.A. (2006). Biologic properties of mesenchymal stem cells derived from bone marrow and adipose tissue. *Journal of Cellular Biochemistry*, 99(5), 1285-1297.
- Jaffe, E.A., Nachman, R.L., Becker, C.G., Minick, C.R. (1973). Culture of human endothelial cells derived from umbilical veins. Identification by morphologic and immunologic criteria. *The Journal of Clinical Investigation*, 52(11), 2745-2756.
- Jakob, M., Saxer, F., Scotti, C., Schreiner, S., Studer, P., Scherberich, A., Heberer, M., Martin, I. (2012). Perspective on the evolution of cell-based bone tissue engineering strategies. *European Surgical Research*, 49(1), 1-7.
- James, R., Kesturu, G., Balian, G., Chhabra, A.B. (2008). Tendon: biology, biomechanics, repair, growth factors, and evolving treatment options. *The Journal of Hand Surgery*, 33(1), 102-112.

- James, R., Kumbar, S.G., Laurencin, C.T., Balian, G., Chhabra, A.B. (2011). Tendon tissue engineering: adipose-derived stem cell and GDF-5 mediated regeneration using electrospun matrix systems. *Biomedical Materials (Bristol, England)*, 6(2), 025011.
- Jaroszeski, M.J., & Radcliff, G. (1999). Fundamentals of flow cytometry. *Molecular Biotechnology*, 11(1), 37-53.
- Jenner, J.M., van Eijk, F., Saris, D.B., Willems, W.J., Dhert, W.J., Creemers, L.B. (2007). Effect of transforming growth factor-beta and growth differentiation factor-5 on proliferation and matrix production by human bone marrow stromal cells cultured on braided poly lactic-co-glycolic acid scaffolds for ligament tissue engineering. *Tissue Engineering*, 13(7), 1573-1582.
- Jensen, J., Hyllner, J., Bjorquist, P. (2009). Human embryonic stem cell technologies and drug discovery. *Journal of Cellular Physiology*, 219(3), 513-519.
- Jeon, J.S., Bersini, S., Whisler, J.A., Chen, M.B., Dubini, G., Charest, J.L., Moretti, M., Kamm, R.D. (2014). Generation of 3D functional microvascular networks with human mesenchymal stem cells in microfluidic systems. *Integrative Biology : Quantitative Biosciences from Nano to Macro*, 6(5), 555-563.
- Jia, W., Gungor-Ozkerim, P.S., Zhang, Y.S., Yue, K., Zhu, K., Liu, W., Pi, Q., Byambaa, B., Dokmeci, M.R., Shin, S.R., Khademhosseini, A. (2016). Direct 3D bioprinting of perfusable vascular constructs using a blend bioink. *Biomaterials*, 106, 58-68.
- Jiang, Y., Cai, Y., Zhang, W., Yin, Z., Hu, C., Tong, T., Lu, P., Zhang, S., Neculai, D., Tuan, R.S., Ouyang, H.W. (2016). Human Cartilage-Derived Progenitor Cells From Committed Chondrocytes for Efficient Cartilage Repair and Regeneration. *Stem Cells Translational Medicine*, 5(6), 733-744.
- Jones, J.R. (2015). Reprint of: Review of bioactive glass: From Hench to hybrids. *Acta Biomaterialia*, 23 Suppl, S53-82.
- Josh, F., Kobe, K., Tobita, M., Tanaka, R., Suzuki, K., Ono, K., Hyakusoku, H., Mizuno, H. (2012). Accelerated and safe proliferation of human adipose-derived stem cells in medium supplemented with human serum. *Journal of Nippon Medical School = Nippon Ika Daigaku Zasshi*, 79(6), 444-452.
- Jungbluth, P., Spitzhorn, L.S., Grassmann, J., Tanner, S., Latz, D., Rahman, M.S., Bohndorf, M., Wruck, W., Sager, M., Grotheer, V., Kropil, P., Hakimi, M., Windolf, J., Schneppendahl, J., Adjaye, J. (2019). Human iPSC-derived iMSCs improve bone regeneration in mini-pigs. *Bone Research*, 7, 32.
- Kamat, P., Schweizer, R., Kaenel, P., Salemi, S., Calcagni, M., Giovanoli, P., Gorantla, V.S., Eberli, D., Andres, A.C., Plock, J.A. (2015). Human Adipose-Derived Mesenchymal Stromal Cells May Promote Breast Cancer Progression and Metastatic Spread. *Plastic and Reconstructive Surgery*, 136(1), 76-84.
- Kang, Y., Kim, S., Fahrenholtz, M., Khademhosseini, A., Yang, Y. (2013). Osteogenic and angiogenic potentials of monocultured and co-cultured human-bone-marrow-derived mesenchymal stem cells and human-umbilical-vein endothelial cells on three-dimensional porous beta-tricalcium phosphate scaffold. *Acta Biomaterialia*, 9(1), 4906-4915.
- Kannus, P. (2000). Structure of the tendon connective tissue. *Scandinavian Journal of Medicine & Science in Sports*, 10(6), 312-320.
- Kant, R.J., & Coulombe, K.L.K. (2018). Integrated approaches to spatiotemporally directing angiogenesis in host and engineered tissues. *Acta Biomaterialia*, 69, 42-62.

- Kargozar, S., Baino, F., Hamzehlou, S., Hill, R.G., Mozafari, M. (2018). Bioactive Glasses: Sprouting Angiogenesis in Tissue Engineering. *Trends in Biotechnology*, 36(4), 430-444.
- Karvinen, J., Koivisto, J.T., Jonkkari, I., Kellomaki, M. (2017). The production of injectable hydrazone crosslinked gellan gum-hyaluronan-hydrogels with tunable mechanical and physical properties. *Journal of the Mechanical Behavior of Biomedical Materials*, 71, 383-391.
- Kazemzadeh-Narbat, M., Rouwkema, J., Annabi, N., Cheng, H., Ghaderi, M., Cha, B.H., Aparnathi, M., Khalilpour, A., Byambaa, B., Jabbari, E., Tamayol, A., Khademhosseini, A. (2017). Engineering Photocrosslinkable Bicomponent Hydrogel Constructs for Creating 3D Vascularized Bone. *Advanced Healthcare Materials*, 6(10), 10.1002/adhm.201601122.
- Keating, M., Kurup, A., Alvarez-Elizondo, M., Levine, A.J., Botvinick, E. (2017). Spatial distributions of pericellular stiffness in natural extracellular matrices are dependent on cell-mediated proteolysis and contractility. *Acta Biomaterialia*, 57, 304-312.
- Keifer, O.P., O'Connor, D.M., Boulis, N.M. (2014). Gene and protein therapies utilizing VEGF for ALS. *Pharmacology & Therapeutics*, 141(3), 261-271.
- Khademhosseini, A., & Langer, R. (2016). A decade of progress in tissue engineering. *Nature Protocols*, 11(10), 1775-1781.
- Khanna-Jain, R., Mannerstrom, B., Vuorinen, A., Sandor, G.K., Suuronen, R., Miettinen, S. (2012). Osteogenic differentiation of human dental pulp stem cells on beta-tricalcium phosphate/poly (l-lactic acid/caprolactone) three-dimensional scaffolds. *Journal of Tissue Engineering*, 3(1), 2041731412467998.
- Killion, J.A., Kehoe, S., Geever, L.M., Devine, D.M., Sheehan, E., Boyd, D., Higginbotham, C.L. (2013). Hydrogel/bioactive glass composites for bone regeneration applications: synthesis and characterisation. *Materials Science & Engineering, C, Materials for Biological Applications*, 33(7), 4203-4212.
- Kim, K.M., Choi, Y.J., Hwang, J.H., Kim, A.R., Cho, H.J., Hwang, E.S., Park, J.Y., Lee, S.H., Hong, J.H. (2014). Shear stress induced by an interstitial level of slow flow increases the osteogenic differentiation of mesenchymal stem cells through TAZ activation. *PLoS One*, 9(3), e92427.
- Kirkpatrick, C.J., Fuchs, S., Unger, R.E. (2011). Co-culture systems for vascularization--learning from nature. *Advanced Drug Delivery Reviews*, 63(4-5), 291-299.
- Kishore, V., Bullock, W., Sun, X., Van Dyke, W.S., Akkus, O. (2012). Tenogenic differentiation of human MSCs induced by the topography of electrochemically aligned collagen threads. *Biomaterials*, 33(7), 2137-2144.
- Kniazeva, E., & Putnam, A.J. (2009). Endothelial cell traction and ECM density influence both capillary morphogenesis and maintenance in 3-D. *American Journal of Physiology. Cell Physiology*, 297(1), C179-87.
- Ko, H.C., Milthorpe, B.K., McFarland, C.D. (2007). Engineering thick tissues--the vascularisation problem. *European Cells & Materials*, 14, 1-18;
- Kobolak, J., Dinnyes, A., Memic, A., Khademhosseini, A., Mobasheri, A. (2016). Mesenchymal stem cells: Identification, phenotypic characterization, biological properties and potential for regenerative medicine through biomaterial micro-engineering of their niche. *Methods (San Diego, Calif.)*, 99, 62-68.
- Koellensperger, E., Bollinger, N., Dexheimer, V., Gramley, F., Germann, G., Leimer, U. (2014). Choosing the right type of serum for different applications of human

- adipose tissue-derived stem cells: influence on proliferation and differentiation abilities. *Cytotherapy*, 16(6), 789-799.
- Kohane, D.S., & Langer, R. (2010). Biocompatibility and drug delivery systems. *Chemical Science*, 1(4), 441-446.
- Koivisto, J.T., Gering, C., Karvinen, J., Maria Cherian, R., Belay, B., Hyttinen, J., Aalto-Setälä, K., Kellomäki, M., Parraga, J. (2019). Mechanically Biomimetic Gelatin-Gellan Gum Hydrogels for 3D Culture of Beating Human Cardiomyocytes. *ACS Applied Materials & Interfaces*, 11(23), 20589-20602.
- Koivisto, J.T., Joki, T., Parraga, J.E., Paakkonen, R., Ylä-Outinen, L., Salonen, L., Jonkkari, I., Peltola, M., Ihalainen, T.O., Narkilahti, S., Kellomäki, M. (2017). Bioamine-crosslinked gellan gum hydrogel for neural tissue engineering. *Biomedical Materials*, 12(2), 025014.
- Kolbe, M., Xiang, Z., Dohle, E., Tonak, M., Kirkpatrick, C.J., Fuchs, S. (2011). Paracrine effects influenced by cell culture medium and consequences on microvessel-like structures in cocultures of mesenchymal stem cells and outgrowth endothelial cells. *Tissue Engineering, Part A*, 17(17-18), 2199-2212.
- Kolind, K., Leong, K.W., Besenbacher, F., Foss, M. (2012). Guidance of stem cell fate on 2D patterned surfaces. *Biomaterials*, 33(28), 6626-6633.
- Kondiah, P.J., Choonara, Y.E., Kondiah, P.P., Marimuthu, T., Kumar, P., du Toit, L.C., Pillay, V. (2016). A Review of Injectable Polymeric Hydrogel Systems for Application in Bone Tissue Engineering. *Molecules*, 21(11), 1580.
- Kramer, J., Dazzi, F., Dominici, M., Schlenke, P., Wagner, W. (2012). Clinical perspectives of mesenchymal stem cells. *Stem Cells International*, 2012, 684827.
- Kuo, C.K., Marturano, J.E., Tuan, R.S. (2010). Novel strategies in tendon and ligament tissue engineering: Advanced biomaterials and regeneration motifs. *Sports Medicine, Arthroscopy, Rehabilitation, Therapy & Technology : SMARTT*, 2, 20-2555-2-20.
- Kuo, C.K., & Tuan, R.S. (2008). Mechanoactive tenogenic differentiation of human mesenchymal stem cells. *Tissue Engineering, Part A*, 14(10), 1615-1627.
- Kuo, K.C., Lin, R.Z., Tien, H.W., Wu, P.Y., Li, Y.C., Melero-Martin, J.M., Chen, Y.C. (2015). Bioengineering vascularized tissue constructs using an injectable cell-laden enzymatically crosslinked collagen hydrogel derived from dermal extracellular matrix. *Acta Biomaterialia*, 27, 151-166.
- Kyllönen, L., Haimi, S., Mannerström, B., Huhtala, H., Rajala, K.M., Skottman, H., Sandor, G.K., Miettinen, S. (2013). Effects of different serum conditions on osteogenic differentiation of human adipose stem cells in vitro. *Stem Cell Research & Therapy*, 4(1), 17.
- LaCroix, A.S., Duenwald-Kuehl, S.E., Lakes, R.S., Vanderby, R., Jr. (2013). Relationship between tendon stiffness and failure: a metaanalysis. *Journal of Applied Physiology (Bethesda, Md.: 1985)*, 115(1), 43-51.
- Langer, R., & Vacanti, J.P. (1993). Tissue engineering. *Science*, 260(5110), 920-926.
- Laranjeira, M., Domingues, R.M.A., Costa-Almeida, R., Reis, R.L., Gomes, M.E. (2017). 3D Mimicry of Native-Tissue-Fiber Architecture Guides Tendon-Derived Cells and Adipose Stem Cells into Artificial Tendon Constructs. *Small*, 13(31), 10.1002/smll.201700689.
- Laschke, M.W., & Menger, M.D. (2016). Prevascularization in tissue engineering: Current concepts and future directions. *Biotechnology Advances*, 34(2), 112-121.

- Lasprilla, A.J., Martinez, G.A., Lunelli, B.H., Jardini, A.L., Filho, R.M. (2012). Poly-lactic acid synthesis for application in biomedical devices - a review. *Biotechnology Advances*, 30(1), 321-328.
- Lee, J.M., Jung, J., Lee, H., Jeong, S.J., Cho, K.J., Hwang, S., Kim, G.J. (2012). Comparison of immunomodulatory effects of placenta mesenchymal stem cells with bone marrow and adipose mesenchymal stem cells. *International Immunopharmacology*, 13(2), 219-224.
- Lee, V.K., Lanzi, A.M., Haygan, N., Yoo, S.S., Vincent, P.A., Dai, G. (2014). Generation of Multi-Scale Vascular Network System within 3D Hydrogel using 3D Bio-Printing Technology. *Cellular and Molecular Bioengineering*, 7(3), 460-472.
- Lee, V.K., Kim, D.Y., Ngo, H., Lee, Y., Seo, L., Yoo, S., Vincent, P.A., Dai, G. (2014). Creating perfused functional vascular channels using 3D bio-printing technology. *Biomaterials*, 35(28), 8092-8102.
- Li, H., Li, J., Jiang, J., Lv, F., Chang, J., Chen, S., Wu, C. (2017). An osteogenesis/angiogenesis-stimulation artificial ligament for anterior cruciate ligament reconstruction. *Acta Biomaterialia*, 54, 399-410.
- Li, J., & Mooney, D.J. (2016). Designing hydrogels for controlled drug delivery. *Nature Reviews. Materials*, 1(12), 16071.
- Lian, J.B., & Stein, G.S. (1995). Development of the osteoblast phenotype: molecular mechanisms mediating osteoblast growth and differentiation. *The Iowa Orthopaedic Journal*, 15, 118-140.
- Lian, J.B., Stein, G.S., van Wijnen, A.J., Stein, J.L., Hassan, M.Q., Gaur, T., Zhang, Y. (2012). MicroRNA control of bone formation and homeostasis. *Nature Reviews. Endocrinology*, 8(4), 212-227.
- Lindroos, B., Suuronen, R., Miettinen, S. (2011). The potential of adipose stem cells in regenerative medicine. *Stem Cell Reviews*, 7(2), 269-291.
- Little, D., Guilak, F., Ruch, D.S. (2010). Ligament-derived matrix stimulates a ligamentous phenotype in human adipose-derived stem cells. *Tissue Engineering. Part A*, 16(7), 2307-2319.
- Liu, X., Chen, W., Zhang, C., Thein-Han, W., Hu, K., Reynolds, M.A., Bao, C., Wang, P., Zhao, L., Xu, H.H.K. (2017). Co-Seeding Human Endothelial Cells with Human-Induced Pluripotent Stem Cell-Derived Mesenchymal Stem Cells on Calcium Phosphate Scaffold Enhances Osteogenesis and Vascularization in Rats. *Tissue Engineering. Part A*, 23(11-12), 546-555.
- Liu, Y., Chan, J.K., Teoh, S.H. (2015). Review of vascularised bone tissue-engineering strategies with a focus on co-culture systems. *Journal of Tissue Engineering and Regenerative Medicine*, 9(2), 85-105.
- Liu, Y., Ramanath, H.S., Wang, D.A. (2008). Tendon tissue engineering using scaffold enhancing strategies. *Trends in Biotechnology*, 26(4), 201-209.
- Loaiza, S., Ferreira, S.A., Chinn, T.M., Kirby, A., Tsolaki, E., Dondi, C., Parzych, K., Strange, A.P., Bozec, L., Bertazzo, S., Hedegaard, M.A.B., Gentleman, E., Auner, H.W. (2018). An engineered, quantifiable in vitro model for analysing the effect of proteostasis-targeting drugs on tissue physical properties. *Biomaterials*, 183, 102-113.
- Loh, Y.H., Agarwal, S., Park, I.H., Urbach, A., Huo, H., Heffner, G.C., Kim, K., Miller, J.D., Ng, K., Daley, G.Q. (2009). Generation of induced pluripotent stem cells from human blood. *Blood*, 113(22), 5476-5479.
- Long, F. (2011). Building strong bones: molecular regulation of the osteoblast lineage. *Nature Reviews. Molecular Cell Biology*, 13(1), 27-38.

- Lopes, D., Martins-Cruz, C., Oliveira, M.B., Mano, J.F. (2018). Bone physiology as inspiration for tissue regenerative therapies. *Biomaterials*, 185, 240-275.
- Lopez-Cebral, R., Paolicelli, P., Romero-Caamano, V., Seijo, B., Casadei, M.A., Sanchez, A. (2013). Spermidine-cross-linked hydrogels as novel potential platforms for pharmaceutical applications. *Journal of Pharmaceutical Sciences*, 102(8), 2632-2643.
- Lu, H.H., Cooper, J.A., Jr, Manuel, S., Freeman, J.W., Attawia, M.A., Ko, F.K., Laurencin, C.T. (2005). Anterior cruciate ligament regeneration using braided biodegradable scaffolds: in vitro optimization studies. *Biomaterials*, 26(23), 4805-4816.
- Lv, F.J., Tuan, R.S., Cheung, K.M., Leung, V.Y. (2014). Concise review: the surface markers and identity of human mesenchymal stem cells. *Stem Cells (Dayton, Ohio)*, 32(6), 1408-1419.
- Ma, J., Yang, F., Both, S.K., Prins, H.J., Helder, M.N., Pan, J., Cui, F.Z., Jansen, J.A., van den Beucken, J.J. (2014). In vitro and in vivo angiogenic capacity of BM-MSCs/HUVECs and AT-MSCs/HUVECs cocultures. *Biofabrication*, 6(1), 015005.
- Maes, C., Kobayashi, T., Selig, M.K., Torrekens, S., Roth, S.I., Mackem, S., Carmeliet, G., Kronenberg, H.M. (2010). Osteoblast precursors, but not mature osteoblasts, move into developing and fractured bones along with invading blood vessels. *Developmental Cell*, 19(2), 329-344.
- Marelli, B., Ghezzi, C.E., Mohn, D., Stark, W.J., Barralet, J.E., Boccaccini, A.R., Nazhat, S.N. (2011). Accelerated mineralization of dense collagen-nano bioactive glass hybrid gels increases scaffold stiffness and regulates osteoblastic function. *Biomaterials*, 32(34), 8915-8926.
- Marques, C.F., Diogo, G.S., Pina, S., Oliveira, J.M., Silva, T.H., Reis, R.L. (2019). Collagen-based bioinks for hard tissue engineering applications: a comprehensive review. *Journal of Materials Science: Materials in Medicine*, 30(3), 32.
- Marro, A., Bandukwala, T., Mak, W. (2016). Three-Dimensional Printing and Medical Imaging: A Review of the Methods and Applications. *Current Problems in Diagnostic Radiology*, 45(1), 2-9.
- Martin, R.J., Hausman, G.J., Hausman, D.B. (1998). Regulation of adipose cell development in utero. *Proceedings of the Society for Experimental Biology and Medicine. Society for Experimental Biology and Medicine (New York, N.Y.)*, 219(3), 200-210.
- Mazini, L., Rochette, L., Amine, M., Malka, G. (2019). Regenerative Capacity of Adipose Derived Stem Cells (ADSCs), Comparison with Mesenchymal Stem Cells (MSCs). *International Journal of Molecular Sciences*, 20(10), 2523.
- McBlane, J.W., Phul, P., Sharpe, M. (2018). Preclinical Development of Cell-Based Products: a European Regulatory Science Perspective. *Pharmaceutical Research*, 35(8), 165-018-2437-y.
- McIntosh, K., Zvonic, S., Garrett, S., Mitchell, J.B., Floyd, Z.E., Hammill, L., Kloster, A., Di Halvorsen, Y., Ting, J.P., Storms, R.W., Goh, B., Kilroy, G., Wu, X., Gimble, J.M. (2006). The immunogenicity of human adipose-derived cells: temporal changes in vitro. *Stem Cells (Dayton, Ohio)*, 24(5), 1246-1253.
- McKenzie, J.L., & Webster, T.J. (2009). Protein Interactions at Material Surfaces. In R. Narayan (Ed.), *Biomedical Materials* (pp. 215-237). New York: Springer.
- Meng, Z., Chen, G., Chen, J., Yang, B., Yu, M., Feng, L., Jiang, Z., Guo, W., Tian, W. (2015). Tumorigenicity analysis of heterogeneous dental stem cells and its self-modification for chromosome instability. *Cell Cycle (Georgetown, Tex.)*, 14(21), 3396-3407.

- Middleton, J.C., & Tipton, A.J. (2000). Synthetic biodegradable polymers as orthopedic devices. *Biomaterials*, 21(23), 2335-2346.
- Midwood, K.S., Chiquet, M., Tucker, R.P., Orend, G. (2016). Tenascin-C at a glance. *Journal of Cell Science*, 129(23), 4321-4327.
- Mihaila, S.M., Frias, A.M., Pirraco, R.P., Rada, T., Reis, R.L., Gomes, M.E., Marques, A.P. (2013). Human adipose tissue-derived SSEA-4 subpopulation multi-differentiation potential towards the endothelial and osteogenic lineages. *Tissue Engineering, Part A*, 19(1-2), 235-246.
- Mihaila, S.M., Resende, M.F., Reis, R.L., Gomes, M.E., Marques, A.P. (2017). Interactive endothelial phenotype maintenance and osteogenic differentiation of adipose tissue stromal vascular fraction SSEA-4(+) -derived cells. *Journal of Tissue Engineering and Regenerative Medicine*, 11(7), 1998-2013.
- Miranda, C.S., Ribeiro, A.R.M., Homem, N.C., Felgueiras, H.P. (2020). Spun Biotextiles in Tissue Engineering and Biomolecules Delivery Systems. *Antibiotics (Basel, Switzerland)*, 9(4), 174.
- Miranville, A., Heeschen, C., Sengenès, C., Curat, C.A., Busse, R., Bouloumie, A. (2004). Improvement of postnatal neovascularization by human adipose tissue-derived stem cells. *Circulation*, 110(3), 349-355.
- Miri, A.K., Muja, N., Kamranpour, N.O., Lepry, W.C., Boccaccini, A.R., Clarke, S.A., Nazhat, S.N. (2016). Ectopic bone formation in rapidly fabricated acellular injectable dense collagen-Bioglass hybrid scaffolds via gel aspiration-ejection. *Biomaterials*, 85, 128-141.
- Mitchell, J.B., McIntosh, K., Zvonic, S., Garrett, S., Floyd, Z.E., Kloster, A., Di Halvorsen, Y., Storms, R.W., Goh, B., Kilroy, G., Wu, X., Gimble, J.M. (2006). Immunophenotype of human adipose-derived cells: temporal changes in stromal-associated and stem cell-associated markers. *Stem Cells (Dayton, Ohio)*, 24(2), 376-385.
- Mohamed-Ahmed, S., Fristad, I., Lie, S.A., Suliman, S., Mustafa, K., Vindenes, H., Idris, S.B. (2018). Adipose-derived and bone marrow mesenchymal stem cells: a donor-matched comparison. *Stem Cell Research & Therapy*, 9(1), 168-018-0914-1.
- Molloy, T., Wang, Y., Murrell, G. (2003). The roles of growth factors in tendon and ligament healing. *Sports Medicine (Auckland, N.Z.)*, 33(5), 381-394.
- Muehleder, S., Ovsianikov, A., Zipperle, J., Redl, H., Holnthoner, W. (2014). Connections matter: channeled hydrogels to improve vascularization. *Frontiers in Bioengineering and Biotechnology*, 2, 52.
- Muehleder, S., Pill, K., Schappner, M., Labuda, K., Priglinger, E., Hofbauer, P., Charwat, V., Marx, U., Redl, H., Holnthoner, W. (2018). The role of fibrinolysis inhibition in engineered vascular networks derived from endothelial cells and adipose-derived stem cells. *Stem Cell Research & Therapy*, 9(1), 35.
- Nagoshi, N., Tsuji, O., Nakamura, M., Okano, H. (2019). Cell therapy for spinal cord injury using induced pluripotent stem cells. *Regenerative Therapy*, 11, 75-80.
- Nair, L.S., & Laurencin, C.T. (2006). Polymers as biomaterials for tissue engineering and controlled drug delivery. *Advances in Biochemical Engineering/ Biotechnology*, 102, 47-90.
- Narayan, R. (Ed.). (2009). *Biomedical materials*. New York: Springer.
- Neri, S. (2019). Genetic Stability of Mesenchymal Stromal Cells for Regenerative Medicine Applications: A Fundamental Biosafety Aspect. *International Journal of Molecular Sciences*, 20(10), 2406.



- Norwegian Nobel Committee. (2012). The Nobel Prize in Physiology or Medicine 2012. [WWW]. Accessed 23.11.2019. Retrieved from <https://www.nobelprize.org/prizes/medicine/2012/press-release/>.
- Nunez-Toldra, R., Montori, S., Bosch, B., Hupa, L., Atari, M., Miettinen, S. (2019). S53P4 Bioactive Glass Ions for Vascularized Bone Tissue Engineering by DPPSC Co-cultures. *Tissue Engineering.Part A*, 25(17-8), 1213-1224.
- Oedayrajsingh-Varma, M.J., van Ham, S.M., Knippenberg, M., Helder, M.N., Klein-Nulend, J., Schouten, T.E., Ritt, M.J., van Milligen, F.J. (2006). Adipose tissue-derived mesenchymal stem cell yield and growth characteristics are affected by the tissue-harvesting procedure. *Cytotherapy*, 8(2), 166-177.
- Ojansivu, M., Hyvari, L., Kellomaki, M., Hupa, L., Vanhatupa, S., Miettinen, S. (2018). Bioactive glass induced osteogenic differentiation of human adipose stem cells is dependent on cell attachment mechanism and mitogen-activated protein kinases. *European Cells & Materials*, 35, 54-72.
- Ojansivu, M., Mishra, A., Vanhatupa, S., Juntunen, M., Larionova, A., Massera, J., Miettinen, S. (2018). The effect of S53P4-based borosilicate glasses and glass dissolution products on the osteogenic commitment of human adipose stem cells. *PLoS One*, 13(8), e0202740.
- Ojansivu, M., Vanhatupa, S., Bjorkvik, L., Hakkanen, H., Kellomaki, M., Autio, R., Ihalainen, J.A., Hupa, L., Miettinen, S. (2015). Bioactive glass ions as strong enhancers of osteogenic differentiation in human adipose stem cells. *Acta Biomaterialia*, 21, 190-203.
- Okubo, T., Nagoshi, N., Kohyama, J., Tsuji, O., Shinozaki, M., Shibata, S., Kase, Y., Matsumoto, M., Nakamura, M., Okano, H. (2018). Treatment with a Gamma-Secretase Inhibitor Promotes Functional Recovery in Human iPSC-Derived Transplants for Chronic Spinal Cord Injury. *Stem Cell Reports*, 11(6), 1416-1432.
- Oliveira, J.T., Martins, L., Picciochi, R., Malafaya, P.B., Sousa, R.A., Neves, N.M., Mano, J.F., Reis, R.L. (2010). Gellan gum: a new biomaterial for cartilage tissue engineering applications. *Journal of Biomedical Materials Research.Part A*, 93(3), 852-863.
- Oliveira, M.B., Custodio, C.A., Gasperini, L., Reis, R.L., Mano, J.F. (2016). Autonomous osteogenic differentiation of hASCs encapsulated in methacrylated gellan-gum hydrogels. *Acta Biomaterialia*, 41, 119-132.
- Orimo, H. (2010). The mechanism of mineralization and the role of alkaline phosphatase in health and disease. *Journal of Nippon Medical School = Nippon Ika Daigaku Zasshi*, 77(1), 4-12.
- Osmalek, T., Froelich, A., Tasarek, S. (2014). Application of gellan gum in pharmacy and medicine. *International Journal of Pharmaceutics*, 466(1-2), 328-340.
- Papadimitropoulos, A., Scherberich, A., Guven, S., Theilgaard, N., Crooijmans, H.J., Santini, F., Scheffler, K., Zallone, A., Martin, I. (2011). A 3D in vitro bone organ model using human progenitor cells. *European Cells & Materials*, 21, 445-58.
- Park, A., Hogan, M.V., Kesturu, G.S., James, R., Balian, G., Chhabra, A.B. (2010). Adipose-derived mesenchymal stem cells treated with growth differentiation factor-5 express tendon-specific markers. *Tissue Engineering.Part A*, 16(9), 2941-2951.
- Park, I.S., Han, M., Rhie, J.W., Kim, S.H., Jung, Y., Kim, I.H., Kim, S.H. (2009). The correlation between human adipose-derived stem cells differentiation and cell adhesion mechanism. *Biomaterials*, 30(36), 6835-6843.
- Patrikoski, M., Juntunen, M., Boucher, S., Campbell, A., Vemuri, M.C., Mannerstrom, B., Miettinen, S. (2013). Development of fully defined xeno-free culture system for the

- preparation and propagation of cell therapy-compliant human adipose stem cells. *Stem Cell Research & Therapy*, 4(2), 27.
- Patrikoski, M., Mannerstrom, B., Miettinen, S. (2019). Perspectives for Clinical Translation of Adipose Stromal/Stem Cells. *Stem Cells International*, 2019, 5858247.
- Pauly, S., Klatte, F., Strobel, C., Schmidmaier, G., Greiner, S., Scheibel, M., Wildemann, B. (2010). Characterization of tendon cell cultures of the human rotator cuff. *European Cells & Materials*, 20, 84-97.
- Pedersen, T.O., Blois, A.L., Xing, Z., Xue, Y., Sun, Y., Finne-Wistrand, A., Akslen, L.A., Lorens, J.B., Leknes, K.N., Fristad, I., Mustafa, K. (2013). Endothelial microvascular networks affect gene-expression profiles and osteogenic potential of tissue-engineered constructs. *Stem Cell Research & Therapy*, 4(3), 52.
- Pereira, D.R., Canadas, R.F., Silva-Correia, J., da Silva Morais, A., Oliveira, M.B., Dias, I.R., Mano, J.F., Marques, A.P., Reis, R.L., Oliveira, J.M. (2018). Injectable gellan-gum/hydroxyapatite-based bilayered hydrogel composites for osteochondral tissue regeneration. *Applied Materials Today*, 12, 309-321.
- Pfaffl, M.W. (2001). A new mathematical model for relative quantification in real-time RT-PCR. *Nucleic Acids Research*, 29(9), e45.
- Picot, J., Guerin, C.L., Le Van Kim, C., Boulanger, C.M. (2012). Flow cytometry: retrospective, fundamentals and recent instrumentation. *Cytotechnology*, 64(2), 109-130.
- Pill, K., Melke, J., Muhleder, S., Pultar, M., Rohringer, S., Priglinger, E., Redl, H.R., Hofmann, S., Holthoner, W. (2018). Microvascular Networks From Endothelial Cells and Mesenchymal Stromal Cells From Adipose Tissue and Bone Marrow: A Comparison. *Frontiers in Bioengineering and Biotechnology*, 6, 156.
- Pina, S., Ribeiro, V.P., Marques, C.F., Maia, F.R., Silva, T.H., Reis, R.L., Oliveira, J.M. (2019). Scaffolding Strategies for Tissue Engineering and Regenerative Medicine Applications. *Materials (Basel, Switzerland)*, 12(11), 1824.
- Piroso, A., Gottardi, R., Alexander, P.G., Tuan, R.S. (2018). Engineering in-vitro stem cell-based vascularized bone models for drug screening and predictive toxicology. *Stem Cell Research & Therapy*, 9(1), 112.
- Pirracco, R.P., Iwata, T., Yoshida, T., Marques, A.P., Yamato, M., Reis, R.L., Okano, T. (2014). Endothelial cells enhance the in vivo bone-forming ability of osteogenic cell sheets. *Laboratory Investigation; a Journal of Technical Methods and Pathology*, 94(6), 663-673.
- Przekora, A. (2019). The summary of the most important cell-biomaterial interactions that need to be considered during in vitro biocompatibility testing of bone scaffolds for tissue engineering applications. *Materials Science & Engineering.C, Materials for Biological Applications*, 97, 1036-1051.
- Qiu, X., Zhang, Y., Zhao, X., Zhang, S., Wu, J., Guo, H., Hu, Y. (2015). Enhancement of endothelial differentiation of adipose derived mesenchymal stem cells by a three-dimensional culture system of microwell. *Biomaterials*, 53, 600-608.
- Raabe, O., Shell, K., Fietz, D., Freitag, C., Ohrndorf, A., Christ, H.J., Wenisch, S., Arnhold, S. (2013). Tenogenic differentiation of equine adipose-tissue-derived stem cells under the influence of tensile strain, growth differentiation factors and various oxygen tensions. *Cell and Tissue Research*, 352(3), 509-521.
- Raghavan, S.S., Woon, C.Y., Kraus, A., Megerle, K., Pham, H., Chang, J. (2012). Optimization of human tendon tissue engineering: synergistic effects of growth

- factors for use in tendon scaffold repopulation. *Plastic and Reconstructive Surgery*, 129(2), 479-489.
- Raisz, L.G. (1999). Physiology and pathophysiology of bone remodeling. *Clinical Chemistry*, 45(8 Pt 2), 1353-1358.
- Rao, R.R., Ceccarelli, J., Vigen, M.L., Gudur, M., Singh, R., Deng, C.X., Putnam, A.J., Stegemann, J.P. (2014). Effects of hydroxyapatite on endothelial network formation in collagen/fibrin composite hydrogels in vitro and in vivo. *Acta Biomaterialia*, 10(7), 3091-3097.
- Rao, R.R., Peterson, A.W., Ceccarelli, J., Putnam, A.J., Stegemann, J.P. (2012). Matrix composition regulates three-dimensional network formation by endothelial cells and mesenchymal stem cells in collagen/fibrin materials. *Angiogenesis*, 15(2), 253-264.
- Rasal, R.M., Janorkar, A.V., Hirt, D.E. (2010). Poly(lactic acid) modifications. *Progress in Polymer Science*, 35(3), 338-356.
- Raub, C.B., Putnam, A.J., Tromberg, B.J., George, S.C. (2010). Predicting bulk mechanical properties of cellularized collagen gels using multiphoton microscopy. *Acta Biomaterialia*, 6(12), 4657-4665.
- Raya-Rivera, A., Esquiliano, D.R., Yoo, J.J., Lopez-Bayghen, E., Soker, S., Atala, A. (2011). Tissue-engineered autologous urethras for patients who need reconstruction: an observational study. *Lancet*, 377(9772), 1175-1182.
- Raya-Rivera, A.M., Esquiliano, D., Fierro-Pastrana, R., Lopez-Bayghen, E., Valencia, P., Ordorica-Flores, R., Soker, S., Yoo, J.J., Atala, A. (2014). Tissue-engineered autologous vaginal organs in patients: a pilot cohort study. *Lancet*, 384(9940), 329-336.
- Rehman, J., Traktuev, D., Li, J., Merfeld-Clauss, S., Temm-Grove, C.J., Bovenkerk, J.E., Pell, C.L., Johnstone, B.H., Considine, R.V., March, K.L. (2004). Secretion of angiogenic and antiapoptotic factors by human adipose stromal cells. *Circulation*, 109(10), 1292-1298.
- Ribeiro, A.J.S., Denisin, A.K., Wilson, R.E., Pruitt, B.L. (2016). For whom the cells pull: Hydrogel and micropost devices for measuring traction forces. *Methods*, 94, 51-64.
- Rodriguez, J.P., Gonzalez, M., Rios, S., Cambiazo, V. (2004). Cytoskeletal organization of human mesenchymal stem cells (MSC) changes during their osteogenic differentiation. *Journal of Cellular Biochemistry*, 93(4), 721-731.
- Rouwkema, J., de Boer, J., Van Blitterswijk, C.A. (2006). Endothelial cells assemble into a 3-dimensional prevascular network in a bone tissue engineering construct. *Tissue Engineering*, 12(9), 2685-2693.
- Rouwkema, J., & Khademosseini, A. (2016). Vascularization and Angiogenesis in Tissue Engineering: Beyond Creating Static Networks. *Trends in Biotechnology*, 34(9), 733-745.
- Ruhrberg, C. (2003). Growing and shaping the vascular tree: multiple roles for VEGF. *BioEssays : News and Reviews in Molecular, Cellular and Developmental Biology*, 25(11), 1052-1060.
- Ruokola, P., Dadu, E., Kazmertsuk, A., Hakkanen, H., Marjomaki, V., Ihalainen, J.A. (2014). Raman spectroscopic signatures of echovirus 1 uncoating. *Journal of Virology*, 88(15), 8504-8513.
- Russell, K.C., Phinney, D.G., Lacey, M.R., Barrilleaux, B.L., Meyertholen, K.E., O'Connor, K.C. (2010). In vitro high-capacity assay to quantify the clonal

- heterogeneity in trilineage potential of mesenchymal stem cells reveals a complex hierarchy of lineage commitment. *Stem Cells (Dayton, Ohio)*, 28(4), 788-798.
- Sakurai, T., & Kudo, M. (2011). Signaling pathways governing tumor angiogenesis. *Oncology*, 81 Suppl 1, 24-29.
- Saleh, F.A., Whyte, M., Genever, P.G. (2011). Effects of endothelial cells on human mesenchymal stem cell activity in a three-dimensional in vitro model. *European Cells & Materials*, 22, 242-57; discussion 257.
- Sarkanen, J.R., Mannerstrom, M., Vuorenmaa, H., Uotila, J., Ylikomi, T., Heinonen, T. (2011). Intra-Laboratory Pre-Validation of a Human Cell Based in vitro Angiogenesis Assay for Testing Angiogenesis Modulators. *Frontiers in Pharmacology*, 1, 147.
- Schaffler, A., & Buchler, C. (2007). Concise review: adipose tissue-derived stromal cells—basic and clinical implications for novel cell-based therapies. *Stem Cells (Dayton, Ohio)*, 25(4), 818-827.
- Schindelin, J., Arganda-Carreras, I., Frise, E., Kaynig, V., Longair, M., Pietzsch, T., Preibisch, S., Rueden, C., Saalfeld, S., Schmid, B., Tinevez, J.Y., White, D.J., Hartenstein, V., Eliceiri, K., Tomancak, P., Cardona, A. (2012). Fiji: an open-source platform for biological-image analysis. *Nature Methods*, 9(7), 676-682.
- Selich, A., Daudert, J., Hass, R., Philipp, F., von Kaisenberg, C., Paul, G., Cornils, K., Fehse, B., Rittinghausen, S., Schambach, A., Rothe, M. (2016). Massive Clonal Selection and Transiently Contributing Clones During Expansion of Mesenchymal Stem Cell Cultures Revealed by Lentiviral RGB-Barcode Technology. *Stem Cells Translational Medicine*, 5(5), 591-601.
- Seoane-Vazquez, E., Shukla, V., Rodriguez-Monguio, R. (2019). Innovation and competition in advanced therapy medicinal products. *EMBO Molecular Medicine*, 11(3), 9992.
- Seok, J., Warren, H.S., Cuenca, A.G., Mindrinos, M.N., Baker, H.V., Xu, W., Richards, D.R., McDonald-Smith, G.P., Gao, H., Hennessy, L., Finnerty, C.C., Lopez, C.M., Honari, S., Moore, E.E., Minei, J.P., Cuschieri, J., Bankey, P.E., Johnson, J.L., Sperry, J., Nathens, A.B., Billiar, T.R., West, M.A., Jeschke, M.G., Klein, M.B., Gamelli, R.L., Gibran, N.S., Brownstein, B.H., Miller-Graziano, C., Calvano, S.E., Mason, P.H., Cobb, J.P., Rahme, L.G., Lowry, S.F., Maier, R.V., Moldawer, L.L., Herndon, D.N., Davis, R.W., Xiao, W., Tompkins, R.G., Inflammation and Host Response to Injury, Large Scale Collaborative Research Program. (2013). Genomic responses in mouse models poorly mimic human inflammatory diseases. *Proceedings of the National Academy of Sciences of the United States of America*, 110(9), 3507-3512.
- SFS-EN ISO 604. (2002). *Plastics. Determination of compressive properties*. (No. 604). Helsinki: Finnish Standards Association SFS.
- Shafiee, A., & Atala, A. (2017). Tissue Engineering: Toward a New Era of Medicine. *Annual Review of Medicine*, 68, 29-40.
- Shah, S.B., & Singh, A. (2017). Cellular self-assembly and biomaterials-based organoid models of development and diseases. *Acta Biomaterialia*, 53, 29-45.
- Shahabipour, F., Ashammakhi, N., Oskuee, R.K., Bonakdar, S., Hoffman, T., Shokrgozar, M.A., Khademhosseini, A. (2019). Key components of engineering vascularized 3-dimensional bioprinted bone constructs. *Translational Research : The Journal of Laboratory and Clinical Medicine*, (Sep 5), Epub ahead of print.

- Sharma, R.I., & Snedeker, J.G. (2012). Paracrine interactions between mesenchymal stem cells affect substrate driven differentiation toward tendon and bone phenotypes. *PLoS One*, 7(2), e31504.
- Sharma, R.I., & Snedeker, J.G. (2010). Biochemical and biomechanical gradients for directed bone marrow stromal cell differentiation toward tendon and bone. *Biomaterials*, 31(30), 7695-7704.
- Shearn, J.T., Kinneberg, K.R., Dymont, N.A., Galloway, M.T., Kenter, K., Wylie, C., Butler, D.L. (2011). Tendon tissue engineering: progress, challenges, and translation to the clinic. *Journal of Musculoskeletal & Neuronal Interactions*, 11(2), 163-173.
- Shen, Y., Cho, H., Papa, A.E., Burke, J.A., Chan, X.Y., Duh, E.J., Gerecht, S. (2016). Engineered human vascularized constructs accelerate diabetic wound healing. *Biomaterials*, 102, 107-119.
- Shum, L., Rabie, A.B., Hagg, U. (2004). Vascular endothelial growth factor expression and bone formation in posterior glenoid fossa during stepwise mandibular advancement. *American Journal of Orthodontics and Dentofacial Orthopedics : Official Publication of the American Association of Orthodontists, its Constituent Societies, and the American Board of Orthodontics*, 125(2), 185-190.
- Sidney, L.E., Branch, M.J., Dunphy, S.E., Dua, H.S., Hopkinson, A. (2014). Concise review: evidence for CD34 as a common marker for diverse progenitors. *Stem Cells*, 32(6), 1380-1389.
- Sieminski, A.L., Was, A.S., Kim, G., Gong, H., Kamm, R.D. (2007). The stiffness of three-dimensional ionic self-assembling peptide gels affects the extent of capillary-like network formation. *Cell Biochemistry and Biophysics*, 49(2), 73-83.
- Silva, M., Ferreira, F.N., Alves, N.M., Paiva, M.C. (2020). Biodegradable polymer nanocomposites for ligament/tendon tissue engineering. *Journal of Nanobiotechnology*, 18(1), 23-019-0556-1.
- Silva-Correia, J., Gloria, A., Oliveira, M.B., Mano, J.F., Oliveira, J.M., Ambrosio, L., Reis, R.L. (2013). Rheological and mechanical properties of acellular and cell-laden methacrylated gellan gum hydrogels. *Journal of Biomedical Materials Research. Part A*, 101(12), 3438-3446.
- Smith, A.M., Shelton, R.M., Perrie, Y., Harris, J.J. (2007). An initial evaluation of gellan gum as a material for tissue engineering applications. *Journal of Biomaterials Applications*, 22(3), 241-254.
- Song, H.G., Park, K.M., Gerecht, S. (2014). Hydrogels to model 3D in vitro microenvironment of tumor vascularization. *Advanced Drug Delivery Reviews*, 79-80, 19-29.
- Soto, A.M., Koivisto, J.T., Parraga, J.E., Silva-Correia, J., Oliveira, J.M., Reis, R.L., Kellomaki, M., Hyttinen, J., Figueiras, E. (2016). Optical Projection Tomography Technique for Image Texture and Mass Transport Studies in Hydrogels Based on Gellan Gum. *Langmuir : The ACS Journal of Surfaces and Colloids*, 32(20), 5173-5182.
- Sowa, Y., Imura, T., Numajiri, T., Takeda, K., Mabuchi, Y., Matsuzaki, Y., Nishino, K. (2013). Adipose stromal cells contain phenotypically distinct adipogenic progenitors derived from neural crest. *PLoS One*, 8(12), e84206.
- Stevens, L.R., Gilmore, K.J., Wallace, G.G., In Het Panhuis, M. (2016). Tissue engineering with gellan gum. *Biomaterials Science*, 4(9), 1276-1290.
- Strioga, M., Viswanathan, S., Darinskas, A., Slaby, O., Michalek, J. (2012). Same or not the same? Comparison of adipose tissue-derived versus bone marrow-derived mesenchymal stem and stromal cells. *Stem Cells and Development*, 21(14), 2724-2752.

- Suga, H., Matsumoto, D., Eto, H., Inoue, K., Aoi, N., Kato, H., Araki, J., Yoshimura, K. (2009). Functional implications of CD34 expression in human adipose-derived stem/progenitor cells. *Stem Cells and Development*, 18(8), 1201-1210.
- Takahashi, K., & Yamanaka, S. (2006). Induction of pluripotent stem cells from mouse embryonic and adult fibroblast cultures by defined factors. *Cell*, 126(4), 663-676.
- Takao, K., & Miyakawa, T. (2015a). Correction for Takao and Miyakawa, Genomic responses in mouse models greatly mimic human inflammatory diseases. *Proceedings of the National Academy of Sciences of the United States of America*, 112(10), E1163-7.
- Takao, K., & Miyakawa, T. (2015b). Genomic responses in mouse models greatly mimic human inflammatory diseases. *Proceedings of the National Academy of Sciences of the United States of America*, 112(4), 1167-1172.
- Tan, S.L., Ahmad, R.E., Ahmad, T.S., Merican, A.M., Abbas, A.A., Ng, W.M., Kamarul, T. (2012). Effect of growth differentiation factor 5 on the proliferation and tenogenic differentiation potential of human mesenchymal stem cells in vitro. *Cells, Tissues, Organs*, 196(4), 325-338.
- Tapp, H., Hanley, E.N., Jr, Patt, J.C., Gruber, H.E. (2009). Adipose-derived stem cells: characterization and current application in orthopaedic tissue repair. *Experimental Biology and Medicine*, 234(1), 1-9.
- Thesleff, T., Lehtimäki, K., Niskakangas, T., Mannerström, B., Miettinen, S., Suuronen, R., Ohman, J. (2011). Cranioplasty with adipose-derived stem cells and biomaterial: a novel method for cranial reconstruction. *Neurosurgery*, 68(6), 1535-1540.
- Tirkkonen, L., Haimi, S., Huttunen, S., Wolff, J., Pirhonen, E., Sandor, G.K., Miettinen, S. (2013). Osteogenic medium is superior to growth factors in differentiation of human adipose stem cells towards bone-forming cells in 3D culture. *European Cells & Materials*, 25, 144-158.
- Tiruvannamalai Annamalai, R., Rioja, A.Y., Putnam, A.J., Stegemann, J.P. (2016). Vascular Network Formation by Human Microvascular Endothelial Cells in Modular Fibrin Microtissues. *ACS Biomaterials Science & Engineering*, 2(11), 1914-1925.
- Traktuev, D.O., Merfeld-Clauss, S., Li, J., Kolonin, M., Arap, W., Pasqualini, R., Johnstone, B.H., March, K.L. (2008). A population of multipotent CD34-positive adipose stromal cells share pericyte and mesenchymal surface markers, reside in a periendothelial location, and stabilize endothelial networks. *Circulation Research*, 102(1), 77-85.
- Trounson, A., & McDonald, C. (2015). Stem Cell Therapies in Clinical Trials: Progress and Challenges. *Cell Stem Cell*, 17(1), 11-22.
- Tsiapalis, D., & Zeugolis, D.I. (2019). Hypoxia Preconditioning of Bone Marrow Mesenchymal Stem Cells Before Implantation in Orthopaedics. *The Journal of the American Academy of Orthopaedic Surgeons*, 27(23), e1040-e1042.
- Turinetti, V., Orlando, L., Giachino, C. (2017). Induced Pluripotent Stem Cells: Advances in the Quest for Genetic Stability during Reprogramming Process. *International Journal of Molecular Sciences*, 18(9), 10.3390/ijms18091952.
- Turner, I.G. (2009). Ceramics and Glasses. In R. Narayan (Ed.), *Biomedical Materials* (pp. 3-39). New York: Springer.
- Van Blitterswijk, C. (Ed.). (2008). *Tissue engineering* (1st ed.). Amsterdam: Academic Press.
- Vaquette, C., Kahn, C., Frochet, C., Nouvel, C., Six, J.L., De Isla, N., Luo, L.H., Cooper-White, J., Rahouadj, R., Wang, X. (2010). Aligned poly(L-lactic-co-ε-caprolactone)

- electrospun microfibers and knitted structure: a novel composite scaffold for ligament tissue engineering. *Journal of Biomedical Materials Research. Part A*, 94(4), 1270-1282.
- Varma, M.J., Breuls, R.G., Schouten, T.E., Jurgens, W.J., Bontkes, H.J., Schuurhuis, G.J., van Ham, S.M., van Milligen, F.J. (2007). Phenotypical and functional characterization of freshly isolated adipose tissue-derived stem cells. *Stem Cells and Development*, 16(1), 91-104.
- Vert, M., Doi, Y., Hellwich, K., Hess, M., Hodge, P., Kubisa, P., Rinaudo, M., Schué, F. (2012). Terminology for biorelated polymers and applications (IUPAC Recommendations 2012). *Pure and Applied Chemistry*, 84(2), 377-410.
- Vieira, S., da Silva Morais, A., Garet, E., Silva-Correia, J., Reis, R.L., González-Fernández, Á, Miguel Oliveira, J. (2019). Self-mineralizing Ca-enriched methacrylated gellan gum beads for bone tissue engineering. *Acta Biomaterialia*, 93, 74-85.
- Vieira, S., Vial, S., Maia, F.R., Carvalho, M., Reis, R.L., Granja, P.L., Oliveira, J.M. (2015). Gellan gum-coated gold nanorods: an intracellular nanosystem for bone tissue engineering. *RSC Advances*, 5(95), 77996-78005.
- Viinikainen, A., Goransson, H., Taskinen, H.S., Roytta, M., Kellomaki, M., Tormala, P., Rokkanen, P. (2014). Flexor tendon healing within the tendon sheath using bioabsorbable poly-L/D-lactide 96/4 suture. A histological in vivo study with rabbits. *Journal of Materials Science. Materials in Medicine*, 25(5), 1319-1325.
- Vindigni, V., Tonello, C., Lancerotto, L., Abatangelo, G., Cortivo, R., Zavan, B., Bassetto, F. (2013). Preliminary report of in vitro reconstruction of a vascularized tendonlike structure: a novel application for adipose-derived stem cells. *Annals of Plastic Surgery*, 71(6), 664-670.
- Vogel, V. (2018). Unraveling the Mechanobiology of Extracellular Matrix. *Annual Review of Physiology*, 80, 353-387.
- Volarevic, V., Markovic, B.S., Gazdic, M., Volarevic, A., Jovicic, N., Arsenijevic, N., Armstrong, L., Djonov, V., Lako, M., Stojkovic, M. (2018). Ethical and Safety Issues of Stem Cell-Based Therapy. *International Journal of Medical Sciences*, 15(1), 36-45.
- Volponi, A.A., Gentleman, E., Fatscher, R., Pang, Y.W., Gentleman, M.M., Sharpe, P.T. (2015). Composition of Mineral Produced by Dental Mesenchymal Stem Cells. *Journal of Dental Research*, 94(11), 1568-1574.
- Walters, N.J., & Gentleman, E. (2015). Evolving insights in cell-matrix interactions: Elucidating how non-soluble properties of the extracellular niche direct stem cell fate. *Acta Biomaterialia*, 11, 3-16.
- Wan, Z., Zhang, P., Liu, Y., Lv, L., Zhou, Y. (2020). Four-dimensional bioprinting: Current developments and applications in bone tissue engineering. *Acta Biomaterialia*, 101, 26-42.
- Wang, Y., Yin, P., Bian, G.L., Huang, H.Y., Shen, H., Yang, J.J., Yang, Z.Y., Shen, Z.Y. (2017). The combination of stem cells and tissue engineering: an advanced strategy for blood vessels regeneration and vascular disease treatment. *Stem Cell Research & Therapy*, 8(1), 194-017-0642-y.
- Webber, M.J., Khan, O.F., Sydlik, S.A., Tang, B.C., Langer, R. (2015). A perspective on the clinical translation of scaffolds for tissue engineering. *Annals of Biomedical Engineering*, 43(3), 641-656.

- Wen, J.H., Vincent, L.G., Fuhrmann, A., Choi, Y.S., Hribar, K.C., Taylor-Weiner, H., Chen, S., Engler, A.J. (2014). Interplay of matrix stiffness and protein tethering in stem cell differentiation. *Nature Materials*, 13(10), 979-987.
- Williams, D. F. (Ed.). (1990). *Biocompatibility, an overview, in Concise Encyclopedia of Medical and Dental Materials*. New York: Pergammon Press.
- Williams, D.F. (2014). There is no such thing as a biocompatible material. *Biomaterials*, 35(38), 10009-10014.
- Wittkowske, C., Reilly, G.C., Lacroix, D., Perrault, C.M. (2016). In Vitro Bone Cell Models: Impact of Fluid Shear Stress on Bone Formation. *Frontiers in Bioengineering and Biotechnology*, 4, 87.
- Wu, J., Zhang, K., Yu, X., Ding, J., Cui, L., Yin, J. (2017). Hydration of hydrogels regulates vascularization in vivo. *Biomaterials Science*, 5(11), 2251-2267.
- Wubneh, A., Tsekoura, E.K., Ayranci, C., Uludag, H. (2018). Current state of fabrication technologies and materials for bone tissue engineering. *Acta Biomaterialia*, 80, 1-30.
- Wystrychowski, W., McAllister, T.N., Zagalski, K., Dusserre, N., Cierpka, L., L'Heureux, N. (2014). First human use of an allogeneic tissue-engineered vascular graft for hemodialysis access. *Journal of Vascular Surgery*, 60(5), 1353-1357.
- Xu, Z., Li, Z., Jiang, S., Bratlie, K.M. (2018). Chemically Modified Gellan Gum Hydrogels with Tunable Properties for Use as Tissue Engineering Scaffolds. *ACS Omega*, 3(6), 6998-7007.
- Xue, Y., Lim, S., Yang, Y., Wang, Z., Jensen, L.D., Hedlund, E.M., Andersson, P., Sasahara, M., Larsson, O., Galter, D., Cao, R., Hosaka, K., Cao, Y. (2011). PDGF-BB modulates hematopoiesis and tumor angiogenesis by inducing erythropoietin production in stromal cells. *Nature Medicine*, 18(1), 100-110.
- Xynos, I.D., Hukkanen, M.V., Batten, J.J., Buttery, L.D., Hench, L.L., Polak, J.M. (2000). Bioglass 45S5 stimulates osteoblast turnover and enhances bone formation In vitro: implications and applications for bone tissue engineering. *Calcified Tissue International*, 67(4), 321-329.
- Yang, G., Rothrauff, B.B., Lin, H., Gottardi, R., Alexander, P.G., Tuan, R.S. (2013). Enhancement of tenogenic differentiation of human adipose stem cells by tendon-derived extracellular matrix. *Biomaterials*, 34(37), 9295-9306.
- Yang, S., Leong, K.F., Du, Z., Chua, C.K. (2001). The design of scaffolds for use in tissue engineering. Part I. Traditional factors. *Tissue Engineering*, 7(6), 679-689.
- Yi, T., Kim, S.N., Lee, H.J., Kim, J., Cho, Y.K., Shin, D.H., Tak, S.J., Moon, S.H., Kang, J.E., Ji, I.M., Lim, H.J., Lee, D.S., Jeon, M.S., Song, S.U. (2015). Manufacture of Clinical-Grade Human Clonal Mesenchymal Stem Cell Products from Single Colony Forming Unit-Derived Colonies Based on the Subfractionation Culturing Method. *Tissue Engineering. Part C, Methods*, 21(12), 1251-1262.
- Yoon, D.M., & Fisher, J.P. (2009). Natural and Synthetic Polymeric Scaffolds. In R. Narayan (Ed.), *Biomedical Materials* (pp. 415-442). New York: Springer.
- Yoshihara, M., Hayashizaki, Y., Murakawa, Y. (2017). Genomic Instability of iPSCs: Challenges Towards Their Clinical Applications. *Stem Cell Reviews and Reports*, 13(1), 7-16.
- Yoshimura, K., Shigeura, T., Matsumoto, D., Sato, T., Takaki, Y., Aiba-Kojima, E., Sato, K., Inoue, K., Nagase, T., Koshima, I., Gonda, K. (2006). Characterization of freshly isolated and cultured cells derived from the fatty and fluid portions of liposuction aspirates. *Journal of Cellular Physiology*, 208(1), 64-76.



- Zelzer, E., & Olsen, B.R. (2004). Multiple Roles of Vascular Endothelial Growth Factor (VEGF) in Skeletal Development, Growth, and Repair. *Current Topics in Developmental Biology*, 65, 169-187.
- Zhang, J.M., & An, J. (2007). Cytokines, inflammation, and pain. *International Anesthesiology Clinics*, 45(2), 27-37.
- Zhao, X., Qiu, X., Zhang, Y., Zhang, S., Gu, X., Guo, H. (2016). Three-Dimensional Aggregates Enhance the Therapeutic Effects of Adipose Mesenchymal Stem Cells for Ischemia-Reperfusion Induced Kidney Injury in Rats. *Stem Cells International*, 2016, 9062638.
- Zhu, J., & Marchant, R.E. (2011). Design properties of hydrogel tissue-engineering scaffolds. *Expert Review of Medical Devices*, 8(5), 607-626.
- Zimmerlin, L., Donnenberg, V.S., Rubin, J.P., Donnenberg, A.D. (2013). Mesenchymal markers on human adipose stem/progenitor cells. *Cytometry.Part A : The Journal of the International Society for Analytical Cytology*, 83(1), 134-140.
- Zouani, O.F., Chanseau, C., Brouillaud, B., Bareille, R., Deliane, F., Foulc, M.P., Mehdi, A., Durrieu, M.C. (2012). Altered nanofeature size dictates stem cell differentiation. *Journal of Cell Science*, 125(Pt 5), 1217-1224.
- Zuk, P.A., Chou, Y.F., Mussano, F., Benhaim, P., Wu, B.M. (2011). Adipose-derived stem cells and BMP2: part 2. BMP2 may not influence the osteogenic fate of human adipose-derived stem cells. *Connective Tissue Research*, 52(2), 119-132.
- Zuk, P.A., Zhu, M., Ashjian, P., De Ugarte, D.A., Huang, J.I., Mizuno, H., Alfonso, Z.C., Fraser, J.K., Benhaim, P., Hedrick, M.H. (2002). Human adipose tissue is a source of multipotent stem cells. *Molecular Biology of the Cell*, 13(12), 4279-4295.
- Zuk, P.A., Zhu, M., Mizuno, H., Huang, J., Futrell, J.W., Katz, A.J., Benhaim, P., Lorenz, H.P., Hedrick, M.H. (2001). Multilineage cells from human adipose tissue: implications for cell-based therapies. *Tissue Engineering*, 7(2), 211-228.



# PUBLICATIONS



# PUBLICATION

I

## **Human Adipose Stem Cells Differentiated on Braided Polylactide Scaffolds Is a Potential Approach for Tendon Tissue Engineering**

Vuornos K., Björninen M., Talvitie E., Kellomäki M., Paakinaho K.,  
Huhtala H., Miettinen S., Seppänen-Kaijansinkko R., Haimi S.

*Tissue Engineering Part A* (2016) 22 (5-6), 513-523.

**Publication reprinted with the permission from the Mary Ann Liebert, Inc;  
New Rochelle, NY, USA.**

## CORRIGENDA

In publication **I**:

An error in reporting in human adipose stem cell isolation and cell expansion chapter in collagenase type I solution composition and consequently missing information on the composition of maintenance medium (MM). Error corrected as follows: “The adipose tissue was cut up and tissue was digested by collagenase type I (1.5 mg/mL; Thermo Fisher Scientific) solution containing DMEM/F-12 1:1 (Thermo Fisher Scientific), 1 % L-glutamine (GlutaMAX; Thermo Fisher Scientific), and 1 % antibiotics (100 U/mL penicillin/100 U/mL streptomycin; P/S; Lonza, Basel, Switzerland). The cells were expanded in maintenance medium (MM) containing DMEM/F-12, 5-10 % human serum (HS; PAA Laboratories, Pasching, Austria), 1 % L-glutamine, and 1 % P/S.”

ORIGINAL ARTICLE

# Human Adipose Stem Cells Differentiated on Braided Polylactide Scaffolds Is a Potential Approach for Tendon Tissue Engineering

Kaisa Vuornos, MSc,<sup>1,2</sup> Miina Björninen, PhD,<sup>1,2</sup> Elina Talvitie, MSc,<sup>3</sup>  
Kaarlo Paakinaho, PhD,<sup>3</sup> Minna Kellomäki, PhD,<sup>3</sup> Heini Huhtala, MSc,<sup>4</sup> Susanna Miettinen, PhD,<sup>1,2</sup>  
Riitta Seppänen-Kajjansinkko, MD, DDS, PhD, Dr Tech (hc), FEBOMS<sup>5,6</sup> and Suvi Haimi, PhD<sup>5,7</sup>

Growing number of musculoskeletal defects increases the demand for engineered tendon. Our aim was to find an efficient strategy to produce tendon-like matrix *in vitro*. To allow efficient differentiation of human adipose stem cells (hASCs) toward tendon tissue, we tested different medium compositions, biomaterials, and scaffold structures in preliminary tests. This is the first study to report that medium supplementation with 50 ng/mL of growth and differentiation factor-5 (GDF-5) and 280  $\mu$ M L-ascorbic acid are essential for tenogenic differentiation of hASCs. Tenogenic medium (TM) was shown to significantly enhance tendon-like matrix production of hASCs compared to other tested media groups. Cell adhesion, proliferation, and tenogenic differentiation of hASCs were supported on braided poly(L/D)lactide (PLA) 96L/4D copolymer filament scaffolds in TM condition compared to foamed poly(L-lactide-co- $\epsilon$ -caprolactone) (PLCL) 70L/30CL scaffolds. A uniform cell layer formed on braided PLA 96/4 scaffolds when hASCs were cultured in TM compared to maintenance medium (MM) condition after 14 days of culture. Furthermore, total collagen content and gene expression of tenogenic marker genes were significantly higher in TM condition after 2 weeks of culture. The elastic modulus of PLA 96/4 scaffold was more similar to the elastic modulus reported for native Achilles tendon. Our study showed that the optimized TM is needed for efficient and rapid *in vitro* tenogenic extracellular matrix production of hASCs. PLA 96/4 scaffolds together with TM significantly stimulated hASCs, thus demonstrating the potential clinical relevance of this novel and emerging approach to tendon injury treatments in the future.

## Introduction

**T**HE RATE OF serious tendon injuries that require surgical treatment is ~200,000 cases each year and increasing.<sup>1–3</sup> The current tendon reconstruction therapies after serious injury are limited due to lack of suitable tendon grafts. In addition, the use of autografts is restricted because most often it is not possible to graft again in case of a reinjury.<sup>4</sup> The combination of cells with a supporting biomaterial scaffold has been considered as a potential approach to treat tendon injuries.<sup>4–7</sup> Harvesting and culturing of tenocytes have not been efficient for clinical applications<sup>8</sup> due to their low *in vitro* proliferation capacity.<sup>9</sup> To evade these problems, human adipose stem cells (hASCs) could be used as a cell

source for tendon tissue engineering as they are an accessible, abundant, and multipotent cell population.<sup>10–12</sup> Tenogenic potential of hASCs has also been shown with induction by animal tendon derived extracellular matrix (ECM),<sup>13,14</sup> mechanical stress,<sup>15</sup> and coculture with tenocytes.<sup>16</sup> Different inducing factors such as growth and differentiation factor-5 (GDF-5) and transforming growth factor beta (TGF- $\beta$ ) have been used to trigger differentiation toward tendon or ligament,<sup>17–19</sup> however, an efficient tenogenic differentiation protocol for hASCs has not yet been reported.

Large tendons of the body transmit significant forces between muscle and bone.<sup>20–22</sup> To date, no functional scaffold structures have been available with appropriate mechanical properties for tendon tissue engineering.<sup>7,23</sup> For instance,

<sup>1</sup>Adult Stem Cells, BioMediTech, University of Tampere, Tampere, Finland.

<sup>2</sup>Science Center, Tampere University Hospital, Tampere, Finland.

<sup>3</sup>Department of Electronics and Communications Engineering, BioMediTech, Tampere University of Technology, Tampere, Finland.

<sup>4</sup>Tampere School of Health Sciences, University of Tampere, Tampere, Finland.

<sup>5</sup>Department of Oral and Maxillofacial Sciences, Clinicum, Faculty of Medicine, University of Helsinki, Helsinki, Finland.

<sup>6</sup>Department of Oral and Maxillofacial Diseases, Head and Neck Center, Helsinki University Hospital, Helsinki, Finland.

<sup>7</sup>Department of Biomaterials Science and Technology, University of Twente, Enschede, The Netherlands.

poly(L-lactide-co- $\epsilon$ -caprolactone) (PLCL) is a highly elastic copolymer,<sup>24,25</sup> which has been previously demonstrated to support tenocyte proliferation.<sup>26</sup> In comparison, lactide stereocopolymers are widely applied as medical implant material due to their more tailorable mechanical properties.<sup>27,28</sup> In addition, the mechanical load bearing of polylactides matches the requirements of tendon tissue regeneration.<sup>29</sup> Furthermore, poly-L-lactic acid (PLLA) filament scaffolds have demonstrated excellent biocompatibility and supported high cellular proliferation of rabbit anterior cruciate cells together with tendon-like ECM production.<sup>29,30</sup>

While foamed 96/4 poly(L/D)lactide (PLA) is a hard and brittle material due to its properties and therefore not suited for soft tissue applications such as tendon,<sup>7</sup> on the other hand, filaments fabricated from PLCL 70/30 are highly adhesive, which makes them unsuitable for braiding into filamentous structures. Therefore, due to these differences in polymer properties, we chose to compare braided PLA 96/4 and foamed PLCL 70/30 structures as highly biocompatible and pliable biomaterials<sup>27</sup> for tendon tissue applications. The aim of this study was to develop an effective *in vitro* tendon tissue engineering approach; first, by optimizing tenogenic medium (TM) for the hASCs, and second, by differentiating hASCs on different three-dimensional (3D) structures in the optimized TM, and third, we compared braided PLA 96/4 and foamed PLCL 70/30 scaffolds as potential structures for tendon tissue engineering.

## Materials and Methods

### Scaffold manufacture and characterization

**Braided PLA 96/4 scaffolds.** PLA fibers were melt spun from medical grade PLA 96/4 copolymer with an inherent viscosity of 2.18 dL/g (Corbion Purac, Amsterdam, The Netherlands) using Gimac microextruder (Gimac, Gastronno, Italy). The multifilament fiber was oriented by means of caterpillars and infrared ovens. PLA 96/4 scaffolds were machine braided by Scaffoldex Ltd. (Tampere, Finland). The finished braid of 4 mm width and 1.1 mm height was washed with ethanol and manually cut into scaffolds of 10 mm of length with a heated blade. The scaffolds were gamma irradiated for sterility with a minimum irradiation dose of 25 kGy before cell culture by a commercial service supplier.

**Foamed PLCL scaffolds.** The foamed scaffolds were fabricated from PLCL (PURASORB PLC-7015; Corbion Purac) with an inherent viscosity of 1.6 dL/g. The polymer was melt extruded into rods and processed with a supercritical CO<sub>2</sub> reactor system (Waters Operating Corporation, Milford, MA) to create a porous structure as previously described.<sup>24</sup> The samples were manually cut to final dimensions of 10 mm length, 4 mm width, and 1.4 mm height. Before cell culture experiments, all the scaffolds were gamma irradiated for sterility with a minimum irradiation dose of 25 kGy by a commercial service supplier.

### Scaffold characterization with micro-computed tomography

The micro-computed tomography (micro-CT) characterization was done for the braided PLA 96/4 and the foamed PLCL scaffolds with MicroXCT-400 microscope (Carl

Zeiss X-ray Microscopy, Pleasanton, CA) and image analysis was performed with Fiji open-source platform<sup>31</sup> with BoneJ plugin (ImageJ; U.S. National Institutes of Health, Bethesda, MD)<sup>32</sup> to characterize the structures.

### Mechanical testing

The mechanical properties of the braided PLA 96/4 scaffolds and the foamed PLCL scaffolds were tested by a tensile test method with a universal material testing machine (Instron 4411, series IX Automated Materials Testing System, Norwood, MA). The direct tensile test was performed with a crosshead speed of 30 mm/minute. A 500 N load cell was used in the tests. The elastic modulus under tension was calculated by system integrated software based on the slope of the linear region of the stress versus strain curve in which Hooke's law holds.

### Isolation and cell culture

This study was conducted in accordance with the Ethics Committee of the Pirkanmaa Hospital District (Tampere, Finland) to obtain adipose tissue samples for research purposes (R15161). Human ASCs were isolated from subcutaneous adipose tissue of seven healthy female donors of 52 ± 9 years of age in surgeries at the Tampere University Hospital Department of Plastic Surgery with the patient's written informed consent. Isolation of hASCs was performed as described previously.<sup>33,34</sup> First, the adipose tissue was mechanically minced and digested further with collagenase type I (1.5 mg/mL; Life Technologies; Thermo Fisher Scientific, Waltham, MA) in maintenance medium (MM) containing Dulbecco's Modified Eagle Medium (DMEM/F-12 1:1, Gibco; Life Technologies), 5–10% human serum (PAA Laboratories, Pasching, Austria), 1% L-glutamine (GlutaMAX, Gibco; Life Technologies), and 1% antibiotics (50 U/mL penicillin/50 mg/mL streptomycin; Lonza, Basel, Switzerland).

For the medium optimization, cells were plated at a density of 15,000 cells/cm<sup>2</sup>, in 24-well plate wells (Nunc; Sigma-Aldrich, St. Louis, MO). Tenogenic induction was initiated 5 days after plating by adding TM with different concentrations of L-ascorbic acid (Sigma-Aldrich) and/or GDF-5 (Biomol, Hamburg, Germany) (Table 1). The control cell cultures were maintained in MM. Medium was changed every other day. The experiments were carried out at passage 5. Tenogenic medium 3 (TM3) was selected as the TM condition for the subsequent scaffold experiments based on the obtained results (see Tenogenic Medium Optimization section).

TABLE 1. TENOGENIC DIFFERENTIATION MEDIA COMPOSITIONS

<i>Medium compositions</i>	
MM	10% HS
TM1	100 ng/mL GDF-5
TM2	50 ng/mL GDF-5
TM3	50 ng/mL GDF-5 50 $\mu$ g/mL (280 $\mu$ M) L-ascorbic acid

GDF-5, growth and differentiation factor-5; HS, human serum; MM, maintenance medium; TM, tenogenic medium.



For the scaffold experiments, PLA 96/4 and PLCL scaffolds were pretreated for 72 h with DMEM/F-12 (Gibco; Life Technologies) with 1% P/S (Lonza). Cells were seeded on top of the scaffolds at a density of 15,000 hASCs in a volume of 30  $\mu$ L in 48-well plate wells (Nunc/Delta Surface; Sigma-Aldrich), as described in previous studies.<sup>30</sup> The cell seeded scaffolds were incubated 3 h after plating at +37°C to induce cell attachment. The tenogenic induction was initiated 24 h after plating by adding TM. For the braided PLA 96/4 scaffolds, hASCs were also cultured in MM to study the effect of the scaffold structure. Medium was changed every other day. The experiments were carried out at passage 4. For the analyses, the scaffolds were removed from the initial plates in which the differentiation was induced and treated separately.

#### *Flow cytometric surface marker expression analysis*

Flow cytometry was used to characterize undifferentiated hASCs of passage 1–2. Briefly, hASCs were analyzed for the multipotency cell surface markers<sup>12</sup> with fluorescence-activated cell sorter (FACS Aria; BD Biosciences, Franklin Lakes, NJ) by measuring monoclonal antibodies against CD3-PE, CD14-PE-Cy7, CD19-PE-Cy7, CD45RO-APC, CD54-FITC, CD73-PE, CD90-APC (BD Biosciences), CD11a-APC, CD80-PE, CD86-PE, CD105-PE (R&D Systems, Minneapolis, MN), CD34-APC, and HLA-DR-PE (ImmunoTools, Friesoythe, Germany). Fluorescence-activated cell sorter (FACS) analysis was performed with 10,000 cells per sample, and the positive expression was defined as a level of fluorescence 99% greater than that of the corresponding unstained cell sample.<sup>35,36</sup>

The flow cytometric analysis showed that hASCs expressed the surface markers CD73, CD90, and CD105, and lacked the expression of the CD3, CD11a, CD14, CD19, CD45, CD80, and CD86, whereas the expression of CD34, CD54, and HLA-DR was moderate. The surface marker analysis confirmed overall the mesenchymal origin of the cells in agreement with literature.<sup>12,37,38</sup>

#### *Cell viability and cell number*

Cell viability was evaluated qualitatively at 7 and 14 days using Live/Dead fluorescence staining (Invitrogen; Life Technologies) as described previously.<sup>39</sup> The samples were incubated for 45 min at room temperature with a mixture containing 0.5  $\mu$ M calcein acetoxymethyl ester (Calcein-AM; green fluorescent dye) and 0.25  $\mu$ M ethidium homodimer-1 (EthD-1; red fluorescent dye). Images of viable green stained cells and necrotic cells stained red were obtained using an epifluorescence Olympus IX51 microscope (Olympus, Tokyo, Japan).

Cell number based on the total amount of DNA of the sample was determined quantitatively with CyQUANT Cell Proliferation Assay Kit (Invitrogen; Life Technologies) according to the manufacturer's protocol at 1, 7, and 14 days. Briefly, the cells were lysed with 0.1% Triton-X 100 buffer (Sigma-Aldrich) and stored at  $-70^{\circ}\text{C}$  until analysis. Alternatively, at 7 and 14 days, the cell seeded PLCL and PLA 96/4 scaffold samples were digested overnight with 1.25 U/mL papain (Sigma-Aldrich) at pH 6.5 and +65°C. The amount of DNA was quantified using 0.2  $\mu\text{g}/\text{mL}$  Hoechst 33258 nucleic acid stain (Bio-Rad Laboratories, Hercules, CA) with purified calf thymus DNA as a standard (Bio-Rad Laboratories). After

a freeze-thaw cycle, working solution for each sample was prepared with CyQUANT GR dye and lysis buffer. The blue-green fluorescence of three parallel samples was measured at 480/520 nm with Victor 1420 Multilabel Counter microplate reader (Wallac, Turku, Finland).

#### *Immunocytochemical analysis*

For qualitative immunocytochemical analysis, the samples were fixed with 4% paraformaldehyde (Sigma-Aldrich). The sample cells were permeabilized with 0.05% Triton-X 100 buffer (Sigma-Aldrich) and blocked with 10% goat serum (Invitrogen; Life Technologies). The samples were incubated with antibodies detecting collagen type I (Abcam, Cambridge, United Kingdom) and TNMD (Santa Cruz Biotechnology, Dallas, TX), and cell nuclei were stained with DAPI (Sigma-Aldrich). Highly cross-adsorbed Alexa Fluor secondary antibodies (Life Technologies) were used and samples were visualized with a confocal LSM 780 microscope (ZEISS, Oberkochen, Germany). COL1 stained in cyan-green was detected at 488 nm, and TNMD stained in orange-red was detected at 594 nm, and cell nuclei stained in blue color by DAPI were detected at 461 nm.

#### *Total collagen content*

The total collagen content was analyzed at day 14 using a quantitative Sircol Soluble Collagen Assay (Biocolor, Carrickfergus, United Kingdom) as described previously.<sup>40</sup> In brief, acid soluble collagen was extracted from the samples with 0.5 M acetic acid (Merck, Darmstadt, Germany) containing 0.1 mg/mL pepsin (Sigma-Aldrich). Sircol Dye reagent (Biocolor), comprised of Sirius Red and picric acid, was added to liquid samples and incubated for 30 min for the mammalian collagen types I–V with a [Gly-X-Y] peptide sequence to form a complex with the dye. The collagen-dye pellet was washed to remove any unbound dye and alkali reagent of 0.5 M sodium hydroxide solution (Biocolor) was added to resolubilize the collagen. Finally, the intensity of red dye in two parallel samples was measured with Victor 1420 microplate reader at 540 nm (Wallac).

#### *Mineralization*

Cellular mineralization was measured with a quantitative Alizarin Red S (Sigma-Aldrich) assay, as described previously,<sup>34</sup> at 14-day time point to exclude unwanted mineralization indicating bone-like matrix formation.

#### *Quantitative real-time polymerase chain reaction*

Quantitative real-time polymerase chain reaction (qRT-PCR) analysis was used to compare the relative expression of tenogenic genes. Total sample RNA was isolated at 14-day time point for the medium optimization experiments, and at 7 and 14 days for the scaffold experiments with the NucleoSpin RNA II kit (Macherey-Nagel, Düren, Germany) according to manufacturer's instructions. First strand complementary DNA (cDNA) of total RNA was synthesized using High-Capacity cDNA Reverse Transcriptase Kit (Applied Biosystems, Foster City, CA). The gene expression of *collagen type I* (TAG Copenhagen, Frederiksberg, Denmark), *collagen type II*, *collagen type III*, *scleraxis (SCX)*, and *tenomodulin (TNMD)* (Oligomer, Helsinki, Finland) was

TABLE 2. THE PRIMER SEQUENCES FOR qRT-PCR

Name	Primer	5'-Sequence-3'	Product size (bp)	Accession No.
<i>hRPLP0</i>	Fwd	AATCTCCAGGGGCACCATT	70	NM_001002
	Rev	CGCTGGCTCCCACTTTGT		
<i>hSCX</i>	Fwd	CAGCGGCACACGGCGAAC	163	BK000280
	Rev	CGTTGCCCAGGTGCGAGATG		
<i>hCOL3A1</i>	Fwd	CAGCGGTTCTCCAGGCAAGG	179	NM_000090
	Rev	CTCCAGTGATCCCAAGCAATCCC		
<i>hCOL1</i>	Fwd	CCAGAAGAACTGGTACATCAGCAA	94	NM_000088.3
	Rev	CGCCATACTCGAACTGGAATC		
<i>hCOL2A1</i>	Fwd	GAGACAGCATGACGCCGAG	5087	NM_001844
	Rev	GCGGATGCTCTCAATCTGGT		
<i>hTNMD</i>	Fwd	CCATGCTGGATGAGAGAGGTT	123	NM_022144
	Rev	TTGGTAGCAGTATGGATATGGGT		

Gene primer sequences of human (1) *acidic ribosomal phosphoprotein P0* (*hRPLP0*); (2) *scleraxis* (*hSCX*); (3) *collagen type III* (*hCOL3A1*); (4) *collagen type I* (*hCOL1*); (5) *collagen type II* (*hCOL2A1*); and (6) *tenomodulin* (*hTNMD*). qRT-PCR, quantitative real-time polymerase chain reaction.

measured. The obtained data were normalized using human *acidic ribosomal phosphoprotein P0* (*hRPLP0*) as a house-keeping gene.<sup>41,42</sup> Relative gene expression of each sample in relation to *hRPLP0* was calculated according to a mathematical data analysis model.<sup>43</sup> The qRT-PCR mixture contained 50 ng cDNA, 300 nM forward and reverse primers, and SYBR Green PCR Master Mix (Applied Biosystems). The used primer sequences and accession numbers are presented in Table 2. The qRT-PCR reactions were performed with ABI PRISM 7300 Sequence Detection System (Applied Biosystems) initially at +95°C for 10 min enzyme activation, and by 45 cycles at +95°C for 15 s denaturation followed by 60 s at +60°C for annealing and extension.

#### Statistical analysis

The significance of differences between means was determined using one-way analysis of variance with Bonferroni's *post hoc* test for statistical significance with *p*-values <0.05. The scaffold experiments were repeated thrice and a different hASC donor was used in each experimental repeat, resulting in *n*=3 for each assay. All the results were standardized to the control condition of MM. Data were analyzed with IBM SPSS Statistics 19 software (IBM, Armonk, NY).

## Results

#### Scaffold characterization

The micro-CT images show the structure of the braided PLA 96/4 and foamed PLCL scaffolds (Fig. 1). The foamed PLCL scaffolds possessed complex irregular structure with 66% ± 2% porosity and pore size of 300–500 μm. Due to the structure's two-dimensional nature, it was not possible to analyze the porosity of the braided PLA 96/4 scaffolds. The measured elastic modulus of PLCL scaffolds was 1.6 ± 0.6 MPa, whereas for the braided PLA 96/4 scaffolds the elastic modulus was 280 ± 20 MPa.

#### Tenogenic medium optimization

TM3 was chosen for the TM condition based on higher DNA content (Fig. 2A) at 7- and 14-day time points and higher relative total collagen content (Fig. 2B) at 14 days. Stronger gene expression of *collagen type III* and *I* was

visible in TM3 at 14-day time point compared with other medium compositions (Fig. 2C, D).

#### Cell viability and cell number in scaffolds

The Live/Dead results showed that the majority of cells were viable with only a negligible number of dead cells (Fig. 3). Also, hASCs cultured in TM formed a uniform cell layer on PLA 96/4 scaffolds at day 14 (Fig. 3; lower row, middle), whereas hASCs cultured on PLCL scaffolds in TM (Fig. 3; lower row, far left), or on PLA 96/4 in MM (Fig. 3; lower row, far right), formed only small aggregates.

The cell number was higher in PLA 96/4 scaffolds compared to PLCL scaffolds at both measured time points in TM, although no significant differences were found due to high donor-dependent variation (Fig. 4A). The cell number was higher in PLA 96/4 scaffolds cultured in TM at 7 and 14 days showing the stimulatory effect of TM on proliferation compared with MM (Fig. 4B).

#### Expression of tenogenic markers in scaffolds

Quantitative RT-PCR was used to detect relative changes in the expression of tenogenic marker genes; *collagen type I*, *collagen type III*, *SCX* and *TNMD* at 7- and 14-day time points in PLA 96/4 scaffolds, in addition to *collagen type II*, which was measured to exclude chondrogenesis (Fig. 5). Due to the poor proliferation results and low expression of *collagen type I* and *TNMD* in PLCL scaffolds, only PLA 96/4 scaffolds were further analyzed. The expression of early tenogenic marker *SCX* was significantly higher in TM condition compared with MM at 7 and 14 days (Fig. 5A). Furthermore, the gene expression of *collagen type III* and *I*, respectively, an early and a late tenogenic marker, peaked in TM already at the 7-day time point and remained higher compared to MM at 14-day time point. The difference was significant at 7 days for both markers (Fig. 5B, C). Although a similar trend was detected also for *TNMD* expression, no significant differences were detected during 2 weeks culture period for *TNMD* expression (Fig. 5D). The expression of *collagen type II* increased in MM with time, whereas in TM, the expression decreased. At 14 days, the expression was lower in TM compared to MM, however, the difference was not statistically significant (Fig. 5E).

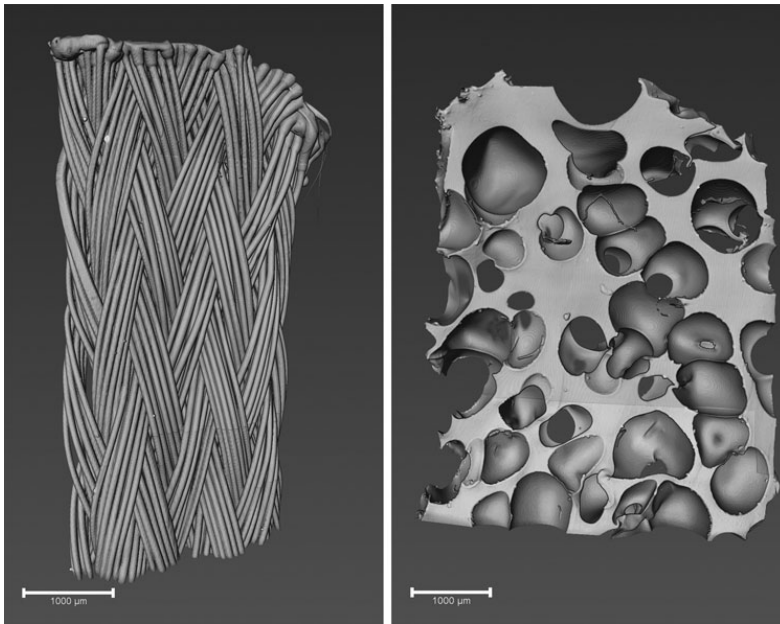


**FIG. 1.** Micro-CT imaging. Micro-CT images of braided 8-filament PLA 96/4 (*left*) and foamed PLCL 70/30 (*right*) scaffolds. Scale bar 1000 µm. Micro-CT, micro-computed tomography; PLA, polylactide; PLCL, poly(L-lactide-co-ε-caprolactone).

*Immunocytochemical staining in scaffolds*

Immunofluorescence staining of the tenogenic proteins COL1 and TNMD was used to analyze hASCs seeded on the braided PLA 96/4 and the foamed PLCL scaffolds (Fig. 6).

Collagen I was strongly expressed in the hASCs cultured on PLA 96/4 scaffolds under tenogenic conditions (Fig. 6; middle row, middle). In contrast, only few hASCs expressed collagen type I when cultured on PLCL scaffolds in tenogenic conditions (Fig. 6; bottom row, middle). Human ASCs

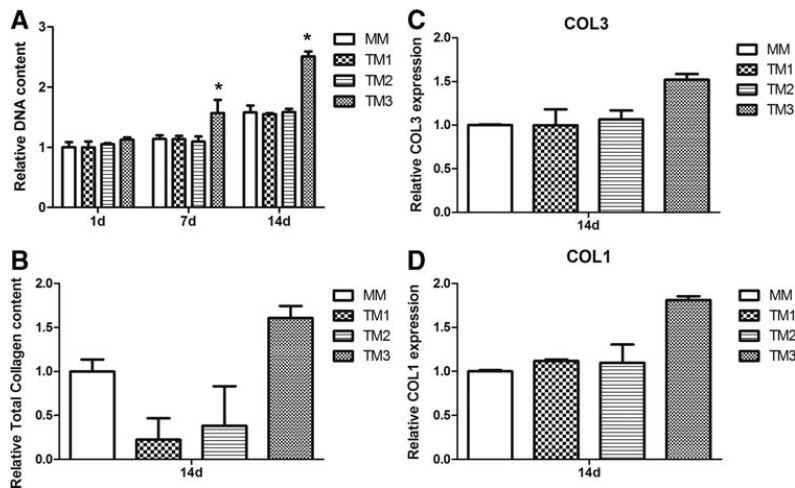


**FIG. 2.** TM optimization. (A) Cell proliferation. Relative DNA content of hASC monolayer in TM1, TM2, TM3, and MM at 1-, 7-, and 14-day time points. Results relative to MM 1-day time point. Significantly higher relative DNA content in TM3 at 7 and 14 days ( $p < 0.05$ ). (B) Collagen production. Relative total collagen content of hASC monolayer in TM1, TM2, TM3, and MM at 14-day time point. Results relative to MM; quantitative real-time PCR results. The relative expression of tenogenic genes. (C) *Collagen type III (COL3)*. (D) *Collagen type I (COL1)* in hASCs in TM1, TM2, TM3, and MM at 14-day time point. The hASCs were isolated from one donor. Data are presented as mean + SD. \*Indicates significant difference with  $p < 0.05$ . hASCs, human adipose stem cells; MM, maintenance medium; SD, standard deviation; TM, tenogenic medium.

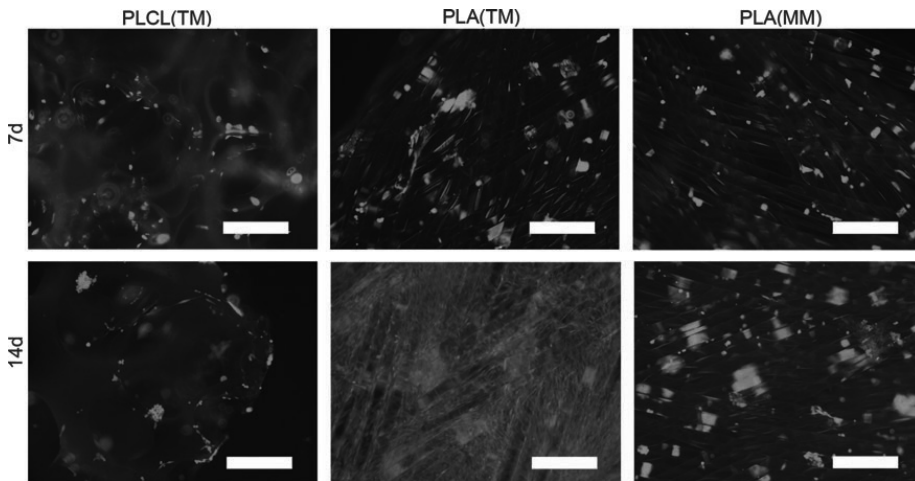


**FIG. 3.** Cell viability. Representative fluorescence images of viable (green) and dead (red) hASCs in TM in PLA 96/4 and PLCL scaffolds compared to control in MM in PLA 96/4 scaffolds at 7- and 14-day time points. The hASCs were isolated from one donor. Magnification  $\times 40$ . Scale bar 500  $\mu\text{m}$ . Color images available online at [www.liebertpub.com/tea](http://www.liebertpub.com/tea)

cultured in MM expressed little collagen type I at 14-day time point (Fig. 6; top row, middle). TNMD was strongly expressed in hASCs in PLA 96/4 scaffolds in TM (Fig. 6; middle row, far right), whereas TNMD staining was scarce for cells on PLCL scaffolds in tenogenic conditions (Fig. 6; bottom row, far right) and negative for hASCs cultured in MM (Fig. 6; top row, far right) at 2 weeks.

#### Total collagen content in scaffolds

Significantly higher total collagen content was measured for hASCs cultured in PLA 96/4 scaffolds in TM compared with MM at 14-day time point (Fig. 7).

#### Mineralization

There was no significant difference in hASC mineralization in PLA 96/4 scaffolds between the MM and TM conditions after 14 days of culture (data not shown).

#### Discussion

Currently, no efficient strategies for engineering tendon *in vitro* exist. Here, we describe a potential approach to produce tendon-like cellular phenotype *in vitro* using the combination of GDF-5 and L-ascorbic acid for the differentiation of hASCs in PLA 96/4 scaffolds. To obtain competent tendon differentiation, the *in vitro* differentiation medium for hASCs was first optimized. We selected ascorbic acid over L-ascorbate-2-phosphate due to the fact that the latter compound has been shown to enhance mineralization, and it has been used as an osteogenic inducer for hASCs.<sup>34</sup> L-ascorbic acid has also been shown to promote collagen type I production.<sup>44–46</sup> Furthermore, ascorbic acid is considered essential for catalyzing cross-linking of collagen in ECM during collagen fibril formation.<sup>47</sup> In combination with tenogenic growth factors, ascorbic acid has been shown to enhance expression of tenogenic genes and proteins such as tenomodulin and collagen type I<sup>48,49</sup> or to

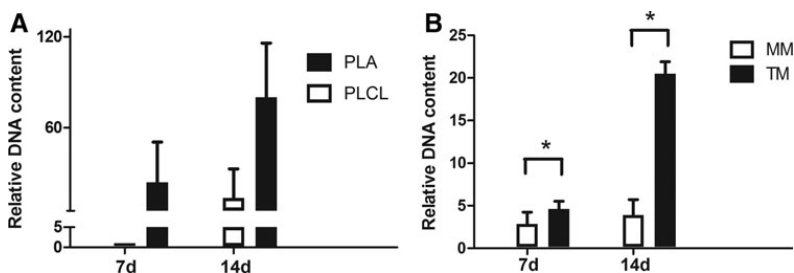
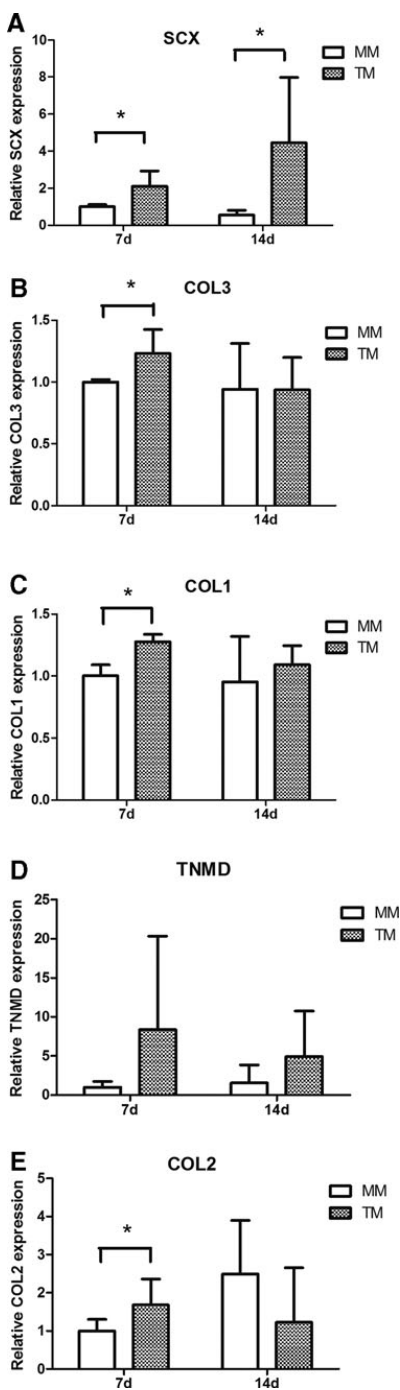


**FIG. 4.** Cell proliferation. Relative DNA content of hASCs in (A) PLA 96/4 and PLCL scaffolds in TM at 7 and 14 days. Results are relative to PLCL at 7-day time point. (B) PLA 96/4 scaffolds in TM and in MM at 7- and 14-day time points. Results are relative to MM at 1-day time point (data not shown). The hASCs were isolated from three donors. Data are presented as mean + SD. \*Indicates significant difference with  $p < 0.05$ .



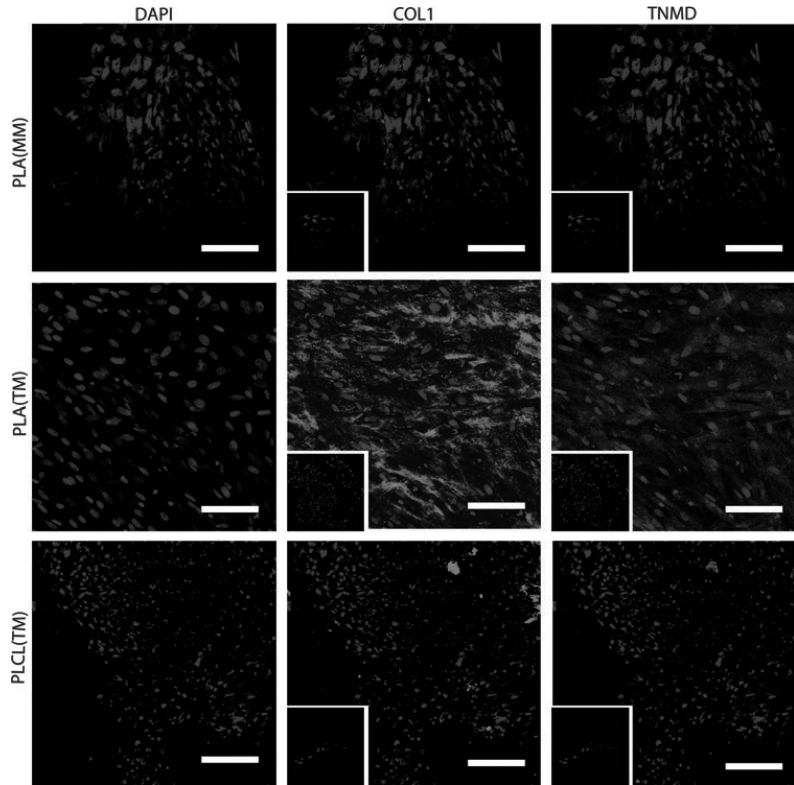
promote cell sheet and ECM formation.<sup>50</sup> The importance of GDF-5 for the tenogenesis of hASCs *in vitro* has been previously reported,<sup>17,50,51</sup> however, to the best of our knowledge, this was the first study to combine GDF-5 and L-ascorbic acid to stimulate tenogenic differentiation of hASCs. TM3 containing both GDF-5 and L-ascorbic acid was superior for the stimulation of collagen production and tenogenic gene expression of hASCs compared to the media containing only GDF-5. This result is consistent with previous studies with human bone marrow-derived mesenchymal stem cells differentiated toward tendon-like lineages using the combination.<sup>19</sup>

In addition to the response to diffusible biochemical species, the chemistry of the material and its surface structure have an important role to support stem cell differentiation.<sup>52-55</sup> Our group and others have previously studied the effect of chemical properties of PLA and PLCL to stem cell response and according to these results, PLA and PLCL do not produce significantly different responses when tested with mesenchymal stem cells.<sup>30,56,57</sup> While differences in polymer properties prevented us from using a similar structure for both materials and because of the adhesive character of PLCL 70/30 fibers, which makes them unsuitable for braided structures, we chose to compare foamed PLCL and braided PLA 96/4 structures, both suited to support hASC differentiation. We showed that hASCs formed a uniform, continuous monolayer on the surface of braided PLA 96/4 filaments, whereas hASCs on foamed PLCL scaffolds formed only small clusters during the same culture period. Moreover, the results of the immunofluorescence staining showed that PLA 96/4 scaffolds promoted the production of a uniform collagenous sheet of hASCs, whereas only minor collagen production was detected on PLCL scaffolds in TM. Our result is consistent with a previous study demonstrating the beneficial effect of fibrous scaffolds for tenogenic differentiation of human mesenchymal stem cells.<sup>58</sup> Our result with PLA 96/4 scaffolds is remarkable due to the fact that we obtained an abundant collagen production in a 3D structure in a static condition without mechanical stimulation. Mechanical stimulation has been shown to induce tendon-like matrix production in previous works.<sup>13,15,23,51,59</sup>

The mechanical stability of the 3D structure is another important factor since tendon transmits the mechanical force of muscle contraction to bone. For the mechanical testing results of the tested scaffolds; the Young's modulus of PLA 96/4 scaffold at  $280 \pm 20$  MPa resembled more than that of human Achilles tendon measured at  $870 \pm 200$  MPa<sup>4</sup> thus providing further evidence of the mechanical properties and suitability of the braided PLA 96/4 scaffolds to bear loads more similar to native tendon. In addition, PLA 96/4 has

**FIG. 5.** Quantitative real-time polymerase chain reaction results. The relative expression of tenogenic genes in hASCs in PLA 96/4 scaffolds cultured in TM or MM at 7- and 14-day time points; (A) *Scleraxis* (SCX); (B) *Collagen type III* (COL3); (C) *Collagen type I* (COL1); (D) *Tenomodulin* (TNMD); (E) *Collagen type II* (COL2). All results were standardized to the control condition of MM at day 7. The hASCs were isolated from three donors. Data are presented as mean  $\pm$  SD. \*Indicates significant difference with  $p < 0.05$ .

**FIG. 6.** Immunofluorescence staining. Teno-genic proteins COL1 and TNMD detected with confocal microscope. COL1 was stained in *green* color, TNMD in *red*, and cell nuclei in *blue* color by DAPI in hASCs at 14 days of culture in PLA 96/4 scaffolds in TM or MM and in PLCL scaffolds in TM. Negative controls for COL1 and TNMD imaged in *bottom left corner*. The hASCs were isolated from one donor. Scale bar 100  $\mu$ m. COL1, collagen type I; TNMD, tenomodulin; DAPI, 4',6'-diamidino-2-phenylindole. Color images available online at [www.liebertpub.com/tea](http://www.liebertpub.com/tea)



been found suitable for tendon repair *in vivo*.<sup>60</sup> However, the foamed PLCL scaffolds were highly elastic and could provide low mechanical support during tissue healing.

Our results showed that soluble factors are needed to support hASC commitment toward tenogenic lineage as the structure alone was not sufficient to promote hASC tenogenesis. According to the results, collagen production was significantly enhanced in the presence of TM compared to MM. Furthermore, the *collagen types I and III*, the major

collagens of tendon ECM, were significantly upregulated in TM at 7 days. The decreasing *collagen II* gene expression profile suggests that hASC chondrogenesis was prohibited in TM condition. To further verify the obtained tendon phenotype, we quantified tendon-specific markers *SCX* and *TNMD* on gene level.<sup>16</sup> *SCX*, a transcription factor for tenomodulin, was significantly upregulated in TM at both time points. Also, the expression of *TNMD* was higher in TM, although no significant differences were found due to patient variation. The obtained mineralization results indicated the L-ascorbic acid containing TM supported tenogenic differentiation over osteogenic differentiation of hASCs. The obtained significant hASC proliferation in TM is also important to gain sufficient cellular mass, which is needed to produce mature and functional tissue *in vivo*.<sup>61</sup>

In short, the results with hASCs seeded on PLA 96/4 scaffolds and cultured in tenogenic conditions show potential clinical relevance. In the future, *in vivo* studies are needed to test the functionality of the engineered tendon construct.

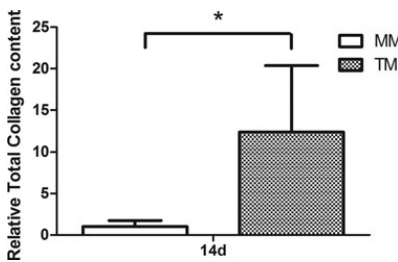


**FIG. 7.** Collagen production. Relative total collagen content of hASCs in PLA 96/4 scaffolds in TM compared to hASCs in MM at 14-day time point. The hASCs were isolated from three donors. Data are presented as mean + SD. \*Indicates significant difference with  $p < 0.05$ .

## Conclusions

In this study, we initially demonstrated that stimulation under GDF-5 and L-ascorbic acid allows efficient differentiation of hASCs toward tendon tissue. The comparison of two different scaffolds showed that the braided PLA 96/4

scaffold was more potential for an engineered tendon construct over the foamed PLCL scaffold. PLA 96/4 structure allowed uniform cell attachment and spreading compared to PLCL scaffolds when cultured in tenogenic conditions. Tendon markers collagen type I and TNMD were strongly expressed in hASCs cultured on PLA 96/4 scaffolds under tenogenic conditions. The braided PLA 96/4 scaffold was also shown to have suitable mechanical properties for tendon tissue engineering applications. However, PLA 96/4 scaffold alone was not sufficient for effective proliferation and tenogenic induction of hASCs. Thus, the optimized TM was needed to provide a favorable tenogenic gene expression profile and abundant collagen production of hASCs. In conclusion, hASCs seeded on the braided PLA 96/4 scaffolds and cultured in tenogenic conditions present an efficient strategy to produce tendon-like cellular phenotype.

### Acknowledgments

The authors thank Dr. Hannu Kuokkanen for the delivery of fat samples for stem cell isolation; Scaffold Ltd. and the Unit of Electronics and Communications Engineering of Tampere University of Technology for the biomaterials; Anna-Majja Honkala, Miia Juntunen, and Mimmi Patrikoski for technical assistance and FACS analysis; Professor Jari Hyttinen and Tampere University of Technology Computational Biophysics and Imaging Group ([www.tut.fi/cbig](http://www.tut.fi/cbig)); and Markus Hannula for micro-CT imaging and analysis. This study was financially supported by the Finnish Funding Agency for Technology and Innovation (TEKES) and the Academy of Finland.

### Authors' Contributions

K.V. carried out majority of the cell culture studies and data analysis, drafted the article, and participated in article editing. M.B. assisted in the cell culture studies and data analysis, and participated in article editing. E.T. and K.P. carried out biomaterial production work and helped to draft and edit the article. H.H. was consulted for statistical analyses, contributed to the interpretation of data, and participated in article editing. M.K. and R.S.-K. participated in the study design, coordination, and article editing. S.M. participated in the study design and coordination, contributed to the interpretation of data, and participated in article editing. S.H. designed and coordinated the study, had a major contribution in interpretation of data, and participated in writing and editing of the article. All authors read and approved the final article.

### Disclosure Statement

No competing financial interests exist.

### References

- Pennisi, E. Tending tender tendons. *Science* **295**, 1011, 2002.
- Vitale, M.A., Vitale, M.G., Zivin, J.G., Braman, J.P., Bigliani, L.U., and Flatow, E.L. Rotator cuff repair: an analysis of utility scores and cost-effectiveness. *J Shoulder Elbow Surg* **16**, 181, 2007.
- Caliari, S.R., and Harley, B.A. Composite growth factor supplementation strategies to enhance tenocyte bioactivity in aligned collagen-GAG scaffolds. *Tissue Eng Part A* **19**, 1100, 2013.
- Kuo, C.K., Marturano, J.E., and Tuan, R.S. Novel strategies in tendon and ligament tissue engineering: advanced biomaterials and regeneration motifs. *Sports Med Arthrosc Rehabil Ther Technol* **2**, 20, 2010.
- Ho, J.O., Sawadkar, P., and Mudera, V. A review on the use of cell therapy in the treatment of tendon disease and injuries. *J Tissue Eng* **5**, 2041731414549678, 2014.
- Lomas, A.J., Ryan, C.N., Sorushanova, A., Shologu, N., Sideri, A.L., Tsioli, V., *et al.* The past, present and future in scaffold-based tendon treatments. *Adv Drug Deliv Rev* **84**, 257, 2015.
- Font Tellado, S., Balmayor, E.R., and Van Griensven, M. Strategies to engineer tendon/ligament-to-bone interface: biomaterials, cells and growth factors. *Adv Drug Deliv Rev* **94**, 126, 2015.
- Huang, D., Balian, G., and Chhabra, A.B. Tendon tissue engineering and gene transfer: the future of surgical treatment. *J Hand Surg Am* **31**, 693, 2006.
- Kryger, G.S., Chong, A.K., Costa, M., Pham, H., Bates, S.J., and Chang, J. A comparison of tenocytes and mesenchymal stem cells for use in flexor tendon tissue engineering. *J Hand Surg Am* **32**, 597, 2007.
- Zuk, P.A., Zhu, M., Ashjian, P., De Ugarte, D.A., Huang, J.I., Mizuno, H., *et al.* Human adipose tissue is a source of multipotent stem cells. *Mol Biol Cell* **13**, 4279, 2002.
- Zuk, P.A., Zhu, M., Mizuno, H., Futrell, J.W., Katz, A.J., *et al.* Multilineage cells from human adipose tissue: implications for cell-based therapies. *Tissue Eng* **7**, 211, 2001.
- Lindroos, B., Suuronen, R., and Miettinen, S. The potential of adipose stem cells in regenerative medicine. *Stem Cell Rev* **7**, 269, 2011.
- Yang, G., Rothrauff, B.B., Lin, H., Gottardi, R., Alexander, P.G., and Tuan, R.S. Enhancement of tenogenic differentiation of human adipose stem cells by tendon-derived extracellular matrix. *Biomaterials* **34**, 9295, 2013.
- Chainani, A., Hippensteel, K.J., Kishan, A., Garrigues, N.W., Ruch, D.S., Guilak, F., *et al.* Multilayered electrospun scaffolds for tendon tissue engineering. *Tissue Eng Part A* **19**, 2594, 2013.
- Vindigni, V., Tonello, C., Lancerotto, L., Abatangelo, G., Cortivo, R., Zavan, B., *et al.* Preliminary report of in vitro reconstruction of a vascularized tendonlike structure: a novel application for adipose-derived stem cells. *Ann Plast Surg* **71**, 664, 2013.
- Kraus, A., Woon, C., Raghavan, S., Megerle, K., Pham, H., and Chang, J. Co-culture of human adipose-derived stem cells with tenocytes increases proliferation and induces differentiation into a tenogenic lineage. *Plast Reconstr Surg* **132**, 754e, 2013.
- James, R., Kumbar, S.G., Laurencin, C.T., Balian, G., and Chhabra, A.B. Tendon tissue engineering: adipose-derived stem cell and GDF-5 mediated regeneration using electrospun matrix systems. *Biomed Mater* **6**, 025011, 2011.
- Park, A., Hogan, M.V., Kesturu, G.S., James, R., Balian, G., and Chhabra, A.B. Adipose-derived mesenchymal stem cells treated with growth differentiation factor-5 express tendon-specific markers. *Tissue Eng Part A* **16**, 2941, 2010.
- Jenner, J.M., van Eijk, F., Saris, D.B., Willems, W.J., Dhert, W.J., and Creemers, L.B. Effect of transforming growth factor-beta and growth differentiation factor-5 on proliferation and matrix production by human bone marrow

- stromal cells cultured on braided poly lactic-co-glycolic acid scaffolds for ligament tissue engineering. *Tissue Eng* **13**, 1573, 2007.
20. Butler, D.L., Juncosa, N., and Dressler, M.R. Functional efficacy of tendon repair processes. *Annu Rev Biomed Eng* **6**, 303, 2004.
  21. James, R., Kesturu, G., Balian, G., and Chhabra, A.B. Tendon: biology, biomechanics, repair, growth factors, and evolving treatment options. *J Hand Surg Am* **33**, 102, 2008.
  22. Kannus, P. Structure of the tendon connective tissue. *Scand J Med Sci Sports* **10**, 312, 2000.
  23. Gaspar, D., Spanoudes, K., Holladay, C., Pandit, A., and Zeugolis, D. Progress in cell-based therapies for tendon repair. *Adv Drug Deliv Rev* **84**, 240, 2015.
  24. Kim, S.H., Jung, Y., and Kim, S.H. A biocompatible tissue scaffold produced by supercritical fluid processing for cartilage tissue engineering. *Tissue Eng Part C Methods* **19**, 181, 2013.
  25. Jung, Y., Kim, S.H., Kim, Y.H., and Kim, S.H. The effect of hybridization of hydrogels and poly(L-lactide-co-epsilon-caprolactone) scaffolds on cartilage tissue engineering. *J Biomater Sci Polym Ed* **21**, 581, 2010.
  26. Lee, J., Guarino, V., Gloria, A., Ambrosio, L., Tae, G., Kim, Y.H., *et al.* Regeneration of Achilles' tendon: the role of dynamic stimulation for enhanced cell proliferation and mechanical properties. *J Biomater Sci Polym Ed* **21**, 1173, 2010.
  27. Nair, L.S., and Laurencin, C.T. Polymers as biomaterials for tissue engineering and controlled drug delivery. *Adv Biochem Eng Biotechnol* **102**, 47, 2006.
  28. Rasal, R.M., Janorkar, A.V., and Hirt, D.E. Poly(lactic acid) modifications. *Prog in Polym Sci* **35**, 338, 2010.
  29. Lu, H.H., Cooper, J.A., Jr., Manuel, S., Freeman, J.W., Attawia, M.A., Ko, F.K., *et al.* Anterior cruciate ligament regeneration using braided biodegradable scaffolds: in vitro optimization studies. *Biomaterials* **26**, 4805, 2005.
  30. Sartoneva, R., Haaparanta, A.M., Lahdes-Vasama, T., Mannerstrom, B., Kellomaki, M., Salomaki, M., *et al.* Characterizing and optimizing poly-L-lactide-co-epsilon-caprolactone membranes for urothelial tissue engineering. *J R Soc Interface* **9**, 3444, 2012.
  31. Schindelin, J., Arganda-Carreras, I., Frise, E., Kaynig, V., Longair, M., Pietzsch, T., *et al.* Fiji: an open-source platform for biological-image analysis. *Nat Methods* **9**, 676, 2012.
  32. Doube, M., Klosowski, M.M., Arganda-Carreras, I., Cordelières, F.P., Dougherty, R.P., Jackson, J.S., *et al.* BoneJ: free and extensible bone image analysis in ImageJ. *Bone* **47**, 1076, 2010.
  33. Haimi, S., Suuriniemi, N., Haaparanta, A.M., Ella, V., Lindroos, B., Huhtala, H., *et al.* Growth and osteogenic differentiation of adipose stem cells on PLA/bioactive glass and PLA/beta-TCP scaffolds. *Tissue Eng Part A* **15**, 1473, 2009.
  34. Kyllonen, L., Haimi, S., Mannerstrom, B., Huhtala, H., Rajala, K.M., Skottman, H., *et al.* Effects of different serum conditions on osteogenic differentiation of human adipose stem cells in vitro. *Stem Cell Res Ther* **4**, 17, 2013.
  35. Jaroszeski, M.J., and Radcliff, G. Fundamentals of flow cytometry. *Mol Biotechnol* **11**, 37, 1999.
  36. Picot, J., Guerin, C.L., Le Van Kim, C., and Boulanger, C.M. Flow cytometry: retrospective, fundamentals and recent instrumentation. *Cytotechnology* **64**, 109, 2012.
  37. Dominici, M., Le Blanc, K., Mueller, I., Slaper-Cortenbach, I., Marini, F., Krause, D., *et al.* Minimal criteria for defining multipotent mesenchymal stromal cells. The International Society for Cellular Therapy position statement. *Cytotherapy* **8**, 315, 2006.
  38. McIntosh, K., Zvonice, S., Garrett, S., Mitchell, J.B., Floyd, Z.E., Hammill, L., *et al.* The immunogenicity of human adipose-derived cells: temporal changes in vitro. *Stem Cells* **24**, 1246, 2006.
  39. Tirkkonen, L., Haimi, S., Huttunen, S., Wolff, J., Pirhonen, E., Sandor, G.K., *et al.* Osteogenic medium is superior to growth factors in differentiation of human adipose stem cells towards bone-forming cells in 3D culture. *Eur Cell Mater* **25**, 144, 2013.
  40. Kyllonen, L., Haimi, S., Sakkinen, J., Kuokkanen, H., Mannerstrom, B., Sandor, G.K., *et al.* Exogenously added BMP-6, BMP-7 and VEGF may not enhance the osteogenic differentiation of human adipose stem cells. *Growth Factors* **31**, 141, 2013.
  41. Fink, T., Lund, P., Pilgaard, L., Rasmussen, J.G., Duroux, M., and Zachar, V. Instability of standard PCR reference genes in adipose-derived stem cells during propagation, differentiation and hypoxic exposure. *BMC Mol Biol* **9**, 98, 2008.
  42. Gabriellsson, B.G., Olofsson, L.E., Sjogren, A., Jernas, M., Elander, A., Lonn, M., *et al.* Evaluation of reference genes for studies of gene expression in human adipose tissue. *Obes Res* **13**, 649, 2005.
  43. Pfaffl, M.W. A new mathematical model for relative quantification in real-time RT-PCR. *Nucleic Acids Res* **29**, e45, 2001.
  44. Kim, A.Y., Lee, E.M., Lee, E.J., Min, C.W., Kang, K.K., Park, J.K., *et al.* Effects of vitamin C on cytotherapy-mediated muscle regeneration. *Cell Transplant* **22**, 1845, 2013.
  45. Wei, C., Liu, X., Tao, J., Wu, R., Zhang, P., Bian, Y., *et al.* Effects of vitamin C on characteristics retaining of in vitro-cultured mouse adipose-derived stem cells. *In Vitro Cell Dev Biol Anim* **50**, 75, 2014.
  46. Yu, J., Tu, Y.K., Tang, Y.B., and Cheng, N.C. Stemness and transdifferentiation of adipose-derived stem cells using L-ascorbic acid 2-phosphate-induced cell sheet formation. *Biomaterials* **35**, 3516, 2014.
  47. Kishore, V., Bullock, W., Sun, X., Van Dyke, W.S., and Akkus, O. Tenogenic differentiation of human MSCs induced by the topography of electrochemically aligned collagen threads. *Biomaterials* **33**, 2137, 2012.
  48. Ni, M., Rui, Y.F., Tan, Q., Liu, Y., Xu, L.L., Chan, K.M., *et al.* Engineered scaffold-free tendon tissue produced by tendon-derived stem cells. *Biomaterials* **34**, 2024, 2013.
  49. Theiss, F., Mirsaidi, A., Mhanna, R., Kummerle, J., Glanz, S., Bahrenberg, G., *et al.* Use of biomimetic microtissue spheroids and specific growth factor supplementation to improve tenocyte differentiation and adaptation to a collagen-based scaffold in vitro. *Biomaterials* **69**, 99, 2015.
  50. Lui, P.P., Wong, O.T., and Lee, Y.W. Application of tendon-derived stem cell sheet for the promotion of graft healing in anterior cruciate ligament reconstruction. *Am J Sports Med* **42**, 681, 2014.
  51. Raabe, O., Shell, K., Fietz, D., Freitag, C., Ohrndorf, A., Christ, H.J., *et al.* Tenogenic differentiation of equine adipose-tissue-derived stem cells under the influence of tensile strain, growth differentiation factors and various oxygen tensions. *Cell Tissue Res* **352**, 509, 2013.



52. Murphy, W.L., McDevitt, T.C., and Engler, A.J. Materials as stem cell regulators. *Nat Mater* **13**, 547, 2014.
53. McMurray, R.J., Gadegaard, N., Tsimbouri, P.M., Burgess, K.V., McNamara, L.E., Tare, R., *et al.* Nanoscale surfaces for the long-term maintenance of mesenchymal stem cell phenotype and multipotency. *Nat Mater* **10**, 637, 2011.
54. Kolind, K., Leong, K.W., Besenbacher, F., and Foss, M. Guidance of stem cell fate on 2D patterned surfaces. *Biomaterials* **33**, 6626, 2012.
55. Iannone, M., Ventre, M., Formisano, L., Casalino, L., Patriarca, E.J., and Netti, P.A. Nanoengineered surfaces for focal adhesion guidance trigger mesenchymal stem cell self-organization and tenogenesis. *Nano Lett* **15**, 1517, 2015.
56. Yin, Z., Chen, X., Chen, J.L., Shen, W.L., Hieu Nguyen, T.M., Gao, L., *et al.* The regulation of tendon stem cell differentiation by the alignment of nanofibers. *Biomaterials* **31**, 2163, 2010.
57. Farnig, E., Urdaneta, A.R., Barba, D., Esmende, S., and McAllister, D.R. The effects of GDF-5 and uniaxial strain on mesenchymal stem cells in 3-D culture. *Clin Orthop Relat Res* **466**, 1930, 2008.
58. Czaplewski, S.K., Tsai, T.L., Duenwald-Kuehl, S.E., Vanderby, R., Jr., and Li, W.J. Tenogenic differentiation of human induced pluripotent stem cell-derived mesenchymal stem cells dictated by properties of braided submicron fibrous scaffolds. *Biomaterials* **35**, 6907, 2014.
59. Kuo, C.K., and Tuan, R.S. Mechanoactive tenogenic differentiation of human mesenchymal stem cells. *Tissue Eng Part A* **14**, 1615, 2008.
60. Viinikainen, A., Goransson, H., Taskinen, H.S., Roytta, M., Kellomaki, M., Tormala, P., *et al.* Flexor tendon healing within the tendon sheath using bioabsorbable poly-L/D-lactide 96/4 suture. A histological in vivo study with rabbits. *J Mater Sci Mater Med* **25**, 1319, 2014.
61. Weinand, C., Xu, J.W., Peretti, G.M., Bonassar, L.J., and Gill, T.J. Conditions affecting cell seeding onto three-dimensional scaffolds for cellular-based biodegradable implants. *J Biomed Mater Res B Appl Biomater* **91**, 80, 2009.

Address correspondence to:  
Kaisa Vuornos, MSc  
Adult Stem Cells  
BioMediTech  
University of Tampere  
FI-33014 Tampere  
Finland

E-mail: [kaisa.vuornos@uta.fi](mailto:kaisa.vuornos@uta.fi)

Received: September 3, 2015

Accepted: January 25, 2016

Online Publication Date: February 24, 2016



# PUBLICATION II

## **Bioactive Glass Ions Induce Efficient Osteogenic Differentiation of Human Adipose Stem Cells Encapsulated in Gellan Gum and Collagen Type I Hydrogels**

Vuornos K., Ojansivu M., Koivisto J.T., Häkkänen H., Belay B., Montonen T., Huhtala H., Kääriäinen M., Hupa L., Kellomäki M., Hyttinen J., Ihalainen J., Miettinen S.

*Mater Sci Eng C Mater Biol Appl.* 2019 Jun; 99: 905-918.

**Publication reprinted with the permission of Elsevier Ltd.**

## CORRIGENDA

In publication **II**:

1. An error in reporting in human adipose stem cell isolation and cell expansion chapter in collagenase type I solution composition and consequently missing information on the composition of maintenance medium (MM). Error corrected as follows: “The adipose tissue was cut up and tissue was digested by collagenase type I (1.5 mg/mL; Thermo Fisher Scientific) solution containing DMEM/F-12 1:1 (Thermo Fisher Scientific), 1 % L-glutamine (GlutaMAX; Thermo Fisher Scientific), and 1 % P/S. The cells were expanded in maintenance medium containing DMEM/F-12, 5 % human serum (HS; Biowest, Nuaille, France), 1 % L-glutamine, and 1 % P/S.”
2. An error in section 2.5 LIVE/DEAD staining protocol dye concentrations, corrected as follows: “The living cells were stained with 0.5  $\mu$ M calcein acetoxymethyl ester (green stain) and necrotic cells were stained with 0.25  $\mu$ M ethidium homodimer-1 (red stain) for 45 min in RT.”
3. An error in Fig. 4 Gene expression: Error in scales of *OSX* (Fig. 4B) and *RUNX2* (Fig. 4C) gene expressions and single missing box plot values from figure. Corrected as follows, with the upper limit of the y axis scale of *OSX* gene expression adjusted to 1 000 000 instead of 100 000. Also, the y axis scale of *RUNX2* gene expression adjusted to include all values below 5.0.
4. An error in Authors' contributions: missing author Minna Kääriäinen, MD, PhD, from listed authors' contributions. Corrected as follows: “MKä provided adipose tissue samples for stem cell isolation and participated in manuscript preparation and editing.”



## Bioactive glass ions induce efficient osteogenic differentiation of human adipose stem cells encapsulated in gellan gum and collagen type I hydrogels

Kaisa Vuornos<sup>a,b,\*</sup>, Miina Ojansivu<sup>a,b</sup>, Janne T. Koivisto<sup>c,d</sup>, Heikki Häkkänen<sup>e</sup>, Birhanu Belay<sup>f</sup>, Toni Montonen<sup>f</sup>, Heini Huhtala<sup>g</sup>, Minna Kääriäinen<sup>h</sup>, Leena Hupa<sup>i</sup>, Minna Kellomäki<sup>c</sup>, Jari Hyttinen<sup>f</sup>, Janne A. Ihalainen<sup>e</sup>, Susanna Miettinen<sup>a,b</sup>

<sup>a</sup> Adult Stem Cell Group, BioMediTech, Faculty of Medicine and Health Technology, Tampere University, P.O. BOX 100, FI-33014 Tampere, Finland

<sup>b</sup> Research, Development and Innovation Centre, Tampere University Hospital, P.O. BOX 2000, FI-33521, Tampere, Finland

<sup>c</sup> Biomaterials and Tissue Engineering Group, BioMediTech, Faculty of Medicine and Health Technology, Tampere University, P.O. BOX 527, FI-33101 Tampere, Finland

<sup>d</sup> Heart Group, BioMediTech, Faculty of Medicine and Health Technology, Tampere University, P.O. BOX 100, FI-33014 Tampere, Finland

<sup>e</sup> Nanoscience Center, University of Jyväskylä, P.O. BOX 35, FI-40014 Jyväskylä, Finland

<sup>f</sup> Computational Biophysics and Imaging Group, BioMediTech, Faculty of Medicine and Health Technology, Tampere University, P.O. BOX 527, FI-33101 Tampere, Finland

<sup>g</sup> Faculty of Social Sciences, Tampere University, P.O. BOX 100, FI-33014 Tampere, Finland

<sup>h</sup> Department of Plastic and Reconstructive Surgery, Tampere University Hospital, P.O. BOX 2000, FI-33521 Tampere, Finland

<sup>i</sup> Johan Gadolin Process Chemistry Centre, Åbo Akademi University, Biskopsgatan 8, FI-20500 Åbo, Finland

### ARTICLE INFO

#### Keywords:

Adipose stem cell  
Bioactive glass  
Osteogenic differentiation  
Gellan gum hydrogel  
Collagen type I hydrogel

### ABSTRACT

**Background:** Due to unmet need for bone augmentation, our aim was to promote osteogenic differentiation of human adipose stem cells (hASCs) encapsulated in gellan gum (GG) or collagen type I (COL) hydrogels with bioactive glass (experimental glass 2-06 of composition [wt-%]: Na<sub>2</sub>O 12.1, K<sub>2</sub>O 14.0, CaO 19.8, P<sub>2</sub>O<sub>5</sub> 2.5, B<sub>2</sub>O<sub>3</sub> 1.6, SiO<sub>2</sub> 50.0) extract based osteogenic medium (BaG OM) for bone construct development. GG hydrogels were crosslinked with spermidine (GG-SPD) or BaG extract (GG-BaG).

**Methods:** Mechanical properties of cell-free GG-SPD, GG-BaG, and COL hydrogels were tested in osteogenic medium (OM) or BaG OM at 0, 14, and 21 d. Hydrogel embedded hASCs were cultured in OM or BaG OM for 3, 14, and 21 d, and analyzed for viability, cell number, osteogenic gene expression, osteocalcin production, and mineralization. Hydroxyapatite-stained GG-SPD samples were imaged with Optical Projection Tomography (OPT) and Selective Plane Illumination Microscopy (SPIM) in OM and BaG OM at 21 d. Furthermore, Raman spectroscopy was used to study the calcium phosphate (CaP) content of hASC-secreted ECM in GG-SPD, GG-BaG, and COL at 21 d in BaG OM.

**Results:** The results showed viable rounded cells in GG whereas hASCs were elongated in COL. Importantly, BaG OM induced significantly higher cell number and higher osteogenic gene expression in COL. In both hydrogels, BaG OM induced strong mineralization confirmed as CaP by Raman spectroscopy and significantly improved mechanical properties. GG-BaG hydrogels rescued hASC mineralization in OM. OPT and SPIM showed homogeneous 3D cell distribution with strong mineralization in BaG OM. Also, strong osteocalcin production was visible in COL.

**Conclusions:** Overall, we showed efficacious osteogenesis of hASCs in 3D hydrogels with BaG OM with potential for bone-like grafts.

### 1. Introduction

Increasing number of musculoskeletal defects and the growth of the

ageing population augment the demand for functional engineered bone grafts. Autologous bone is limited while, besides shortage of allograft bone, it might also pose a risk of adverse effects and graft rejection

\* Corresponding author at: Tampere University, BioMediTech, Faculty of Medicine and Health Technology, Adult Stem Cell Group, P.O. BOX 100, FI-33014, Finland.

**E-mail addresses:** [kaisa.vuornos@tuni.fi](mailto:kaisa.vuornos@tuni.fi) (K. Vuornos), [miina.ojansivu@ki.se](mailto:miina.ojansivu@ki.se) (M. Ojansivu), [janne.t.koivisto@tuni.fi](mailto:janne.t.koivisto@tuni.fi) (J.T. Koivisto), [heikki.hakkanen@jyu.fi](mailto:heikki.hakkanen@jyu.fi) (H. Häkkänen), [birhanu.belay@tuni.fi](mailto:birhanu.belay@tuni.fi) (B. Belay), [toni.montonen@tuni.fi](mailto:toni.montonen@tuni.fi) (T. Montonen), [heini.huhtala@tuni.fi](mailto:heini.huhtala@tuni.fi) (H. Huhtala), [minna.kaariainen@pshp.fi](mailto:minna.kaariainen@pshp.fi) (M. Kääriäinen), [leena.hupa@abo.fi](mailto:leena.hupa@abo.fi) (L. Hupa), [minna.kellomaki@tuni.fi](mailto:minna.kellomaki@tuni.fi) (M. Kellomäki), [jari.hyttinen@tuni.fi](mailto:jari.hyttinen@tuni.fi) (J. Hyttinen), [janne.ihalainen@jyu.fi](mailto:janne.ihalainen@jyu.fi) (J.A. Ihalainen), [susanna.miettinen@tuni.fi](mailto:susanna.miettinen@tuni.fi) (S. Miettinen).

<https://doi.org/10.1016/j.msec.2019.02.035>

Received 20 August 2018; Received in revised form 5 February 2019; Accepted 10 February 2019

Available online 13 February 2019

0928-4931/ © 2019 Elsevier B.V. All rights reserved.

[1,2]. Human adipose stem cells (hASCs) are abundant and accessible adult stem cells and suitable for the development of bone constructs [3]. For bone applications, 3D hydrogels offer an adaptable approach of a free form construct with high elasticity and malleable mechanical properties, instead of limited conventional scaffold structure. 3D hydrogel culture simulates more effectively the natural elastic cell microenvironment allowing higher degrees of freedom to form cellular interactions compared to traditional stiffer biomaterials. For instance, natural polymers have been studied as native microenvironments for stem cells, such as protein based collagen type I (COL), while inexpensive polysaccharide gellan gum (GG) offers more tailorable mechanical properties to support stem cell differentiation. Moreover, GG and COL hydrogels have been already reported as hydrophilic, biocompatible, bioresorbable, and also, adaptable hydrogel scaffolds suitable for bone tissue engineering applications [4–9]. On the other hand, bioactive glasses (BaGs) have been widely applied as medical implant materials and have been shown well applicable for bone grafts [10–12] and, in addition, as strong osteogenic inducers of the hASCs without any added chemical supplements such as growth factors [13,14].

Despite their suitability for bone applications, hydrogel biomaterials in themselves lack bone mineralization enhancing components. To date, the majority of the GG and COL hydrogel studies for bone applications have sought to increase hydrogel mineralization and mechanical properties by the addition of nanosized or larger BaG particles to the hydrogel matrix [4,7,15,16]. Hydrogel mineralization requires robust support from added components in *in vitro* conditions mimicking the physiological conditions. To achieve this, in an earlier study, we demonstrated that BaG dissolution ions were strong inducers of hASC osteogenic differentiation, and showed that the ions dissolved from the specific composition of experimental silica-based BaG 2-06 combined with osteogenic medium (OM) components induced calcium phosphate (CaP) mineral accumulation already after 14 days of culture in 2D culture conditions [13]. The ionic dissolution products of experimental glass 2-06 have been previously analyzed high in  $\text{Ca}^{2+}$ ,  $\text{K}^+$ , and  $\text{B}^+$ , and the detailed ionic composition of the bioactive glass extract (BaG ext) of experimental glass 2-06 has been reported in a published study [13]. Thus, we hypothesized that the BaG ext ionic dissolution products would promote equally strong osteogenic differentiation of hASCs in 3D hydrogel culture. In addition, since small molecules like cationic spermidine (SPD) have been demonstrated to interact with anionic polymers such as GG [17,18], we hypothesized the divalent  $\text{Ca}^{2+}$  cations in the BaG ext to function as potential ionic crosslinkers for GG hydrogel. To the best of our knowledge, GG and COL have not been previously combined with BaG ionic species alone for bone tissue engineering applications with embedded hASCs. We also used efficient imaging techniques to assess the cell distribution, form and mineralization with in-house-built Optical Projection Tomography (OPT) and Selective Plane Illumination Microscopy (SPIM) systems that have been already applied to cell imaging in 3D hydrogel culture, mass transport studies, and characterization of 3D hydrogels [19–21].

Therefore, the aim of this study was to develop an effective hASC-laden hydrogel mineralization method for the development of engineered bone constructs. The mechanical properties of cell-free hydrogels were tested for bone applications with or without incubation in serum-containing OM and BaG ext. based osteogenic medium (BaG OM) media. GG and COL hydrogels combined with BaG OM induction were compared for osteogenic differentiation of hydrogel-encapsulated hASCs, and to that end hASC viability, adhesion, cell number, osteocalcin production by immunofluorescence staining, mineralization, and the gene expression of osteogenic marker genes were analyzed. Additionally, the potential of GG ionic crosslinkers SPD and BaG ext to support hASC mineralization was tested in the control OM. The transparent GG-SPD cell-hydrogel sample mineralized residues were imaged with OPT and SPIM in OM and BaG OM at 3 weeks. Also, the Raman spectra of hASC-secreted ECM and mineralized residues in GG-SPD, GG-BaG, and COL was measured at 3 weeks of culture in the BaG OM

condition.

## 2. Materials and methods

### 2.1. Hydrogel scaffolds

#### 2.1.1. Gellan gum hydrogel scaffolds

GG (low acyl,  $M_w$  1.0 kg/mol; Gelzan CM; Sigma-Aldrich, St. Louis, MO, USA) sterile filtered (0.2  $\mu\text{m}$ ) solution of 0.5% (w/v) concentration was crosslinked with either 16% (v/v) SPD (BioXtra; Sigma-Aldrich) of 1 mg/mL concentration in 10% (w/w) sucrose (Sigma-Aldrich) in deionized water or with BaG ext (experimental glass 2-06) [13] containing Dulbecco's Modified Eagle Medium/Ham's Nutrient Mixture F-12 (DMEM/F-12 1:1; Thermo Fisher Scientific, Waltham, MA, USA), 1% L-glutamine (GlutaMAX; Thermo Fisher Scientific), and 1% antibiotics/antimycotic containing 100 U/mL penicillin/100 U/mL streptomycin (P/S; Lonza, Basel, Switzerland) to yield GG-BaG hydrogel samples. The cell pellet was resuspended into GG solution at +37 °C for hASC encapsulation into 3D hydrogel. The cell-hydrogel solution was manually mixed to an ionic crosslinker for immediate gelation. The cell culture medium was added on top of the gelled hASC-laden hydrogel samples.

#### 2.1.2. Collagen type I hydrogel scaffolds

Commercially available COL (rat tail collagen type I, 3.0 mg/mL, Gibco; Thermo Fisher Scientific) was gelled with 10 $\times$  phosphate buffered saline (10 $\times$  PBS; Lonza) and 1 N NaOH (Sigma-Aldrich) according to the manufacturer's protocol. Briefly, the ice cold 10 $\times$  PBS and 1 N NaOH were mixed and COL stock was added while kept on ice. The cell pellet was resuspended and mixed into the non-gelated COL mixture followed by immediate gelation in RT and the cell culture medium was added on top of the gelled hydrogels.

### 2.2. Mechanical testing

The acellular GG-SPD, GG-BaG, and COL hydrogel samples were mechanically tested by compression testing. The 0.875 cm<sup>3</sup> samples ( $n = 3-6$ ) of approximately 4.0–6.5 mm of height and 12.2 mm diameter were cast in custom-made molds and incubated overnight at +37 °C under parafilm without media to ensure complete hydrogel gelation before compression testing or media incubation initiation. Unconfined compression was performed with a constant 10 mm/min strain rate in air environment in RT to 65% strain from their original height at 0, 14, and 21 days of incubation in OM or BaG OM media. The compressive load was measured by the Bose 5100 BioDynamic ElectroForce (TA Instruments, New Castle, DE, USA) instrument equipped with a 225 N load sensor and the data was recorded with the WinTest 4.1 software (WinTest, Yokohama, Japan). The compressive modulus under tension was calculated by MS Excel (Microsoft, Redmond, WA, USA) based on the slope of the linear region of the stress versus strain curve where the Hooke's law holds [17].

### 2.3. Adipose stem cell isolation and cell expansion

The hASCs were obtained from subcutaneous adipose tissue of six healthy female donors of 52  $\pm$  5 years in surgeries at the Tampere University Hospital Department of Plastic Surgery between 2014 and 2015 with the patients' written informed consent, in accordance with the Ethics Committee of the Pirkanmaa Hospital District's, Tampere, Finland, ethical approval (R15161). The hASCs were isolated as reported previously [22]. Briefly, the adipose tissue was cut up and tissue was digested by collagenase type I (1.5 mg/mL; Thermo Fisher Scientific) in maintenance medium containing DMEM/F-12 1:1 (Thermo Fisher Scientific), 5% human serum (Biowest, Nuaille, France), 1% L-glutamine (GlutaMAX; Thermo Fisher Scientific), and 1% P/S. The cells were expanded in maintenance medium. Flow cytometry analysis was performed, and the overall results of the cell surface marker flow

cytometry analysis (see Supplementary file 1) indicated the mesenchymal origin of the cells in accordance with literature [3,23,24]. The isolated hASCs were tested and reported negative for mycoplasma contamination.

#### 2.4. Osteogenic induction and cell culture

Osteogenic induction was initiated immediately after plating by adding 0.3 cm<sup>3</sup> either OM optimized for hASC osteogenic differentiation [22] or BaG OM to the hydrogel encapsulated cell constructs. The cells were plated at a density of 950,000 cells/cm<sup>3</sup>, encapsulated in respective hydrogels which were cast in 48-well plate wells (Nunclon; Sigma-Aldrich) in a volume of 0.2 cm<sup>3</sup>. The BaG ext was prepared as reported previously from bioactive glass 2-06 (wt-%: Na<sub>2</sub>O 12.1; K<sub>2</sub>O 14.0; CaO 19.8; P<sub>2</sub>O<sub>5</sub> 2.5; B<sub>2</sub>O<sub>3</sub> 1.6; SiO<sub>2</sub> 50.0) [13]. Briefly, 87.5 mg/mL of BaG granules (500–1000 μm) of bioactive glass 2-06 were disinfected with 70% ethanol washes for 10 min repeated twice and air dried in RT for 2 h followed by incubation for 24 h at +37 °C to dissolve ions into the maintenance medium without human serum. After incubation, 5% human serum (Biowest) was added to the sterile filtered (0.2 μm) BaG ext. The BaG ext was prepared fresh each 14 days to avoid any risk of precipitates. For the Raman spectroscopy analyses, the cells were cultured in phenol red free media to avoid fluorescence interference with the Raman spectra [13]. The control cell cultures were maintained in OM. Different media compositions are listed in Table 1. During the experiments, medium was changed every other day. The experiments were carried out at hASC passage 3–6.

MM, maintenance medium; OM, osteogenic medium; BaG OM, bioactive glass extract osteogenic medium; HS, human serum (Biowest); P/S, 100 U/mL penicillin/streptomycin (Lonza); Dex, dexamethasone (Sigma-Aldrich); AsA2P, L-ascorbic acid 2-phosphate (Sigma-Aldrich); β-GP, beta-glycerophosphate (Sigma-Aldrich); L-glutamine (Thermo Fisher Scientific).

#### 2.5. Cell viability and cell number

Cell viability was analyzed with Live/Dead fluorescence staining (Thermo Fisher Scientific) at 3 and 14 days, as described previously [25]. The living cells were stained with 0.5 mM calcein acetoxyethyl ester (green stain) and necrotic cells were stained with 0.25 mM ethidium homodimer-1 (red stain) for 45 min in RT. The samples were imaged using an epifluorescence Olympus IX51 microscope and Olympus DP30BW digital camera (Olympus, Tokyo, Japan).

Cell number was measured based on the total amount of DNA with CyQUANT Cell Proliferation Assay Kit (Thermo Fisher Scientific) according to the manufacturer's protocol at 14 and 21 days. Briefly, the cells were lysed with 0.1% Triton X-100 buffer (Sigma-Aldrich) and the hydrogel samples were homogenized mechanically by the Ultra-Turrax tissue homogenizer (IKA Labortechnik, Staufen, Germany). The lysed samples were stored at –80 °C until analysis after a freeze-thaw cycle. A working solution was prepared with the kit provided CyQUANT GR dye and Cell lysis buffer. Fluorescence of 3 parallel samples was measured at 480/520 nm with Victor 1420 Multilabel Counter microplate reader (PerkinElmer, Waltham, MA, USA).

#### 2.6. Immunocytochemical analysis

For the immunocytochemical analysis, the hydrogel samples with encapsulated cells were fixed with 4% paraformaldehyde (PFA; Sigma-Aldrich). The cells were permeabilized with 0.1% Triton X-100 buffer (Sigma-Aldrich) in blocking solution of 10% normal donkey serum (Sigma-Aldrich) and 1% bovine serum albumin (Sigma-Aldrich) for 1 h in RT. After washes with solution of 0.1% Triton X-100 buffer, 1% normal donkey serum, and 1% bovine serum albumin, the hydrogel embedded cells were incubated with a mouse monoclonal anti-osteocalcin antibody (OCG3; dilution 1:100) detecting human osteocalcin (OC; Abcam, Cambridge, United Kingdom) for 72 h at +4 °C [17]. Highly cross-adsorbed donkey anti-mouse IgG Alexa Fluor 488 secondary antibody (dilution 1:400; Thermo Fisher Scientific) was used for overnight staining at +4 °C, and the cell nuclei were stained with 4',6-diamidino-2-phenylindole (DAPI; dilution 1:2000; Sigma-Aldrich). The samples were imaged using an epifluorescence Olympus IX51 microscope and Olympus DP30BW digital camera (Olympus). OC stained in cyan-green was imaged at 488 nm and cell nuclei stained in blue color by DAPI were detected at 361 nm.

#### 2.7. Mineralization

For the hASC mineralization assay, the hASC secreted hydroxyapatite residues of the cell matrix in 3D hydrogel were stained with the Osteolmage assay according to manufacturer's protocol (Osteolmage Mineralization Assay; Lonza) at 21 days [26]. Briefly, the cells were fixed with 4% PFA (Sigma-Aldrich) for 30 min in RT and the hydroxyapatite residues were stained with the Osteolmage Staining Reagent for 45 min and immediately measured at 490/535 nm with Victor 1420 Multilabel Counter microplate reader (PerkinElmer). After quantitative measurement, the cell nuclei were stained with DAPI (dilution 1:2000) and detected at 361 nm together with the stained hydroxyapatite residues imaged at 492/520 nm with an epifluorescence Olympus IX51 microscope and Olympus DP30BW digital camera (Olympus).

#### 2.8. Quantitative real-time polymerase chain reaction

Quantitative real-time polymerase chain reaction (qRT-PCR) method was applied to analyze the relative expression of osteogenic marker genes. Total sample RNA from 2 parallel samples was isolated at 7 and 14 days with the NucleoSpin RNA II kit (Macherey-Nagel, Düren, Germany) according to the kit protocol. High-Capacity cDNA Reverse Transcriptase Kit (Applied Biosystems, Foster City, CA, USA) was used to synthesize first strand complementary DNA (cDNA) of the total RNA. The gene expression of human intestinal *alkaline phosphatase* (*ALPL*), *runt related transcription factor 2* (*RUNX2*), *distal-less homeobox 5* (*DLX5*), and *osterix* (*OSX*) was measured. A mathematical data analysis model was applied to calculate the relative gene expression of each sample in relation to a housekeeping gene human *ribosomal protein lateral stalk subunit P0* (*RPLP0*) [27]. The measured gene expression data was normalized to that of *RPLP0* [28,29]. The mixture for qRT-PCR analysis consisted of 50 ng cDNA, 300 nM forward and reverse primers, and SYBR Green PCR Master Mix (Applied Biosystems). The primer sequences and accession numbers are listed in Table 2. All primers were

**Table 1**  
Composition of media.

Medium	Composition
Maintenance medium (MM)	DMEM/F-12 1:1, 5% HS, 1% L-glutamine, 1% P/S
Osteogenic medium (OM)	5 nM Dex, 250 μM AsA2P, 10 nM β-GP in MM
BaG osteogenic medium (BaG OM)	OM in BaG ext base
Raman spectroscopy cell culture medium	Phenol red free DMEM/F-12 1:1 including L-glutamine, 5% HS, 1% P/S
Raman spectroscopy phenol red free BaG OM	OM in phenol red free BaG ext base

**Table 2**  
The primer sequences for qRT-PCR.

Name	Primer	5'-Sequence-3'	Product size (bp)	Accession number
RPLP0	Fwd	AATCTCCAGGGGCCACATT	70	NM_001002
	Rev	CGGTGGCTCCCACTTTGT		
ALPL	Fwd	CCCCGTGGAACTCTATCT	73	NM_000478.5
	Rev	GATGGCAGTGAAGGGCTTCTT		
RUNX2	Fwd	CTTCATTGCGCTCACAAACAAC	62	NM_001024630.3
	Rev	TCTCTCTGGAGAAAGTTTGCA		
DLX5	Fwd	ACCATCCGTCTCAGGAATCG	75	NM_005221.5
	Rev	CCCCGTAGGGCTGTAGTAGT		
OSX	Fwd	TGAGCTGGAGCGTCATGTG	79	NM_152860.1
	Rev	TCGGTAAAGCGCTTGGGA		

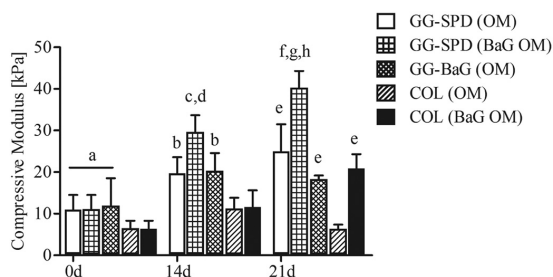


**Fig. 1.** Compressive moduli. Cell-free GG-SPD, GG-BaG, and COL hydrogels after 0-day, 14-day, and 21-day incubation in OM and BaG OM media, where GG-BaG in OM only ( $n = 3-6$ ). Data are presented as mean + SD. Significant difference with  $p < 0.05$ . a Significant difference from COL hydrogel samples at 0 days; b Significant difference from COL (OM) at 14 days; c Significant difference from GG-SPD (OM) at 14 days; d Significant difference from GG-BaG (OM) at 14 days; e Significant difference from COL (OM) at 21 days; f Significant difference from GG-SPD (OM) at 21 days; g Significant difference from GG-BaG (OM) at 21 days; h Significant difference from COL (BaG OM) at 21 days.

purchased from Oligomer (Helsinki, Finland). The ABI PRISM 7300 Sequence Detection System (Applied Biosystems) was used for the qRT-PCR initial reactions at +95 °C for 10 min enzyme activation, and followed by 45 cycles at +95 °C for 15 s denaturation, and 60 s annealing and extension at +60 °C.

### 2.9. Optical projection tomography and selective plane illumination microscopy

In-house-built SPIM and OPT multimodal 3D imaging systems were used to image hASCs encapsulated in the transparent GG-SPD hydrogels [20,21], whereas the opacity of the COL hydrogel prevented its imaging. The structure and distribution of the hASCs and their ECM in the 3D hydrogel was obtained with the brightfield OPT, and 3D fluorescence signal of the OsteoImage (Lonza) stained hydroxyapatite residues was captured with the SPIM. The hydrogel-cell samples cultured initially in 1.0-cm inside diameter fluorinated ethylene propylene (FEP; Adtech Polymer Engineering, Stroud, United Kingdom) tubes were punctured with 1.0-mm inside diameter FEP tubes to insert the cell-laden hydrogels into the smaller tubes for imaging. For the brightfield OPT imaging of the samples, a white light LED source (LTCL23; Opto Engineering, Mantova, Italy) was used to illuminate the sample in transmission mode without any contrasting agents. A total of 400 projection images were captured with 0.9°-degree intervals using a 20× water-immersed objective while rotating the sample 360° degrees. The 3D images of hASCs and ECM were reconstructed using filtered back projection algorithm (Matlab; MathWorks, Natick, MA, USA) [19]. The brightfield OPT imaged a smaller cylindrical volume ( $d = 0.67$  mm,  $h = 0.67$  mm) within a larger cylindrical volume

( $d = 1$  mm,  $h =$  sample height) inside the spatial area of the 1.0-mm diameter FEP tube whereas the fluorescence SPIM imaged a larger rectangular volume ( $x = 0.67$  mm,  $y = 0.67$  mm,  $z = 1$  mm) due to differences in technical imaging modalities.

For the SPIM fluorescence imaging, the cell-laden GG hydrogels inside the 1.0-cm inside diameter FEP tube were fixed with 4% PFA (Sigma-Aldrich) for 1 h and the hydroxyapatite residues were stained for 90 min in RT to allow stain diffusion throughout the hydrogel volume (OsteoImage Mineralization Assay, Lonza). The SPIM illumination light sheet at 488 nm wavelength (Custom multi-wavelength laser system, Modulight, Tampere, Finland) was used to excite sample fluorescence. In the detection path, notch filter (NF03-405/488/561/635E-25 StopLine Quad-Notch filter; Semrock, Rochester, NY, USA) was used to cut out the excitation light from the fluorescent signal emitted by mineralized residues. The fluorescence image stack was acquired by translating the sample in the axial direction of the detection path and capturing an image every 3 μm with a x20 objective. The image stack was acquired in z direction while x and y directions formed the actual image. Both OPT and SPIM images were visualized in 3D using Avizo 9.3 (FEI Visualization Sciences Group; Thermo Fisher Scientific).

### 2.10. Raman spectroscopy

The inorganic phosphate  $\text{PO}_4^{3-}$  containing hydroxyapatite mineral residues of the hASC-secreted cell matrix in different hydrogels were analyzed semi-quantitatively by Raman spectroscopic methods [30]. In the preliminary experiments, we verified that the Raman spectra of the mineralized hASC matrix in 3D hydrogels in the BaG OM condition and that of added pure hydroxyapatite powder (0.5 or 2.5 mg/mL) acellular hydrogels were identical in terms of observed Raman shift at  $960 \text{ cm}^{-1}$  (see Supplementary file 2). For the Raman experiments, hASCs from 1 donor, and GG-SPD, GG-BaG, and COL cell-laden and parallel cell-free samples in a phenol red free BaG OM condition were analyzed at 21 days avoiding interference of phenol red fluorescence to Raman spectra. The OM condition was omitted from analysis due to COL hydrogel contraction and the low detection of the GG-SPD mineralized matrix in OM. The Raman spectroscopy was conducted as described in [30] and prior to analysis, the cell-hydrogel samples were washed with  $1 \times$  PBS. Briefly, the Raman scattering was generated with a fiber coupled pulsed laser (532 nm, 150 ps, 40–100 kHz) (TimeGate Instruments, Oulu, Finland). The spectra were collected from a single location by averaging Raman signal from 2.1 million laser pulses produced in 47 s. The reference spectra of cell-free samples measured in identical conditions were subtracted from the measured data. The obtained spectra for each sample were normalized to average intensity between 475 and  $560 \text{ cm}^{-1}$ .

### 2.11. Statistical methods

The significance of differences between mean ranks for equal



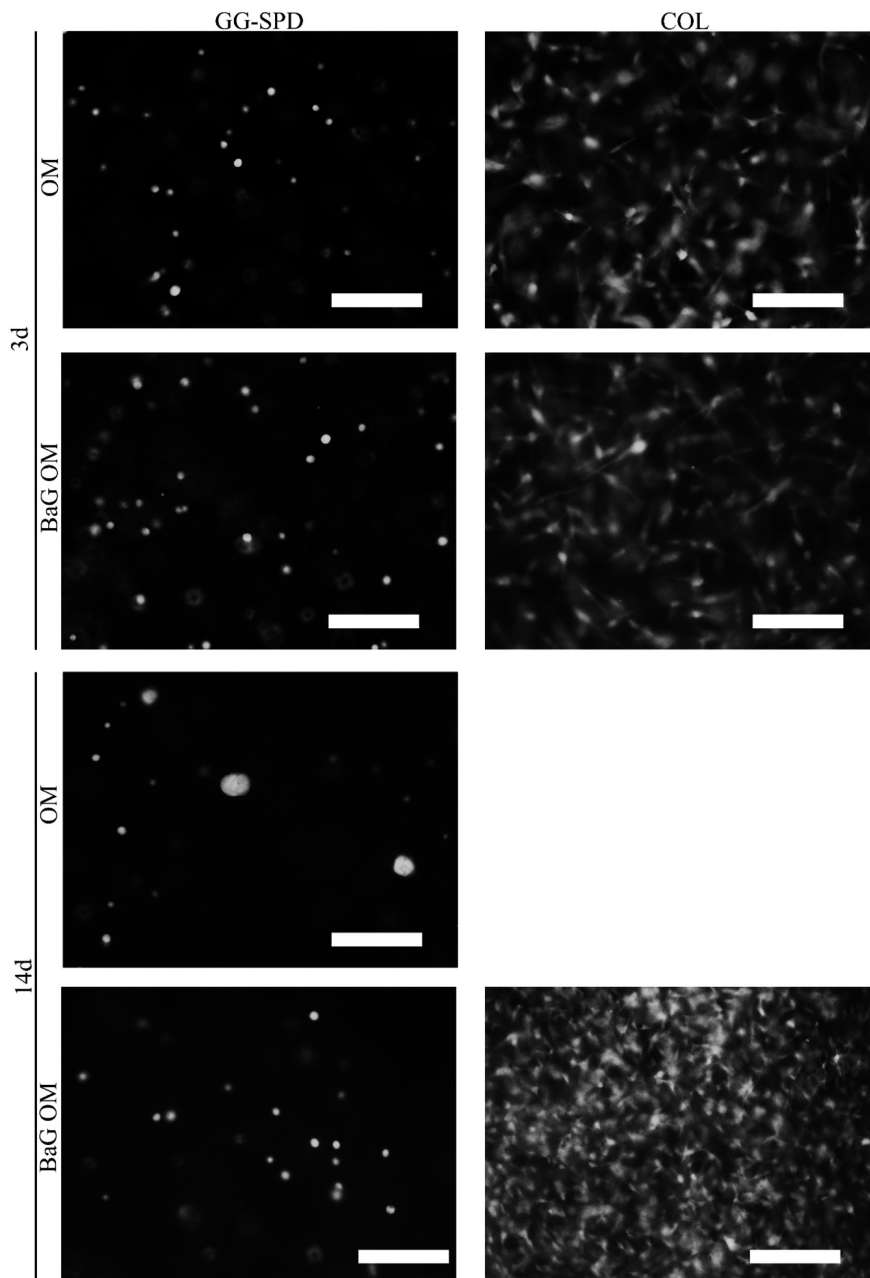


**Fig. 2.** Cell viability. Viability of hASCs encapsulated in GG-SPD (OM), GG-SPD (BaG OM), COL (OM) and COL (BaG OM) 3D hydrogels at 3 and 14 days. The COL (OM) samples contracted after 3 days. Representative images with hASCs from 1 donor ( $n = 1$ ). Scale bar 200  $\mu\text{m}$ .

distributions was determined using Mann-Whitney  $U$  Test for statistical significance with  $p$ -values  $< 0.05$ . For the mechanical testing results, 3–6 parallel samples were tested in each experiment group ( $n = 3$ –6). The cell number analyses were repeated with 3 different hASC donors with 3 parallel samples for each condition ( $n = 9$ ). The gene expression analyses were repeated for 3 different donors with 2 parallel samples

for each condition ( $n = 6$ ). The mineralization assay was conducted with hASCs from 3 donors with 1–2 parallel samples for the GG-SPD in OM and BaG OM groups ( $n = 5$ ), whereas for COL in BaG OM, hASCs from only 2 donors were tested with 2 parallel samples ( $n = 4$ ) due to contracted gels. All the COL in OM hydrogel mineralization samples were contracted after 3 days of culture, and therefore, unavailable for

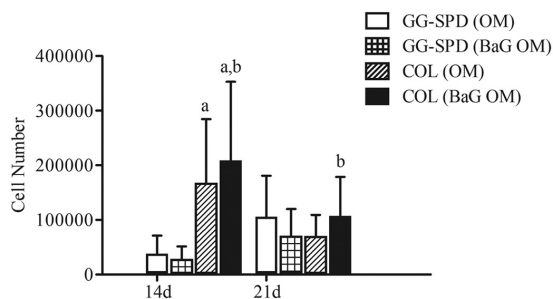


**Fig. 3.** Cell number. Cell number based on total DNA content of hASCs encapsulated in 3D hydrogels at 14 and 21 days. The analyzed hASCs were from 3 donors ( $n = 9$ ). Data are presented as mean + SD. Significant difference with  $p < 0.05$ . a The combined COL (OM) and COL (BaG OM) cell numbers are significantly higher compared to the combined GG-SPD (OM) and GG-SPD (BaG OM) cell numbers at 14 days; b The combined 14- and 21-day COL (BaG OM) cell numbers are significantly higher compared to the combined 14- and 21-day GG-SPD (BaG OM) cell numbers.

mineralization quantification analysis at 21 days. The data was analyzed with IBM SPSS Statistics 23 software (IBM, Armonk, NY, USA).

### 3. Results

#### 3.1. Mechanical properties of hydrogels improved by serum-containing media incubation

The acellular GG-SPD and COL hydrogel samples in OM and BaG OM media, and GG-BaG in OM alone, were mechanically tested by compression testing at 0, 14, and 21 days of incubation (Fig. 1).

The measured compressive moduli of acellular GG-SPD hydrogels with both the OM and BaG OM incubation and those of GG-BaG with the OM incubation increased, indicating additional ionic crosslinking. At day 0, the compressive moduli of all the GG samples without medium incubation were statistically significantly higher than those for the COL hydrogel samples. The OM condition increased the moduli of all hydrogels in the beginning, however, only GG-SPD moduli continued to increase in OM after the 14-day time point. Furthermore, the modulus of GG-SPD was significantly higher than that of GG-BaG in OM although the modulus of GG-BaG with the OM incubation was significantly higher compared to COL in OM at both 14- and 21-day time points. Indeed, the BaG OM incubation alone increased COL compressive modulus significantly at 21 days. Additionally, at 21 days, the GG-SPD (BaG OM) samples had the highest compressive moduli measured at approximately 40.0 kPa and significantly higher compared to GG-SPD (OM) and COL (BaG OM). For both GG-SPD and COL hydrogels, the BaG OM condition had significantly higher compressive modulus compared to the OM condition at the 21-day time point. Overall, the COL as well as GG-BaG samples showed ductile behavior and plastic deformation properties without a fracture point, whereas by default, the GG-SPD samples had higher resistance to deformation and more brittle behavior which indicated a stiffer structure, and also had a clear fracture point in the stress-strain curve (See Supplementary file 3).

#### 3.2. Adipose stem cell viability maintained and cell number increased in 3D hydrogels

The viability of hASCs was analyzed at 3 and 14 days of 3D hydrogel culture (Fig. 2, see Supplementary file 4). The cells remained well viable during culture. The COL (OM) samples contracted after 4 days and were therefore unavailable for a later time point.

The cell number based on total DNA content was analyzed at 14- and 21-day time points (Fig. 3).

The cell number increased the most for the BaG OM cultured samples with the significantly highest cell number for the COL (BaG OM) at 14 days. Also, at 14 days, the COL hydrogels in OM and BaG OM combined together had a significantly higher cell number compared to the combined GG-SPD hydrogels in OM and BaG OM. Further, the combined cell number results at 14 and 21 days of the COL (BaG OM) condition showed a significantly higher cell number compared to the combined 14- and 21-day GG-SPD (BaG OM) cell numbers.

#### 3.3. Higher expression of osteogenic marker genes of adipose stem cells in collagen type I hydrogel scaffolds

The gene expression of osteogenic marker genes was analyzed by qRT-PCR at 14 and 21 days (Fig. 4).

All the osteogenic marker genes were statistically significantly higher in gene expression in COL in OM or in BaG OM compared to GG-SPD at 3 weeks, excluding *ALPL* expression. Due to the non-Gaussian distribution, the statistical analyses of the gene expression medians was conducted with the Mann-Whitney test. The *DLX5* expression was significantly higher for the COL (BaG OM) compared to GG-SPD (OM) at 21 days. The *OSX* expression was significantly higher for the combined COL (BaG OM) results at 14 and 21 days compared to the combined results for GG-SPD (OM) at 14 and 21 days. The gene expression of *RUNX2* of the combined COL in OM and BaG OM samples at 21 days was statistically significantly higher than that of the combined GG-SPD samples in OM and BaG OM at the 21-day time point.

#### 3.4. Strong immunocytochemical osteocalcin staining of adipose stem cells in collagen type I hydrogel scaffolds

Immunocytochemical staining results of OC and DAPI stained hASCs encapsulated in GG and COL hydrogels in different media conditions at 21 days are shown in Fig. 5 (see Supplementary file 5).

Strong OC immunofluorescence staining was detected in the COL samples in both media conditions, although some OC staining in GG-SPD was visible.

#### 3.5. Efficient mineralization of adipose stem cells in 3D hydrogel scaffolds

The hASC secreted mineralized matrix of hydroxyapatite residues were stained with the OsteoImage assay and hASC nuclei with DAPI and imaged in 3D hydrogels at 21 days (Fig. 6A). The hydroxyapatite content was also quantified with the OsteoImage assay analysis (Fig. 6B).

The OsteoImage stained hydroxyapatite residue imaging supported the quantified mineralization results with the strongest hydroxyapatite staining for the COL (BaG OM), while also strong staining was seen in the GG-SPD (BaG OM) condition, and where moderate staining was visible in the GG-SPD (OM) at the 21-day time point.

#### 3.6. Optical projection tomography and selective plane illumination microscopy for high resolution 3D hydrogel scaffold imaging

OPT and SPIM images were acquired for brightfield transmission and fluorescence emission modes, respectively (Fig. 7). Optical opacity of the COL hydrogel prevented its OPT and SPIM imaging.

For the brightfield OPT 3D reconstructed images, the variation in light attenuation between the cells and the hydrogel structure allowed to visualize the distribution of the cells in each projection image (Fig. 7A; C; see Supplementary files 9, 10; 3D reconstruction videos). The cells and the surrounding shaded mineralized ECM were visible in transmission mode brightfield images, and thus offered proof of concept that label-free OPT can be applied to 3D hydrogel cell culture mineralization studies. The 3D stack of multi-focal fluorescence SPIM imaging showed the fluorescent-labeled mineralization clearly with strong hydroxyapatite stain in the GG-SPD (BaG OM) sample (Fig. 7B, D; see Supplementary files 11, 12; 3D reconstruction videos) whereas the

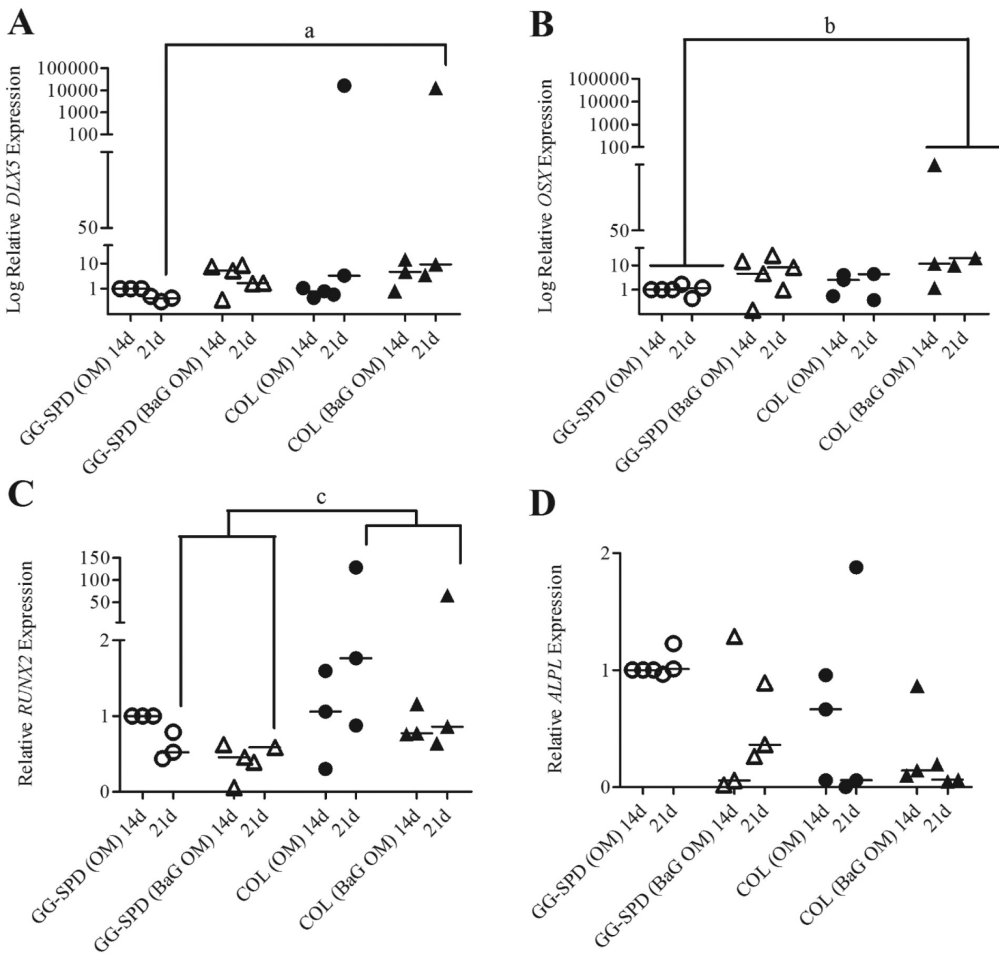


**Fig. 4.** Gene expression. Gene expression of osteogenic marker genes of hASCs in GG-SPD (OM), GG-SPD (BaG OM), COL (OM), and COL (BaG OM) 3D hydrogels at 14 and 21 days. Significant difference with  $p < 0.05$ . (A) *DLX5* gene expression significantly higher in a COL (BaG OM) compared to GG-SPD (OM) at 21 days; (B) *OSX* gene expression significantly higher for b the combined COL (OM) and COL (BaG OM) sample expression at 14 and 21 days compared to the combined GG-SPD (OM) and GG-SPD (BaG OM) sample expression at 14 and 21 days; (C) *RUNX2* gene expression significantly higher for c the combined COL (OM) and COL (BaG OM) sample expression at 21 days compared to the combined GG-SPD (OM) and GG-SPD (BaG OM) sample expression at 21 days; (D) *ALPL* gene expression. The results were relativised to the control condition of GG-SPD (OM) at 14 days. The relative expression of *DLX5* and *OSX* had high variance and are presented partly in Log(10) scale. The hASCs were isolated from 3 donors ( $n = 6$ ). Group medians are indicated with a horizontal line.

fluorescent-stained hydroxyapatite was scarce in the OM condition (see Supplementary files 13, 14; 3D reconstruction video). Any closer inspection of cell morphology was restricted by the optically dense mineralization.

**3.7. Raman spectroscopic analysis verified mineralized hydroxyapatite residues and gellan gum mineralization improved with bioactive glass extract ionic crosslinking**

The Raman spectra of hASCs in GG-SPD (BaG OM), GG-BaG (BaG OM) and COL (BaG OM) were measured at 21 days (Fig. 8).

The measured Raman spectra showed the detected phosphate peak at Raman shift  $960\text{ cm}^{-1}$  indicating semi-quantitatively hydroxyapatite residue content for all the measured samples with the highest result for the COL (BaG OM) sample which confirmed the quantified OsteoImage mineralization as well as the imaged hydroxyapatite staining results

(Fig. 6). Additionally, Fig. 9 presents measured fluorescence of the hydroxyapatite residues in GG-SPD (OM) and GG-BaG (OM) samples at 3 weeks (see Supplementary file 6 for crosslinker comparison results on cell viability; Supplementary file 7 for crosslinker comparison cell number results; Supplementary file 8 for crosslinker comparison hydroxyapatite mineralization imaging results).

The slightly higher semi-quantitative phosphate peak detected at Raman shift  $960\text{ cm}^{-1}$  for the GG-BaG (BaG OM) (Fig. 8) followed a similar trend to the measured significantly higher hydroxyapatite content for the GG-BaG (OM) compared to GG-SPD (OM) at 3 weeks (Fig. 9).

**4. Discussion**

Presently, efficient bone grafts are urgently called for, and in order to help answer this demand, we studied a novel bone tissue engineering

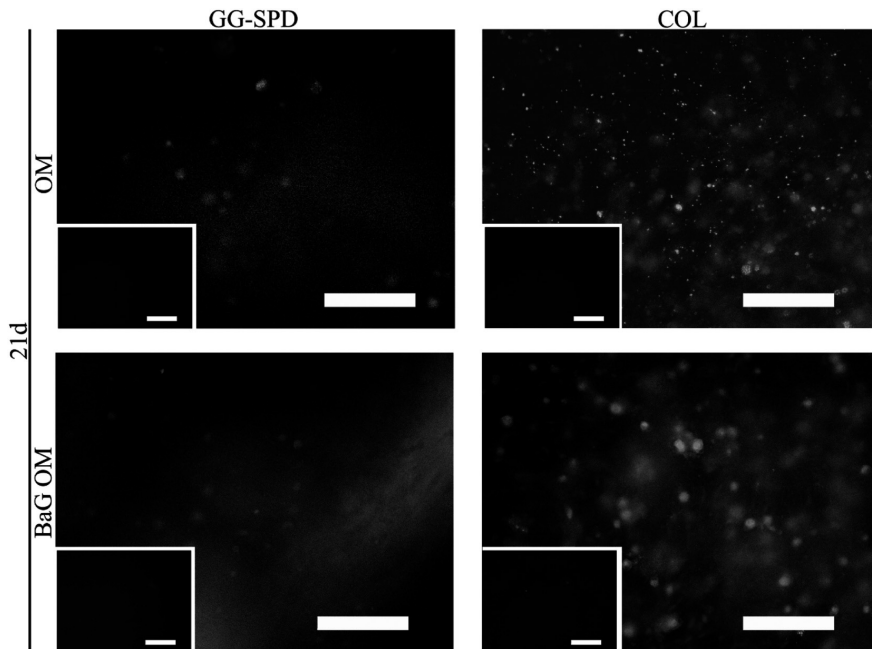


Fig. 5. Osteocalcin immunofluorescence staining. Representative images of osteocalcin and DAPI stained hASCs in GG-SPD (OM), GG-SPD (BaG OM), COL (OM), and COL (BaG OM) 3D hydrogels at 21 days. The blank controls are shown in lower left corner. The hASCs were isolated from 2 donors ( $n = 2$ ). Scale bar 200  $\mu\text{m}$ .

approach with BaG OM induction of hASCs embedded in GG and COL 3D hydrogels. The BaG OM induction of hASCs has been found promising for bone applications and to support rapid hASC osteogenic differentiation already in our previous work [13]. In the present study, we hypothesized that the BaG OM could induce hASCs osteogenesis in 3D when embedded into GG and COL hydrogels together with gradually evolving hydrogel mechanical properties, and thus yield a sufficiently stiff, while also flexible and osteoinductive matrix mimicking bone organic and inorganic phase composite structure [31,32] for the development of engineered bone constructs. Also, injectable hydrogels are especially attractive biomaterials due to their malleability as bone defects are typically of varied dimensions [15]. To ensure hydrogel construct suitability for bone applications, the mechanical properties of GG-SPD, GG-BaG, and COL hydrogels were analyzed with compression testing. Our results for non-incubated GG and COL hydrogel moduli were supported by previous reports [33,34]. The softer COL and GG-BaG hydrogel scaffolds followed a similar trend in the OM with a seeming improvement of mechanical properties up to 14 days, and then degrading at 21 days. Interestingly, the GG-BaG hydrogel resulted in a weaker gel compared to the GG-SPD in OM, albeit the GG-BaG hydrogels were stable and showed sufficient mechanical properties and a modulus comparable to COL hydrogel in BaG OM at 3 weeks. The relatively weak mechanical properties of GG and the lack of COL stability have limited their potential for hard tissue applications [6,16]. However, we demonstrated significantly improved mechanical properties for both GG-SPD and COL hydrogels with the BaG OM incubation. Indeed, the GG-SPD (BaG OM) samples had the highest compressive modulus measured at 40 kPa, and therefore, potential for bone-like graft development when compared to the approximated 30 kPa modulus required for an osteoblastic matrix [4,35–37]. Even though these mechanical properties would be sufficient in small bone cavities to support the development of an osteoblastic matrix, in load-bearing bone defects a scaffold for additional stabilization would be required. Significantly, also COL hydrogel mechanical properties were gradually

reinforced with the BaG OM incubation. Although a similar strengthening by added BaG particles in GG and COL hydrogels has been reported [4,16], we significantly improved hydrogel scaffold mechanical properties with ionic BaG dissolution products alone. Importantly, the gradual hydrogel stiffening in BaG OM incubation might mimic the evolving bone matrix mechanical properties of natural bone formation process [31,36–38].

We tested 3D hydrogel culture cytocompatibility, and the hydrogel encapsulated hASCs were mostly alive at 14 days, as expected since the GG-SPD cell-hydrogel constructs have shown previously good cytocompatibility in 3D culture with human pluripotent stem cell-derived neuronal cells [17]. Moreover, the observed rounded morphology of hASCs embedded in GG-SPD in both OM and BaG OM was expected and suggested lack of adhesion sites, since GG hydrogel encapsulated human cells have been found to require functionalization also in other studies [17,39]. Interestingly, rounded cell morphology could be irrelevant regarding hASC capacity for osteogenic differentiation encapsulated in GG [6,37]. Conversely, in COL efficient cell adhesion was seen not only in the spreading of the hASCs embedded in COL hydrogel, but also in the strong tendency of the cells to pull on the matrix and make the COL samples contract in the OM condition. This issue has been reported in various studies [7,16,33,40], however, importantly for novelty, we showed that the BaG OM incubation significantly improved the COL mechanical stability and rendered the COL hydrogel scaffolds more resistant to cell-induced contraction. We also detected a decrease in the cell number from 14 to 21 days in the COL hydrogels in parallel with enhanced osteogenic differentiation, similarly to a previously reported 2D study in our group [13], whereas there was a small albeit nonsignificant increase in cell number in the GG-SPD hydrogels between day 14 and 21.

According to our initial hypothesis of strong osteogenic induction of hASCs with BaG ionic species, we saw that the hASC osteogenic marker gene expression results of *DLX5* and *OSX* were significantly higher in COL (BaG OM) hydrogels, although the gene expression medians were

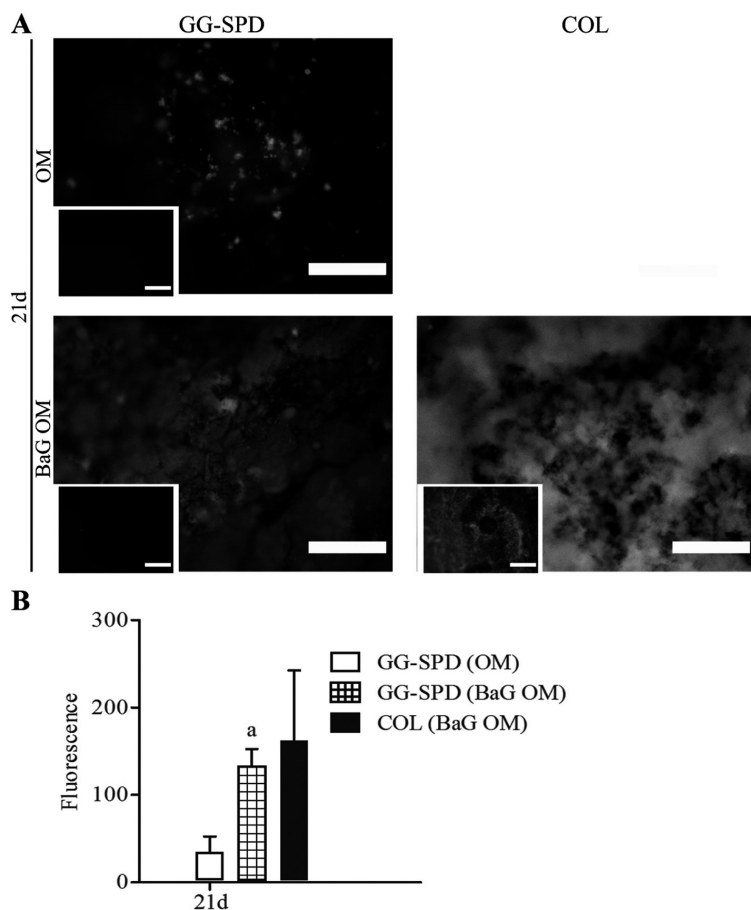


**Fig. 6.** Mineralization. (A) Representative images of hydroxyapatite residues and cell nuclei of hASCs stained with the OsteoImage assay and DAPI in 3D hydrogels at 21 days in GG-SPD (OM), GG-SPD (BaG OM), and COL (BaG OM). The COL (OM) samples are presented in the lower left corner. The hASCs were contracted before 21 days. The blank controls are presented in the lower left corner. Scale bar 200  $\mu\text{m}$ ; (B) The measured OsteoImage hydroxyapatite mineralization fluorescence count of hASCs in 3D hydrogel at 21 days. Data are presented as mean + SD. A significant difference from GG-SPD (OM) with  $p < 0.05$ . The hASCs were isolated from 3 donors and 2 parallel samples of each condition were tested, out of which for GG-SPD (OM) and (BaG OM) groups a total of 5 samples ( $n = 5$ ), and for COL (BaG OM) 4 samples ( $n = 4$ ) were available for analysis at 21-day time point.

also elevated in the GG-SPD (BaG OM) condition. This showed the effect of the BaG OM incubation with additional synergistic support of the 3D COL hydrogel matrix for hASC osteogenesis. Similarly to the current results, the bioactive glass 2-06 based BaG OM has been previously reported to increase hASC gene expression of *RUNX2* [13]. Moreover, the gene expression of *RUNX2* was more strongly enhanced in the control condition of OM for COL hydrogel samples which attested further of the COL 3D hydrogel support for efficient hASC osteogenic differentiation. Instead, no visible trend was discernible in gene expression of early bone marker *ALPL*, however, the bioactive glass 2-06 based BaG OM has been shown to promote efficacious hASC mineralization despite low alkaline phosphatase activity [13]. Indeed, low gene expression of *ALPL* might be due to the more advanced state of mineralization. Also, the mineralization results attested of robust hASC osteogenesis with the strong hydroxyapatite residue accumulation in the hASC-secreted matrix with BaG OM in both the GG and COL hydrogels. Importantly, the clear peak of inorganic phosphate containing hydroxyapatite mineral residues visible in the Raman spectra attested of considerable mineralized cell matrix accumulation. The Raman spectroscopic results verified the hASC osteogenic activity and hydroxyapatite accumulation in the cell-secreted mineralized ECM, also seen in the OsteoImage mineralization results. Furthermore, the semi-quantitative Raman spectra attested similar succession of samples as the mineralization assay in the BaG OM condition, where COL had the

highest hydroxyapatite content, followed by GG-BaG and the lesser amount detected for hASCs in the GG-SPD hydrogel samples. However, the non-homogenous character of the cell-secreted mineralized matrix might have interfered with the semi-quantitative Raman measurement results. The 3D reconstructed OPT and stacked fluorescence SPIM images showed homogeneously deposited hydroxyapatite surrounding or in close proximity to hydrogel encapsulated hASCs approximating ECM growth. The cell distribution was similar by visual inspection in both conditions as seen in the brightfield OPT 3D reconstructed images, however, the fluorescence SPIM images showed a stronger mineral deposition of the hASC secreted matrix in the BaG OM condition compared to OM. These 3D reconstructed images supported further the measured OsteoImage results where hydroxyapatite fluorescence count was significantly higher for the hASC-laden GG-SPD (BaG OM) samples compared to OM at 3 weeks. Our results demonstrated the attractiveness and efficacy of high resolution OPT and SPIM imaging techniques for 3D mesoscopic imaging of transparent wet-state cell-laden hydrogel samples with a refractive index close to water providing a real 3D image of the sample while avoiding issues of photobleaching or low spatial resolution of conventional fluorescence microscopy. While OPT has been applied for high resolution ( $< 1 \mu\text{m}$ ) imaging of optically transparent small animal embryos in developmental biology [41–44], our in-house built OPT system has also been employed to assess hydrogel macrostructure [19] as well as 3D cell cultures [21]. Additionally,

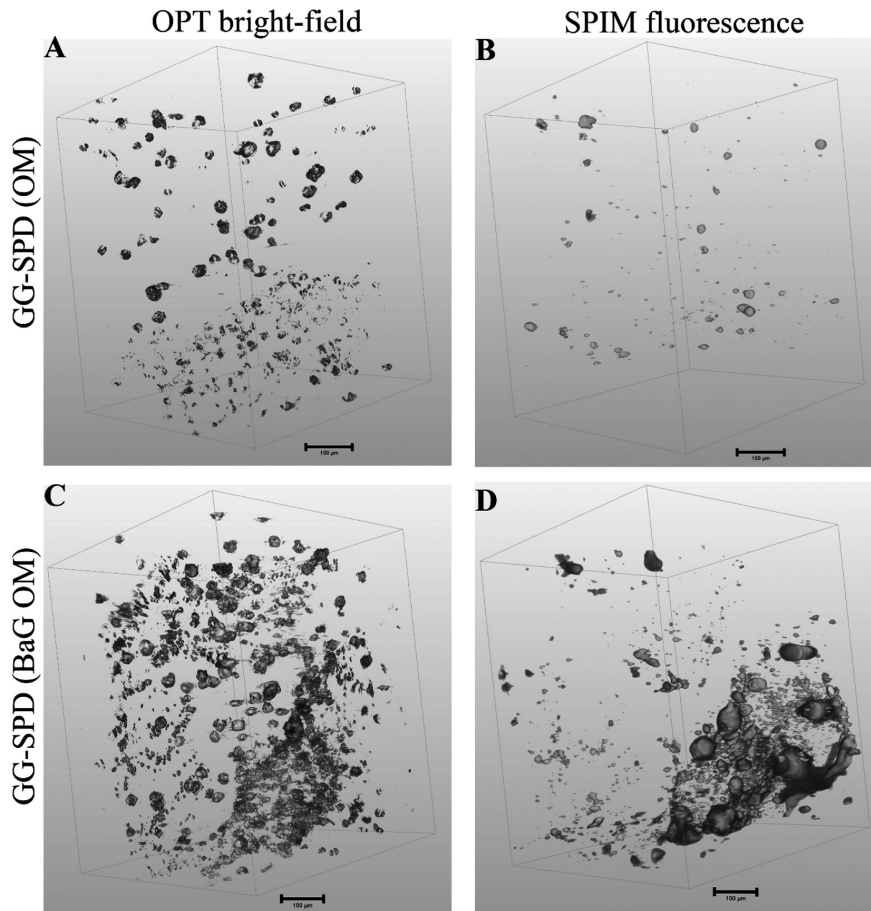
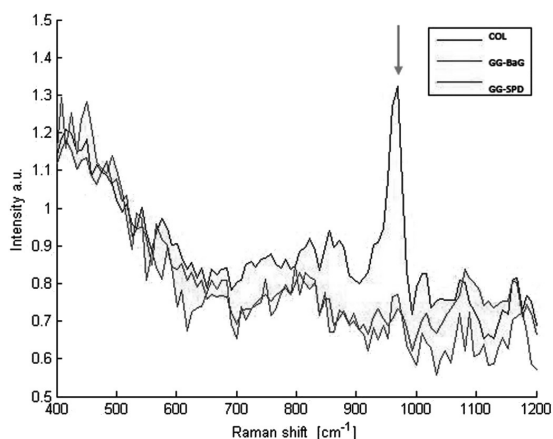


Fig. 7. OPT and SPIM 3D imaging of hASC-hydrogel constructs. Representative label-free brightfield OPT 3D reconstructed images of hASCs encapsulated in (A) GG-SPD (OM); (C) GG-SPD (BaG OM); and OsteoImage hydroxyapatite stained fluorescence SPIM 3D images of hASCs in 3D hydrogels in (B) GG-SPD (OM); (D) GG-SPD (BaG OM) at 21 days. The hASCs were isolated from 1 donor ( $n = 1$ ). Scale bar 100  $\mu\text{m}$ .

brightfield OPT allowed to inspect the general aspect of the mineral depositions together with the cells, however, the signal was label-free and therefore non-specific. Nonetheless, the brightfield OPT imaging showed potential for a label-free mineralization imaging technique for future studies. What is more, these techniques permitted the 3D imaging of cells in an unaltered hydrogel microstructure in a wet-state. Importantly, the SPIM and also the label-free OPT imaging allowed to study the cell and mineralized matrix distribution spanning the whole 3D volume and thus avoiding the mere surface effect of hydrogel mineralization where an apatite layer has been deposited on top of the incubated hydrogel samples [45]. Indeed, the BaG ability to cause hydroxyapatite precipitation in 3D hydrogel culture with embedded cells in the presence of biological fluid has been reported also in other studies [4,5,15,46–48]. However, previously only moderate hydroxyapatite staining of human mesenchymal stem cells with osteogenic induction has been shown in 3D hydrogel culture [26] compared to our robust results. Similarly to a prior study by Gantar et al., we achieved hydroxyapatite deposition in hASC-secreted ECM in central parts of GG-SPD hydrogel samples, whereas in contrast, we used BaG OM ionic dissolution products alone without embedded BaG nanoparticles [4]. Although the cell-free COL samples showed some background as

expected, due to the fact that COL functions as a natural platform for mineral crystal accumulation in acellular mineralization processes [5,7], the mineral deposition was clearly accelerated in interactions with the cell-secreted matrix in our present results. Moreover, these results verified that the GG-SPD hydrogels allowed the steady unobstructed diffusion [20] of the ionic species supporting hASC osteogenic differentiation and homogeneous mineral deposition. What is more, the cell-containing samples were also positively stained for the late osteogenic marker OC, which was shown to increase together with the quantitatively measured and imaged mineralized content thus confirming hASC osteogenic differentiation towards bone-like cells in 3D hydrogel culture. All in all, the strong OC and hydroxyapatite staining in the COL hydrogel, in addition to the highest Raman spectroscopic measurement result indicated that COL hydrogel combined with the BaG OM as the most efficient osteogenic inducer of the hydrogel encapsulated hASCs. In the future and especially for *in vivo* studies for larger critical sized bone defects, however, cell survival, diffusion of nutrients, and removal of waste products also in the central parts of the construct should be secured with an adequate vessel structure for vascularized bone-like graft development. Also, the effect of mineralization on collagen hydrogel *in vivo* degradation would



**Fig. 8.** Raman spectroscopic analysis. The hASC secreted mineralized residue Raman shifts in 3D hydrogel at 21 days in GG-SPD (BaG OM) (red), GG-BaG (BaG OM) (green) and COL (BaG OM) (blue) conditions. The red arrow points to the phosphate peak at Raman shift  $960\text{ cm}^{-1}$ . The hASCs were isolated from 1 donor ( $n = 1$ ). The spectra were normalized to average intensity between  $475$  and  $560\text{ cm}^{-1}$ . (For interpretation of the references to color in this figure legend, the reader is referred to the web version of this article.)

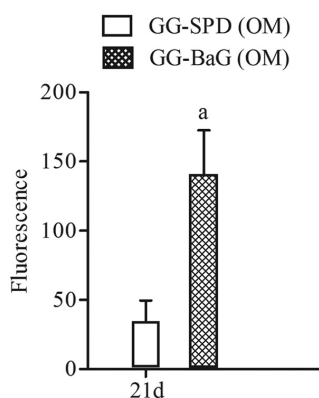


**Fig. 9.** Mineralization with different gellan gum crosslinkers. The measured fluorescence count for the OsteoImage stained hydroxyapatite mineralization of hASCs in GG-SPD and GG-BaG hydrogel samples in OM at 21 days. The analyzed hASCs were from 3 donors ( $n = 9$ ). Data are presented as mean + SD. A Significant difference from GG-SPD (OM) with  $p = 0.002$ .

require further investigation in the future.

While COL hydrogel has been extensively tested for potential injectable bone tissue engineering applications [5,49–51], we also tested an abundant and economic GG hydrogel for hASC osteogenic differentiation. On the whole, our results indicated that the BaG OM induction was required for efficient hASC osteogenic differentiation encapsulated in 3D GG-SPD and COL hydrogels. The BaG OM was chosen based on previous studies in our group that showed in 2D culture the efficiency of the bioactive glass 2-06 BaG ext for hASC osteogenic induction [13]. Importantly, the current results confirmed that the dissolved BaG ions with the OM supplements together with evolving hydrogel mechanical properties were efficient to induce hASC osteogenic differentiation. Further, we hypothesized that crosslinking GG hydrogel with the BaG ext would enhance hASC mineralization encapsulated in 3D GG, based on the rich  $\text{Ca}^{2+}$  content of the BaG ext and since GG

crosslinking requires small cations [52]. Also,  $\text{Ca}^{2+}$  ions are implicated in the ECM mineralization process [46]. Indeed, the poor performance of cell-loaded GG hydrogel samples in control OM was rescued by  $\text{Ca}^{2+}$  crosslinking with the BaG ext. What is more, the mineralization results suggested that a separate cationic crosslinker might be omitted when using the novel BaG ext for GG gelation, where a statistically significantly higher hydroxyapatite content of the hASC-laden GG-BaG hydrogels was compared to GG-SPD samples in control OM at 3 weeks. Further studies are still required to determine the potential of the BaG ext hydrogel crosslinking for the hASC mineralization process in more detail.

Overall, BaG OM induced efficient osteogenic differentiation and strong mineralization of hASCs in 3D hydrogels thus supporting further the osteoblast-like cell maturation combined with enhanced mechanical properties of the mineralized matrix in both the GG and COL hydrogels. Therefore, these novel results combining osteoinducing BaG ions and 3D hydrogel stem cell culture have considerable potential for the development of a wide variety of applications for bone tissue engineered constructs.

## 5. Conclusions

In this study, we studied enhanced hASC osteogenic induction with BaG ionic dissolution products in GG-SPD and COL 3D hydrogel culture in BaG OM compared to regular OM. Incubation in BaG OM significantly reinforced GG and COL hydrogel mechanical properties and showed a stiffening behavior similar to an evolving bone matrix. In both media conditions, the hASCs were well viable embedded within 3D hydrogel, where the GG-SPD encapsulated hASCs had a tight and round cell morphology, whereas in COL hydrogel elongated and spread morphologies were observed. With the BaG OM induction, the hASCs in COL hydrogel showed significantly higher osteogenic marker gene expression. On the whole, the BaG OM culture significantly enhanced hASC potency to mineralize in both the GG-SPD and COL 3D hydrogels, however, hASC-laden COL (BaG OM) hydrogels showed highest mineralization and hydroxyapatite content confirmed by Raman spectroscopy analysis together with the strongest OC staining results. Importantly, the BaG ext-crosslinked GG-BaG hydrogels promoted significantly higher hASC mineralization even in the control OM. The OPT and SPIM techniques were evaluated as efficient methods for emerging 3D hydrogel cell culture imaging and analysis applications. These results demonstrated the significant potential of BaG OM induction and novel 3D hydrogel culture methods for the osteogenic differentiation of hASCs towards bone-like cells and for bone regeneration applications.

Supplementary data to this article can be found online at <https://doi.org/10.1016/j.msec.2019.02.035>.

## Competing interests

The authors declare that they have no competing interests.

## Funding

This study was financially supported by the Finnish Funding Agency for Innovation (TEKES Business Finland), the Human Spare Parts Project, the Academy of Finland, The City of Tampere Science Fund, The Finnish Cultural Foundation's Pirkanmaa Regional Fund, The Finnish Foundation for Technology Promotion, and the Competitive State Research Financing of the Expert Responsibility area of Tampere University Hospital.

## Authors' contributions

KV contributed to planning of the work, carried out most of the data collection and analysis, drafted and edited the manuscript. MO contributed to planning of the work and participated in manuscript

preparation and editing. JK, HHä, BB, and TM participated in data collection and analysis and manuscript preparation and editing. HHu was consulted for statistical analyses, contributed to the data analysis and participated in manuscript preparation and editing. LH, MK, JH, and JI participated in the planning of the work and manuscript preparation and editing. SM contributed to planning and coordination of the work, interpretation of data, and participated in manuscript preparation and editing.

## Acknowledgements

The authors wish to thank Mari Lehti-Poljörvi, MSc, for the OPT and SPIM imaging cell culture platforms, Computational Biophysics and Imaging Group, BioMediTech, Faculty of Medicine and Health Technology, Tampere University, Tampere, Finland, the Tampere Imaging Facility (TIF), Tampere University, for their support in imaging services, and Jenny Parraga Meneses, PhD, Biomaterials and Tissue Engineering Group, BioMediTech, Faculty of Medicine and Health Technology, Tampere University, Finland, and Nick Walters, PhD, Adult Stem Cell Group, BioMediTech, Faculty of Medicine and Health Technology, Tampere University, Tampere, Finland, and for technical support Adult Stem Cell Group laboratory technicians Miia Juntunen, MSc, Anna-Majja Honkala, laboratory engineer, and Sari Kalliokoski.

## References

- [1] A. Chatterjea, G. Meijer, C. van Blitterswijk, J. de Boer, Clinical application of human mesenchymal stromal cells for bone tissue engineering, *Stem Cells Int.* (2010) 215625, <https://doi.org/10.4061/2010/215625>.
- [2] M. Jakob, F. Saxer, C. Scotti, S. Schreiner, P. Studer, A. Scherberich, M. Heberer, I. Martin, Perspective on the evolution of cell-based bone tissue engineering strategies, *Eur. Surg. Res.* 49 (1) (2012) 1–7, <https://doi.org/10.1159/000338362>.
- [3] B. Lindroos, R. Suuronen, S. Miettinen, et al., *Stem Cell Rev.* 7 (2) (2011) 269–291, <https://doi.org/10.1007/s12015-010-9193-7>.
- [4] A. Gantar, L.P. da Silva, J.M. Oliveira, A.P. Marques, V.M. Correlo, S. Novak, R.L. Reis, Nanoparticulate bioactive-glass-reinforced gellan-gum hydrogels for bone-tissue engineering, *Mater. Sci. Eng. C Mater. Biol. Appl.* 43 (2014) 27–36, <https://doi.org/10.1016/j.msec.2014.06.045>.
- [5] A.K. Miri, N. Muja, N.O. Kamranpour, W.C. Lepry, A.R. Boccaccini, S.A. Clarke, S.N. Nazhat, Ectopic bone formation in rapidly fabricated acellular injectable dense collagen-Bioglass hybrid scaffolds via gel aspiration-ejection, *Biomaterials* 85 (2016) 128–141, <https://doi.org/10.1016/j.biomaterials.2016.01.047>.
- [6] M.B. Oliveira, C.A. Custodio, L. Gasperini, R.L. Reis, J.F. Mano, Autonomous osteogenic differentiation of hASCs encapsulated in methacrylated gellan-gum hydrogels, *Acta Biomater.* 41 (2016) 119–132, <https://doi.org/10.1016/j.actbio.2016.05.033>.
- [7] B. Marelli, C.E. Ghezzi, D. Mohn, W.J. Stark, J.E. Barralet, A.R. Boccaccini, S.N. Nazhat, Accelerated mineralization of dense collagen-nano bioactive glass hybrid gels increases scaffold stiffness and regulates osteoblastic function, *Biomaterials* 32 (34) (2011) 8915–8926, <https://doi.org/10.1016/j.biomaterials.2011.08.016>.
- [8] T.E.L. Douglas, A. Lapa, S.K. Samal, H.A. Declercq, D. Schaubroeck, A.C. Mendes, P.V. der Voort, A. Dokupil, A. Pliš, K. De Schampheleere, I.S. Chronakis, E. Pamula, A.G. Skirtach, Enzymatic, urease-mediated mineralization of gellan gum hydrogel with calcium carbonate, magnesium-enriched calcium carbonate and magnesium carbonate for bone regeneration applications, *J. Tissue Eng. Regen. Med.* 11 (12) (2017) 3556–3566, <https://doi.org/10.1002/term.2273>.
- [9] M.G. Mandá, L.P. da Silva, M.T. Cerqueira, D.R. Pereira, M.B. Oliveira, J.F. Mano, A.P. Marques, J.M. Oliveira, V.M. Correlo, R.L. Reis, Gellan gum-hydroxyapatite composite spongy-like hydrogels for bone tissue engineering, *J. Biomed. Mater. Res. A* 106 (2) (2018) 479–490, <https://doi.org/10.1002/jbm.a.36248>.
- [10] L.L. Hench, Biomaterials: a forecast for the future, *Biomaterials* 19 (16) (1998) 1419–1423 (S0142-9612(98)00133-1 [pii]).
- [11] L.L. Hench, The future of bioactive ceramics, *J. Mater. Sci. Mater. Med.* 26 (2) (2015), <https://doi.org/10.1007/s10856-015-5425-3> (86-015-5425-3. Epub 2015 Feb 3).
- [12] L.L. Hench, J. Wilson, Biocompatibility of silicates for medical use, *CIBA Found. Symp.* 121 (1986) 231–246.
- [13] M. Ojansivu, S. Vanhatupa, L. Björkvik, H. Hakkanen, M. Kellomäki, R. Autio, J.A. Ihalainen, L. Hupa, S. Miettinen, Bioactive glass ions as strong enhancers of osteogenic differentiation in human adipose stem cells, *Acta Biomater.* 21 (2015) 190–203, <https://doi.org/10.1016/j.actbio.2015.04.017>.
- [14] M. Ojansivu, L. Hyvari, M. Kellomäki, L. Hupa, S. Vanhatupa, S. Miettinen, Bioactive glass induced osteogenic differentiation of human adipose stem cells is dependent on cell attachment mechanism and mitogen-activated protein kinases, *Eur. Cell. Mater.* 35 (2018) 54–72, <https://doi.org/10.22203/eCm.v035a05>.
- [15] T.E. Douglas, W. Piwowarczyk, E. Pamula, J. Liskova, D. Schaubroeck, S.C. Leeuwenburgh, G. Brackman, L. Balcaen, R. Detsch, H. Declercq, K. Cholewa-Kowalska, A. Dokupil, V.M. Cuijpers, F. Vanhaecke, R. Cornelissen, T. Coenye, A.R. Boccaccini, P. Dubrue, Injectable self-gelling composites for bone tissue engineering based on gellan gum hydrogel enriched with different bioglasses, *Biomed. Mater.* 9 (4) (2014), <https://doi.org/10.1088/1748-6041/9/4/045014> (045014-6041/9/4/045014. Epub 2014 Jul 25).
- [16] A. El-Fiqi, J.H. Lee, E.J. Lee, H.W. Kim, Collagen hydrogels incorporated with surface-aminated mesoporous nanobioactive glass: improvement of physicochemical stability and mechanical properties is effective for hard tissue engineering, *Acta Biomater.* 9 (12) (2013) 9508–9521, <https://doi.org/10.1016/j.actbio.2013.07.036>.
- [17] J.T. Koivisto, T. Joki, J.E. Parraga, R. Paakkonen, L. Yla-Outinen, L. Salonen, I. Jonkkari, M. Peltola, T.O. Ihalainen, S. Narkilahti, M. Kellomäki, Biomine-crosslinked gellan gum hydrogel for neural tissue engineering, *Biomed. Mater.* 12 (2) (2017), <https://doi.org/10.1088/1748-605X/aa62b0> (025014-605X/aa62b0).
- [18] R. Lopez-Cebral, P. Paolicelli, V. Romero-Caamano, B. Seijo, M.A. Casadei, A. Sanchez, Spermidine-cross-linked hydrogels as novel potential platforms for pharmaceutical applications, *J. Pharm. Sci.* 102 (8) (2013) 2632–2643, <https://doi.org/10.1002/jps.23631>.
- [19] E. Figueiras, A.M. Soto, D. Jesus, M. Lehti, J. Koivisto, J.E. Parraga, J. Silva-Correia, J.M. Oliveira, R.L. Reis, M. Kellomäki, J. Hyttinen, Optical projection tomography as a tool for 3D imaging of hydrogels, *Biomed. Opt. Express* 5 (10) (2014) 3443–3449, <https://doi.org/10.1364/BOE.5.003443>.
- [20] A.M. Soto, J.T. Koivisto, J.E. Parraga, J. Silva-Correia, J.M. Oliveira, R.L. Reis, M. Kellomäki, J. Hyttinen, E. Figueiras, Optical projection tomography technique for image texture and mass transport studies in hydrogels based on gellan gum, *Langmuir* 32 (20) (2016) 5173–5182, <https://doi.org/10.1021/acs.langmuir.6b00554>.
- [21] B. Belay, J.T. Koivisto, K. Vuornos, T. Montonen, O. Koskela, M. Lehti-Poljörvi, S. Miettinen, M. Kellomäki, E. Figueiras, J. Hyttinen, Optical Projection Tomography Imaging of Single Cells in 3D Gellan Gum Hydrogel, (2017), IFMBE Proceedings EMBEC & NBC 2017, Springer Nature Singapore Pte Ltd, Singapore, 2018.
- [22] L. Kyllönen, S. Haimi, B. Mannerstrom, H. Huhtala, K.M. Rajala, H. Skottman, G.K. Sandor, S. Miettinen, Effects of different serum conditions on osteogenic differentiation of human adipose stem cells in vitro, *Stem Cell Res Ther* 4 (1) (2013) 17, <https://doi.org/10.1186/scr1165>.
- [23] M. Dominici, K. Le Blanc, I. Mueller, I. Slaper-Cortenbach, F. Marini, D. Krause, R. Deans, A. Keating, D. Prockop, E. Horwitz, Minimal criteria for defining multipotent mesenchymal stromal cells: The International Society for Cellular Therapy position statement, *Cytotherapy* 8 (4) (2006) 315–317, <https://doi.org/10.1080/14653240600855905>.
- [24] K. McIntosh, S. Zvonc, S. Garrett, J.B. Mitchell, Z.E. Floyd, L. Hammill, A. Kloster, Y. Di Halvorsen, J.P. Ting, R.W. Storms, B. Goh, G. Kilroy, X. Wu, J.M. Gimble, The immunogenicity of human adipose-derived cells: temporal changes in vitro, *Stem Cells* 24 (5) (2006) 1246–1253 (2005-0235 [pii]).
- [25] L. Tirkkonen, S. Haimi, S. Huttunen, J. Wolff, E. Pirhonen, G.K. Sandor, S. Miettinen, Osteogenic medium is superior to growth factors in differentiation of human adipose stem cells towards bone-forming cells in 3D culture, *Eur. Cell. Mater.* 25 (2013) 144–158.
- [26] L.A. Castillo Diaz, M. Elsayi, A. Saijani, J.E. Gough, A.F. Miller, Osteogenic differentiation of human mesenchymal stem cells promotes mineralization within a biodegradable peptide hydrogel, *J. Tissue Eng.* 7 (2016), <https://doi.org/10.1177/2041731416649789> (2041731416649789).
- [27] M.W. Pfaffl, A new mathematical model for relative quantification in real-time RT-PCR, *Nucleic Acids Res.* 29 (9) (2001) e45.
- [28] T. Fink, P. Lund, L. Pilgaard, J.G. Rasmussen, M. Duroux, V. Zachar, Instability of standard PCR reference genes in adipose-derived stem cells during propagation, differentiation and hypoxic exposure, *BMC Mol. Biol.* 9 (2008), <https://doi.org/10.1186/1471-2199-9-98> (98-2199-9-98).
- [29] B.G. Gabriellson, L.E. Olofsson, A. Sjogren, M. Jernas, A. Elander, M. Lonn, M. Rudemo, L.M. Carlsson, Evaluation of reference genes for studies of gene expression in human adipose tissue, *Obes. Res.* 13 (4) (2005) 649–652, <https://doi.org/10.1038/oby.2005.72>.
- [30] P. Ruokola, E. Dadu, A. Kazmertsuk, H. Hakkanen, V. Marjomaki, J.A. Ihalainen, Raman spectroscopic signatures of echovirus 1 uncoating, *J. Virol.* 88 (15) (2014) 8504–8513, <https://doi.org/10.1128/JVI.03398-13>.
- [31] W.L. Murphy, T.C. McDevitt, A.J. Engler, Materials as stem cell regulators, *Nat. Mater.* 13 (6) (2014) 547–557, <https://doi.org/10.1038/nmat3937>.
- [32] N. Ramesh, S.C. Moratti, G.J. Dias, Hydroxyapatite-polymer biocomposites for bone regeneration: a review of current trends, *J. Biomed. Mater. Res B Appl. Biomater.* (2017), <https://doi.org/10.1002/jbm.b.33950>.
- [33] C.B. Raub, A.J. Putnam, B.J. Tromberg, S.C. George, Predicting bulk mechanical properties of cellularized collagen gels using multiphoton microscopy, *Acta Biomater.* 6 (12) (2010) 4657–4665, <https://doi.org/10.1016/j.actbio.2010.07.004>.
- [34] J. Silva-Correia, A. Gloria, M.B. Oliveira, J.F. Mano, J.M. Oliveira, L. Ambrosio, R.L. Reis, Rheological and mechanical properties of acellular and cell-laden methacrylated gellan gum hydrogels, *J. Biomed. Mater. Res. A* 101 (12) (2013) 3438–3446, <https://doi.org/10.1002/jbm.a.34650>.
- [35] J.H. Wen, L.G. Vincent, A. Fuhrmann, Y.S. Choi, K.C. Hribar, H. Taylor-Weiner, S. Chen, A.J. Engler, Interplay of matrix stiffness and protein tethering in stem cell differentiation, *Nat. Mater.* 13 (10) (2014) 979–987, <https://doi.org/10.1038/nmat4051>.
- [36] A.J. Engler, S. Sen, H.L. Sweeney, D.E. Discher, Matrix elasticity directs stem cell lineage specification, *Cell* 126 (4) (2006) 677–689 (S0092-8674(06)00961-5 [pii]).
- [37] N. Huebsch, P.R. Arany, A.S. Mao, D. Shvartsman, O.A. Ali, S.A. Bencherif,



- J. Rivera-Feliciano, D.J. Mooney, Harnessing traction-mediated manipulation of the cell/matrix interface to control stem-cell fate, *Nat. Mater.* 9 (6) (2010) 518–526, <https://doi.org/10.1038/nmat2732>.
- [38] E.V. Alakpa, V. Jayawarna, A. Lampel, K.V. Burgess, C.C. West, S.C.J. Bakker, S. Roy, N. Javid, S. Fleming, D.A. Lamprou, J. Yang, A. Miller, A.J. Urquhart, P.W.J.M. Frederix, N.T. Hunt, B. Péault, R.V. Ulijn, M.J. Dalby, Tunable supra-molecular hydrogels for selection of lineage-guiding metabolites in stem cell cultures, *Chem 1* (2) (2016) 298–319, <https://doi.org/10.1016/j.chempr.2016.07.001>.
- [39] J. Karvinen, J.T. Koivisto, I. Jonkkari, M. Kellomaki, The production of injectable hydrazone crosslinked gellan gum-hyaluronan-hydrogels with tunable mechanical and physical properties, *J. Mech. Behav. Biomed. Mater.* 71 (2017) 383–391 (S1751-6161(17)30155-8 [pii]).
- [40] R.A. Perez, M. Kim, T.H. Kim, J.H. Kim, J.H. Lee, J.H. Park, J.C. Knowles, H.W. Kim, Utilizing core-shell fibrous collagen-alginate hydrogel cell delivery system for bone tissue engineering, *Tissue Eng. A* 20 (1–2) (2014) 103–114, <https://doi.org/10.1089/ten.TEA.2013.0198>.
- [41] J. Mayer, A. Robert-Moreno, R. Danuser, J.V. Stein, J. Sharpe, J. Swoger, OPTISPIM: integrating optical projection tomography in light sheet microscopy extends specimen characterization to nonfluorescent contrasts, *Opt. Lett.* 39 (4) (2014) 1053–1056, <https://doi.org/10.1364/OL.39.001053>.
- [42] J. Sharpe, Optical projection tomography, *Annu. Rev. Biomed. Eng.* 6 (2004) 209–228, <https://doi.org/10.1146/annurev.bioeng.6.040803.140210>.
- [43] J. Sharpe, U. Ahlgren, P. Perry, B. Hill, A. Ross, J. Hecksher-Sorensen, R. Baldock, D. Davidson, Optical projection tomography as a tool for 3D microscopy and gene expression studies, *Science* 296 (5567) (2002) 541–545, <https://doi.org/10.1126/science.1068206>.
- [44] H.C. Chen, H.P. Lee, M.L. Sung, C.J. Liao, Y.C. Hu, A novel rotating-shaft bioreactor for two-phase cultivation of tissue-engineered cartilage, *Biotechnol. Prog.* 20 (6) (2004) 1802–1809, <https://doi.org/10.1021/bp049740s>.
- [45] J.A. Killion, S. Kehoe, L.M. Geever, D.M. Devine, E. Sheehan, D. Boyd, C.L. Higginbotham, Hydrogel/bioactive glass composites for bone regeneration applications: synthesis and characterisation, *Mater. Sci. Eng. C Mater. Biol. Appl.* 33 (7) (2013) 4203–4212, <https://doi.org/10.1016/j.msec.2013.06.013>.
- [46] H. Orimo, The mechanism of mineralization and the role of alkaline phosphatase in health and disease, *J. Nippon Med. Sch.* 77 (1) (2010) 4–12 (JST.JSTAGE/jnms/77.4 [pii]).
- [47] A.J. Leite, B. Sarker, T. Zehnder, R. Silva, J.F. Mano, A.R. Boccacini, Bioplotting of a bioactive alginate dialdehyde-gelatin composite hydrogel containing bioactive glass nanoparticles, *Biofabrication* 8 (3) (2016), <https://doi.org/10.1088/1758-5090/8/3/035005> (035005-5090/8/3/035005).
- [48] J. Lewandowska-Lancucka, S. Fiejdasz, L. Rodzik, M. Koziel, M. Nowakowska, Bioactive hydrogel-nanosilica hybrid materials: a potential injectable scaffold for bone tissue engineering, *Biomed. Mater.* 10 (1) (2015), <https://doi.org/10.1088/1748-6041/10/1/015020> (015020-6041/10/1/015020).
- [49] B. Sarker, J. Hum, S.N. Nazhat, A.R. Boccacini, Combining collagen and bioactive glasses for bone tissue engineering: a review, *Adv. Healthc. Mater.* 4 (2) (2015) 176–194, <https://doi.org/10.1002/adhm.201400302>.
- [50] M.M. Villa, L. Wang, J. Huang, D.W. Rowe, M. Wei, Bone tissue engineering with a collagen-hydroxyapatite scaffold and culture expanded bone marrow stromal cells, *J Biomed Mater Res B Appl Biomater* 103 (2) (2015) 243–253, <https://doi.org/10.1002/jbm.b.33225>.
- [51] T. Long, J. Yang, S.S. Shi, Y.P. Guo, Q.F. Ke, Z.A. Zhu, Fabrication of three-dimensional porous scaffold based on collagen fiber and bioglass for bone tissue engineering, *J Biomed Mater Res B Appl Biomater* 103 (7) (2015) 1455–1464, <https://doi.org/10.1002/jbm.b.33328>.
- [52] E. Miyoshi, T. Takaya, K. Nishinari, Rheological and thermal studies of gel-sol transition in gellan gum aqueous solutions, *Carbohydr. Polym.* 30 (2–3) (1996) 109–119.



**Miina Ojansivu**, PhD, works as a post doctoral researcher at the Karolinska Institutet, Solna, Sweden, in the Department of Medical Biochemistry and Biophysics.



**Janne T Koivisto**, MSc, works as a doctoral student in the Biomaterials and Tissue Engineering Group, BioMediTech, Faculty of Medicine and Health Technology, Tampere University, Tampere, Finland, and also works in the Heart Group, BioMediTech, Faculty of Medicine and Health Technology, Tampere University, Tampere, Finland.



**Heikki Häkkänen** works as a Laboratory Engineer in the Spectroscopy for Detecting Dynamics of Biomolecules Group, Nanoscience Center, in the Department of Biological and Environmental Science in the University of Jyväskylä, Jyväskylä, Finland.



**Birhanu Belay**, MSc, works as a doctoral student in the Computational Biophysics and Imaging Group, BioMediTech, at the Faculty of Medicine and Health Technology, Tampere University, Tampere, Finland.



**Kaisa Vuornos**, MSc, works as a doctoral student in the Adult Stem Cell Group, BioMediTech, Faculty of Medicine and Health Technology, Tampere University, Tampere, Finland.



**Toni Montonen**, MSc, works as a doctoral student in the Computational Biophysics and Imaging Group, BioMediTech, at the Faculty of Medicine and Health Technology, Tampere University, Tampere, Finland.

**Heini Huhtala**, MSc, works as a University Instructor in the Faculty of Social Sciences, Tampere University, Tampere, Finland.



**Minna Kääriäinen**, MD, PhD, works as a plastic surgeon and chief physician in the Department of Plastic and Reconstructive Surgery at the Tampere University Hospital, Tampere, Finland.



**Jari Hyttinen**, DSc, is the Principal Investigator in the Computational Biophysics and Imaging Group ([www.tut.fi/cbig](http://www.tut.fi/cbig)), BioMediTech, at the Faculty of Medicine and Health Technology, Tampere University, Tampere, Finland.



**Leena Hupa**, DSc, is the Professor of Inorganic Chemistry at the Johan Gadolin Process Chemistry Centre, Åbo Akademi University, Åbo, Finland.



**Janne A Ihalainen**, PhD, is the Principal Investigator in the Spectroscopy for Detecting Dynamics of Biomolecules Group, Nanoscience Center, and the Head of Department in the Department of Biological and Environmental Science in the University of Jyväskylä, Jyväskylä, Finland.



**Minna Kellomäki**, DSc, is the Principal Investigator of the Biomaterials and Tissue Engineering Group, BioMediTech, Faculty of Medicine and Health Technology, Tampere University, Finland.



**Susanna Miettinen**, PhD, is an Associate Professor in the Faculty of Medicine and Health Technology in the Tampere University and the Principal Investigator in the Adult Stem Cell Group, BioMediTech, Faculty of Medicine and Health Technology, Tampere University, Tampere, Finland.

## Publication II supplementary data

### **Bioactive glass ions induce efficient osteogenic differentiation of human adipose stem cells encapsulated in gellan gum and collagen type I hydrogels.**

Vuornos K., Ojansivu M., Koivisto J.T., Häkkänen H., Belay B., Montonen T., Huhtala H., Kääriäinen M., Hupa L., Kellomäki M., Hyttinen J., Ihalainen J.A., Miettinen S.

*Materials Science and Engineering: C*, 99 (2019): 905-918.

Supplementary data available at:

<https://doi.org/10.1016/j.msec.2019.02.035>

## Supplementary file 1

### Flow cytometric analysis and cell characterization

Following stem cell isolation, the undifferentiated human adipose stem cells (hASCs) of passage 1–2 were characterized. Briefly, hASCs were analyzed for the cell surface markers [1] with flow cytometry (FACSARIA; BD Biosciences, Franklin Lakes, NJ, USA). The following fluorophore-conjugated monoclonal antibodies were used: anti-CD3-PE, anti-CD14-PECy7, anti-CD19-PE-Cy7, anti-CD45RO-APC, anti-CD54-FITC, anti-CD73-PE, anti-CD90-APC (BD Biosciences), anti-CD11a-APC, anti-CD80-PE, anti-CD86-PE, anti-CD105-PE (R&D Systems, Minneapolis, MN, USA), CD34-APC, and anti-HLA-DR-PE (ImmunoTools, Friesoythe, Germany). Flow cytometry analysis was performed with 10,000 cells per sample, and the positive expression was defined as a level of fluorescence 99 % greater than that of the corresponding unstained cell sample [2, 3]. In the analysis, the majority of hASCs expressed the surface markers CD73, CD90, and CD105, expression of CD34 and CD54 was moderate and expression of CD3, CD11a, CD14, CD19, CD45, CD80, CD86, and HLA-DR was low (Table S1).

**Table S1 Flow cytometry surface markers analysis results of hASCs. n=3.**

Antigen	Surface protein	Mean	SD
CD3	T cell signal transduction	0.5	0.4
CD11a	Cell interactions and T cell mediated killing	1.3	0.6
CD14	Innate immune response to bacterial lipopolysaccharide	0.9	0.8
CD19	B lymphocyte-lineage differentiation antigen	0.6	0.4
CD34	Sialomucin-like adhesion molecule	31.9	19.4
CD45	Leukocyte common antigen	2.2	0.7
CD54	Cell adhesion, lymphocyte activation and migration	13.8	6.0
CD73	Ecto-5'-nucleotidase	93.4	7.7
CD80	Lymphocyte activation	0.9	0.8
CD86	Regulates T cell activation	0.9	0.8
CD90	Thy-1 (T cell surface glycoprotein)	98.9	1.3
CD105	SH-2 endoglin	98.2	1.1
HLA-DR	Major histocompatibility class II antigens	1.0	0.7

The flow cytometry analysis confirmed the mesenchymal origin of the hASCs and the small elevation of CD34 and CD54 was attributed to the low passage of the hASCs and the use of human serum as a cell culture medium supplement [4].

## References

[1] B. Lindroos, R. Suuronen, S. Miettinen, The potential of adipose stem cells in regenerative medicine, *Stem Cell.Rev.*, 7 No. 2 (2011) 269-291. 10.1007/s12015-010-9193-7.

[2] M.J. Jaroszeski & G. Radcliff, Fundamentals of flow cytometry, *Mol.Biotechnol.*, 11 No. 1 (1999) 37-53. 10.1007/BF02789175.

[3] J. Picot, C.L. Guerin, C. Le Van Kim, C.M. Boulanger, Flow cytometry: retrospective, fundamentals and recent instrumentation, *Cytotechnology*, 64 No. 2 (2012) 109-130. 10.1007/s10616-011-9415-0; 10.1007/s10616-011-9415-0.

[4] M. Patrikoski, M. Juntunen, S. Boucher, A. Campbell, M.C. Vemuri, B. Mannerstrom, S. Miettinen, Development of fully defined xeno-free culture system for the preparation and propagation of cell therapy-compliant human adipose stem cells, *Stem Cell.Res.Ther.*, 4 No. 2 (2013) 27. 10.1186/scrt175 [doi].

## Supplementary file 2

### Raman spectra of acellular hydrogels

The Raman spectroscopy was conducted as described in [1]. The samples were incubated in phenol red free bioactive glass extract based osteogenic medium (BaG OM) for 21 days. Prior to analysis, the samples were washed with 1x PBS (Lonza, Basel, Switzerland). The Raman spectra were measured from a single location. Briefly, a laser excitation wavelength of 785 nm and 100 mW power was focused onto a wet sample with an objective (x10, 0.30 N.A.; Zeiss, Oberkochen, Germany), and the same objective was used to collect backscattered light recorded with a CCD camera (Andor, Belfast, United Kingdom), and imaging spectrograph (Princeton Instruments, Trenton, NJ, USA) with an entrance slit of 50  $\mu\text{m}$  and 600 grooves/mm grating. The data accumulation time was 50x 500 s per sample. The dark noise was subtracted from the detected data using AIR-PLS algorithm. The dark background was subtracted and the spectra normalized to vibration of water at 1600–1700  $\text{cm}^{-1}$  [1].

The Raman spectra of acellular gellan gum hydrogels crosslinked with spermidine (GG-SPD) with 0.5 and 2.5 mg/mL added hydroxyapatite (HA) powder (Sigma-Aldrich, St. Louis, MO, USA) incubated in BaG OM condition for 21 days showed a Raman shift at 960  $\text{cm}^{-1}$  (Fig. S1A).

The semi-quantitative Raman measurement results showed the highest phosphate peak at 960  $\text{cm}^{-1}$  for GG-SPD (BaG OM) hydrogels with added 2.5 mg/mL HA powder and a smaller peak for the acellular sample with 0.5 mg/mL of added HA, whereas the acellular blank sample showed no phosphate peak, as expected.

Similarly, the Raman spectra of acellular collagen type I (COL) hydrogels in BaG OM medium incubation with added 2.5 mg/mL HA powder and that of human adipose stem cell (hASC)-laden (1 million cells/mL) COL (BaG OM) hydrogels without added HA showed a Raman shift at 960  $\text{cm}^{-1}$  (Fig. S1B).

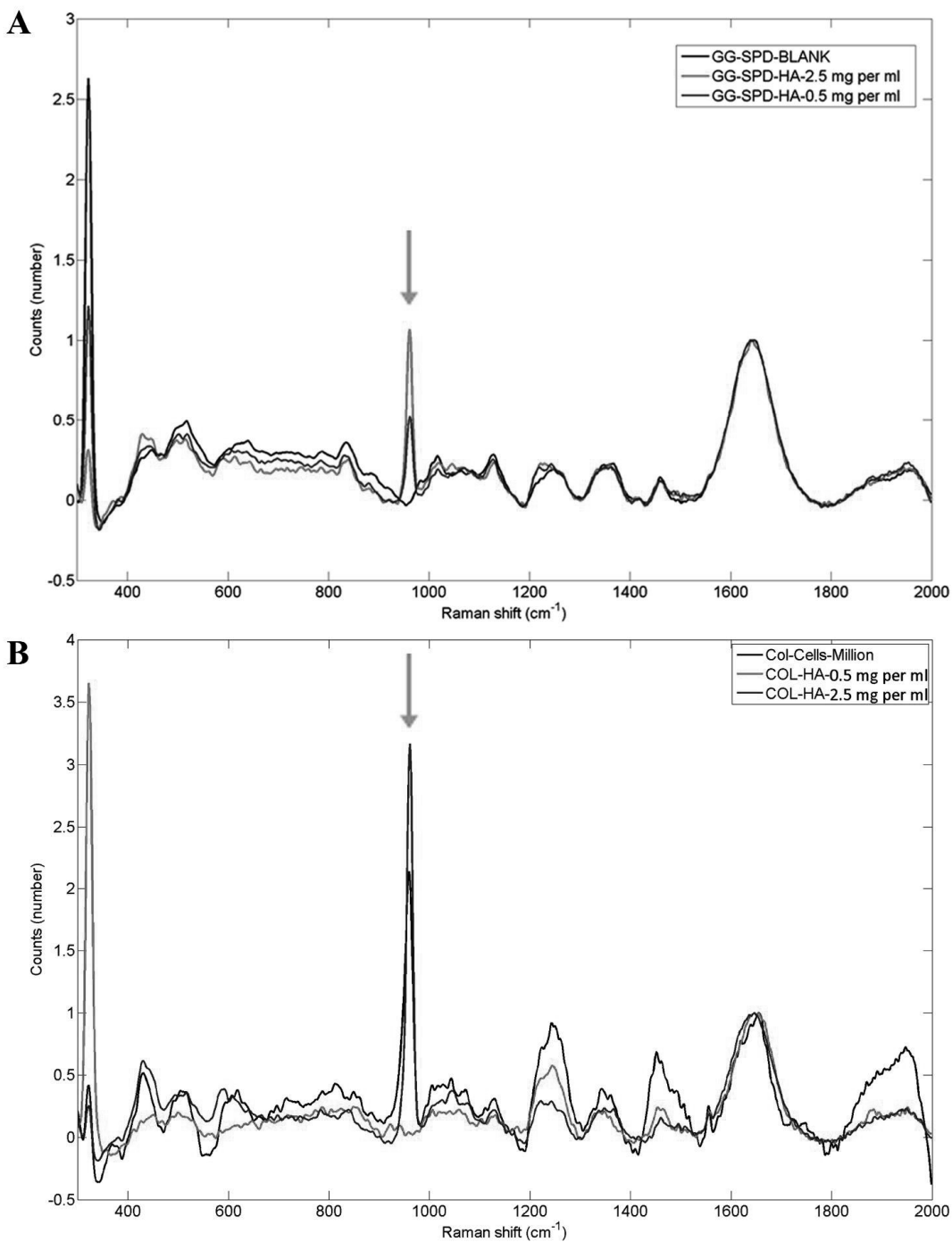


**Fig. S1 Raman spectra of acellular hydrogels.** (A) Raman spectra of acellular GG-SPD (BaG OM) hydrogels. GG-SPD blank (black); GG-SPD with 0.5 mg/mL added pure HA powder (green);

GG-SPD with 2.5 mg/mL HA (red); **(B)** Raman spectra of acellular and hASC-laden COL (BaG OM) hydrogels. COL with 0.5 mg/mL added HA powder (red); COL with 2.5 mg/mL added HA (green); COL with embedded hASCs (1 million cells/mL) cultured in (BaG OM) (black). The red arrow points to the phosphate peak at Raman shift  $960\text{ cm}^{-1}$ . The hASCs were isolated from 1 donor.

The phosphate peaks at  $960\text{ cm}^{-1}$  for hASC-laden COL (BaG OM) and for the acellular COL (BaG OM) with added 2.5 mg/mL HA powder were strong, whereas the phosphate peak at  $960\text{ cm}^{-1}$  was absent for the acellular COL (BaG OM) with added 0.5 mg/mL HA powder which indicated unhomogeneous distribution of added HA into the hydrogel. This might have been due to the fact that the Raman spectra were measured from a single location in each case.

## References

- [1] P. Ruokola, E. Dadu, A. Kazmertsuk, H. Hakkanen, V. Marjomaki, J.A. Ihalainen, Raman spectroscopic signatures of echovirus 1 uncoating, *J.Virol.*, 88 No. 15 (2014) 8504-8513. 10.1128/JVI.03398-13 [doi].



## Supplementary file 3

### Representative stress-strain curves

The representative stress-strain curves of mechanical compression testing of acellular gellan gum hydrogels crosslinked with spermidine (GG-SPD) and collagen type I (COL) hydrogel samples in regular osteogenic medium (OM) and bioactive glass extract based osteogenic medium (BaG OM), and GG hydrogels crosslinked with bioactive glass extract (GG-BaG) in OM alone, at 0, 14, and 21 days of incubation (Fig. S2).

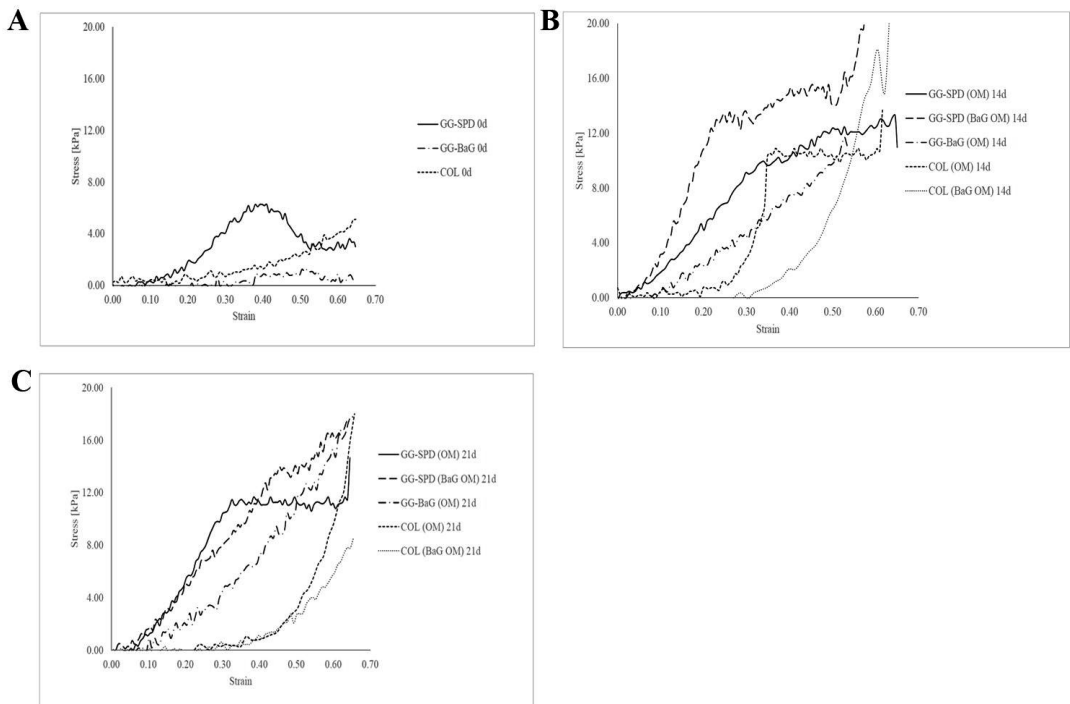


**Fig. S2 Representative stress-strain curves of acellular hydrogels.** Compressive modulus mechanical testing of cell-free GG-SPD, GG-BaG, and COL hydrogels after (A) 0-day; (B) 14-day; (C) 21-day incubation in OM and BaG OM media ( $n=3-6$ ), where GG-BaG in OM only.

## **Supplementary file 4**

### **Cell viability**

The hASC viability was analyzed at 3 and 14 days encapsulated within 3D hydrogel (Fig. S3). All samples showed good cell viability results with few dead cells. The COL (OM) samples contracted after 3 days.

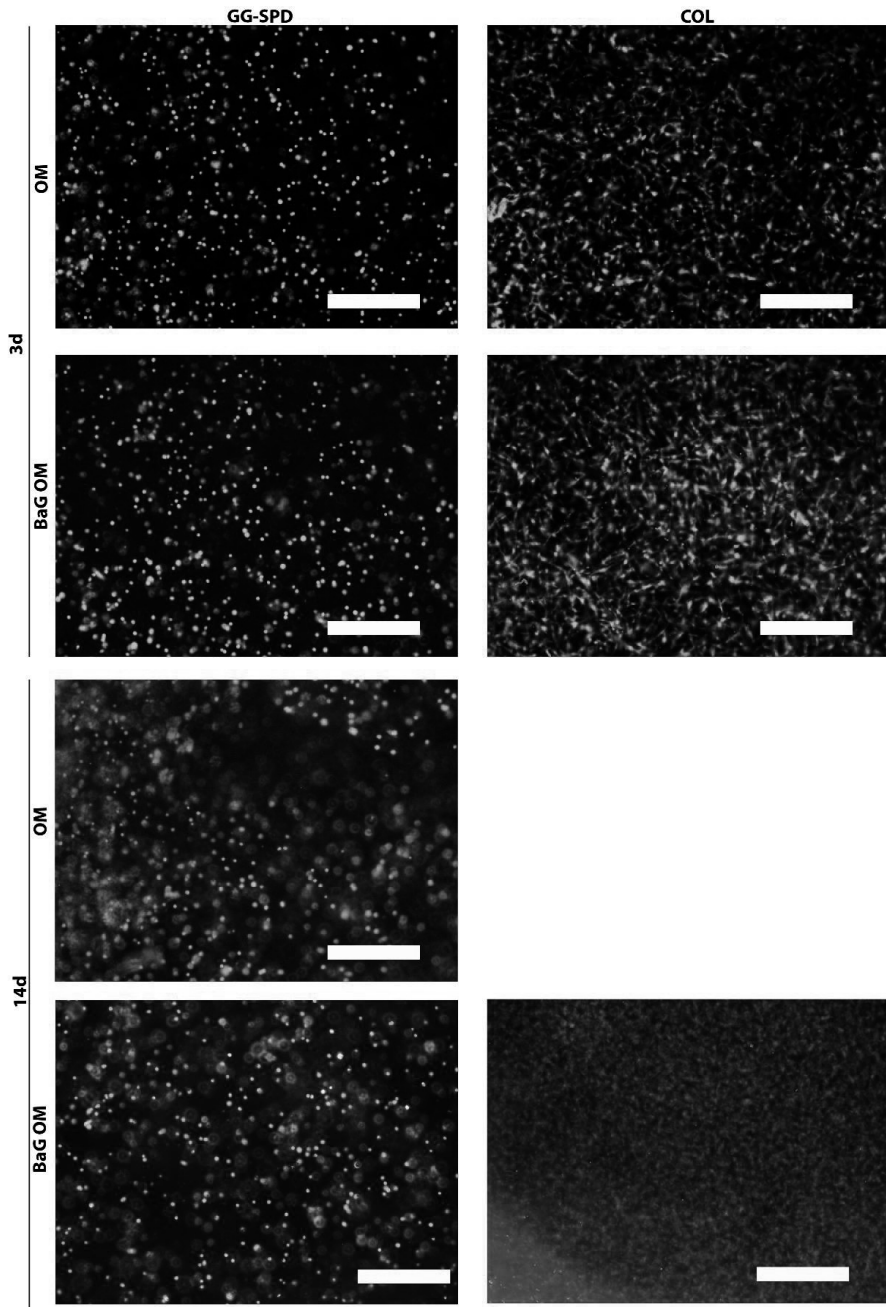


**Fig. S3 Cell viability. Representative fluorescence images of Live/Dead stained cell-laden hydrogels.** Viability of hASCs encapsulated in GG-SPD (OM), GG-SPD (BaG OM), COL (OM) and COL (BaG OM) 3D hydrogels at 3 and 14 days ( $n=3$ ). The COL (OM) samples contracted after 3 days. Scale bar 500  $\mu\text{m}$ .

## Supplementary file 5

### Immunocytochemical staining of osteocalcin

The supplementary immunocytochemical staining results of osteocalcin and DAPI stained hASCs encapsulated in GG and COL hydrogels in different media conditions at 21 days are shown in (Fig. S4).

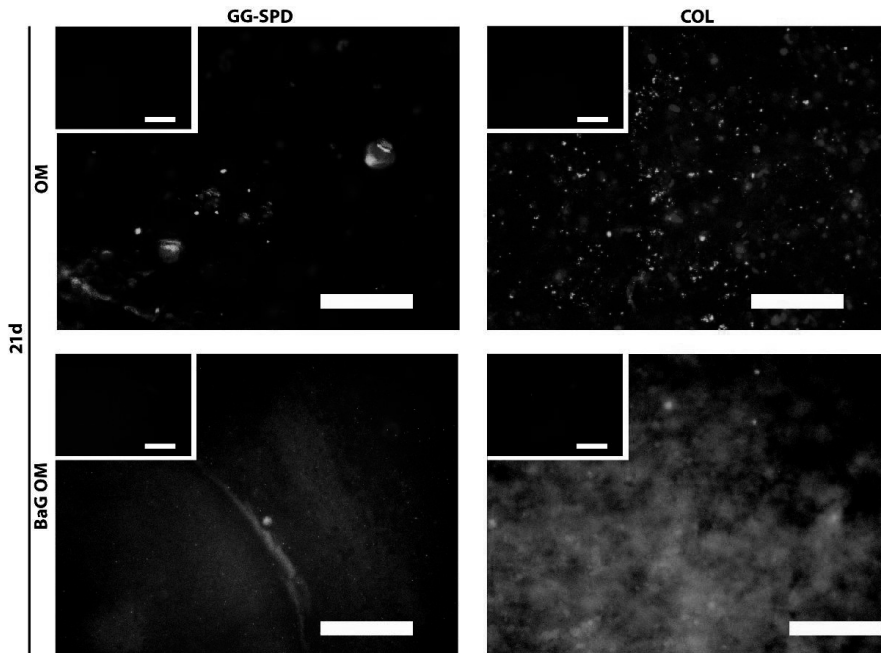


**Fig. S4 Immunocytochemistry. Representative fluorescence images of osteocalcin and DAPI stained hASC-laden hydrogels.** Osteocalcin production and nuclei of hASCs encapsulated in GG-SPD (OM), GG-SPD (BaG OM), COL (OM) and COL (BaG OM) 3D hydrogels at 21 days ( $n=3$ ). Cell free blank controls in upper left corner. Scale bar 200  $\mu\text{m}$ .

The supplementary images confirmed the strong osteocalcin production detected in the COL samples in both media conditions, while some osteocalcin staining was also seen in the GG-SPD hASC-laden hydrogels.

## **Supplementary file 6**

### **Cell viability crosslinker comparison**

The hASC viability was analyzed at 3, 14, and 21 days encapsulated within 3D GG-SPD and GG-BaG hydrogels in OM (Fig. S5). In all the analyzed time points, good cell viability was observed in all samples with few dead cells visible.

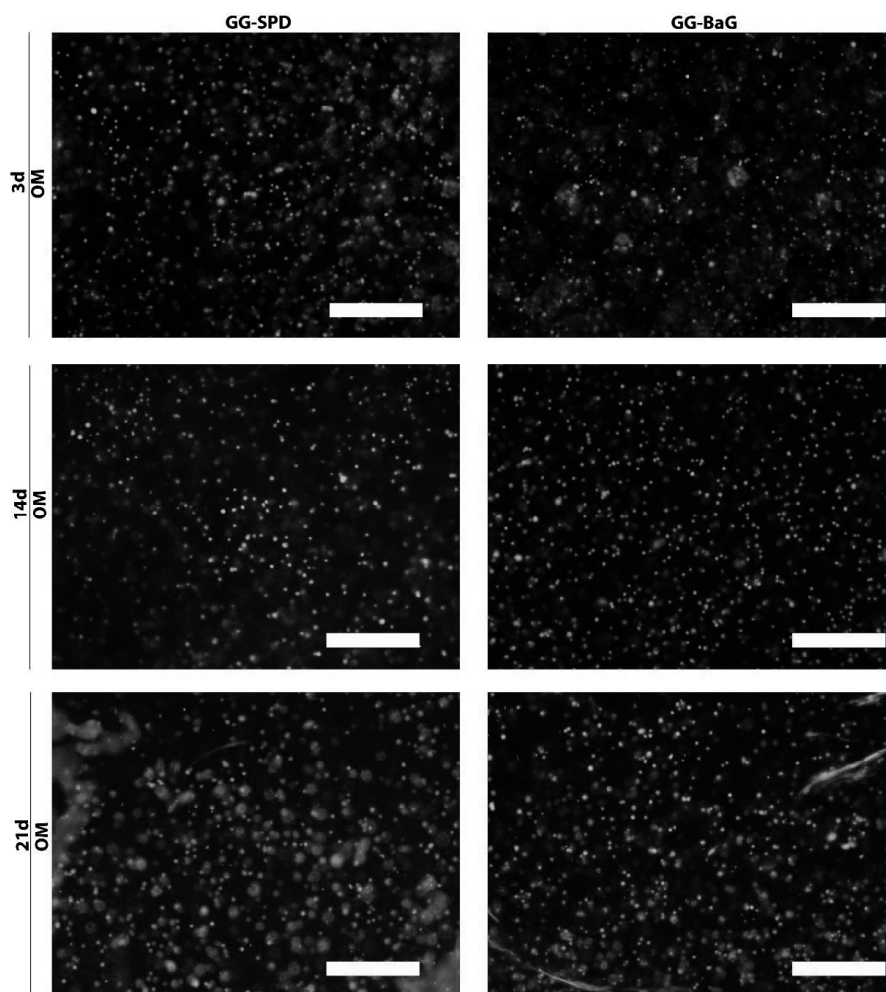


**Fig. S5 Cell viability crosslinker comparison. Representative fluorescence images of Live/Dead stained cell-laden hydrogels.** Viability of hASCs encapsulated in GG-SPD (OM) and GG-BaG (OM) 3D hydrogels at 3, 14, and 21 days ( $n=3$ ). Scale bar 500  $\mu\text{m}$ .

Both of the compared crosslinkers produced similar results supporting hASC viability up to 3 weeks embedded within GG hydrogel in regular OM.

## Supplementary file 7

### Cell number crosslinker comparison

The cell number based on total DNA content in GG-SPD (OM) and GG-BaG (OM) groups was analyzed at 14- and 21-day time points (Fig. S6).

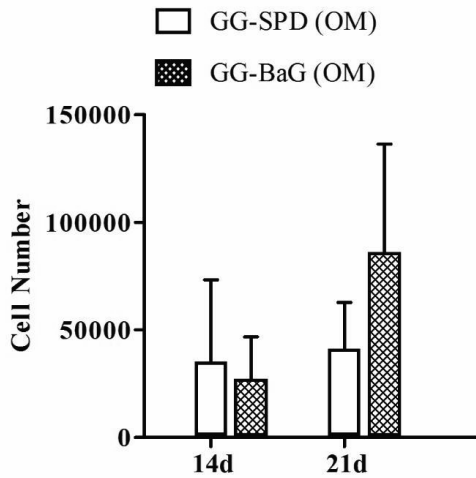


**Fig. S6 Cell number crosslinker comparison.** Cell number based on total DNA content of hASCs encapsulated in 3D hydrogels at 14 and 21 days. The analyzed hASCs were from 3 donors ( $n=9$ ). Data are presented as mean + SD.

The highest cell number was detected in the GG-BaG (OM) condition at 21 days. However, there were no statistically significant differences between the compared GG crosslinkers, namely SPD and BaG ext, either between the crosslinkers or between the tested time points.

## Supplementary file 8

### Mineralization crosslinker comparison

The hASC secreted mineralized matrix hydroxyapatite residues were stained with the OsteoImage assay and hASC nuclei with DAPI. The GG-SPD (OM) and GG-BaG (OM) samples were imaged in 3D hydrogels at 21 days (Fig. S7).

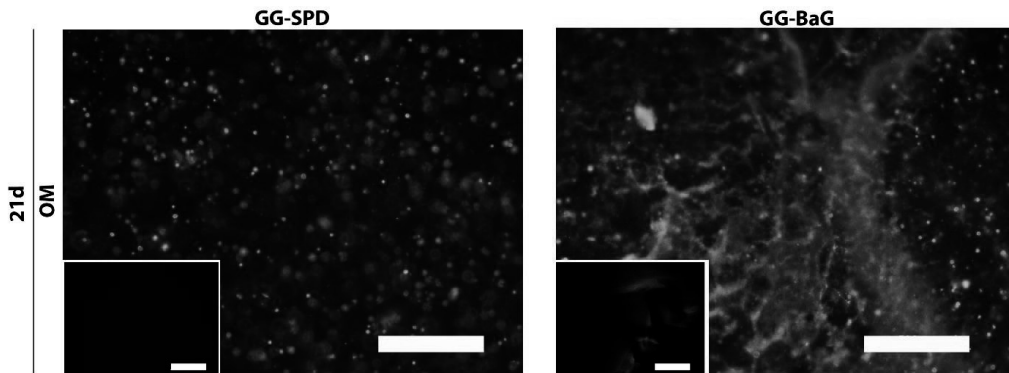
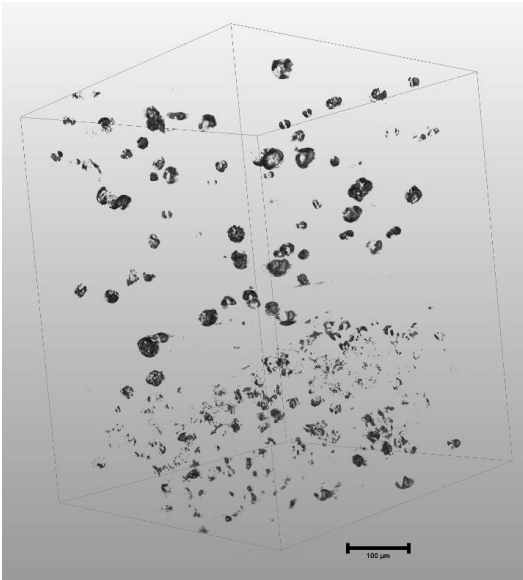


**Fig. S7 Mineralization crosslinker comparison.** Representative images of hydroxyapatite residues and cell nuclei of hASCs stained with the OsteoImage assay and DAPI in 3D hydrogels at 21 days in GG-SPD (OM) and GG-BaG (OM) hydrogels. The blank controls are presented in the lower left corner. Scale bar 500  $\mu\text{m}$ .

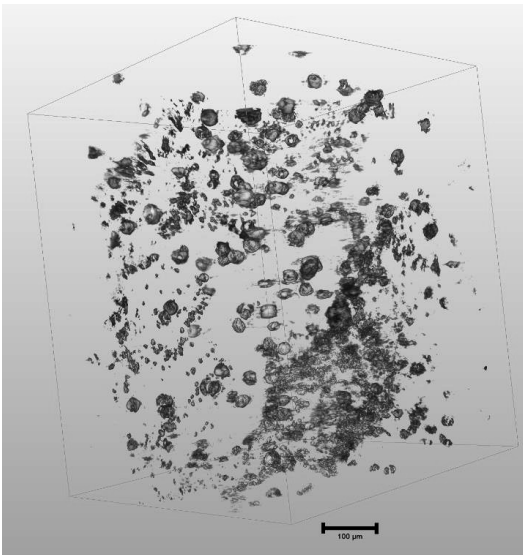
The OsteoImage stained hydroxyapatite residue imaging supported the quantified mineralization results with the stronger hydroxyapatite staining for the GG-BaG (OM) condition, while also some staining in the GG-SPD (OM) condition at the 21-day time point. Some background staining was observed in the cell-free blank GG-BaG (OM) samples.



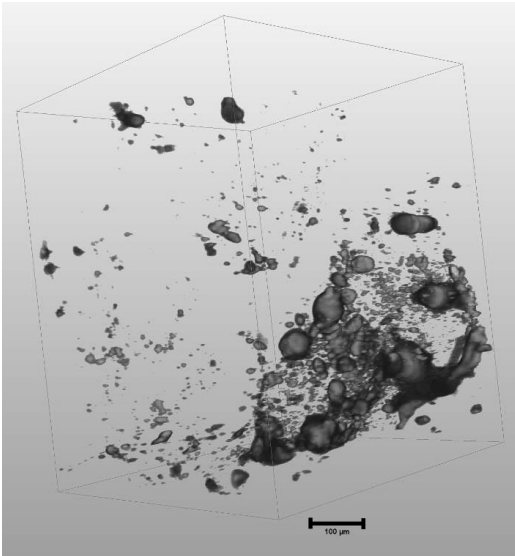
**Video supplementary files 9-14**



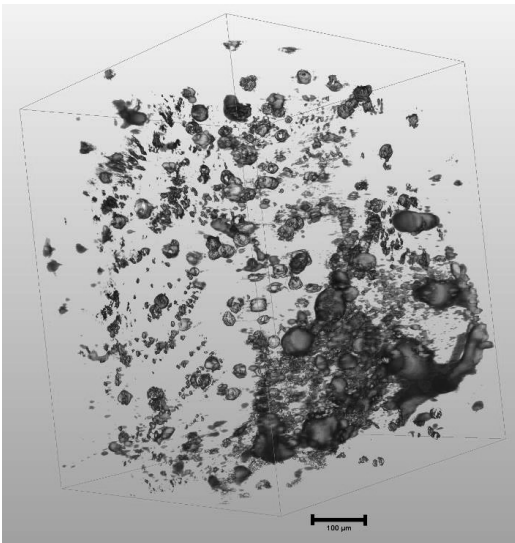
**Video supplementary file 9.** Brightfield OPT imaging of GG-SPD in OM. Representative 3D reconstruction of brightfield OPT still image showing hASC 3D distribution within GG-SPD hydrogel in the OM condition. Scale bar 100 μm.



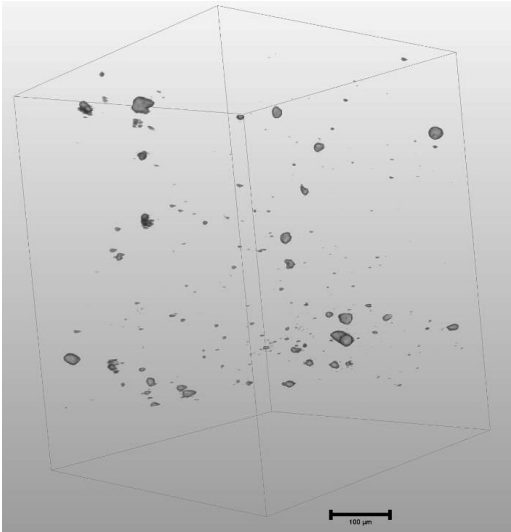
**Video supplementary file 10.** Brightfield OPT imaging of GG-SPD in BaG OM. Representative 3D reconstruction brightfield OPT still image showing hASC 3D distribution within GG-SPD hydrogel in the BaG OM condition. Scale bar 100 μm.



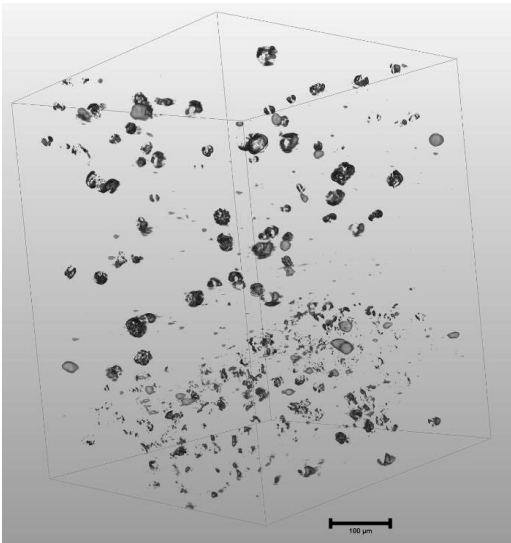
**Video supplementary file 11.** Fluorescence SPIM imaging of GG-SPD in BaG OM. Representative 3D reconstruction fluorescence SPIM still image showing OsteoImage-stained hydroxyapatite 3D distribution within GG-SPD hydrogel in the BaG OM condition. Scale bar 100 μm.



**Video supplementary file 12.** Combined OPT and SPIM imaging of GG-SPD in BaG OM. Representative 3D reconstruction still image of combined brightfield OPT and fluorescence SPIM images showing hASC and hydroxyapatite 3D distribution within GG-SPD hydrogel in the BaG OM condition. Scale bar 100 μm.



**Video supplementary file 13.** Fluorescence SPIM imaging of GG-SPD in OM. Representative 3D reconstruction fluorescence SPIM still image showing OsteoImage-stained hydroxyapatite 3D distribution within GG-SPD hydrogel in the OM condition. Scale bar 100 μm.



**Video supplementary file 14.** Combined OPT and SPIM imaging of GG-SPD in OM. Representative 3D reconstruction still image of combined brightfield OPT and fluorescence SPIM images showing hASC and hydroxyapatite 3D distribution within GG-SPD hydrogel in the OM condition. Scale bar 100 μm.



**PUBLICATION**  
**III**

**Bioactive Glass Ions for *In Vitro* Osteogenesis and Microvascularization in  
Gellan Gum-Collagen Hydrogels**

Vuornos K., Huhtala H., Kääriäinen M., Kuismanen K., Hupa L., Kellomäki M.,  
Miettinen S.


*J Biomed Mater Res B Appl Biomater.* 2019 Aug 31.

**Publication reprinted with the permission of  
the John Wiley and Sons Publisher.**



**ORIGINAL RESEARCH REPORT**

# Bioactive glass ions for *in vitro* osteogenesis and microvascularization in gellan gum-collagen hydrogels

Kaisa Vuornos<sup>1,2</sup>  | Heini Huhtala<sup>3</sup> | Minna Kääriäinen<sup>4</sup> | Kirsi Kuismanen<sup>5</sup> |  
Leena Hupa<sup>6</sup> | Minna Kellomäki<sup>7</sup> | Susanna Miettinen<sup>1,2</sup>

<sup>1</sup>Adult Stem Cell Group, BioMediTech, Faculty of Medicine and Health Technology, Tampere University, Tampere, Finland

<sup>2</sup>Research, Development and Innovation Centre, Tampere University Hospital, Tampere, Finland

<sup>3</sup>Faculty of Social Sciences, Tampere University, Tampere, Finland

<sup>4</sup>Department of Plastic and Reconstructive Surgery, Tampere University Hospital, Tampere, Finland

<sup>5</sup>Department of Obstetrics and Gynecology, Tampere University Hospital, Tampere, Finland

<sup>6</sup>Johan Gadolin Process Chemistry Centre, Åbo Akademi University, Åbo, Finland

<sup>7</sup>Biomaterials and Tissue Engineering Group, BioMediTech, Faculty of Medicine and Health Technology, Tampere University, Tampere, Finland

**Correspondence**

Kaisa Vuornos, Adult Stem Cell Group, BioMediTech, Faculty of Medicine and Health Technology, Tampere University, P.O. BOX 100, FI-33014 Tampere, Finland.  
Email: kaisa.vuornos@tuni.fi

**Abstract**

Lack of bone grafts appeals for bone augmentation solutions. We aimed at osteogenic differentiation of human adipose stem cells (hASCs) and microvascularization in coculture with human umbilical vein endothelial cells (HUVECs) embedded in three-dimensional (3D) gellan gum (GG) and collagen type I (COL) hydrogel mixture. We compared endothelial growth medium-2 (EGM-2) and bioactive glass extract-based endothelial and osteogenic medium (BaG EM-OM) for vascularized bone-like graft development *in vitro*. Cell viability, cell number, and osteogenic and endothelial gene expression were analyzed. Mineralized hydroxyapatite residues, immunocytochemical staining of endothelial marker CD31 production and late osteogenic marker osteocalcin were imaged. With both media, good cell viability was observed within 3D hydrogel. EGM-2 condition induced significantly higher cell number compared to BaG EM-OM condition at both 7 and 14 days. Interestingly, both media supported osteogenic as well as endothelial marker gene expression. Moreover, formation of reticulated cellular structures was observed in both EGM-2 and BaG EM-OM conditions. However, hydroxyapatite mineralization and strong osteocalcin staining were detected only in BaG EM-OM condition. Importantly, strong production of CD31 and elongated tube-like structures were apparent in EGM-2 culture alone. In conclusion, we demonstrated efficient hASC osteogenic differentiation and microvessel-like network formation in coculture with HUVECs.

**KEYWORDS**

adipose stem cell, bioactive glass, collagen type I hydrogel, gellan gum hydrogel, human umbilical vein endothelial cell, osteogenic differentiation, vascularization

**1 | INTRODUCTION**

There is an unmet need for bone augmentation solutions due to growth of aging population and increasing number of musculoskeletal defects (Przekora, 2019). In addition, lack of bone grafts is growing because autologous bone is limited in supply and its harnessing might involve complications (Chatterjea, Meijer, van Blitterswijk, & de Boer, 2010). Consequently, engineered tissue grafts present an attractive alternative.

In addition, sufficient *in vitro* prevascularization of tissue-engineered constructs is needed to support graft survival. Moreover, *in vitro* microvascularization has been reported to support rapid ingrowth of host tissue vasculature to ensure graft viability after implantation (Laschke & Menger, 2016). Previously, abundant and readily available human adipose stem cells (hASCs) have been shown applicable for bone augmentation (Lindroos, Suuronen, & Miettinen, 2011). What is more, coculture of mesenchymal stem cells with human umbilical vein endothelial cells

(HUVECs) has been deemed relevant to formation of vascular-like structures (Kang, Kim, Fahrenholtz, Khademhosseini, & Yang, 2013; Mihaila, Resende, Reis, Gomes, & Marques, 2017; Pill et al., 2018). Furthermore, coculture of osteoblastic cells with endothelial cells has been proven feasible for prevascularization of bone-like grafts (Laschke & Menger, 2016; Mihaila et al., 2017). On the other hand, three-dimensional (3D) cell culture in hydrogels offers stem cells a microenvironment mimicking the natural. Indeed, according to reports, collagen type I (COL) and polysaccharide gellan gum (GG) are besides biocompatible and bioresorbable hydrophilic natural polymer hydrogels, also suited to bone and vascularization applications (Gantar et al., 2014; Koivisto et al., 2019; Manda et al., 2018; Marelli et al., 2011; Oliveira, Custodio, Gasperini, Reis, & Mano, 2016). Also, injectable hydrogel biomaterials facilitate minimally invasive procedures thus avoiding risks of adverse complications (Kondiah et al., 2016). Additionally, bioactive glasses (BaGs) have been shown besides fitting for medical bone implants (Jones, 2015), also to induce bone tissue vascular network formation (Bi et al., 2013). Furthermore, soluble ion species of BaG extracts have been shown to promote strong osteogenic differentiation of hASCs in 2D cell culture (Ojansivu et al., 2015), and in addition, uniform mineralization distribution within 3D hydrogels (Vuornos et al., 2019). Moreover, osteogenic priming by osteogenic medium (OM) culture prior to cell seeding has been reported to enhance hASC osteogenesis (Mihaila et al., 2017). Therefore, our aim was to enhance hASC osteogenic differentiation while, at the same time, support formation of microvascularization in coculture with HUVECs within 3D GG-COL composite hydrogels. Furthermore, we compared endothelial cell growth medium-2 (EGM-2) and bioactive glass 2-06 extract-based endothelial and osteogenic medium (BaG EM-OM) for efficacious hASC osteogenic differentiation and HUVEC coculture along with osteogenic conditioning of hASCs for *in vitro* prevascular network and mineralized matrix formation within 3D GG-COL hybrid hydrogels.

## 2 | MATERIALS AND METHODS

### 2.1 | Materials preparation

#### 2.1.1 | Gellan gum hydrogel

For the preparation of 0.5% w/v GG hydrogel, GG powder (Mw 1,000 g/mol; Gelzan CM; Merck, Kenilworth, NJ) was dissolved into 10% w/v sucrose (BioXtra; Merck) in deionized water with a magnetic stirrer overnight. After dissolving, the GG solution was heated to +60°C on a heat plate and sterile filtered (Acrodisc 0.2 µm syringe filters with Supor polyethersulfone membrane, Pall Corporation, Port Washington, NY). GG was physically crosslinked with 16% v/v bioamine spermidine trihydrochloride (SPD, BioXtra; Merck) of 0.1% w/v concentration. The 0.1% w/v SPD solution was prepared into 10% w/v sucrose (BioXtra; Merck) in deionized water and sterile filtered (Acrodisc 0.2 µm).

#### 2.1.2 | Collagen type I hydrogel

Rat tail collagen type I (COL; Gibco; Thermo Fisher Scientific, Waltham, MA) hydrogel solution of 3 mg/ml concentration was neutralized with

1 N NaOH (Sigma; Merck) and 10× PBS (Lonza, Basel, Switzerland) according to manufacturer protocol and prepared by manual mixing by pipetting at +4°C while kept on ice.

### 2.1.3 | Composite gellan gum-collagen type I hydrogel scaffolds

Prior to cell encapsulation, the 0.5% w/v GG hydrogel solutions and 0.1% w/v SPD crosslinker solutions were heated to +37°C on a heat plate. The 3 mg/ml COL hydrogel solution was kept on ice at +4°C. For cell encapsulation, hASCs resuspended into MM and HUVECs resuspended into EGM-2 were mixed in 1:1 ratio for final cell concentration of  $1 \times 10^6$  cells/ml. Following centrifugation, the combined cell pellet was resuspended into either GG or COL hydrogel solution by manual mixing by pipetting. The cell-laden GG hydrogel solution was manually mixed by pipetting with 16% v/v SPD and with cell-laden COL hydrogel solution in 1:1 volume ratio for a total volume of 0.2 cm<sup>3</sup>. The composite GG-COL hydrogel scaffolds with embedded hASCs and HUVECs were cast into 48-well plate wells (Nunclon; Merck), followed by immediate gelation, and after which 0.3 cm<sup>3</sup> of according media were added on top.

### 2.2 | Mechanical testing

For mechanical compression testing, cell-free GG and COL hydrogel solutions in 1:1 volume ratio together with 16% v/v of SPD crosslinker solution were manually mixed by pipetting for a total volume of 0.875 cm<sup>3</sup> GG-COL composite hydrogel scaffolds. The mechanical compression testing of acellular GG-COL hydrogel scaffolds of approximate height of 5.0 mm and of 12.2 mm cross-section diameter cast in cut syringe (BD Biosciences, Franklin Lakes, NJ) molds was performed by unconfined compression rate, as previously described (Vuornos et al., 2019), at 0, 7, and 14 days of incubation in EGM-2 (Lonza, Basel, Switzerland) or BaG EM-OM media (Table 1). The Young's modulus was determined based on the Hooke's law (Koivisto et al., 2017).

### 2.3 | Cell isolation

Human ASCs of three female donors of 52, 56, and 60 years of age were obtained with the patients' written informed consent at the Tampere University Hospital Department of Plastic Surgery together with the favorable opinion of the Regional Ethics Committee of the Expert Responsibility area of Tampere University Hospital, Tampere, Finland (R15161). Adipose tissue was cut and digested as previously reported (Kyllonen et al., 2013). The hASCs were either expanded in maintenance medium (MM) or primed with osteogenic medium (OM; see Table 1). The flow cytometric analysis indicated the mesenchymal origin of the hASCs (Dominici et al., 2006; see Supporting Information S1).

HUVECs were obtained from 1 donor of 38 years in planned cesarean section at the Tampere University Hospital with the patient's written informed consent together with the favorable opinion of the Regional Ethics Committee of the Expert Responsibility area of Tampere University Hospital, Tampere, Finland (R13019), and isolated



**TABLE 1** Media compositions

Medium	Composition
Maintenance medium (MM)	$\alpha$ -MEM, 5% HS, 1% P/S
Osteogenic medium (OM)	5 nM Dex, 250 $\mu$ M AsA2P, 10 mM $\beta$ -GP in MM
Endothelial cell growth medium-2 (EGM-2)	2% HS, hEGF*, VEGF*, R3-IGF-1*, ascorbic acid*, hydrocortisone*, hFGF- $\beta$ *, 0.1% GA* in EBM-2 media base
BaG endothelial-osteogenic medium (BaG EM-OM)	5% HS, 5 nM Dex, 250 $\mu$ M AsA2P, 10 mM $\beta$ -GP in BaG EM ext

Abbreviations: \*indicates EGM-2 SingleQuots supplement (Lonza); AsA2P, L-ascorbic acid 2-phosphate (Merck); BaG EM ext, endothelial basal medium bioactive glass 2-06 extract; BaG EM-OM, bioactive glass 2-06 extract endothelial-osteogenic medium; Dex, dexamethasone (Merck); EBM-2, endothelial cell growth basal medium-2 (Lonza); EGM-2, endothelial cell growth medium-2 (Lonza); GA, gentamicin/amphotericin-B (Lonza); hEGF, human epidermal growth factor (Lonza); hFGF- $\beta$ , human fibroblast growth factor-beta (Lonza); HS, human serum (Biowest, Nuailé, France); MM, maintenance medium; OM, osteogenic medium; P/S, 100 U/ml penicillin/streptomycin (Lonza); R3-IGF-1, R3-insulin-like growth factor-1 (Lonza); VEGF, vascular endothelial growth factor (Lonza);  $\alpha$ -MEM, minimum essential medium-alpha (Gibco);  $\beta$ -GP, beta-glycerophosphate (Merck).

according to a previously reported method (Jaffe, Nachman, Becker, & Minick, 1973). Briefly, umbilical vein was rinsed with collagenase type II (1.0 mg/ml; Merck) in EBM-2 (Endothelial cell growth basal medium-2, Lonza) containing 2% P/S and 0.1% gentamicin/amphotericin-B (30  $\mu$ g/ml gentamicin; 15 ng/ml amphotericin-B; Lonza; EGM-2 SingleQuots supplements). HUVECs were expanded in EGM-2 medium prepared according to manufacturer's instructions with SingleQuots supplements (Lonza) except that 2% human serum (HS) was used.

## 2.4 | Osteogenic priming

Seven-day osteogenic priming of hASCs in selected experiment groups was initiated by OM culture in cell culture flasks prior to cell seeding. Nonprimed hASCs were expanded in MM.

## 2.5 | Cell culture and cell differentiation

Osteogenic differentiation and formation of microvascularization were induced immediately after plating by adding either EGM-2 or BaG EM-OM to the cell-laden hydrogel samples. Coculture of cells consisted of hASCs and HUVECs in 1:1 ratio (Mihaila et al., 2017) with  $5 \times 10^5$  HUVECs/ml and  $5 \times 10^5$  hASCs/ml for a total cell density of  $1 \times 10^6$  cells/ml. The hASCs and HUVECs were encapsulated into nongelated GG and COL hydrogels. GG and COL cell-laden hydrogels were manually mixed in 1:1 volume ratio of 0.2 cm<sup>3</sup> total volume and cast into 48-well plate wells, followed by immediate gelation, and after which 0.3 cm<sup>3</sup> of according media were added on top.

The endothelial basal medium bioactive glass 2-06 extract (BaG EM ext) was prepared from bioactive glass 2-06 (wt %: Na<sub>2</sub>O 12.1; K<sub>2</sub>O 14.0; CaO 19.8; P<sub>2</sub>O<sub>5</sub> 2.5; B<sub>2</sub>O<sub>3</sub> 1.6; SiO<sub>2</sub> 50.0; Vuornos et al., 2019). Briefly, ethanol washed BaG granules (87.5 mg/ml; 500–1,000  $\mu$ m) were incubated 24 hr at +37°C in EBM-2 with 0.1% gentamicin/amphotericin-B. For the BaG EM-OM, 5% HS and osteogenic supplements were added to the BaG EM ext (see Table 1). Media were changed every other day.

## 2.6 | Cell viability and cell number

Live/Dead analysis (Thermo Fisher Scientific, Waltham, MA) was performed as reported (Tirkkonen et al., 2013) and samples imaged with Olympus IX51 microscope (Olympus, Tokyo, Japan). Total amount of DNA was measured by CyQUANT cell number analysis (Thermo Fisher Scientific) according to manufacturer's protocol. Briefly, cell lysis with 0.1% Triton X-100 buffer (Merck) was followed by mechanical homogenization with Ultra-Turrax tissue homogenizer (IKA Labortechnik, Staufen, Germany). After a freeze–thaw cycle, fluorescence of three parallel samples was measured with a microplate reader (PerkinElmer, Waltham, MA).

## 2.7 | Quantitative real-time polymerase chain reaction

The relative expression of osteogenic and endothelial marker genes was analyzed with quantitative real-time polymerase chain reaction (qRT-PCR) method. Total RNA was isolated using the NucleoSpin RNA II kit (Macherey-Nagel, Düren, Germany), according to the kit protocol. First-strand cDNA of total RNA was synthesized with High-Capacity cDNA Reverse Transcriptase Kit (Applied Biosystems, Foster City, CA). The gene expression of *runx-related transcription factor 2* (*RUNX2*, Oligomer, Helsinki, Finland), *distal-less homeobox 5* (*DLX5*, Oligomer), *osterix* (*OSX*, Oligomer), *Von Willebrand Factor* (*VWF*, QuantiTect Primer Assays; 10x; Qiagen, Hilden, Germany) and *platelet endothelial cell adhesion molecule-1* (*PECAM-1*, QuantiTect Primer Assays) was measured. For calculation of relative gene expression of each sample of 50 ng cDNA, 300 nM forward and reverse primers, and SYBR Green PCR Master Mix (Applied Biosystems) in relation to *human ribosomal protein lateral stalk subunit P0* (*RPLP0*, Oligomer) housekeeping gene, a mathematical data analysis model was applied (Pfaffl, 2001), and the measured data was normalized (Fink et al., 2008; Gabrielsson et al., 2005). The primer sequences are listed in Table 2. The ABI PRISM 7300 Sequence Detection System (Applied Biosystems) was used to analyze qRT-PCR reactions at +95°C for 10 min enzyme activation, followed by 15 s denaturation in 45 cycles at +95°C, and by 60 s of annealing and extension at +60°C.

## 2.8 | Immunocytochemistry

About 4% paraformaldehyde (PFA; Merck) was used to fix samples. In the following, cellular samples were blocked for 6 hr in +4°C in blocking solution of 10% goat serum (GS; Thermo Fisher Scientific), 0.1%

Name	Primer	5'-Sequence-3'	Product size (bp)	Accession number
RPLP0	Fwd	AATCTCCAGGGGCACCATT	70	NM_001002
	Rev	CGCTGGCTCCCACTTTGT		
DLX5	Fwd	ACCATCCGTCTCAGGAATCG	75	NM_005221.5
	Rev	CCCCCGTAGGGCTGTAGTAGT		
OSX	Fwd	TGAGCTGGAGCGTCATGTG	79	NM_152860.1
	Rev	TCGGGTAAGCGCTTGA		
RUNX2	Fwd	CTTCATTGCCTCACAACAAC	62	NM_001024630.3
	Rev	TCCTCCTGGAGAAAGTTTGCA		
PECAM-1	Fwd	AAGTGAGTCCAGCCGCATATC	133	NM_000442.4
	Rev	ATGGAGCAGGACAGTTCAGTC		
VWF	Fwd	AGAAACGCTCCTTCTCGATTATTG	84	NM_000552
	Rev	TGTCAAAAAATCCCAAGATACAC		

**TABLE 2** The primer sequences for qRT-PCR

Triton X-100, and 1% bovine serum albumin (BSA; Merck) in PBS (Lonza). After washes with a solution of 0.1% Triton X-100 buffer, 1% GS, and 1% BSA, the samples were incubated in similar solution with 1:25 polyclonal IgG rabbit anti-osteocalcin antibody (Bio-Rad, Hercules, CA) and 1:20 monoclonal mouse anti-CD31 (Dako, Glostrup, Denmark) for 48 hr in +4°C (Koivisto et al., 2017). Next, secondary antibodies Alexa Fluor 488 goat anti-mouse IgG 1:200 (Thermo Fisher Scientific) and Alexa Fluor 594 goat anti-rabbit IgG 1:100 (Thermo Fisher Scientific) were incubated for 24 hr in +4°C, followed by DAPI 1:2000 (Merck) staining of nuclei. The cell-free control GG-COL hydrogel samples were similarly treated with either both primary and secondary antibodies or with secondary antibodies alone. Z-stacks from the middle of the samples were scanned through high precision #1.5 cover glasses (Carl Zeiss, Oberkochen, Germany) with confocal LSM 780 microscope (Carl Zeiss).

## 2.9 | Mineralization

The hydroxyapatite residues of cellular samples along with cell-free controls were stained with Osteolmage assay according to kit protocol (Osteolmage Mineralization Assay; Lonza) (Castillo Diaz, Elsayy, Saiani, Gough, & Miller, 2016; Vuornos et al., 2019). Following sample fixing with 4% PFA (Merck) for 30 min in RT, the samples were stained for 45 min with kit hydroxyapatite fluorescence stain and the cell nuclei with DAPI 1:2,000. The samples were imaged with Olympus IX51 microscope.

## 2.10 | Statistical analysis

The significance of differences between mean ranks for equal distributions was determined using Mann-Whitney U test for statistical significance with  $p$ -values <0.05. For the mechanical testing results, three parallel samples were tested in each experiment group ( $n = 3$ ). The cell number analyses were repeated with three different hASC donors with three samples for each condition ( $n = 9$ ). The gene expression analyses were repeated for three different hASC donors

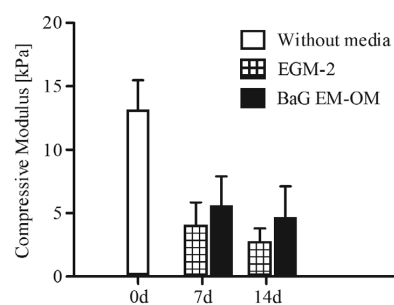


**FIGURE 1** Hydrogel compressive moduli. Acellular GG-COL hydrogel sample mechanical testing at 0 days without media, and after 7 and 14 days of EGM-2 or BaG EM-OM media incubation ( $n = 3$ ). Data are presented as mean + SD

( $n = 3$ ). The data were analyzed with IBM SPSS Statistics 23 software (IBM, Armonk, NY).

## 3 | RESULTS

### 3.1 | Hydrogel scaffold mechanical properties

The acellular GG-COL hydrogel samples were mechanically tested by compression testing at 0, 7, and 14 days (Figure 1).

The results demonstrated the degradation of GG-COL mechanical properties over 2 weeks where the decrease of the compressive moduli was more moderate for the BaG EM-OM media incubated samples.

### 3.2 | Cell viability

Most hASCs and HUVECs remained viable encapsulated in 3D GG-COL hydrogel over 2 weeks with only few necrotic cells (Figure 2).

Live/dead staining showed the cell morphologies in different conditions. In EGM-2 culture regardless of preconditioning status, the hASCs and HUVECs elongated and formed reticulated structures,

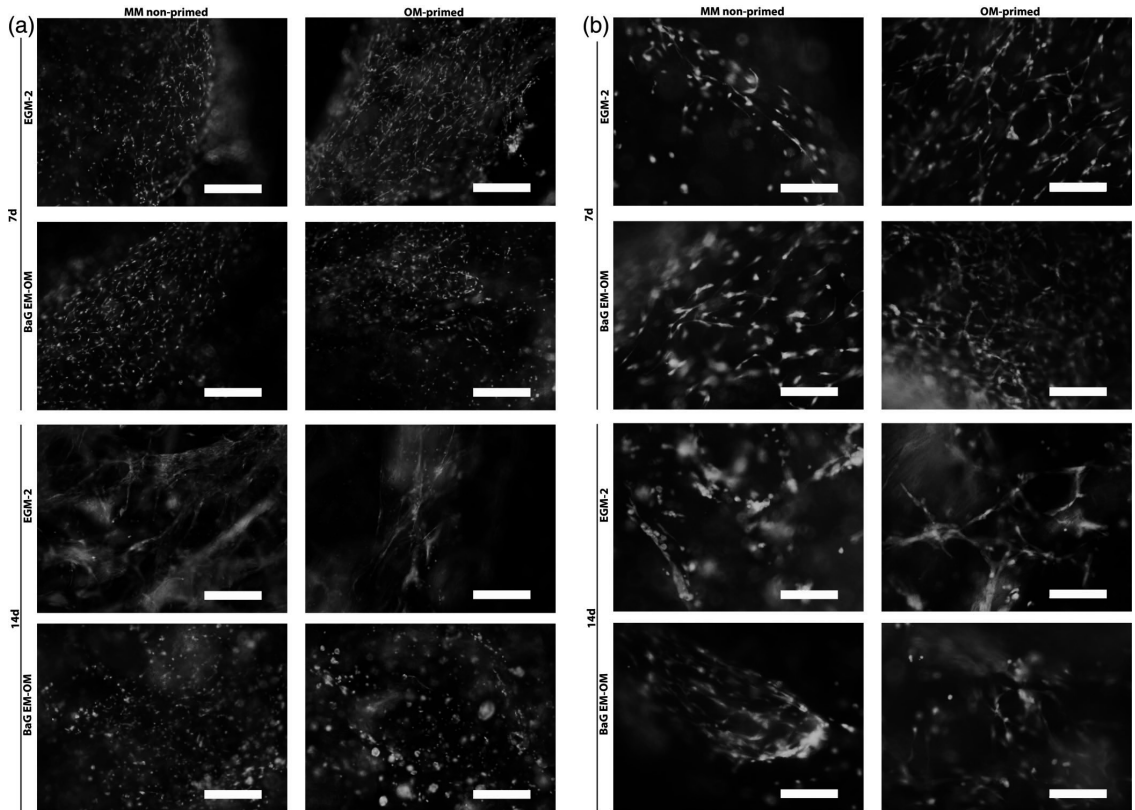


**FIGURE 2** Cell viability. Viability of hASCs and HUVECs within 3D hydrogels cultured with EGM-2 or BaG EM-OM media for 7 and 14 days (living cells stained green; necrotic cells stained red). (a) Imaged with 4× objective. Scale bar 500 μm; (b) imaged with 10× objective. Scale bar 200 μm. The hASCs were OM-primed or nonprimed (MM) prior to cell encapsulation into hydrogels. Representative images with hASCs from 2 donors and HUVECs from 1 donor

whereas the BaG EM-OM culture-induced truncated cell shapes without any elongated cellular structures formed.

### 3.3 | Cell number

The combined EGM-2 (MM) and EGM-2 (OM) cell numbers were significantly higher compared to the combined BaG EM-OM (MM) and BaG EM-OM (OM) cell numbers at 7 days (Figure 3). At 14-day time point, the combined EGM-2 (MM) and EGM-2 (OM) cell numbers were significantly higher compared to the combined BaG EM-OM (MM) and BaG EM-OM (OM) cell numbers, which showed no significant increase in cell amount from 7 to 14 days. The combined cell amount results of EGM-2 (MM) and EGM-2 (OM) conditions at 14 days were significantly higher compared to the combined cell amounts of EGM-2 (MM) and EGM-2 (OM) conditions at 7 days.

### 3.4 | Gene expression

For the osteogenic markers, the gene expression of *DLX5* peaked at 14 days for the BaG EM-OM condition with the highest medians with both

OM-primed and nonprimed hASCs (Figure 4). The gene expression of *RUNX2* peaked with the highest medians for the EGM-2 (OM) condition at 7 and 14 days. For *OSX* gene expression, the peak in gene expression at 7 days was elevated in the EGM-2 (MM) condition and peaked also in EGM-2 (OM) at both 7 and 14 days. *OSX* gene expression median for the BaG EM-OM (OM) condition was equally elevated at 7 days. The highest peak of *VWF* endothelial marker gene expression was detected for the BaG EM-OM (OM) condition at 14 days, whereas gene expression of late endothelial marker *PECAM-1*, or also known as *CD31*, showed high values for individual hASC donors in the EGM-2 (OM) condition at 7 days and BaG EM-OM (MM) at 14 days. The gene expressions were relativized to the gene expression of the EGM-2 (MM) samples at 7 days. Exceptionally, the *PECAM-1* gene expression was relativized to a single 7-day value of EGM-2 (MM) sample gene expression due to below threshold values.

### 3.5 | Osteocalcin and CD31 production

Immunocytochemical staining results of osteocalcin, CD31, and DAPI within GG-COL hydrogel in different media conditions at 14 days are shown in Figure 5.

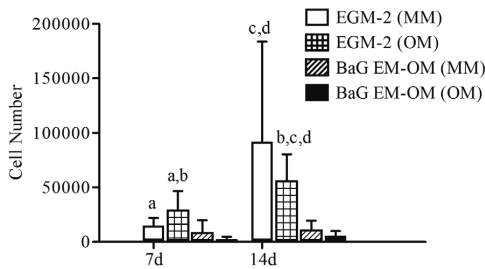


**FIGURE 3** Cell number. Cell number based on total DNA content of hASCs and HUVECs within 3D GG-COL hydrogels cultured with EGM-2 or BaG EM-OM media for 7 and 14 days. The hASCs were OM-primed (OM) or nonprimed (MM). The analyzed three parallel samples for three separate experiment repeats contained hASCs from three donors and HUVECs from one donor ( $n = 9$ ). Data are presented as mean + SD. Significant difference with  $p < .05$ . (a) The combined EGM-2 (MM) and EGM-2 (OM) cell numbers were significantly higher compared to the combined BaG EM-OM (MM) and BaG EM-OM (OM) cell numbers at 7 days ( $p = .026$ ); (b) The combined EGM-2 (OM) cell numbers at 7 and 14 days were significantly higher compared to the combined BaG EM-OM (OM) cell numbers at 7 and 14 days ( $p = .002$ ); (c) The combined EGM-2 (MM) and EGM-2 (OM) cell numbers were significantly higher compared to the combined BaG EM-OM (MM) and BaG EM-OM (OM) cell numbers at 14 days ( $p = .002$ ); (d) The combined EGM-2 (MM) and EGM-2 (OM) cell numbers at 14 days were significantly higher compared to the combined EGM-2 (MM) and EGM-2 (OM) cell numbers at 7 days ( $p = .015$ )

Strong osteocalcin staining was seen in both the BaG EM-OM conditions with even more accentuated osteocalcin production with the OM-primed hASCs. Abundant tubular-like structures and vessel-like networks with strong endothelial marker CD31 production were seen in the EGM-2 conditions alone.

### 3.6 | Hydroxyapatite mineralization

The hASC mineralized matrix hydroxyapatite residues were stained with the OsteoImage assay and the cell nuclei with DAPI in 3D hydrogels at 14 days (Figure 6).

There was no visible OsteoImage hydroxyapatite staining result and no background detected for either of the EGM-2 media conditions. Strong hydroxyapatite staining was seen in both of the BaG EM-OM media conditions while some background was visible in the cell-free blank samples. The strongest hydroxyapatite staining was observed in the BaG EM-OM (OM) condition at 14 days.

## 4 | DISCUSSION

Due to current pressing need for tissue engineered vascularized bone grafts, we studied the effect of soluble BaG ions for osteogenic differentiation of hASCs and formation of microvasculature in coculture with HUVECs in 3D hydrogel culture. Further, we compared endothelial culture media and combined endothelial and BaG ext based

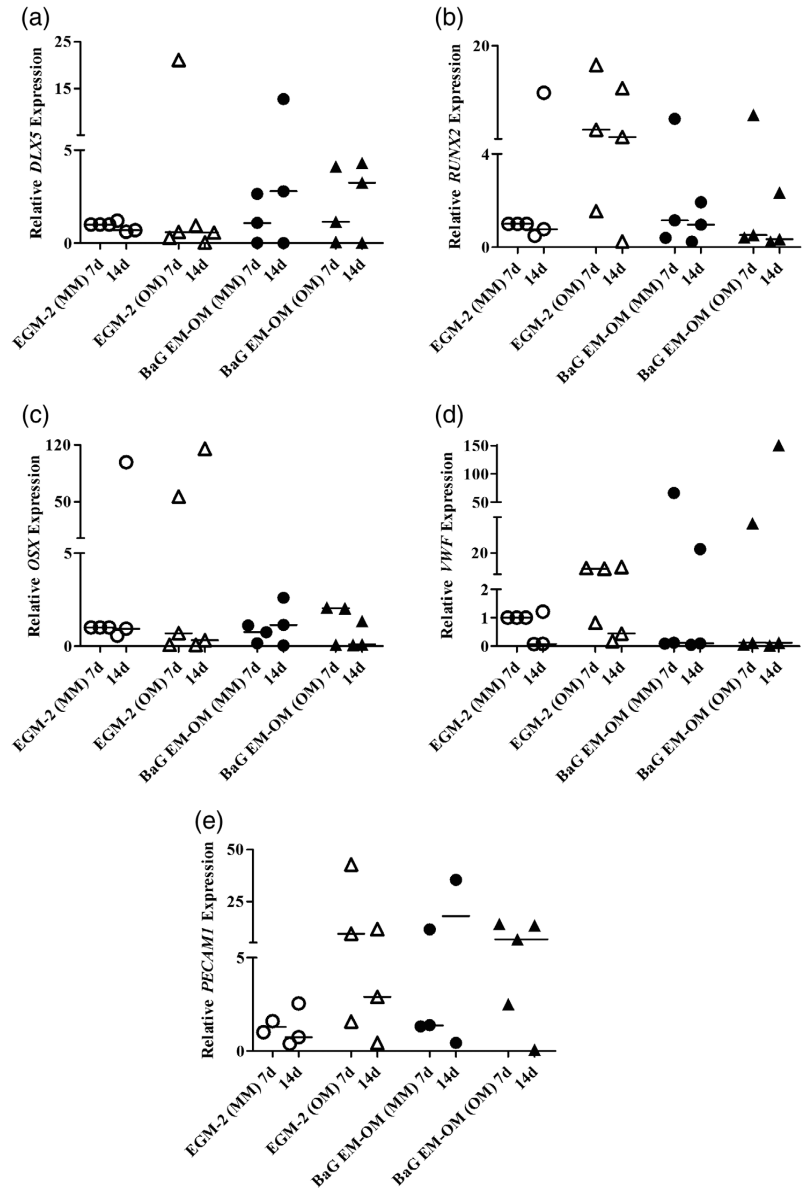
osteogenic media induction, as well as investigated the impact of osteogenic preconditioning for efficient hASC osteogenesis. Presently, there is a keen interest in ions released from BaGs since they are thought to induce the formation of a bioactive hydroxycarbonate apatite layer in contact with physiological fluids thus forming a strong chemical interface with bone tissue (Hench & Wilson, 1986; Jones, 2015; Kargozar, Baino, Hamzehlou, Hill, & Mozafari, 2018a; Rezwani, Chen, Blaker, & Boccaccini, 2006). Moreover, silica and calcium ions dissolved from BaGs are thought to stimulate osteogenic cells to produce bone matrix (Jones, 2015) and possibly to upregulate proangiogenic vascular endothelial growth factor (VEGF) production together with released boron ion (Kargozar, Baino, Hamzehlou, Hill, & Mozafari, 2018b). Furthermore, various bioactive ions released from different BaG compositions and constructs possess vast potential for controlled local delivery of therapeutic agents, among others (Kargozar et al., 2018a; Rezwani et al., 2006). Previously, soluble BaG ions have been proven to induce robust hASC osteogenic differentiation without added chemical supplements (Ojansivu et al., 2015; Vuornos et al., 2019), and importantly, to promote neovascularization (Gorustovich, Roether, & Boccaccini, 2010). However, the attempts to combine simultaneous osteogenic and endothelial commitment of cells especially within 3D matrix have been limited by the contrasting effects of the mineralization and vascular growth processes and challenges connected to hydrogel stability (Unger, Dohle, & Kirkpatrick, 2015). Therefore, we aspired to harness the potential of ionic BaG dissolution products along with osteogenic and endothelial media induction together with hASC and HUVEC cellular crosstalk for efficient mineralization and microvascularization in 3D hydrogel *in vitro* culture for bone-like graft prevascularization.

The hydrogel scaffold mechanical properties influence cell functionality (Haugh, Murphy, McKiernan, Altenbuchner, & O'Brien, 2011). We tested composite GG-COL hydrogels to resist cellular contraction, which has limited feasibility of COL for *in vitro* tissue engineering applications (Marelli et al., 2011). Although the mechanical properties degraded over 2 weeks of media incubation, the moduli decreased less in the BaG EM-OM condition, thus confirming our previous results on the supporting effect of BaG ext based media on hydrogel mechanical properties (Vuornos et al., 2019). According to current literature, the modulus of forming osteoblastic matrix is approximately 30 kPa (Huebsch et al., 2010), and therefore higher than the one measured in the BaG EM-OM condition, whereas for HUVEC capillary-like network formation, the moduli range of 1–3 kPa at 2 weeks of EGM-2 incubated hydrogels indicated soft and malleable hydrogel scaffolds suitable for *in vitro* prevascular network formation (Sieminski, Was, Kim, Gong, & Kamm, 2007).

Cell viability analysis result attested of good hASC and HUVEC cosurvival in both media conditions, and with osteogenic preconditioning. Cell elongation and alignment into tubular-like structures were clearly visible in EGM-2 coculture. Importantly, the Live/Dead images displayed reticulated cellular structures in all the experiment groups thus indicating cellular crosstalk in coculture. Further, significantly lower cell amount was detected in the BaG EM-OM conditions compared to the EGM-2 conditions at both 7 and 14 days. As previously

**FIGURE 4** Gene expression.

Gene expression of osteogenic and endothelial marker genes of hASCs and HUVECs within 3D hydrogels cultured with EGM-2 or BaG EM-OM media for 7 and 14 days. The hASCs were OM-primed or nonprimed (MM). Significant difference with  $p < .05$ . Relative gene expression of (a) *DLX5*; (b) *RUNX2*; (c) *OSX*; (d) *VWF*; (e) *PECAM-1*. Results relativized to control condition of EGM-2 (MM) at 7 days. The experiment was repeated three times with hASCs from three donors ( $n = 3$ ) and HUVECs from one donor. Horizontal line indicates group median



reported, the decrease of cell number has been associated with borosilicate BaG ionic species induced restriction of cell proliferation and accompanying strong osteogenesis (Ojansivu et al., 2018). Moreover, boron ion induced effect on cell morphology has also been indicated by previous research (Brown et al., 2009; Rodriguez, Gonzalez, Rios, & Cambiasso, 2004), together with observed changes to cytoskeleton, cell adhesion, and signaling pathways (Ojansivu et al., 2015, 2018). To the point, we observed a similar effect with borosilicate bioactive glass 2-06 based BaG EM-OM condition with strong osteocalcin production along with cubic cell morphology producing less oriented structures and

truncated tubular growth. In comparison in the EGM-2 condition, the good cell viability along with elongated cell morphologies, high cell number, oriented capillary-like structures, and vascular-like network growth indicated microvascularization formation resulting into the main result of the compared 3D GG-COL coculture conditions.

The gene expression of osteogenic marker genes showed that the BaG EM-OM conditions supported the highest median peaks of *DLX5* gene expression at 2 weeks, similarly with our earlier report on the osteogenic effect of BaG ext conditioned endothelial media on mesenchymal stem cell and HUVEC coculture gene expression in 2D

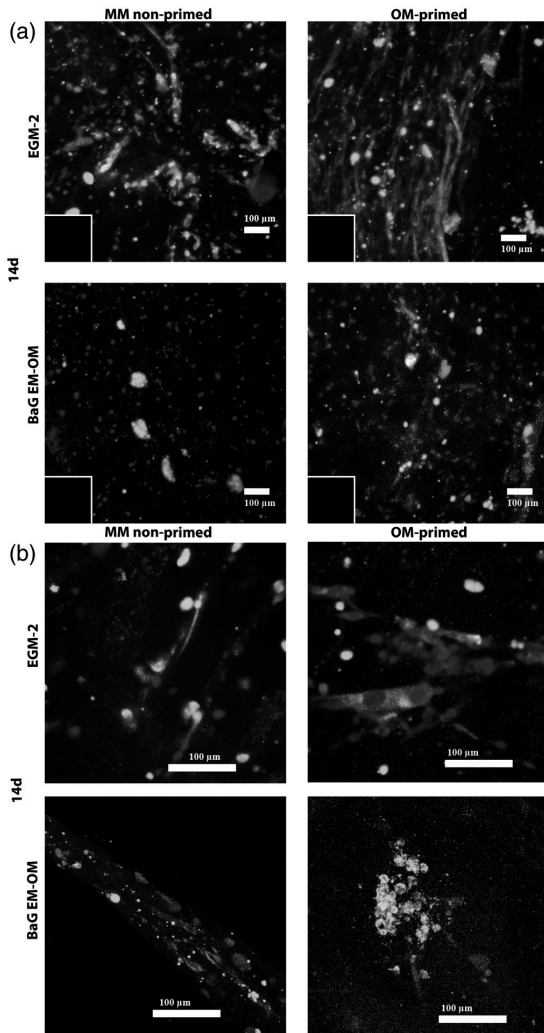


**FIGURE 5** Osteocalcin and CD31 immunofluorescence staining. Representative images of osteocalcin (red), CD31 (green), and DAPI (blue) stained hASCs and HUVECs within GG-COL 3D hydrogels with EGM-2 and BaG EM-OM media at 14 days. (a) Imaged with 10 $\times$  objective. Scale bar 100  $\mu$ m. Blank controls in lower left corner; (b) Imaged with 25 $\times$  objective. Scale bar 100  $\mu$ m. The hASCs were OM-primed or nonprimed (MM). The hASCs were isolated from two donors and HUVECs from one donor

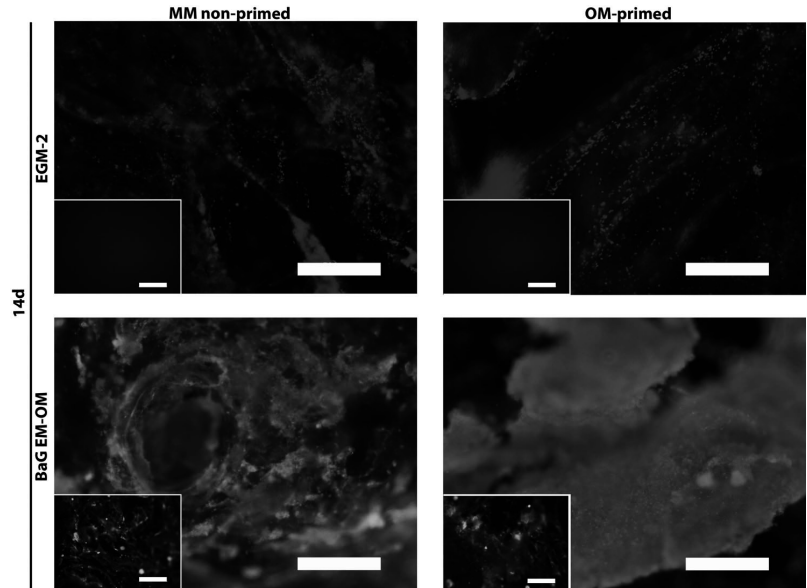
(Nunez-Toldra et al., 2019). Interestingly, also EGM-2 (OM) condition induced a single elevated peak of *DLX5* gene expression at 1 week, together with a consistently higher trend at 7 and 14 days of *RUNX2* osteogenic marker gene expression, whereas for *OSX* gene expression the trend was less clear, although separate peak values were detected with OM-primed hASCs in both media conditions, thus contesting Mihaila et al. (2017) report on lack of osteogenic differentiation in hASC and endothelial cell coculture with EGM-2 media despite

osteogenic preconditioning. Contrastingly, the BaG EM-OM condition induced endothelial marker *VWF* gene expression including the highest peak with OM-primed hASCs at 14 days. Indeed, similar upregulation of hASC *VWF* expression by borosilicate BaG ion stimulation has been reported by Ojansivu, Mishra, et al. (2018). The elevated endothelial gene expression of coculture samples even in the strong osteogenesis inducing BaG EM-OM condition might be in part due to hASC endothelial subpopulation, previously indicated by Mihaila et al., (2017) and Huttala et al. (2015). Importantly, gene expression of *PECAM-1*, or *CD31*, showed elevated values with hASCs from individual donors in the EGM-2 (OM) condition and in both the BaG EM-OM conditions.

The immunofluorescence imaging results showed that the BaG EM-OM condition was required for strong osteocalcin production, whereas the EGM-2 condition supported strong CD31 production and vessel-like structure formation, similarly to a report by Ma et al. (2014). While various in vitro approaches for vascularized hydrogel constructs have been explored (Cerqueira et al., 2014; McCoy, Seo, Choi, & Fischbach, 2016), importantly for novelty, we produced capillary-like growth in 3D GG-COL composite hydrogel with the added mechanical stability offered by GG compared to COL alone (Vuornos et al., 2019). Importantly for novelty, the efficient BaG EM-OM osteogenic capacity was further demonstrated by strong staining of cell-secreted mineralized matrix hydroxyapatite residues in both the BaG EM-OM media conditions, and even accentuated with OM preconditioning of hASCs. As expected, no mineralization was visible in EGM-2 culture, possibly due to lack of any CaP source (Roschger, Paschalis, Fratzl, & Klaushofer, 2008; Veis & Dorvee, 2013). Although some background was detected in cell-free blank samples, and most likely due to known effect of COL hydrogel as COL fibrils function as a natural matrix for CaP apatite precipitation (Veis & Dorvee, 2013), the hydroxyapatite staining was visibly stronger in the cell-laden BaG EM-OM samples. This testified further that the BaG EM-OM condition supported efficient late osteogenic differentiation of hASCs. In this study for novelty value, we compared EGM-2 and BaG EM-OM for concomitant microvessel-like network formation and mineralization for prevascularized bone-like graft development in composite GG-COL hydrogels with hASC and HUVEC coculture. In addition, we tested the effect of osteogenic preconditioning of hASCs for enhanced osteogenesis. Importantly, we demonstrated efficient hASC osteogenic differentiation and formation of microvessel-like structures in coculture with HUVECs encapsulated in 3D GG-COL hydrogels. However, due to absence of endothelial marker CD31-stained vessel-like structures in the BaG EM-OM condition, it can be concluded that hydroxyapatite mineralization and late osteogenic differentiation excluded prevascular network formation. Consequently, this might indicate that the concomitant mineralization and microvascularization formation processes were mutually inhibited. Interestingly, some osteocalcin staining was nevertheless detected in the EGM-2 condition. Therefore, the EGM-2 condition supported moderate osteogenic differentiation which was even further enhanced by hASC osteogenic preconditioning, as indicated by osteogenic marker gene expression and modest osteocalcin production, and thus

## FIGURE 6 Mineralization.

Representative images of stained hydroxyapatite (green) residues and hASC and HUVEC nuclei (DAPI; blue) within 3D hydrogels with EGM-2 and BaG EM-OM media at 14 days. The hASCs were OM-primed or nonprimed (MM). Imaged with 4× objective. Scale bar 500 μm. Blank controls in lower left corner. The mineralization assay was conducted with hASCs from three donors and HUVECs from one donor, with 1–2 parallel samples



warranting more detailed research in the future. Furthermore, this highlighted the role of the chosen media for coculture where besides the cosurvival of both osteogenic and endothelial cells, also the growth of prevascular structures needs to be assured. Indeed, mixture of endothelial-osteogenic media has been assessed beneficial (Bidarra et al., 2011; Usami et al., 2009) for simultaneous osteogenic differentiation and prevascular network formation. However, the optimal composition of media for concomitant osteogenesis and microvascularization requires further study.

## 5 | CONCLUSIONS

Our study examined the effect of soluble cues provided by EGM-2 and BaG EM-OM with dissolved BaG ions for hASC differentiation in coculture with HUVECs embedded within composite GG-COL hydrogel scaffolds. All in all, our results showed that 3D GG-COL hydrogel coculture of hASCs and HUVECs with BaG ionic dissolution product containing osteogenic-endothelial media led to production of osteogenic and endothelial markers. Importantly, osteogenic preconditioning of hASCs intensified hydroxyapatite content of cell-secreted matrix in BaG EM-OM culture. The results showed that endothelial growth media was required for the formation of vessel-like structures mimicking microvasculature. In the future, the effect of dissolved BaG ions on microvessel-like network formation in 3D hydrogel culture would merit further research. To conclude, this study presented efficient hASC osteogenic differentiation and formation of microvessel-like structures in coculture with HUVECs encapsulated in 3D GG-COL composite hydrogels with potential for vascularized bone-like graft development.

## ACKNOWLEDGMENTS

The authors wish to thank Anna-Maija Honkala, Miia Juntunen, Mimmi Patrikoski, and Miina Ojansivu from the Adult Stem Cell Group for cell isolation and flow cytometric analysis, Janne T. Koivisto, Biomaterials and Tissue Engineering Group, BioMediTech, Faculty of Medicine and Health Technology, Tampere University, Tampere, Finland, for GG hydrogel and SPD solutions and consultation on hydrogel mechanical testing, Sari Kalliokoski, Anna-Maija Honkala, and Miia Juntunen for Adult Stem Cell Group technical laboratory expertise, and Tampere Imaging Facility (TIF) for expertise in imaging.

## CONFLICT OF INTEREST

No competing financial interests exist.

## ORCID

Kaisa Vuornos  <https://orcid.org/0000-0003-4731-3314>

## REFERENCES

- Bi, L., Rahaman, M. N., Day, D. E., Brown, Z., Samujh, C., Liu, X., ... Bonewald, L. F. (2013). Effect of bioactive borate glass microstructure on bone regeneration, angiogenesis, and hydroxyapatite conversion in a rat calvarial defect model. *Acta Biomaterialia*, 9(8), 8015–8026.
- Bidarra, S. J., Barrias, C. C., Barbosa, M. A., Soares, R., Amedee, J., & Granja, P. L. (2011). Phenotypic and proliferative modulation of human mesenchymal stem cells via crosstalk with endothelial cells. *Stem Cell Research*, 7(3), 186–197.
- Brown, R. F., Rahaman, M. N., Dwilewicz, A. B., Huang, W., Day, D. E., Li, Y., & Bal, B. S. (2009). Effect of borate glass composition on its

- conversion to hydroxyapatite and on the proliferation of MC3T3-E1 cells. *Journal of Biomedical Materials Research. Part A*, 88(2), 392–400.
- Castillo Diaz, L. A., Elsayw, M., Saiani, A., Gough, J. E., & Miller, A. F. (2016). Osteogenic differentiation of human mesenchymal stem cells promotes mineralization within a biodegradable peptide hydrogel. *Journal of Tissue Engineering*, 7, 2041731416649789.
- Cerqueira, M. T., da Silva, L. P., Santos, T. C., Pirraco, R. P., Correló, V. M., Marques, A. P., & Reis, R. L. (2014). Human skin cell fractions fail to self-organize within a gellan gum/hyaluronic acid matrix but positively influence early wound healing. *Tissue Engineering. Part A*, 20(9–10), 1369–1378.
- Chatterjea, A., Meijer, G., van Blitterswijk, C., & de Boer, J. (2010). Clinical application of human mesenchymal stromal cells for bone tissue engineering. *Stem Cells International*, 2010, 215625.
- Dominici, M., Le Blanc, K., Mueller, I., Slaper-Cortenbach, I., Marini, F., Krause, D., ... Horwitz, E. (2006). Minimal criteria for defining multipotent mesenchymal stromal cells. The International Society for Cellular Therapy position statement. *Cytotherapy*, 8(4), 315–317.
- Fink, T., Lund, P., Pilgaard, L., Rasmussen, J. G., Duroux, M., & Zachar, V. (2008). Instability of standard PCR reference genes in adipose-derived stem cells during propagation, differentiation and hypoxic exposure. *BMC Molecular Biology*, 9, 98.
- Gabrielsson, B. G., Olofsson, L. E., Sjogren, A., Jernas, M., Elander, A., Lonn, M., ... Carlsson, L. M. (2005). Evaluation of reference genes for studies of gene expression in human adipose tissue. *Obesity Research*, 13(4), 649–652.
- Gantar, A., da Silva, L. P., Oliveira, J. M., Marques, A. P., Correló, V. M., Novak, S., & Reis, R. L. (2014). Nanoparticulate bioactive-glass-reinforced gellan-gum hydrogels for bone-tissue engineering. *Materials Science & Engineering. C, Materials for Biological Applications*, 43, 27–36.
- Gorustovich, A. A., Roether, J. A., & Boccaccini, A. R. (2010). Effect of bioactive glasses on angiogenesis: A review of in vitro and in vivo evidences. *Tissue Engineering. Part B, Reviews*, 16(2), 199–207.
- Haugh, M. G., Murphy, C. M., McKiernan, R. C., Altenbuchner, C., & O'Brien, F. J. (2011). Crosslinking and mechanical properties significantly influence cell attachment, proliferation, and migration within collagen glycosaminoglycan scaffolds. *Tissue Engineering. Part A*, 17(9–10), 1201–1208.
- Hench, L. L., & Wilson, J. (1986). Biocompatibility of silicates for medical use. *Ciba Foundation Symposium*, 121, 231–246.
- Huebsch, N., Arany, P. R., Mao, A. S., Shvartsman, D., Ali, O. A., Bencherif, S. A., ... Mooney, D. J. (2010). Harnessing traction-mediated manipulation of the cell/matrix interface to control stem-cell fate. *Nature Materials*, 9(6), 518–526.
- Huttala, O., Vuorenmaa, H., Toimela, T., Uotila, J., Kuokkanen, H., Ylikomi, T., ... Heinonen, T. (2015). Human vascular model with defined stimulation medium—A characterization study. *ALTEX*, 32(2), 125–136.
- Jaffe, E. A., Nachman, R. L., Becker, C. G., & Minick, C. R. (1973). Culture of human endothelial cells derived from umbilical veins. Identification by morphologic and immunologic criteria. *The Journal of Clinical Investigation*, 52(11), 2745–2756.
- Jones, J. R. (2015). Reprint of: Review of bioactive glass: From Hench to hybrids. *Acta Biomaterialia*, 23(Suppl), S53–S82.
- Kang, Y., Kim, S., Fahrenholtz, M., Khademhosseini, A., & Yang, Y. (2013). Osteogenic and angiogenic potentials of monocultured and co-cultured human-bone-marrow-derived mesenchymal stem cells and human-umbilical-vein endothelial cells on three-dimensional porous beta-tricalcium phosphate scaffold. *Acta Biomaterialia*, 9(1), 4906–4915.
- Kargozar, S., Bairo, F., Hamzehlou, S., Hill, R. G., & Mozafari, M. (2018a). Bioactive glasses entering the mainstream. *Drug Discovery Today*, 23(10), 1700–1704.
- Kargozar, S., Bairo, F., Hamzehlou, S., Hill, R. G., & Mozafari, M. (2018b). Bioactive glasses: Sprouting angiogenesis in tissue engineering. *Trends in Biotechnology*, 36(4), 430–444.
- Koivisto, J. T., Gering, C., Karvinen, J., Maria Cherian, R., Belay, B., Hyttinen, J., ... Parraga, J. (2019). Mechanically biomimetic Gellan-Gellan gum hydrogels for 3D culture of beating human cardiomyocytes. *ACS Applied Materials & Interfaces*, 11(23), 20589–20602.
- Koivisto, J. T., Joki, T., Parraga, J. E., Paakkonen, R., Yla-Outinen, L., Salonen, L., ... Kellomaki, M. (2017). Bioamine-crosslinked gellan gum hydrogel for neural tissue engineering. *Biomedical Materials*, 12(2), 025014.
- Kondiah, P. J., Choonara, Y. E., Kondiah, P. P., Marimuthu, T., Kumar, P., du Toit, L. C., & Pillay, V. (2016). A review of injectable polymeric hydrogel Systems for application in bone tissue engineering. *Molecules*, 21(11), E1580. <https://doi.org/10.3390/molecules21111580>
- Kyllonen, L., Haimi, S., Mannerstrom, B., Huhtala, H., Rajala, K. M., Skottman, H., ... Miettinen, S. (2013). Effects of different serum conditions on osteogenic differentiation of human adipose stem cells in vitro. *Stem Cell Research & Therapy*, 4(1), 17.
- Laschke, M. W., & Menger, M. D. (2016). Prevascularization in tissue engineering: Current concepts and future directions. *Biotechnology Advances*, 34(2), 112–121.
- Lindroos, B., Suuronen, R., & Miettinen, S. (2011). The potential of adipose stem cells in regenerative medicine. *Stem Cell Reviews*, 7(2), 269–291.
- Ma, J., Yang, F., Both, S. K., Prins, H. J., Helder, M. N., Pan, J., ... van den Beucken, J. J. (2014). In vitro and in vivo angiogenic capacity of BM-MSCs/HUVECs and AT-MSCs/HUVECs cocultures. *Biofabrication*, 6(1), 015005.
- Manda, M. G., da Silva, L. P., Cerqueira, M. T., Pereira, D. R., Oliveira, M. B., Mano, J. F., ... Reis, R. L. (2018). Gellan gum-hydroxyapatite composite spongy-like hydrogels for bone tissue engineering. *Journal of Biomedical Materials Research. Part A*, 106(2), 479–490.
- Marelli, B., Ghezzi, C. E., Mohn, D., Stark, W. J., Barralet, J. E., Boccaccini, A. R., & Nazhat, S. N. (2011). Accelerated mineralization of dense collagen-nano bioactive glass hybrid gels increases scaffold stiffness and regulates osteoblastic function. *Biomaterials*, 32(34), 8915–8926.
- McCoy, M. G., Seo, B. R., Choi, S., & Fischbach, C. (2016). Collagen I hydrogel microstructure and composition conjointly regulate vascular network formation. *Acta Biomaterialia*, 44, 200–208.
- Mihaila, S. M., Resende, M. F., Reis, R. L., Gomes, M. E., & Marques, A. P. (2017). Interactive endothelial phenotype maintenance and osteogenic differentiation of adipose tissue stromal vascular fraction SSEA-4 (+)-derived cells. *Journal of Tissue Engineering and Regenerative Medicine*, 11(7), 1998–2013.
- Nunez-Toldra, R., Montori, S., Bosch, B., Hupa, L., Atari, M., & Miettinen, S. (2019). S53P4 bioactive glass ions for vascularized bone tissue engineering by DPPSC co-cultures. *Tissue Engineering. Part A*. [Epub ahead of print] <https://doi.org/10.1089/ten.TEA.2018.0256>
- Ojansivu, M., Hyvari, L., Kellomaki, M., Hupa, L., Vanhatupa, S., & Miettinen, S. (2018). Bioactive glass induced osteogenic differentiation of human adipose stem cells is dependent on cell attachment mechanism and mitogen-activated protein kinases. *European Cells & Materials*, 35, 54–72.
- Ojansivu, M., Mishra, A., Vanhatupa, S., Juntunen, M., Larionova, A., Massera, J., & Miettinen, S. (2018). The effect of S53P4-based borosilicate glasses and glass dissolution products on the osteogenic commitment of human adipose stem cells. *PLoS One*, 13(8), e0202740.
- Ojansivu, M., Vanhatupa, S., Bjorkvik, L., Hakkanen, H., Kellomaki, M., Autio, R., ... Miettinen, S. (2015). Bioactive glass ions as strong enhancers of osteogenic differentiation in human adipose stem cells. *Acta Biomaterialia*, 21, 190–203.
- Oliveira, M. B., Custodio, C. A., Gasperini, L., Reis, R. L., & Mano, J. F. (2016). Autonomous osteogenic differentiation of hASCs encapsulated in methacrylated gellan-gum hydrogels. *Acta Biomaterialia*, 41, 119–132.



- Pfaffl, M. W. (2001). A new mathematical model for relative quantification in real-time RT-PCR. *Nucleic Acids Research*, 29(9), e45.
- Pill, K., Melke, J., Muhleder, S., Pultar, M., Rohringer, S., Priglinger, E., ... Holthoner, W. (2018). Microvascular networks from endothelial cells and mesenchymal stromal cells from adipose tissue and bone marrow: A comparison. *Frontiers in Bioengineering and Biotechnology*, 6, 156.
- Przekora, A. (2019). The summary of the most important cell-biomaterial interactions that need to be considered during *in vitro* biocompatibility testing of bone scaffolds for tissue engineering applications. *Materials Science & Engineering. C, Materials for Biological Applications*, 97, 1036–1051.
- Rezwan, K., Chen, Q. Z., Blaker, J. J., & Boccaccini, A. R. (2006). Biodegradable and bioactive porous polymer/inorganic composite scaffolds for bone tissue engineering. *Biomaterials*, 27(18), 3413–3431.
- Rodriguez, J. P., Gonzalez, M., Rios, S., & Cambiazo, V. (2004). Cytoskeletal organization of human mesenchymal stem cells (MSC) changes during their osteogenic differentiation. *Journal of Cellular Biochemistry*, 93(4), 721–731.
- Roschger, P., Paschalis, E. P., Fratzl, P., & Klaushofer, K. (2008). Bone mineralization density distribution in health and disease. *Bone*, 42(3), 456–466.
- Sieminski, A. L., Was, A. S., Kim, G., Gong, H., & Kamm, R. D. (2007). The stiffness of three-dimensional ionic self-assembling peptide gels affects the extent of capillary-like network formation. *Cell Biochemistry and Biophysics*, 49(2), 73–83.
- Tirkkonen, L., Haimi, S., Huttunen, S., Wolff, J., Pirhonen, E., Sandor, G. K., & Miettinen, S. (2013). Osteogenic medium is superior to growth factors in differentiation of human adipose stem cells towards bone-forming cells in 3D culture. *European Cells & Materials*, 25, 144–158.
- Unger, R. E., Dohle, E., & Kirkpatrick, C. J. (2015). Improving vascularization of engineered bone through the generation of pro-angiogenic effects in co-culture systems. *Advanced Drug Delivery Reviews*, 94, 116–125.
- Usami, K., Mizuno, H., Okada, K., Narita, Y., Aoki, M., Kondo, T., ... Ueda, M. (2009). Composite implantation of mesenchymal stem cells with endothelial progenitor cells enhances tissue-engineered bone formation. *Journal of Biomedical Materials Research. Part A*, 90(3), 730–741.
- Veis, A., & Dorvee, J. R. (2013). Biom mineralization mechanisms: A new paradigm for crystal nucleation in organic matrices. *Calcified Tissue International*, 93(4), 307–315.
- Vuornos, K., Ojansivu, M., Koivisto, J. T., Hakkanen, H., Belay, B., Montonen, T., ... Miettinen, S. (2019). Bioactive glass ions induce efficient osteogenic differentiation of human adipose stem cells encapsulated in gellan gum and collagen type I hydrogels. *Materials Science & Engineering. C, Materials for Biological Applications*, 99, 905–918.

## SUPPORTING INFORMATION

Additional supporting information may be found online in the Supporting Information section at the end of this article.

**How to cite this article:** Vuornos K, Huhtala H, Kääriäinen M, et al. Bioactive glass ions for *in vitro* osteogenesis and microvascularization in gellan gum-collagen hydrogels. *J Biomed Mater Res*. 2019;1–11. <https://doi.org/10.1002/jbm.b.34482>

**Publication III supplementary data**

**Bioactive glass ions for *in vitro* osteogenesis and microvascularization in gellan gum-collagen hydrogels.**

Vuornos K., Huhtala H., Kääriäinen M., Kuismanen K., Hupa L., Kellomäki M., Miettinen S.

*J Biomed Mater Res B Appl Biomater.* 2019 Aug 31.

Supplementary data available at: <https://doi.org/10.1002/jbm.b.34482>

## Supplementary Material 1

### *Flow cytometric analysis and human adipose stem cell characterization*

Following stem cell isolation, the undifferentiated human adipose stem cells (hASCs) of passage 1–2 were characterized. Briefly, hASCs were analyzed for the cell surface markers (1) with flow cytometry (FACSaria; BD Biosciences, Franklin Lakes, NJ, USA). The following fluorophore-conjugated monoclonal antibodies were used: anti-CD3-PE, anti-CD14-PECy7, anti-CD19-PE-Cy7, anti-CD45RO-APC, anti-CD54-FITC, anti-CD73-PE, anti-CD90-APC (BD Biosciences), anti-CD11a-APC, anti-CD80-PE, anti-CD86-PE, anti-CD105-PE (R&D Systems, Minneapolis, MN, USA), CD34-APC, and anti-HLA-DR-PE (ImmunoTools, Friesoythe, Germany). Flow cytometric analysis was performed with 10,000 cells per sample, and the positive expression was defined as a level of fluorescence 99 % greater than that of the corresponding unstained cell sample (2,3). The flow cytometric analysis showed that the hASC expression of surface marker CD73 was 89.1(8.8), CD90 was 98.7(1.5), and CD105 was 96.4(3.4), and considered strong. The hASCs lacked the expression of CD3, CD11a, CD14, CD19, CD45, CD80, and CD86, whereas the expression of CD34 was 24.8(19.0), CD54 was 11.9(9.5), and HLA-DR was 1.0(0.9), and considered moderate (Table S1).

**Table S1. Flow cytometry surface markers analysis results of hASCs. *n* = 3.**

<b>Antigen</b>	<b>Surface protein</b>	<b>Mean</b>	<b>SD</b>
CD 3	T cell signal transduction	0.5	0.4
CD 11a	Cell interactions and T cell mediated killing	1.3	0.8
CD 14	Innate immune response to bacterial lipopolysaccharide	1.0	0.8
CD 19	B lymphocyte-lineage differentiation antigen	0.5	0.4
CD 34	Sialomucin-like adhesion molecule	24.8	19.0
CD 45	Leukocyte common antigen	2.0	1.2
CD 54	Cell adhesion, lymphocyte activation and migration	11.9	9.5
CD 73	Ecto-5'-nucleotidase	89.1	8.8
CD 80	Lymphocyte activation	0.9	0.9
CD 86	Regulates T cell activation	1.1	0.8
CD 90	Thy-1 (T cell surface glycoprotein)	98.7	1.5
CD 105	SH-2, endoglin	96.4	3.4
HLA-DR	Major histocompatibility class II antigens	1.0	0.9

The flow cytometric analysis confirmed the mesenchymal origin of the hASCs and the moderate elevation of CD54 was attributed to the low passage of the hASCs and the use of human serum as a cell culture medium supplement (4), whereas the somewhat elevated expression of CD34 has been previously linked to low passage of hASCs (4), while also the role of an endothelial hASC subpopulation has been discussed in literature (5,6).

### *References*

- (1) Lindroos B, Suuronen R, Miettinen S. The potential of adipose stem cells in regenerative medicine. *Stem Cell Rev* 2011 Jun;7(2):269-291.
- (2) Jaroszeski MJ, Radcliff G. Fundamentals of flow cytometry. *Mol Biotechnol* 1999 Feb;11(1):37-53.
- (3) Picot J, Guerin CL, Le Van Kim C, Boulanger CM. Flow cytometry: retrospective, fundamentals and recent instrumentation. *Cytotechnology* 2012 Mar;64(2):109-130.
- (4) Patrikoski M, Juntunen M, Boucher S, Campbell A, Vemuri MC, Mannerstrom B, Miettinen S. Development of fully defined xeno-free culture system for the preparation and propagation of cell therapy-compliant human adipose stem cells. *Stem Cell Res Ther* 2013 Mar 7;4(2):27.

(5) Mihaila SM, Resende MF, Reis RL, Gomes ME, Marques AP. Interactive endothelial phenotype maintenance and osteogenic differentiation of adipose tissue stromal vascular fraction SSEA-4(+) - derived cells. *J Tissue Eng Regen Med* 2017 Jul;11(7):1998-2013.

(6) Huttala O, Vuorenmaa H, Toimela T, Uotila J, Kuokkanen H, Ylikomi T, Sarkanen JR, Heinonen T. Human vascular model with defined stimulation medium - a characterization study. *ALTEX* 2015;32(2):125-136.





